

New Approaches to the Synthesis and Exfoliation of Polymer/Functional Graphene Nanocomposites by Miniemulsion Polymerization

Dissertation presented for the degree of Doctor of Philosophy

(Polymer Science)

at the

University of Stellenbosch



by

Hussein Mohamed Etmimi

Promoter: Prof. Ronald D. Sanderson

Co-promoter: Prof. Peter E. Mallon

Department of Chemistry and Polymer Science
Faculty of Natural Science

March 2012

Declaration

I, Hussein M. Etmimi, hereby declare that the work presented in this dissertation is my own original work, that I am the sole author thereof (save to the extent explicitly otherwise stated), that reproduction and publication thereof by Stellenbosch University will not infringe any third party rights and that I have not previously in its entirety or in part submitted it for obtaining any qualification degree.

March 2012

Copyright © 2012 University of Stellenbosch

All rights reserved

ABSTRACT

New methods are described for the synthesis of polymer/graphite nanocomposites using the miniemulsion polymerization process. Natural graphite was functionalized by oxidation to produce graphite oxide (GO) nanosheets. Poly(styrene-co-butyl acrylate) (poly(St-co-BA)) nanocomposite latices containing GO nanosheets were successfully synthesized using miniemulsion as a one-step nano-incorporation technique. The approach followed included expanding the GO nanosheets *in situ* during the miniemulsification step and then polymerizing the monomers in the presence of these expanded nanosheets. Styrene (St) and butyl acrylate (BA) were mixed with GO and then emulsified in the presence of a surfactant and a hydrophobe to afford pre-mini-emulsion latex particles. The stable pre-mini-emulsions were then polymerized to yield poly(St-co-BA)/GO nanocomposite latices. The polymerization proceeded with relatively high monomer conversion and produced stable nanocomposite latex particles. The nanocomposites exhibited mainly an intercalated morphology, irrespective of the percentage of GO filler loading.

The synthesis of exfoliated polymer nanocomposites made with modified GO is described. GO was modified with a surfmer (reactive surfactant), 2-acrylamido-2-methyl-1-propane sulfonic acid (AMPS), which widened the gap between the GO nanosheets and facilitated monomer intercalation between its nanogalleries. The AMPS-modified GO was used for the synthesis of poly(St-co-BA)/GO nanocomposite latices using a similar miniemulsion procedure. The obtained nanocomposites had exfoliated morphologies and the GO nanosheets were largely exfoliated (about 2–5 nm thick) in the resultant films obtained from the synthesized nanocomposite latices. The synthesized nanocomposites had enhanced thermal and mechanical properties compared to pure polymer as a result of the presence of AMPS-modified GO. Furthermore, the nanocomposites made with AMPS-modified GO had better thermal and mechanical properties than the unmodified GO. The mechanical properties of the nanocomposites depended on the AMPS-modified GO loading in the nanocomposites.

The synthesis of polystyrene/GO (PS-GO) nanocomposites using the reversible addition-fragmentation chain transfer (RAFT) mediated polymerization method is also described. The GO was synthesized and immobilized with a RAFT agent to afford RAFT-functionalized GO nanosheets. The RAFT-immobilized GO was used for the synthesis of PS nanocomposites in a controlled manner using miniemulsion polymerization. The molar mass and dispersity of the PS in the nanocomposites depended on the amount of RAFT-grafted GO in the system, in accordance with the features of the RAFT-mediated polymerization. X-ray diffraction and

transmission electron microscopy analyses revealed that the nanocomposites had exfoliated morphology, even at relatively high GO content. The thermal stability and mechanical properties of the PS-GO nanocomposites were better than those of the neat PS polymer. Furthermore, the mechanical properties were dependent on the modified-GO content (i.e., the amount of RAFT-grafted GO).

The hydrophobicity and barrier properties of the resulting films prepared from the synthesized poly(St-co-BA)/GO nanocomposite latices to water and water vapor were also investigated. The hydrophobicity of the synthesized nanocomposite films was determined using contact angle measurements. The water permeability was determined by measuring the moisture vapor transmission rate of the films. The GO in the nanocomposites was reduced to its original form (i.e., graphite), and the barrier properties of the obtained nanocomposite films were determined and compared to films containing the unmodified GO (as-prepared GO). Results showed that reduction of GO had a significant impact on the water affinity of the resultant films prepared from the synthesized nanocomposite latices. The presence of reduced-GO (RGO) instead of unmodified GO in the miniemulsion formulation significantly improved the hydrophobicity and barrier properties of the final films to water. However, the barrier properties of the nanocomposites were unaffected by the amount of RGO in the nanocomposites.

OPSOMMING

Nuwe metodes is beskryf vir die sintese van polimeer/grafiet nanosamestellings deur gebruik te maak van die miniemulsie polimerisasieproses. Natuurlike grafiet is gefunksionaliseer dmv oksidasie om grafietoksied (GO) nanovelle te vorm. Polistireen-ko-butilakrylaat (poli[St-ko-BA]) nanosamestellinglatekse wat GO nanovelle bevat is suksesvol gesintetiseer deur gebruik te maak van miniemulsie polimerisasie as 'n een-stap nano-insluitingstegniek. Die benadering wat gevolg is het die uitbreiding van die GO nanovelle, in situ, gedurende die miniemulsifiseringstap behels, gevolg deur die polimerisasie van die monomere in die teenwoordigheid van hierdie uitgebreide nanovelle. Stireen (St) en butielakrylaat (BA) is met GO gemeng en daarna emulgeer in die teenwoordigheid van 'n seepmiddel (surfactant) en 'n hidrofoob om pre-miniemulsielateksdeeltjies te lewer. Die stabiele pre-miniemulsies is gepolimeriseer om poli(St-ko-BA)/GO nanosamestellinglatekse te vorm. Die polimerisasie het met redelike hoë monomeeromskakeling verloop en het stabiele nanosamestellinglateksdeeltjies gelewer. Hierdie nanosamestellings het hoofsaaklik geïnterkaleerde morfologie, onafhanklik van die persentasie GO vullers, getoon.

Die sintese van afgeskilferde polimeernanosamestellings berei met gewysigde GO is beskryf. GO is gewysig met 'n 'surfmer' (reaktiewe seepmiddel), 2-akrielamido-2-metiel-1-propaansulfoonsuur (AMPS), wat die gapings tussen die GO nanovelle vergroot het en die monomeer interkalering tussen sy nanogange fasiliteer. Die AMPS-gewysigde GO is gebruik vir die sintese van poli(St-ko-BA)/GO nanosamestellinglatekse deur gebruik te maak van 'n soortgelyke miniemulsie prosedure. Die nanosamestelling só verkry het 'n afgeskilferde morfologie getoon en die GO nanovelle was grotendeels afgeskilfer (ongeveer 2–5 nm dik) in die films wat berei is van die gesintetiseerde nanosamestellinglatekse. Laasgenoemde het verhoogde termiese en meganiese eienskappe gehad in vergelyking met die suiwer polimeer, as gevolg van die teenwoordigheid van die AMPS-gewysigde-GO. Die meganiese eienskappe van die nanosamestellings hang af van persentasie AMPS-gewysigde GO vullers in die nanosamestellings.

Die sintese van PSt/GO nanosamestellings dmv die omkeerbare-addisie-fragmentasie-oordrag- (OAF)-, (Eng. RAFT-) bemiddelde polimerisasie metode is ook beskryf. Die GO is berei en geïmmobiliseer met 'n RAFT verbinding om GO nanovelle met RAFT funksionaliteit te lewer. Die RAFT-geïmmobiliseerde GO is gebruik vir die sintese van PSt nanosamestellings in 'n gekontroleerde manier mbv miniemulsie polimerisasie. Die molêre

massa en dispersie van die PSt in die nanosamestellings hang af van die hoeveelheid RAFT-geënte GO in die sisteem, in ooreenstemming met die kenmerke van RAFT-bemiddelde polimerisasie. X-straaldiffraksie en transmissie-elektronmikroskopie analyses het bewys dat die nanosamestellings, selfs by relatiewe hoë GO inhoud, 'n afgeskilferde morfologie gehad het. Die termiese stabiliteit en meganiese eienskappe van die PSt-GO nanosamestellings was beter as dié van die suiwer PSt polimeer. Verder was die meganiese eienskappe afhanklik van die gewysigde-GO-inhoud (dws, die hoeveelheid RAFT-geënte-GO).

Die hidrofobisiteit en spereienskappe van die films berei vanaf die gesintetiseerde poli(St-ko-BA)/GO nanosamestellinglatekse teenoor water en waterdamp is ook ondersoek. Die hidrofobisiteit is ondersoek deur gebruik te maak van kontakhoekmeting. Die waterdeurlaatbaarheid is bepaal deur die waterdampoordragtempo van die films te bepaal. Die GO in die nanosamestellings is gereduseer tot sy eenvoudigste vorm (grafiet) en die spereienskappe van die nanosamestellingfilms is bepaal en vergelyk met die films wat die ongewysigde GO bevat het. Resultate het getoon dat reduksie van GO 'n groot invloed gehad het op die wateraffiniteit van die films wat berei is vanaf die gesintetiseerde nanosamestellinglatekse. Die teenwoordigheid van die gereduseerde-GO (RGO) in plaas van die onveranderde GO in die miniemulsie formulering het die hidrofobisiteit en spereienskappe van die finale films, teenoor water, baie verbeter. Die spereienskappe van die nanosamestellings is egter nie beïnvloed deur die hoeveelheid RGO in die nanosamestellings nie.

ACKNOWLEDGEMENTS

First and foremost, I would like to thank and be grateful to Allah (God) who gave me the strength, health and opportunity to carry out this study successfully.

My sincere appreciation and gratitude go to my parents, for providing me with opportunities and guidance throughout my life. My father is gratefully thanked for his continuous encouragement and unlimited support that he gave me over the years. Ever since I started school, I could see his aspirations for me and the wish that I continue studying up to PhD level. My mother is especially thanked for her love, caring thoughts and prayers, in making my achievements possible. I would also like to extend my sincere thanks to all my brothers and sisters for their kind thoughts about me, and for being who they are.

On a more personal note, and from the bottom of my heart, I would like to say a very big thank you to my beloved wife, Gamra, for her love, support and patience during our stay in South Africa. She continuously supported and provided me with all the love and the necessary care to finish my Honours, MSc and PhD degrees. My two daughters, Alla and Rawa, are also loved and appreciated, for giving me the pleasure and happiness in my life. I really pray to Allah that He will give me the strength and ability so that I, in turn, can support them and give them the opportunity of a very good education, hopefully to the highest level.

I would also like to express my great thanks to my promoter, Prof. Ronald D. Sanderson, for his help and support, and the opportunity to carry out this PhD study under his guidance in his group. I am also sincerely grateful to my co-promoter, Prof. Peter E. Mallon for his time and constructive advice, after reading my dissertation. The patient assistance I received from Dr. Margie Hurndall in editing this dissertation, and from Dr. Eric van den Dungen in revising it, is also much appreciated and thankfully acknowledged.

Finally, I would like to say thank you to all my colleagues and friends in Stellenbosch, without whom my stay in South Africa would not have been the same.

The International Center for Macromolecular Chemistry and Technology and the Ministry of Education in Libya are gratefully acknowledged for the financial support to make this study possible.

Dedicated to:

- ❖ My parents – they are the reason for me being here and who made me who I am now.
- ❖ My wife and two daughters – who are the inspiration in my life.

LIST OF CONTENTS

<i>ABSTRACT</i>	<i>iii</i>
<i>LIST OF CONTENTS</i>	<i>ix</i>
<i>LIST OF PUBLICATIONS</i>	<i>xiv</i>
<i>CONFERENCE PROCEEDINGS</i>	<i>xv</i>
<i>LIST OF FIGURES</i>	<i>xvi</i>
<i>LIST OF SCHEMES</i>	<i>xix</i>
<i>LIST OF TABLES</i>	<i>xx</i>
<i>LIST OF ABBREVIATIONS</i>	<i>xxi</i>
<i>LIST OF SYMBOLS</i>	<i>xxiii</i>
CHAPTER 1: INTRODUCTION	1
1.1 Introduction	2
1.2 Motivation	5
1.3 Methodology	5
1.4 Objectives	6
1.5 Layout of dissertation	7
1.6 References	8
CHAPTER 2: HISTORICAL AND THEORETICAL BACKGROUND	11
2.1 Polymer/graphite nanocomposites (PGNs)	12
2.1.1 Introduction	12
2.1.2 Features of graphite	13
2.1.2.1 Introduction	13
2.1.2.2 Structure of graphite	14
2.1.2.3 Properties of graphite	16
2.1.2.4 Preparation of exfoliated graphite (ExG)	17
2.1.2.5 Oxidation of graphite flakes	18
2.1.3 Preparation of PGNs	20
2.1.3.1 Introduction	20
2.1.3.2 Methods used for the synthesis of PGNs	21
2.1.4 Degree of dispersion of graphite in PGNs and their final structure	22
2.1.5 Characterization of PGNs	23
2.1.5.1 XRD analysis	24

2.1.5.2 TEM analysis	25
2.1.5.3 SEM analysis	26
2.1.5.4 Mechanical properties by DMA	27
2.1.5.5 Thermal analysis by TGA	27
2.1.6 Properties and applications of PGNs	27
2.1.6.1 Mechanical properties	28
2.1.6.2 Thermal stability and flame retardant properties	28
2.1.6.3 Electrical properties	29
2.1.6.4 Barrier properties	30
2.2 Miniemulsion polymerization	31
2.2.1 Introduction	31
2.2.2 Miniemulsion vs. emulsion polymerization	32
2.2.3 Miniemulsion formulations	34
2.2.4 Preparation of miniemulsions	35
2.2.5 Initiators used in miniemulsions	36
2.2.6 Properties of miniemulsions	37
2.2.7 Miniemulsion stability	37
2.3 Controlled/living radical polymerization (CLRP)	39
2.3.1 Introduction	39
2.3.2 Fundamentals of CLRP	40
2.3.3 Common CLRP techniques	41
2.3.3.1 NMP	41
2.3.3.2 ATRP	42
2.3.3.3 RAFT-mediated polymerization	42
2.3.4 RAFT-mediated emulsion polymerization vs. miniemulsion polymerization	44
2.4 Barrier polymer coatings	45
2.4.1 Introduction	45
2.4.2 Permeability of polymeric barrier coatings	47
2.4.3 Effect of temperature and humidity on permeability	49
2.5 References	50
CHAPTER 3: POLY(STYRENE-CO-BUTYL ACRYLATE)/GRAPHITE NANOCOMPOSITES USING GRAPHITE OXIDE	60
3.1 Introduction	61
3.2 Formation of PGNs	62
3.3 Experimental	64
3.3.1 Materials	65
3.3.2 Preparation of GO from natural graphite	65
3.3.3 Miniemulsion copolymerization of St and BA in the presence of GO	66

3.3.4 Characterization and analytical techniques	67
3.3.4.1 Monomer conversion	67
3.3.4.2 Transmission electron microscopy (TEM)	67
3.3.4.3 Dynamic light scattering (DLS)	68
3.3.4.4 Fourier-transform infrared (FT-IR) spectroscopy	68
3.3.4.5 Nuclear magnetic resonance (NMR) spectroscopy	68
3.3.4.6 X-ray diffraction (XRD)	68
3.3.4.7 Differential scanning calorimetry (DSC)	68
3.3.4.8 Scanning electron microscope (SEM)	69
3.3.4.9 Thermogravimetric analysis (TGA)	69
3.3.4.10 Size exclusion chromatography (SEC)	69
3.4 Results and discussion	70
3.4.1 Characterization of GO	70
3.4.1.1 FT-IR analysis	70
3.4.1.2 XRD measurements	71
3.4.1.3 Thermal analysis by TGA	72
3.4.1.4 Thermal analysis by DSC	73
3.4.1.5 Nanostructure of GO by SEM and TEM	74
3.4.2 Characterization of the nanocomposite latices	75
3.4.2.1 Monomer conversion and latex stability	75
3.4.2.2 FT-IR analysis of nanocomposites	76
3.4.2.3 Chemical composition of poly(St-BA) nanocomposites as determined by NMR spectroscopy	77
3.4.2.4 Effect of GO loading on molecular weight of poly(St-co-BA)	79
3.4.3 Nanocomposite morphology	80
3.4.3.1 XRD analysis	80
3.4.3.2 TEM analysis	81
3.4.3.4 The amount of GO incorporated in the nanocomposites as determined by TGA	85
3.5 Conclusion	88
3.6 References	89
CHAPTER 4: POLY(STYRENE-CO-BUTYL ACRYLATE)/GRAPHITE NANOCOMPOSITES USING FUNCTIONALIZED GRAPHITE OXIDE	92
4.1 Introduction	93
4.2 Methods: Experimental and characterization	97
4.2.1 Materials	97
4.2.2 Preparation of GO	97
4.2.3 Modification of GO with AMPS	98
4.2.4 Typical preparation of poly(St-co-BA)/GO using miniemulsion polymerization	98
4.2.5 Analytical techniques	99
4.2.5.1 Transmission electron microscopy (TEM)	99

4.2.5.2 Scanning electron microscopy (SEM)	100
4.2.5.3 Thermogravimetric analysis (TGA)	100
4.2.5.4 Fourier-transform infrared (FT-IR) spectroscopy	100
4.2.5.5 Size exclusion chromatography (SEC)	100
4.2.5.6 X-ray diffraction (XRD)	101
4.2.5.7 Dynamic mechanical analysis (DMA)	101
4.3 Results and discussion	101
4.3.1 Preparation of GO	101
4.3.2 Characterization of GO	102
4.3.2.1 Interlayer spacing of GO as determined by XRD	102
4.3.2.2 Nanostructure of GO as determined by SEM and TEM	103
4.3.2.3 The organization of AMPS in the GO galleries	105
4.3.3 Characterization of poly(St-co-BA)/GO nanocomposites	107
4.3.3.1 Determination of morphology by TEM	107
4.3.3.2 Determination of nanocomposite structure by XRD	109
4.3.3.3 Mechanical properties of the poly(St-co-BA)/GO nanocomposites	110
4.3.3.4 Thermal stability of poly(St-co-BA)/GO nanocomposites	114
4.4 Conclusion	117
4.5 References	118
CHAPTER 5: POLYSTYRENE/GRAPHITE NANOCOMPOSITES VIA SURFACE RAFT-MEDIATED POLYMERIZATION	122
5.1 Introduction	123
5.2 Experimental	126
5.2.1 Chemicals	126
5.2.2 Analytical techniques	126
5.2.3 Preparation of GO	128
5.2.4 Synthesis of DIBTC RAFT agent	129
5.2.5 Immobilization of the DIBTC RAFT agent on the GO surface	130
5.2.6 Synthesis of PS-GO nanocomposites by RAFT-mediated miniemulsion polymerization	130
5.3 Results and discussion	131
5.3.1 Nanostructure of GO by TEM	131
5.3.2 Immobilization of RAFT agent onto GO surfaces	132
5.3.3 Characterization of PS-GO nanocomposites	135
5.3.3.1 SEC analysis	135
5.3.3.2 TEM analysis	136
5.3.3.3 XRD analysis	138
5.3.3.4 Particle size measurements	139
5.3.3.5 Thermal stability	139
5.3.3.6 Mechanical properties	140

5.4 Conclusion	143
5.5 References	144
CHAPTER 6: WATER BARRIER PROPERTIES OF POLYMER/GRAPHITE NANOCOMPOSITES	147
6.1 Introduction	148
6.2 Experimental	151
6.2.1 Materials	151
6.2.2 Synthesis of poly(St-co-BA)/GO nanocomposite latices	152
6.2.3 Reduction of GO in the nanocomposite latices with hydrazine hydrate	152
6.2.4 Analyses	153
6.2.4.1 SEC analysis	154
6.2.4.2 Hydrophobicity	154
6.2.4.3 MVTR test	154
6.2.4.4 Conductivity and water uptake measurements	156
6.3 Results and discussion	156
6.3.1 SEC analysis	156
6.3.2 Hydrophobicity as determined by contact angle measurements	157
6.3.3 Permeability studies using MVTR measurements	160
6.3.4 Water uptake measurements	162
6.3.5 Conductivity measurements	163
6.4 Conclusion	164
6.5 References	165
CHAPTER 7: CONCLUSIONS, HIGHLIGHTS AND RECOMMENDATIONS	168
7.1 Conclusions	168
7.2 Highlights	169
7.3 Recommendations	170
7.4 References	171
APPENDICES	172

LIST OF PUBLICATIONS

- Hussein M. Etmimi and Ronald D. Sanderson, New approach to the synthesis of exfoliated polymer/graphite nanocomposites by miniemulsion polymerization using functionalized graphene, *Macromolecules*, 44 (21), 8504–8515 (2011).
- Hussein M. Etmimi, Matthew P. Tonge and Ronald D. Sanderson, Synthesis and characterization of polystyrene-graphite nanocomposites via surface RAFT-mediated miniemulsion polymerization, *Journal of Polymer Science Part A: Polymer Chemistry*, 49, 1621–1632 (2011).
- Hussein M. Etmimi and Ronald D. Sanderson, *In situ* intercalation of graphite nanosheets in the synthesis of polymer/graphite oxide nanocomposites using miniemulsion polymerization, submitted to *Polymer* (March, 2012).
- Hussein M. Etmimi and Ronald D. Sanderson, Polymer/graphite nanocomposites: effect of reducing the functional groups of graphite oxide on water barrier properties, submitted to *Macromolecular Materials and Engineering* (March, 2012)

CONFERENCE PROCEEDINGS

The following posters were presented during the course of this study:

- Encapsulated graphene sheets covered with poly (styrene-co-butyl acrylate) nanocomposites prepared by *in situ* miniemulsion polymerization. H. Etmimi, M. Tonge, R. Sanderson, poster presented at Macro2010: 43rd IUPAC World Polymer Congress, 11–16 July 2010, Glasgow, UK.
- New approach to the synthesis of exfoliated poly(styrene-co-butyl acrylate) nanocomposites using functionalized graphene via miniemulsion polymerization. Hussein Etmimi and Ron Sanderson, poster presented at the 11th Annual UNESCO/IUPAC Workshop & Conference on Functional Polymeric Materials Focusing on Synthesis, Characterization, Properties and Applications, 26–29 April 2011, Stellenbosch, South Africa.
- New approach to the synthesis of exfoliated poly(styrene-co-butyl acrylate) nanocomposites using functionalized graphene via miniemulsion polymerization. Hussein Etmimi and Ron Sanderson, poster presented at SPE ANTEC 2011 Conference, 1–5 May 2011, Hynes Convention Center and Boston Marriott Copley Place Hotel, Boston, Massachusetts, USA.

The following oral presentation was presented based on results of this study:

- Free radical polymerization with control by RAFT for the exfoliation of clay and graphene. Ron D. Sanderson, A. Samakande and H. M. Etmimi, talk (invited speaker) presented at the IP'11 International Symposium on Ionic Polymerization, 10–15 July 2011, Goodyear Polymer Center Auditorium, The University of Akron, Akron, Ohio, USA.
- Synthesis and characterization of polystyrene-graphite nanocomposites via surface RAFT-mediated miniemulsion polymerization. Hussein Etmimi and Ron D. Sanderson, talk presented at ICAMR 2012, 7–8 Jan 2012, Chengdu, China.

LIST OF FIGURES

Figure 2.1: SEM images of graphite particles: a) natural spherical graphite and b) synthetic graphite. _____	14
Figure 2.2: Graphene, the building block of all graphitic forms such as graphite, buckyballs and CNTs. _____	16
Figure 2.3: Chemical structure of GO with different oxygen-based groups on the basal plane and around the edges of a graphene layer. _____	19
Figure 2.4: XRD patterns of: a) pristine GO; b) poly(<i>St-co-BA</i>)/GO nanocomposite with 2 wt% GO; and c) poly(<i>St-co-BA</i>)/GO nanocomposite with 3 wt% GO. _____	25
Figure 2.5: Examples of TEM images of a microtomed sample: a) intercalated poly(<i>St-MMA</i>)/graphite nanocomposite and b) exfoliated polyarylenesulfide/graphite nanocomposite. _____	25
Figure 2.6: SEM image of graphite nanosheets. _____	26
Figure 2.7: Permeation in polymer composites: a) conventional composites and b) formation of tortuous path in PGNs. _____	31
Figure 2.8: Coalescence of two droplets in miniemulsion. _____	38
Figure 2.9: Ostwald ripening in miniemulsion. _____	38
Figure 2.10: Basic structure of a typical RAFT agent. _____	43
Figure 2.11: Permeation process in a polymer film of thickness h . _____	48
Figure 3.1: FT-IR spectrum of (a) natural graphite and (b) its oxidized form (GO). _____	70
Figure 3.2: XRD results of natural graphite and its oxidized form (GO). _____	72
Figure 3.3: TGA thermograms of natural graphite and GO. _____	73
Figure 3.4: DSC curves of graphite and GO. _____	73
Figure 3.5: SEM images of natural graphite: a) at low magnification and b) at high magnification. _____	74
Figure 3.6: SEM images of GO at high magnification. _____	74
Figure 3.7: TEM images showing a) thinner nanosheets of GO and b) different area of the same sample of GO. _____	75
Figure 3.8: Monomer conversion of the miniemulsion polymerization of <i>St</i> and <i>BA</i> in the presence of different GO content (0–6 wt%). _____	76
Figure 3.9: Digital photographs showing poly(<i>St-co-BA</i>) miniemulsion latices: a) latex without GO, b) latex containing 1 wt% GO and c) latex containing 5 wt% GO. _____	76
Figure 3.10: ¹ H NMR spectra of poly(<i>St-co-BA</i>) nanocomposites with different GO content: a) 0 wt% GO, b) 1 wt% GO, c) 3 wt% GO and d) 5 wt% GO. _____	78
Figure 3.11: XRD patterns of neat poly(<i>St-co-BA</i>) (0 wt% GO) and poly(<i>St-co-BA</i>)/GO nanocomposites made with different quantities of GO (1–6 wt%). _____	80
Figure 3.12: TEM images of poly(<i>St-co-BA</i>)/GO nanocomposite latices made with a) 1 and b) 2 wt% GO relative to monomer. _____	81
Figure 3.13: TEM images of poly(<i>St-co-BA</i>)/GO nanocomposite latices made with a) 4 and b) 5 wt% GO. _____	82
Figure 3.14: TEM images of poly(<i>St-co-BA</i>)/GO nanocomposites at different magnifications: a) and b) 1 wt% GO loading, and c) and d) 2 wt% GO loading. _____	84
Figure 3.15: TEM images of poly(<i>St-co-BA</i>)/GO nanocomposites at different magnifications: a) and b) 3 wt% GO loading, and c) and d) 4 wt% GO loading. _____	84

Figure 3.16: TEM images of poly(<i>St-co-BA</i>)/GO nanocomposites at different magnifications: a) and b) 5% GO loading, and c) and d) 6% GO loading. _____	85
Figure 3.17: TGA thermograms of Poly(<i>St-co-BA</i>)/GO nanocomposites made with different quantities of GO. The insertion shows the TGA thermogram of GO. _____	86
Figure 3.18: DSC thermograms of poly(<i>St-co-BA</i>) reference and poly(<i>St-co-BA</i>)/GO nanocomposites with different GO content (1–6 wt%). _____	87
Figure 4.1: FT-IR spectra of a) pristine natural graphite and b) its oxidized form (GO). _____	102
Figure 4.2: XRD curves of pristine natural graphite and GO. _____	103
Figure 4.3: SEM images of natural graphite: a) at low magnification and b) at higher magnification. _____	103
Figure 4.4: SEM images of GO: a) at low magnification, and b) and c) at higher magnification. _____	104
Figure 4.5: Microstructure of the graphite flakes and graphite nanosheets consisting of graphene nanoplatelets. _____	104
Figure 4.6: TEM images showing thinner sheets inside GO: a) low magnification image and b) higher magnification image. _____	105
Figure 4.7: XRD patterns of GO and GOs modified with different quantities of AMPS. _____	106
Figure 4.8: TEM images of poly(<i>St-co-BA</i>)/GO nanocomposite latex made with 1 wt% GO relative to monomer: a) latex particles and b) a microtomed film cast from the same latex. _____	108
Figure 4.9: TEM images of poly(<i>St-co-BA</i>)/GO nanocomposite prepared using 1 wt% AMPS-modified GO: a) latex particles and b) a microtomed film cast from the same latex. _____	108
Figure 4.10: XRD results of poly(<i>St-co-BA</i>)/GO nanocomposites made with different amounts of AMPS-modified GO. _____	110
Figure 4.11: Mechanical properties as a function of temperature of poly(<i>St-co-BA</i>)/GO nanocomposites, at AMPS-GO loadings of 0–6 wt%: a) storage modulus and b) loss modulus. _____	111
Figure 4.12: Mechanical properties as a function of temperature of poly(<i>St-co-BA</i>) nanocomposites made with AMPS-GO and GO: a) storage modulus (1 wt% filler loading) and b) loss modulus (2 wt% filler loading). _____	114
Figure 4.13: TGA curves of poly(<i>St-co-BA</i>) nanocomposites prepared using various amounts of AMPS-GO (1–6 wt %). _____	115
Figure 4.14: Thermal properties as a function of temperature of poly(<i>St-co-BA</i>) nanocomposites made with AMPS-GO and GO: a) 1 wt% AMPS-GO and GO loading and b) 2 wt% AMPS-GO and GO loading. _____	117
Figure 5.1: TEM images of natural graphite showing different areas of the same graphite sample. _____	132
Figure 5.2: TEM images of GO dispersed in aqueous solution of SDBS: a) low magnification image and b) higher magnification image. _____	132
Figure 5.3: UV spectrum of GO-DIBTC product after successive washings with DCM. _____	133
Figure 5.4: FT-IR spectra of (a) DIBTC RAFT agent, (b) GO and (c) GO-DIBTC. _____	134
Figure 5.5: Digital photographs of GO and GO-DIBTC dispersed in <i>St</i> monomer: (a) 1 wt% GO relative to monomer and (b) 5 wt% GO-DIBTC relative to monomer. _____	134
Figure 5.6: TGA curves of (a) DIBTC RAFT agent, (b) GO-DIBTC and (c) GO. _____	135
Figure 5.7: TEM images of PS-GO nanocomposite latex particles made with different amounts of GO-DIBTC: (a) 5 wt% GO-DIBTC (at low magnification) and (b) 4 wt% GO-DIBTC (at higher magnification). _____	137

<i>Figure 5.8: TEM images of microtomed films cast from PS-GO nanocomposite latices prepared with different amount of GO-DIBTC: (a) 3 wt% GO-DIBTC, and (b) 5 wt% GO-DIBTC.</i>	138
<i>Figure 5.9: XRD results of PS-GO nanocomposites with different GO-DIBTC loadings: (a) 1 wt% GO-DIBTC, (b) 5 wt% GO-DIBTC and (c) 7 wt% GO-DIBTC.</i>	138
<i>Figure 5.10: Evolution of particle size vs. DIBTC-grafted-GO loading.</i>	139
<i>Figure 5.11: TGA thermograms of PS-GO nanocomposites and a PS reference.</i>	140
<i>Figure 5.12: Storage modulus as function of temperature of PS-GO nanocomposites at GO-DIBTC loadings of 1, 2, 3 and 6 wt%. The insertion shows the storage modulus of PS reference.</i>	141
<i>Figure 5.13: Loss modulus as function of temperature of PS-GO nanocomposites, at GO-DIBTC loadings of 1, 2, 3 and 6 wt%. The insertion shows the loss modulus of PS reference.</i>	141
<i>Figure 5.14: Tan δ as a function of temperature of PS-GO nanocomposites at GO-DIBTC loadings of 1, 2, 3 and 6 wt%.</i>	143
<i>Figure 6.1: Static contact angle of a water drop on a polymer surface.</i>	154
<i>Figure 6.2: Effect of GO loading on the Molecular weight of poly(St-co-BA)</i>	157
<i>Figure 6.3: Static contact angle of a water drop on a solid surface: a) hydrophilic surface ($\theta = 0-30^\circ$) and b) hydrophobic surface ($\theta \geq 90^\circ$).</i>	158
<i>Figure 6.4: Static contact angle of nanocomposite films: a) 2 wt% GO ($\theta = 67^\circ$) and b) 2 wt% RGO ($\theta = 100^\circ$).</i>	158
<i>Figure 6.5: Static contact angle of a poly(St-co-BA) reference film made with no GO ($\theta = 65^\circ$).</i>	159
<i>Figure 6.6: FT-IR spectra of poly(St-co-BA)/GO nanocomposites: a) 1 wt% GO, b) 2 wt% GO, c) 1 wt% RGO and d) 2 wt% RGO.</i>	160
<i>Figure 6.7: MVTR vs. GO and RGO content (wt%) for poly(St-co-BA) nanocomposite films.</i>	161
<i>Figure 6.8: Water uptake vs. GO and RGO content (wt%) for poly(St-co-BA) nanocomposite films.</i>	162
<i>Figure 6.9: Water conductivity vs. GO and RGO content (wt%) for poly(St-co-BA) nanocomposite films.</i>	164

LIST OF SCHEMES

<i>Scheme 2.1: Schematic representation of the crystal structure of graphite.</i>	15
<i>Scheme 2.2: Structure of different types of polymer/graphite composite/nanocomposites: a) conventional, b) intercalated and c) exfoliated nanostructure.</i>	23
<i>Scheme 2.3: Schematic illustration of the effect of different graphite morphology on the conductive network formation in PGNs.</i>	30
<i>Scheme 2.4: Schematic representation of miniemulsion preparation.</i>	36
<i>Scheme 2.5: Nitroxide-mediated polymerization.</i>	41
<i>Scheme 2.6: Atom transfer radical polymerization.</i>	42
<i>Scheme 2.7: The RAFT mechanism.</i>	44
<i>Scheme 3.1: The formation of polymer nanocomposite lattices based on GO using miniemulsion polymerization.</i>	64
<i>Scheme 5.1: The overall synthesis route for the preparation of RAFT-immobilized GO nanosheets.</i>	125

LIST OF TABLES

<i>Table 3.1: Formulations used in the miniemulsion polymerizations for the preparation of Poly(St-co-BA) and Poly(St-co-BA)/GO nanocomposite latices</i>	66
<i>Table 3.2: Assignment of the main FT-IR peaks of GO films and their comparison with data in the literature.</i>	71
<i>Table 3.3: The average interlayer distances of natural graphite and GO</i>	72
<i>Table 3.4: FT-IR data of GO, poly(St-co-BA) and poly(St-co-BA)/GO nanocomposites</i>	77
<i>Table 3.5: The amount of St and BA in the nanocomposites as calculated from ¹H NMR</i>	79
<i>Table 3.6: \bar{M}_n, \bar{M}_w and \bar{D} of poly(St-co-BA) nanocomposites prepared using different quantities of GO (0–6 wt%)</i>	79
<i>Table 3.7: Average particle size of nanocomposite latices made with different quantities of GO (0–6 wt%) obtained from DLS</i>	83
<i>Table 3.8: The initial GO content added and the quantities of GO in the nanocomposites determined from TGA analysis</i>	87
<i>Table 3.9: T_g of poly(St-co-BA) and poly(St-co-BA)/GO nanocomposites prepared with different GO content (1–6 wt%).</i>	88
<i>Table 4.1: Quantities of reagents and monomers used in the miniemulsion polymerizations</i>	99
<i>Table 4.2: Interlayer distance (d-spacing) of GO and GOs modified with different amounts of AMPS</i>	107
<i>Table 4.3: T_g of poly(St-co-BA)/GO nanocomposites, at AMPS-GO loadings of 0–6 wt%</i>	112
<i>Table 4.4: M_n, M_w and \bar{D} of the poly(St-co-BA) reference and poly(St-co-BA)/GO nanocomposites prepared using different quantities of AMPS-GO (0–6 wt%)</i>	113
<i>Table 4.5: Thermogravimetric properties of poly(St-co-BA) and its nanocomposites made with different concentrations of AMPS-GO (0–6 wt%)</i>	115
<i>Table 5.1: Miniemulsion formulations used for the preparation of PS-GO nanocomposites and the PS reference</i>	131
<i>Table 5.2: Molar masses and \bar{D} of the PS-GO nanocomposites and PS reference</i>	136
<i>Table 5.3: T_g values of PS-GO nanocomposites and PS reference obtained from the onset temperature of the $\tan \delta$ curve in the DMA scan</i>	142
<i>Table 6.1: Gas permeability of graphene-based nanocomposites</i>	150
<i>Table 6.2: Formulations used in the miniemulsion polymerization reactions</i>	153
<i>Table 6.3: Static contact angles of the poly(St-co-BA) films prepared using different quantities of GO and RGO</i>	159

LIST OF ABBREVIATIONS

AIBN	2,2'-Azobis(isobutyronitrile)
AMPS	2-Acrylamido-2-methyl-1-propane sulfonic acid
ARG	As-received graphite
ATRP	Atom-transfer radical polymerization
BA	n-Butyl acrylate
CA	Cetyl alcohol
CDCl ₃	Deuterated chloroform
CLRP	Controlled/living radical polymerization
cmc	Critical micelle concentration
CNTs	Carbon nanotubes
DCC	1,3-Dicyclohexyl carbodiimide
DCM	Dichloromethane
DDI	Distilled deionized
DIBTC	Dodecyl isobutyric acid trithiocarbonate
DLS	Dynamic light scattering
DMA	Dynamic mechanical analysis
DMAP	4-Dimethylaminopyridine
DMF	<i>N,N</i> -Dimethylformamide
DMSO- <i>d</i> ₆	Deuterated dimethyl sulfoxide
DSC	Differential scanning calorimetry
EG	Expanded graphite
ExG	Exfoliated graphite
FT-IR	Fourier-transform infrared
GIC	Graphite intercalation compounds
GO	Graphite oxide
GNPs	Graphene nanoplatelets
HD	Hexadecane
iGO	Isocyanate-treated GO
M	Monomer
MMA	Methyl methacrylate
MVTR	Moisture vapor transmission rate
NMP	Nitroxide-mediated polymerization
NMR	Nuclear magnetic resonance

PC	Polycarbonate
PCNs	Polymer-clay nanocomposites
PDMS	Polydimethylsiloxane
PE	Polyethylene
PEN	Poly(ethylene naphthalate)
PGNs	Polymer/graphite nanocomposites
PMMA	Poly(methyl methacrylate)
Poly(St-co-MMA)	Poly(styrene-co-methyl methacrylate)
Poly(St-co-BA)	Poly(styrene-co-butyl acrylate)
Poly(St-co-BA)/GO	Poly(styrene-co-butyl acrylate)/graphite oxide
PP	Polypropylene
PS	Polystyrene
PS-GO	Polystyrene-graphite oxide
PS-PI-PS	Poly(styrene-co-isoprene-co-styrene)
PU	Polyurethane
KPS	Potassium persulfate
RAFT	Reversible addition-fragmentation chain transfer
RGO	Reduced-GO
SEC	Size exclusion chromatography
SEM	Scanning electron microscopy
SDS	Sodium dodecyl sulfate
SDBS	Sodium dodecylbenzene sulfonate
St	Styrene
TEGO	Thermally-exfoliated GO
TEM	Transmission electron microscopy
TGA	Thermogravimetric analysis
THF	Tetrahydrofuran
TRG	Thermally-reduced graphene
TRU	Thermoplastic polyurethane
UV	Ultraviolet
VAc	Vinyl acetate
w.u.	Water uptake
XRD	X-ray diffraction

LIST OF SYMBOLS

D	Diffusion coefficient
S	Solubility coefficient
P	Permeability
E_p	Activation energy for permeation
R	Gas constant
T	Temperature
T_g	Glass transition temperature
θ	Static contact angle
R_p	Rate of polymerization
$[M]_p$	Monomer concentration in the particles
\bar{M}_w	Weight average molecular weight
\bar{M}_n	Number average molecular weight
\mathcal{D}	Dispersity
G'	Storage modulus
G''	Loss modulus
K_d	Dissociation rate coefficient
k_p	Propagation rate coefficient
k_t	Termination rate coefficient
k_{tr}	Trapping rate coefficient
k_{act}	Activation rate coefficient
k_{deact}	Deactivation rate coefficient

INTRODUCTION

Abstract

This chapter provides a brief introduction to, motivation for, and the objectives of this study.

1.1 Introduction

Polymer nanocomposites consist of a filler reinforcement material of a nanometer scale in size, dispersed in a polymer matrix.¹ These multicomponent materials create a new class of polymer composites with unique functional and physical properties, such as superior mechanical and thermal performance as well as improved barrier properties.²⁻⁴ The fillers can be one-dimensional (e.g., nanotubes and fibres), two-dimensional (e.g., clay and graphite), or three-dimensional (e.g., spherical particles).⁵ The optimal combination of properties of these two different materials (i.e., polymer and nanofiller) can often be better achieved with these structured nanocomposites than by blending the two materials. Furthermore, as the mixing of phases occurs over a nanometer-length scale, in comparison to the micrometer-length scale of conventional composites, these nanocomposites may exhibit remarkable improvements in the properties of polymers, even with the addition of only a small weight fraction of the nanofillers relative to polymers.^{6,7} In general, polymer nanocomposites exhibit improved polymer properties, and their use can even lead to certain new properties that can not be derived from pure polymers.⁸

The ability to synthesize such nanostructured materials can be of great scientific and industrial importance due to their potential properties and applications. The synthesis of polymer nanocomposites such as polymer/graphite nanocomposites (PGNs) could provide an opportunity to tailor properties for a range of desired applications. These include applications such as interior and exterior accessories for automobiles, structural components for portable electronic devices, films for food packaging, and in the aerospace industry.^{9,10} Most often, these nanocomposite particles can be used to create polymeric materials with properties that can not be achieved by a physical blend of two or more different polymers.

Unfortunately, pure polymers often have insufficient physical and functional properties. The addition of graphite nanosheets into polymers could improve their properties compared to neat polymers.¹¹ An example of this, is graphite inclusion into polystyrene (PS), which alone has very poor impact strength that limits its applications.¹² Graphite, with its nanolayered structure and high aspect ratio, has exceptional mechanical strength. It is one of the stiffest materials found in nature, with an elastic modulus of > 1 TPa.¹³ By using an additive approach, it can be used as a nanofiller material for the preparation of polymer nanocomposites with improved mechanical performance.^{7,9} Furthermore, most polymers are thermally unstable. Increasing the thermal stability of polymers will, therefore, lead to them

being useful for many new applications, for example, as fire extinguisher agents and flame retardant materials.^{14,15} The graphite nanosheets, often < 100 nm thick, provide good thermal stability. Graphite has an thermal resistance up to 3000 °C.¹⁶ It can, therefore, be added as a nanofiller material into the matrix of many polymers to produce thermally stable polymer nanocomposites.^{17,18}

In recent years, the use of graphite based materials, as reinforcement fillers for polymers, has attracted much attention. Various synthesis techniques are now available and have been widely used for the preparation of PGNs. These include solution blending,¹⁹ exfoliation-adsorption,²⁰ *in situ* intercalative polymerization²¹ and melt intercalation.²² Although great success has been achieved in the preparation of such nanocomposites using *in situ* polymerization of the monomer in the presence of graphite nanosheets,^{21,23,24} reports on the preparation of these composites in emulsion systems are rare. In particular, the use of miniemulsion polymerization for the synthesis of these nanocomposites has not been fully investigated. This study describes the synthesis of poly(styrene-co-butyl acrylate) (poly(St-co-BA)/graphite and polystyrene (PS)/graphite nanocomposites using miniemulsion polymerization as a one-step nano-incorporation technique.

In miniemulsion polymerization most monomer droplets are in principle directly converted into polymer particles, since the droplets are regarded as the locus of polymerization.²⁵ This feature makes miniemulsion polymerization quite efficient as a convenient one-step technique for the incorporation of inorganic solid compounds in polymeric materials. In the miniemulsion process, the oil phase, which consists of the monomer and the nanofiller, is dispersed in the water phase, which contains the surfactant, by a high shear device.^{26,27} This will lead to the formation of monomer droplets containing the nanofiller particles, stabilized by the surfactant, from which polymer particles will be created during the polymerization step.²⁷

In the past, layered silicate clays have received much attention because they can be dispersed in a polymer matrix at the nanometer level to yield reinforced polymer composites known as polymer-clay nanocomposites (PCNs).²⁸ Since then, great success has been achieved in the synthesis of polymer nanocomposites made with clays under different polymerization conditions, including miniemulsion polymerization.²⁹ However, the modification of clay is an essential requirement for the formation of PCNs. 2-Acrylamido-2-methyl-1-propane sulfonic acid (AMPS) has been widely used to modify clay for the preparation of PCNs made with

hydrophobic monomers.^{30,31} Recent studies showed that using AMPS as a clay modifier successfully promoted exfoliation of clay upon copolymerization of styrene (St) with n-butyl acrylate (BA)³² and methyl methacrylate³³ in emulsion systems.

The same concept can be applied, for the first time, to graphite oxide (GO), since GO has a larger interlayer spacing compared to the pristine graphite, and polar groups such as hydroxyl and carboxyl groups on its surface. Thus, the intercalation of AMPS between GO nanosheets becomes possible via the formation of hydrogen bonds between the functional groups of AMPS and GO. As part of this study, the use of AMPS as a modifier of the GO nanosheets was studied. The study also focuses on the preparation of poly(St-co-BA) nanocomposites based on GO, which was functionalized by AMPS, using the miniemulsion polymerization process.

The use of chain transfer agents in controlled/living radical polymerization (CLRP) allows for achieving control of the polymerization process. Among the CLRP methods, the discovery of the reversible addition-fragmentation chain transfer (RAFT)-mediated polymerization has been an outstanding achievement.^{34,35} RAFT-mediated polymerization allows the preparation of polymers with low dispersity and predetermined molecular weights. In addition, the compatibility over a wide range of reaction conditions required for the RAFT process and its versatility toward different monomers make this method the most useful of all the CLRP techniques in designing macromolecular architectures. Thus, use of a combination of RAFT technology and graphite nanosheets for the synthesis of PGNs by RAFT-mediated polymerization is expected to allow for the preparation of tailor-made polymer composites with enhanced properties. To date, the synthesis of PGNs using the RAFT technique has not been reported, except from our own reference.³⁶

Recently, the barrier properties of polymer nanocomposites made with graphite have attracted significant interest.^{4,37} Due to its layered structure, graphite can be used in the synthesis of polymer nanocomposites with improved barrier properties. These nanocomposites can be used in latex formulations, such as coatings, to reduce the unwanted penetration of water and water vapor molecules through a permeable material. However, GO is hydrophilic due to the presence of many oxygen-containing functional groups such as hydroxyl (–OH) and carboxyl (–COOH) on its surface.³⁸ If these functional groups are reduced, the GO can be changed back to its original form (i.e., graphite).^{39,40} This makes graphene nanoplatelets in reduced-GO (RGO) relatively hydrophobic. By reducing the functional groups of GO in the nanocomposite lattices, it is possible to obtain films that consist of a highly hydrophobic

graphene nanoplatelets, intercalated by a relatively hydrophobic polymer, such as poly(St-co-BA). The graphene nanolayers in RGO will act as impermeable obstacles⁴¹ that provide longer diffusion paths across the polymer film, resulting in improved barrier properties.

1.2 Motivation

The motivation for this study was the desire to investigate new methods for the synthesis of PGNs using functionalized graphite. To the best of my knowledge, nothing is yet reported in the literature on studies carried out to prepare polymer nanocomposites based on functionalized graphite using miniemulsion polymerization. The modification of graphite will alter the intercalation behavior of its graphene nanosheets and allows for the complete exfoliation of graphite into individual graphene nanoplatelets. The use of miniemulsion as the polymerization method will also promote the intercalation of monomers into the modified graphite nanosheets.

1.3 Methodology

The synthesis of PGNs requires good compatibility between the graphite nanosheets and the monomer or polymer used. Unfortunately, graphite layers lack both the affinity and space for hydrophilic or hydrophobic polymers to intercalate into its galleries. This is because there are no reactive groups on the graphite layers, which makes it very difficult for a monomer or polymer to be loaded on its surface.¹⁶ In addition, graphite platelets are bound to each other by van der Waals forces, which make the interlayer distance of graphite very narrow (3.35 Å).⁴² Therefore, modification of the natural graphite sheets should be carried out in order to produce functional graphite that can be used for the synthesis of PGNs with enhanced properties.^{43,44}

One approach that can be used for the modification of graphite sheets is the subjection of graphite flakes to oxidation under strong acidic conditions (e.g., H₂SO₄/HNO₃). The oxidation of graphite leads to the formation of functionalized graphite, referred to as GO. Depending on the conditions of oxidation, GO may contain variable amounts of oxygen-containing groups, such as epoxy, hydroxyl and carboxyl.^{45,46} Due to the presence of these functional groups, GO is very hydrophilic and soluble in aqueous media. The presence of these functional groups will also facilitate physical and chemical interaction between the graphite and polar organic molecules and polymers. The incorporation of functional groups into GO could also provide

newly functionalized GO to which organic molecules such as AMPS and RAFT agents can be attached.

This modification of GO sheets will play a vital role in tailoring the structure and properties of GO, and improving its compatibility in polymer systems. This will enable us to prepare novel PGNs with enhanced functional and physical properties.

1.4 Objectives

The objectives of this study were the following:

- 1) Investigate the use of miniemulsion polymerization for the preparation of poly(St-co-BA) nanocomposite latices using unmodified GO (i.e., as-prepared GO) in a one-step nano-incorporation technique. The emphasis will be on investigating the use of miniemulsion polymerization for the synthesis of latices with intercalated or exfoliated morphology based on unmodified GO. The morphology of the obtained nanocomposites latices and their films will be characterized. The synthesized GO will also be characterized in terms of its chemical structure, morphology and thermal stability.
- 2) Modify GO by a surfmer (also called reactive surfactant), 2-acrylamido-2-methyl-1-propane sulfonic acid (AMPS). The AMPS-modified GO will be used for the synthesis of poly(St-co-BA) nanocomposites with exfoliated structure using the miniemulsion process. The obtained nanocomposites will be characterized for their thermal and mechanical properties, and these properties will be compared to the properties of the neat copolymer.
- 3) Modify GO by a RAFT agent, dodecyl isobutyric acid trithiocarbonate (DIBTC). The DIBTC RAFT agent will be synthesized and immobilized onto the GO nanosheets. The RAFT-immobilized GO (GO-DIBTC) will then be used for the synthesis of PS nanocomposites in a controlled manner. The effect of the use of RAFT-mediated polymerization on the control of the PS nanocomposites' morphology and properties using GO-DIBTC will be determined.
- 4) Investigate the barrier properties of poly(St-co-BA) nanocomposite films containing the GO nanosheets to water and water vapor. The functional groups on GO in the

nanocomposites will be reduced using a strong reducing agent, hydrazine hydrate. The water hydrophobicity and permeability of the obtained nanocomposite films containing the RGO will be evaluated, and compared to the same nanocomposite films made with unmodified GO.

1.5 Layout of dissertation

This dissertation consists of seven chapters. Since two papers emanating from this study have already been published, I elected to present my dissertation in the so called ‘publication style’. Chapter 1 provides a general introduction to the research, followed by a motivation for and the objectives of the study.

Chapter 2 gives a detailed historical and theoretical background to the study. It mainly describes the concept of polymer nanocomposites based on graphite. The preparations of PGNs as well as the properties of these nanocomposites, including the thermal, mechanical and barrier properties, are discussed. Miniemulsion polymerizations, and the differences between emulsion and miniemulsion systems, are described. The chapter also describes controlled/living radical polymerization, with emphasis on the RAFT method. A short overview on the barrier properties of polymers used in coating applications is included. The permeability of low molecular weight molecules, such as water, through polymer films is addressed.

Chapters 3–6 comprise the body of the document, and each has its own introduction, experimental, results and discussion, and conclusion sections. Chapter 3 describes the synthesis of poly(St-co-BA) nanocomposites based on unmodified GO (i.e., as-prepared GO). The emphasis was on investigating the ability of miniemulsion polymerization for the synthesis of polymer nanocomposites using as-prepared GO with intercalated or exfoliated structure.

Chapter 4 describes the modification of GO with a surfmer, namely AMPS, and the subsequent use of the AMPS-modified GO for the synthesis of poly(St-co-BA) nanocomposites. The thermal and mechanical properties of the synthesized nanocomposites were determined and compared to those of the pure polymer.

Chapter 5 describes the use of a RAFT agent for the modification of GO and the subsequent

Chapter 1: Introduction

use of the RAFT-modified GO for the control of St polymerization to yield PS nanocomposites with controlled molar mass and dispersity. Synthesis and characterization (i.e., thermal and mechanical properties) of the PS nanocomposites obtained are reported.

Chapter 6 describes the results obtained from the hydrophobicity, water uptake, conductivity and moisture vapor transmission rate measurements. Here the effects of the reduction of functional groups of GO on the hydrophobicity and barrier properties (to water) of the resultant films produced from the synthesized latices are described.

Chapter 7 presents the main conclusions drawn from the results presented in this study, and offers some recommendations for future work.

1.6 References

- (1) Mai, Y.-W.; Yu, Z.-Z., *Polymer Nanocomposites*. 2nd edition; Woodhead Publishing: Cambridge, 2006.
- (2) Alexandre, M.; Dubois, P. *Materials Science and Engineering: Reports* **2000**, 28 (1-2), 1-63.
- (3) Moniruzzaman, M.; Winey, K. I. *Macromolecules* **2006**, 39 (16), 5194-5205.
- (4) Kim, H.; Miura, Y.; Macosko, C. W. *Chemistry of Materials* **2010**, 22 (11), 3441-3450.
- (5) Ray, S.; Bousmina, N., *Polymer Nanocomposites and Their Applications*. American Scientific Publishers: California, 2006.
- (6) Vaia, R. A.; Price, G.; Ruth, P. N.; Nguyen, H. T.; Lichtenhan, J. *Applied Clay Science* **1999**, 15 (1-2), 67-92.
- (7) Yang, J.; Tian, M.; Jia, Q.-X.; Shi, J.-H.; Zhang, L.-Q.; Lim, S.-H.; Yu, Z.-Z.; Mai, Y.-W. *Acta Materialia* **2007**, 55 (18), 6372-6382.
- (8) Hussain, F.; Hojjati, M.; Okamoto, M.; Gorga, R. E. *Journal of Composite Materials* **2006**, 40 (17), 1511-1575.
- (9) Potts, J. R.; Dreyer, D. R.; Bielawski, C. W.; Ruoff, R. S. *Polymer* **2011**, 52 (1), 5-25.
- (10) Kim, H.; Abdala, A. A.; Macosko, C. W. *Macromolecules* **2010**, 43 (16), 6515-6530.
- (11) Stankovich, S.; Dikin, D. A.; Dommett, G. H. B.; Kohlhaas, K. M.; Zimney, E. J.; Stach, E. A.; Piner, R. D.; Nguyen, S. T.; Ruoff, R. S. *Nature* **2006**, 442 (7100), 282-286.
- (12) Mark, H. F.; Bikales, N. M.; Overberger, C. G.; Menger, G., *Encyclopedia of Polymer Science and Engineering*. 2nd edition; John Wiley and Sons Inc.: New York, 1989; Vol. 16, pp 1-246.
- (13) Donghwan, C.; Sangyeob, L.; Gyeongmo, Y.; Hiroyuki, F.; Lawrence, T. D. *Macromolecular Materials and Engineering* **2005**, 290 (3), 179-187.
- (14) Higginbotham, A. L.; Lomeda, J. R.; Morgan, A. B.; Tour, J. M. *ACS Applied Materials & Interfaces* **2009**, 1 (10), 2256-2261.

Chapter 1: Introduction

- (15) Wang, Z.; Han, E.; Ke, W. *Corrosion Science* **2007**, 49 (5), 2237-2253.
- (16) Pierson, H. O., *Handbook of Carbon, Graphite, Diamond and Fullerenes*. 2nd edition; Noyes Publications: New Jersey, 1993; Vol. 3, pp 43-69.
- (17) Uhl, F. M.; Wilkie, C. A. *Polymer Degradation and Stability* **2002**, 76 (1), 111-122.
- (18) Zhang, R.; Hu, Y.; Xu, J.; Fan, W.; Chen, Z. *Polymer Degradation and Stability* **2004**, 85 (1), 583-588.
- (19) Zheng, W.; Wong, S.-C. *Composites Science and Technology* **2003**, 63 (2), 225-235.
- (20) Jing-Wei, S.; Xiao-Mei, C.; Wen-Yi, H. *Journal of Applied Polymer Science* **2003**, 88 (7), 1864-1869.
- (21) Liu, P.-G.; Xiao, P.; Xiao, M.; Gong, K.-c. *Chinese Journal of Polymer Science* **2000**, 18 (5), 413-418.
- (22) Wenge, Z.; Xuehong, L.; Shing-Chung, W. *Journal of Applied Polymer Science* **2004**, 91 (5), 2781-2788.
- (23) Du, X. S.; Xiao, M.; Meng, Y. Z. *Journal of Polymer Science Part B: Polymer Physics* **2004**, 42, 1972-1978.
- (24) Zheng, G.; Wu, J.; Wang, W.; Pan, C. *Carbon* **2004**, 42, 2839-2847.
- (25) Landfester, K.; Bechthold, N.; Forster, S.; Antonietti, M. *Macromolecular Rapid Communications* **1999**, 20, 81-84.
- (26) Sudol, E.; El-Aasser, M. Miniemulsion Polymerization. In *Emulsion Polymerization and Emulsion Polymers*, Lovell, P.; El-Aasser, M., Eds.; John Wiley & Sons Ltd.: New York, 1997; pp 699-722.
- (27) Samakande, A.; Sanderson, R. D.; Hartmann, P. C. *Journal of Polymer Science Part A: Polymer Chemistry* **2008**, 46 (21), 7114-7126.
- (28) Usuki, A.; Kojima, Y.; Kawasumi, M.; Okada, A.; Fukushima, Y.; Kurauchi, T.; Kamigaito, O. *Journal of Materials Research* **1993**, 8, 1179-1184.
- (29) Matej, M.; Reyes, Y.; Mari, P.; Leiza, J. Polymer–Clay Nanocomposites by Miniemulsion Polymerization. In *Polymer Nanocomposites by Emulsion and Suspension Polymerization*, 1st edition; Mittal, V., Ed.; Royal Society of Chemistry: Cambridge, 2011; Vol. 10, pp 198-222.
- (30) Greesh, N.; Hartmann, P. C.; Cloete, V.; Sanderson, R. D. *Journal of Colloid and Interface Science* **2008**, 319 (1), 2-11.
- (31) Choi, Y. S.; Ham, H. T.; Chung, I. J. *Polymer* **2003**, 44 (26), 8147-8154.
- (32) Greesh, N.; Hartmann, P. C.; Cloete, V.; Sanderson, R. D. *Journal of Polymer Science Part A: Polymer Chemistry* **2008**, 46 (11), 3619-3628.
- (33) Xu, M.; Choi, Y. S.; Kim, Y. K.; Wang, K. H.; Chung, I. J. *Polymer* **2003**, 44 (20), 6387-6395.
- (34) Le, T. P.; Moad, G.; Rizzardo, E.; Thang, S. H. PCT Int. Appl. WO 9801478 1998.

Chapter 1: Introduction

- (35) Chiefari, J.; Chong, Y. K.; Ercole, F.; Krstina, J.; Jeffery, J.; Le, T. P. T.; Mayadunne, R. T. A.; Meijs, G. F.; Moad, C. L.; Moad, G.; Rizzardo, E.; Thang, S. H. *Macromolecules* **1998**, 31 (16), 5559-5562.
- (36) Etmimi, H. M.; Tonge, M. P.; Sanderson, R. D. *Journal of Polymer Science Part A: Polymer Chemistry* **2011**, 49 (7), 1621-1632.
- (37) Kim, H.; Macosko, C. W. *Macromolecules* **2008**, 41 (9), 3317-3327.
- (38) Titelman, G. I.; Gelman, V.; Bron, S.; Khalfin, R. L.; Cohen, Y.; Bianco-Peled, H. *Carbon* **2005**, 43 (3), 641-649.
- (39) Stankovich, S.; Dikin, D. A.; Piner, R. D.; Kohlhaas, K. A.; Kleinhammes, A.; Jia, Y.; Wu, Y.; Nguyen, S. T.; Ruoff, R. S. *Carbon* **2007**, 45 (7), 1558-1565.
- (40) Stankovich, S.; Piner, R. D.; Chen, X.; Wu, N.; Nguyen, S. T.; Ruoff, R. S. *Journal of Materials Chemistry* **2006**, 16 (2), 155-158.
- (41) Bunch, J. S.; Verbridge, S. S.; Alden, J. S.; van der Zande, A. M.; Parpia, J. M.; Craighead, H. G.; McEuen, P. L. *Nano Letters* **2008**, 8 (8), 2458-2462.
- (42) Meng, Y. Polymer/graphite nanocomposites. In *Polymer Nanocomposites*, 2nd edition; Mai, Y.-W.; Yu, Z.-Z., Eds.; Woodhead Publishing: Cambridge, 2006; Vol. 19, pp 510-539.
- (43) Dreyer, D. R.; Ruoff, R. S.; Bielawski, C. W. *Angewandte Chemie International Edition* **2010**, 49 (49), 9336-9344.
- (44) Dreyer, D. R.; Park, S.; Bielawski, C. W.; Ruoff, R. S. *Chemical Society Reviews* **2010**, 39 (1), 228-240.
- (45) He, H.; Klinowski, J.; Forster, M.; Lurf, A. *Chemical Physics Letters* **1998**, 287 (1-2), 53-56.
- (46) Lurf, A.; He, H.; Forster, M.; Klinowski, J. *The Journal of Physical Chemistry B* **1998**, 102 (23), 4477-4482.

HISTORICAL AND THEORETICAL BACKGROUND

Abstract

This chapter gives a brief insight and historical overview of the study. Relevant scientific achievements in the synthesis of polymer nanocomposites, particularly polymer/graphite nanocomposites, are discussed, including the numerous synthesis routes currently available. The end-application of these nanostructured materials and the importance of the study are mentioned.

2.1 Polymer/graphite nanocomposites (PGNs)

2.1.1 Introduction

Since the pioneering work of the Toyota research group in the early 1990s,¹ polymer-clay nanocomposites (PCNs) have attracted much attention. If the clay particles are well dispersed within the polymer matrix, either intercalated or exfoliated nanostructures are obtained. This leads to great enhancement of physical and functional performance of the nanocomposites in comparison to pure polymers.² Since then, most researchers have focused on the synthesis and characterization of nanocomposites made with exfoliated clay platelets, mainly because of the availability of clay and the ease of surface modification and intercalation with a variety of polymer systems.³⁻⁵

The same concept can be applied to another nanoreinforcement material, namely graphite, to produce graphene nanoplatelets^{6,7} and PGNs.⁸⁻¹⁰ Similar to clay, graphite is a layered material that consists of many layers known as graphene. Graphene is a monolayer of carbon atoms densely packed in a 2-D hexagonal lattice. These graphene sheets have many characteristic chemical and physical properties in the exfoliated state, including good mechanical, thermal and electrical properties.^{11,12} Furthermore, the use of graphene in polymer nanocomposites has been found to increase the barrier and fire-retardant properties of polymers.^{13,14}

The carbon atoms within the same graphene layers are covalently bonded and the cleavage of bonds between carbon atoms among these layers is very difficult. This results in graphene sheets having very high strength as well as good mechanical properties in the same plane. Contrary to this, the weak van der Waals interaction acting between the graphene layers makes the cleavage of bonds between the graphene layers very easy. Hence, the material can be converted into high aspect ratio (length-to-thickness ratio) nanoreinforcement platelets with thicknesses as small as 2–10 nm through a process of intercalation and exfoliation.¹⁵ During this process of intercalation and exfoliation, the graphite is oxidized and converted to a lamellar solid material with aromatic regions of unoxidized benzene rings and aliphatic six-membered ring regions containing epoxide, hydroxyl and carboxyl groups.^{16,17} The resulting material, known as expanded graphite (EG), consists of a large number of delaminated graphene oxide sheets that are connected in a network with pores of different sizes, ranging from 10 nm to 10 μm .¹⁸ These nanosheets are strongly hydrophilic and are dispersible in water,¹⁹ alkaline solutions²⁰ and organic solvents.²¹ Thus, suitable monomers are able to intercalate into the pores and galleries of EG to form PGNs.²²

The advantage of nanoscale reinforcement in polymers is threefold: (1) The nanofiller particles, which are finely dispersed in the polymer matrix, contribute to polymer chain confinement effects. This may lead to enhanced mechanical properties of polymers, such as high glass transition temperature, stiffness and strength. This enhancement in mechanical properties of polymers can be attributed to the high aspect ratio and large surface area of the nanofiller particles.²³ (2) Due to the intercalation of polymer chains into the lamellae (galleries) of the nanolayered filler, an improvement in thermal stability of polymers is observed. The filler particles act as an insulator between the heat source and the surface area of polymer where the combustion occurs, resulting in better thermal stability.²⁴ (3) The nanolayered fillers act as impermeable obstacles that provide longer diffusion paths across the polymer matrix. Their presence makes diffusion paths of low molecular weight molecules such as oxygen and water across a polymer membrane more tortuous.²⁵ This results in enhanced barrier performance for low molecular weight molecules such as gases through polymers.^{26,27}

2.1.2 Features of graphite

2.1.2.1 Introduction

Graphite has been known and used since the 15th century when the first pencil was manufactured in England. The word graphite derives its name from the Greek word "graphein", meaning to write. The carbon atoms in graphite are arranged in a planar condensed ring system in six-atom hexagonal cells, namely graphene. The material is generally soft and normally gray to black in color, opaque, and has a glossy appearance. Graphite is naturally abundant and has very strong anisotropic properties. For instance graphite has an electrical conductivity that is high along the graphene layers but very poor perpendicular to the graphene layer. Despite its natural abundance, graphite has only recently become known as a nanofiller material of choice.²⁸ This is mainly due to the exceptional physical and chemical properties observed when the sp²-hybridized graphene layers are isolated.¹¹

There are two main classifications of graphite: (a) natural and (b) synthetic graphite.²⁹ Figure 2.1 shows scanning electron microscopy (SEM) images of natural spherical graphite and synthetic graphite. Natural graphite is graphite that is formed in very distinct geological environments. It is a relatively abundant mineral found in nature in the form of flakes of

various particle sizes. Its structure comprises graphitic carbon, regardless of its crystalline perfection.³⁰ Depending on the formation of the natural graphite and crystallite size, the morphology can vary from micro-crystalline to macro-crystalline.³¹ The micro-crystalline form is amorphous and has a low purity, resulting in low conductivity and lubricating properties. On the other hand, the macro-crystalline form is very pure and has a high electrical conductivity. The latter can be further sub-divided into flake graphite or vein graphite.

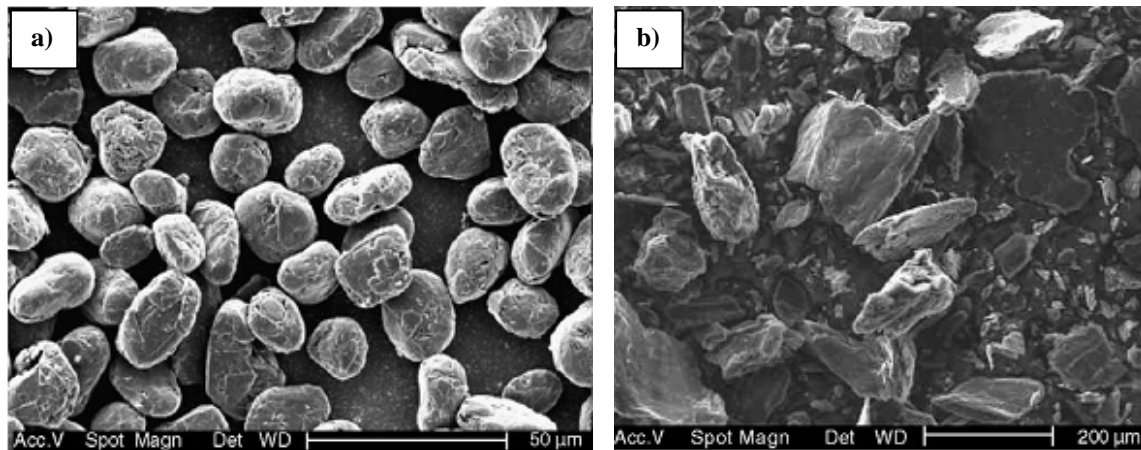


Figure 2.1: SEM images of graphite particles: a) natural spherical graphite and b) synthetic graphite.²⁹

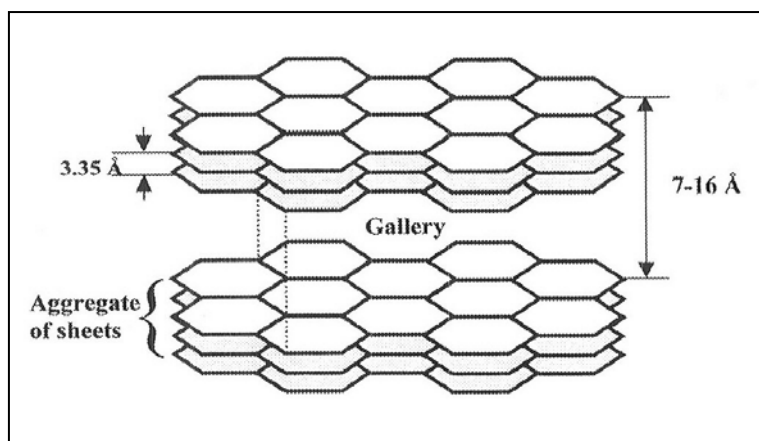
Synthetic graphite is mainly prepared by heating unstructured carbon at high temperature, above 2500 °C.³² This heat treatment orients the disordered layers of carbon atoms into the graphitic structure. The process is called graphitization, which is essentially an ordering of the carbon atoms to a more perfect structure of hexagonal graphite. The quality of the obtained graphite depends on the purity of the raw starting material. Therefore, the characteristics of the synthetic graphite may vary. Different synthetic graphite with different anisotropic properties can be obtained.³³ This includes graphitic materials that have a strong anisotropic structure and properties, which could be similar to those of the perfect graphite crystal.

2.1.2.2 Structure of graphite

Like diamond and fullerenes, graphite is a natural crystalline allotropic form of carbon. The main difference between graphite and diamond is that the carbon bonds in diamond consist of sp^3 hybridization, whereas in graphite they involve sp^2 hybridization. As a result, diamond has a 3-D crystal structure, whereas graphite has a layered structure in which the carbon atoms are arranged in 2-D hexagonal pattern within each layer. These layers are arranged in

the ABA or ABC alternating stacking sequence and are linked together by weak van der Waals interactions.^{11,34}

Scheme 2.1 shows a schematic representation of the graphite crystal structure.³⁵ The aggregate structures have a c-axis lattice constant of 7–16 Å and contain a number of graphene sheets of single carbon atom thickness. The carbon atoms within the same layers are strongly bound by covalent bonds to other carbons in the same plane. The distance between two carbon atoms bonded together in the same sheet is approximately 1.42 Å. The graphene layers, which are stacked parallel to each other, are 3.35 Å apart. The bond strength is much higher within the graphene layers than perpendicular to them. This feature accounts for the high degree of anisotropy in graphite, which results from the two types of contrasting chemical bonds acting in two different directions.



Scheme 2.1: Schematic representation of the crystal structure of graphite.³⁵

For instance, graphite's ability to form a solid film lubricant arises from these two different bonds acting in two different crystalline directions. The strong chemical bond between the carbon atoms in the same plane makes the material solid and very stiff. The weak van der Waals forces between the individual graphene layers allow the layers to slide over each other, making it an ideal lubricant. The latter also explains why inserting atoms and molecules between the graphene layers can be easily achieved. Thus, the interlayer spacings (also called gallery spacing) are increased and a number of graphite intercalation compounds (GICs) may be prepared.^{36,37} A common method, which is widely used for the preparation of these GICs involves subjecting the pristine graphite to sulfuric acid, sodium nitrate and potassium permanganate.³⁸

In addition to graphite, graphene is the building block of other graphitic forms, such as fullerenes (also known as buckyballs) and carbon nanotubes (CNTs) (see Figure 2.2).¹¹ Fullerenes are similar in structure to graphite, in that they are composed of stacked graphene sheets of linked hexagonal rings, but they may also contain pentagonal or sometimes heptagonal rings. CNTs, on the other hand, can be made by rolling graphene sheets to form single- or multi-walled CNTs, as can be seen in Figure 2.2.

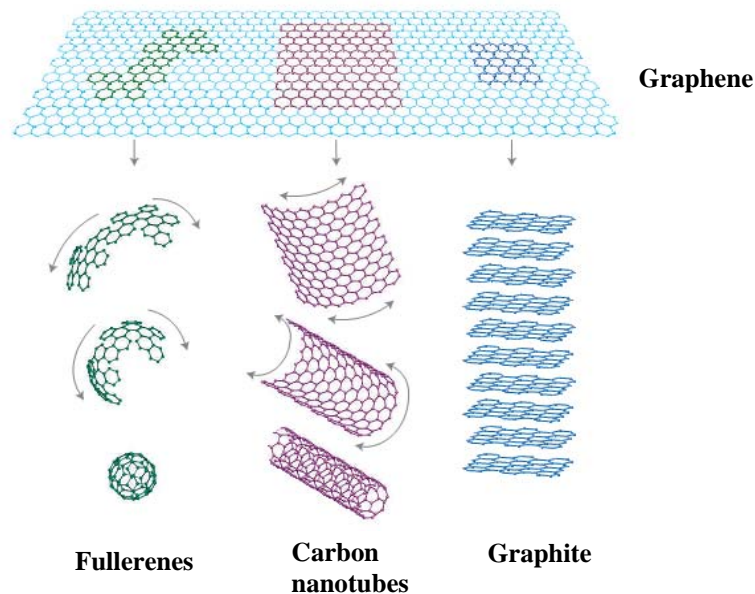


Figure 2.2: Graphene, the building block of all graphitic forms such as graphite, buckyballs and CNTs.¹¹

2.1.2.3 Properties of graphite

Graphite's unusual combination of properties is due to its distinctive crystal structure. As mentioned before, graphite presents a highly anisotropic layered structure of carbon and its properties may vary significantly when measured within the same plane or perpendicular in the c-direction plane. Graphite is also unique in that it exhibits the properties of both a metal and a non-metal material. For instance, graphite has the properties of a metal, such as thermal and electrical conductivity, and of a non-metal, such as inertness, flexibility, and high thermal resistance. It is also one of the strongest materials per unit weight (graphene has a Young's modulus of 1000 GPa)^{39,40} and has good lubricating properties. Graphite has an in-plane stiffness of about 1 TPa, which is many times higher than nanoclays and as high as that of

CNTs.⁴¹ In addition, graphite and graphite nanoplatelets are inexpensive compared to CNTs, and they have a very high aspect ratio in the exfoliated state.^{42,43}

The unique properties of graphite and its chemical inertness make it the material of choice in many applications, such as the synthesis of PGNs. These graphite-based materials find many applications in manufacturing, including electronics, atomic energy, hot metal processing, aerospace, high-temperature gaskets and coatings.⁴⁴ On reviewing the various applications of graphite in polymer nanocomposite systems, a number of very useful properties can be identified, for example:

- Excellent electrical⁴⁵ and thermal conductivity,^{46,47}
- Inertness with specific reactivity under certain conditions,
- Thermal resistance up to 3000 °C,⁴⁸
- Gas and liquid (e.g., oil) absorption.^{49,50}
- Excellent lubricating properties and compressibility,⁵¹
- Environmentally friendly.

2.1.2.4 Preparation of exfoliated graphite (ExG)

ExG, which contain graphene nanoplatelets are obtained by the exfoliation process of GICs. GIC can be obtained by inserting various atoms or molecules, called intercalants, between the layers of graphite sheets.³⁶ The exfoliation occurs when the graphene layers in GICs are forced apart by a rapid heating at very high temperatures (600–1000 °C) under N₂ atmosphere,⁵² which may cause a sudden vaporization of the residual intercalated species.⁴⁴ Furthermore, due to the high thermal shock, the remaining water molecules inserted during the washing step will vaporize, pushing the graphene layers apart. Thus a large unidirectional expansion (up to hundreds of times) of the graphene nanoplatelets in the starting GICs material along the crystallographic c-axis occurs.⁴⁴

The resultant low-density exfoliated material, referred to as ExG, formed with potentially high surface area and high aspect ratio can be utilized as nanoreinforcement platelets in polymers. After exfoliation, the layered structure of the original natural graphite is maintained,⁵³ while the volume expansion ratio, that is, the ratio of the packing volume of ExG to that of GICs, can be typically as high as 200–300.⁴⁴ Exfoliation of graphite to nanoscale platelets with high concentrations can also be achieved by dispersing GIC in

organic and aqueous media using ultrasonic devices.⁵⁴⁻⁵⁶ In comparison with other methods for the preparation of graphene nanoplatelets, this method represents a convenient route for the preparation of graphene sheets on a large scale. Bourlinos et al.⁵⁷ have recently investigated the direct exfoliation of graphite to single-layer graphene via sonication in a series of perfluorinated aromatic solvents. Solvents that were used include hexafluorobenzene, octafluorotoluene, pentafluorobenzonitrile and pentafluoropyridine. The authors demonstrated that, depending on the solvent used, graphite can be dispersed in different concentrations, to yield stable colloids containing solubilized graphenes. The solubility of graphene in such a wide range of solvents is believed to facilitate solution processing of graphene and the synthesis of several PGNs.

Other methods that are simpler than the traditional heating of GIC at high temperature have been used to produce ExG. These include electrochemical oxidation of graphite powder at ambient temperatures,⁵⁸ and microwave irradiation⁵⁹ to produce ExG. Other routes to obtain graphene nanoplatelets include reduction of GO, mechanical exfoliation of graphite and chemical vapor deposition.⁶⁰ Recently, graphite oxide (GO) was chemically reduced to single nanoplatelets of graphene after deposition on a silicon substrate.⁶¹ More recently, graphene nanoplates were isolated by mechanical exfoliation of pyrolytic graphite,⁶² a method which is suitable for small-scale applications.¹¹ Graphene nanoplatelets can also be obtained by the dispersion of graphite in selective organic solvents such as N-methyl-pyrrolidone and chloroform.^{63,64} A direct synthesis method for the preparation of large-scale graphene films by chemical vapor deposition has also been reported.^{65,66}

2.1.2.5 Oxidation of graphite flakes

Oxidation of graphite with strong acids followed by exfoliation is one approach to obtain functionalized graphene (i.e., oxidized graphene nanoplatelets) in bulk. The oxidation chemistry is similar to that used to functionalize CNTs and results in a variety of oxygen-containing functionalities (e.g., epoxy, hydroxyl and carboxyl), primarily at different sites on the graphite surface. After oxidation, the GO still possesses a layered structure,⁵³ but is much lighter in color than pristine graphite due to the loss of electronic conjugation that occurs during the oxidation step. The lamellar structure of graphite is conserved, but its polyaromatic character is lost due to the formation of different functional groups created by the chemical oxidation of the double bonds of graphite.

In recent years, the structure of GO has been widely studied in a number of theoretical⁶⁷⁻⁶⁹ and experimental^{16,70-73} investigations. Similar to graphite, which contains stacks of graphene, GO is composed of graphene oxide nanoplatelets with expanded interlayer spacing. Several authors have proposed that the epoxy and hydroxyl functional groups lie on the surface of each graphene layer, while the carboxyl groups are located near the layers' edges, as shown in Figure 2.3.^{16,74,75} The oxygen functionalities alter the chemistry of the graphene nanoplatelets in GO and render them hydrophilic in nature, thus facilitating their hydration and exfoliation in aqueous media. As a result, GO readily disperses in water and forms stable colloidal dispersions of thin GO nanosheets in water.¹⁹

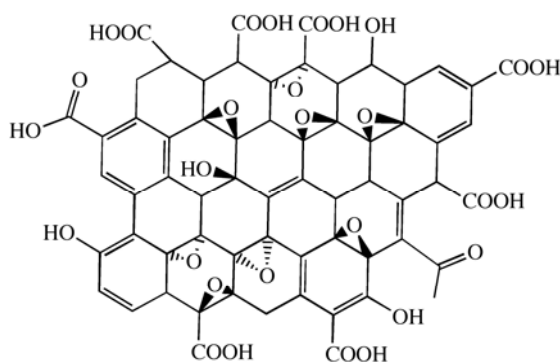


Figure 2.3: Chemical structure of GO with different oxygen-based groups on the basal plane and around the edges of a graphene layer.

The oxidation leads to a huge reduction in the size of graphite nanosheets in GO, compared to the size of the natural graphite flakes.⁷⁶ Furthermore, the oxidation results in an increase in the interlayer spacing of graphite nanosheets in GO relative to natural graphite, which can be attributed to the intercalation of oxygen-based groups between its layers. Hence, the interlayer distance of graphite can be increased from 3.35 Å of the original graphite to 6–10 Å, depending on the interlamellar water content and the extent of the intercalation process.¹² The interlayer spacing also depends strongly on the humidity conditions of the GO sample. As the humidity level increases, an increase in the interlayer spacing can be observed. In a recent study, Buchsteiner et al.⁷⁷ investigated the hydration behavior of GO at different humidity levels. They found that the interlayer distance of GO increases with increasing the water content in the sample, giving rise to different spacings between graphene layers in the range 0.6–1.2 nm.

2.1.3 Preparation of PGNs

2.1.3.1 Introduction

PGNs are a new class of multi-phase composite materials obtained by the dispersion of graphite sheets in a polymer matrix at the nanometer level. They are generally obtained by using an intercalating agent, followed by insertion of a polymer into the galleries of graphite-based material to achieve an intercalated or exfoliated nanocomposite structure. These nanocomposites have a wide range of functional properties that are improved compared to pure polymers. The fundamental properties of graphite can be tailored in these nanocomposites for various applications.²⁸ These include mechanical, thermal and barrier performance, as well as flame retardant properties.^{60,78}

Graphite has a layered nanostructure similar to that of clay nanoparticles, hence the preparation methods used for polymer nanocomposites made with graphite are similar to those used for PCNs. Therefore, many methods, such as exfoliation-adsorption, melt intercalation, and *in situ* intercalation polymerization, which are widely used for the preparation of PCNs, can be used to produce PGNs. However, natural graphite is chemically different from clay; the relatively simple exchange reactions used to modify clay can not be used with graphite. Furthermore, due to the non-dispersibility of graphite in aqueous or organic media, it is very difficult for a monomer or polymer to be loaded onto its surface. In addition, graphite is generally insoluble in common solvents, therefore, modified graphite (e.g., GO) are used for the preparation of PGNs.^{60,78}

In contrast to graphite, GO is very hydrophilic and soluble in aqueous and organic media.^{79,80} In addition, the presence of hydrophilic polar groups (e.g., –OH and –COOH) will facilitate physical and chemical interaction between the graphite and other organic molecules, such as monomers and polymers, which can be then loaded onto its surface. Owing to the presence of such polar groups in GO, the material is quite reminiscent of clay; they share common swelling and intercalation properties. The nanometer-scale sheets and galleries in the GO as well as the polar groups generated by chemical oxidation create favorable conditions allowing for suitable polymers to intercalate and form PGNs.

2.1.3.2 Methods used for the synthesis of PGNs

Several strategies have been proposed to produce PGNs. The following are the three main techniques:⁸¹

i) Exfoliation-adsorption (also called solution intercalation): In this method, the graphite flakes are dispersed and exfoliated into graphene nanoplatelets in an adequate solvent in which the polymer can be dissolved. The exfoliation of graphite into very small graphene nanoplatelets can be achieved using high shear devices such as sonicators. This will also help the polymer chains to intercalate and adsorb into the graphene layers. When the polymer is completely dispersed, the solvent can be removed by evaporation to form PGNs with intercalated or exfoliated structure. This method depends greatly on the choice of solvent—where both aqueous and organic solvents can be used. The solvent facilitates the exfoliation of the graphite nanosheets as well as the intercalation of the polymer into the interlayer spacing of the graphite. Using this method, water-soluble and organic solvent-soluble polymers have been used to produce PGNs such as poly(methyl methacrylate)/graphite,^{82,83} poly(vinyl alcohol)/graphite,⁸⁴ and maleic anhydride grafted polypropylene/graphite.⁸⁵

ii) Melt intercalation or exfoliation (also called melt compounding): This method is solvent-free and mainly used with polyolefins such as polyethylene (PE).^{86,87} The expanded or exfoliated graphite is mixed with the polymer in the molten state above the melting temperature. The polymer chains can then diffuse into the interlayer space of graphite to form PGNs. Mixing graphite with the polymer in the molten state can be achieved using a batch mixer, an extruder, or injection molding.^{87,88}

iii) *In situ* intercalation or exfoliation polymerization: In this process, the monomer is polymerized in the presence of graphite nanosheets.⁸⁹ Prior to the polymerization, the monomer or monomer solution is used to swell the graphite nanosheets. The initiator is then added, which can diffuse into the interlayer spaces of graphite. The polymerization is initiated either by heating or radiation, thus polymer chains can be formed in-between the intercalated graphite sheets. The advantage of this method is that partially or fully-exfoliated PGNs can be obtained. This results in better dispersion, prevention of agglomeration and stronger interaction between the reinforcing graphite nanosheets and the polymer chains. Thus, PGNs made by *in situ* methods have better mechanical properties compared to nanocomposites made by other methods such as melt intercalation and exfoliation-adsorption processes.⁸¹

To promote the intercalation of water insoluble polymers within layered graphite, emulsion polymerization has been used for the *in situ* polymerization. Since the GO has larger c-axis spacing compared to the pristine graphite and polar groups on its surface such as hydroxyl, ether and carboxylate groups, intercalation of polymers into GO in emulsion systems becomes possible. For example, Wang and Pan⁹⁰ reported that the intercalation of methyl methacrylate (MMA), followed by *in situ* polymerization, occurred during the emulsion polymerization of MMA in the presence of GO. Although, they found that a small amount of MMA was grafted on the surface of GO during the emulsion polymerization, spherical particles of GO were homogeneously distributed within the composites in the nanoscale range.

PGNs can also be obtained by other less-used methods, for example:

- i) Direct mixing: This method is often used in the case of low viscosity polymers, where the graphite-based material is directly mixed with the polymer to obtain PGNs.⁹¹
- ii) Electrospinning of nanoscale fibers using polymer/graphite solution or melts: This can be achieved by applying an electric field between the solution and a collection plate that is oppositely charged, thus nanocomposites in the form of nanofibers can be obtained.⁹²

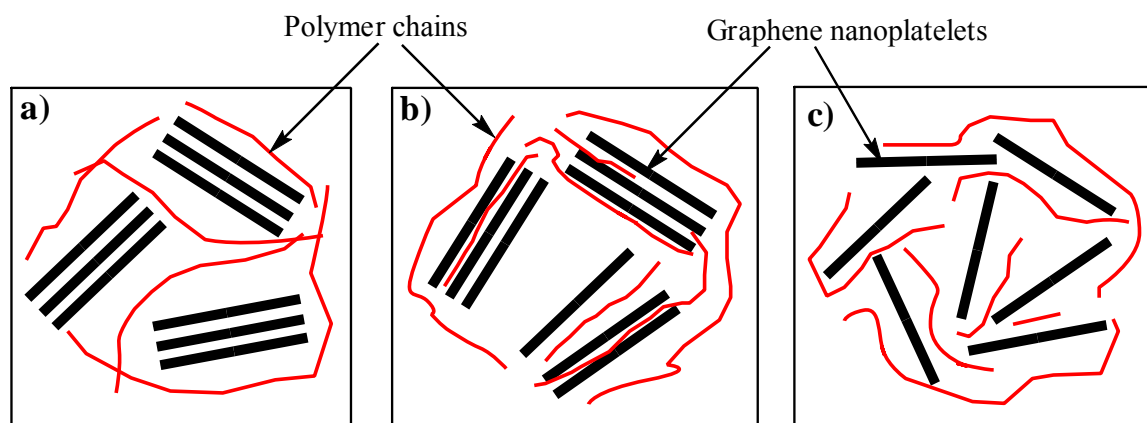
2.1.4 Degree of dispersion of graphite in PGNs and their final structure

The structure of PGNs is mainly determined by the degree of graphite dispersion in the polymer matrix. Polymer composites based on graphite are generally classified into three groups: conventional polymer/graphite composites, intercalated PGNs and exfoliated PGNs.⁸¹

Conventional polymer/graphite composites: This type of composite is obtained when the polymer chains are unable to penetrate into the graphite galleries (see Scheme 2.2 a). The graphene nanoplatelets are still close to each other in an unintercalated manner. Thus a phase-separated material is obtained, where the graphene nanoplatelets exist as agglomerates within the polymer matrix. This type of composite fails to enhance the properties of the polymer in use, which remain in the same range as in the traditional macrocomposites.

Intercalated PGNs: In this type, only a few polymer chains are intercalated between the graphene layers, in a relatively ordered morphology. As seen in Scheme 2.2 b, the graphite sheets are not completely dispersed in the polymer phase, resulting in a slight improvement in polymer properties. Compared to the conventional composites, the structure obtained in intercalated nanocomposites (Scheme 2.2 b) may be considered as a true nanocomposite.

Exfoliated PGNs: In this case, the fine graphene particles are uniformly and completely dispersed in a continuous polymer phase, resulting in randomly separated graphene nanoplatelets (see Scheme 2.2 c). The distance between the graphene layers, which are no longer close to each other, greatly depends on the graphite concentration in the nanocomposite. The large surface area and high aspect ratio of the nanoscale graphite sheets could enhance polymer properties significantly. Thus, these nanocomposites exhibit better properties than their conventional and intercalated counterparts with the same number of graphene particles.



Scheme 2.2: Structure of different types of polymer/graphite composite/nanocomposites: a) conventional, b) intercalated and c) exfoliated nanostructure.

2.1.5 Characterization of PGNs

Generally speaking, the structure of PGNs can be determined using X-ray diffraction (XRD) analysis and transmission electron microscopy (TEM). The graphite structure (either intercalated or exfoliated) may be identified by using XRD to monitor the position of the basal reflections from the graphene layers. TEM allows a qualitative understanding of the internal structure through direct visualization at the nanometer level. However, special care must be applied when TEM is used to guarantee a representative part of the sample. Other analytical techniques such as dynamic mechanical analysis (DMA), thermogravimetric analysis (TGA) and SEM have been used to characterize the PGNs. DMA gives the

mechanical response for a material while TGA shows the chemical degradation behavior as a function of temperature. SEM gives the surface morphology of a material, such as polymer films, by scanning its surface. These analytical techniques are discussed in detail in the following sections:

2.1.5.1 XRD analysis

XRD gives the interlayer distance of an ordered crystalline material, commonly referred to as the d-spacing. PGNs have a recurring nanoscale multilayered structure, allowing the use of XRD to determine the interlayer spacing of graphite in the nanocomposite. The graphene nanoplates in the nanocomposite are ordered in a crystalline form, thus they give rise to Bragg diffraction peaks, from which the interlayer distance can be obtained according to Bragg's law⁹³ (see Equation 2.1).

$$2d \sin \theta = n \lambda \quad (2.1)$$

where d is the distance between two diffractive lattice planes (d-spacing), θ is the measured diffraction angle, n is the order of interference and λ is the wavelength of X-ray radiation used in the diffraction experiment.

The intercalation of guest molecules such as polymers into the graphite layers results in an increase in its d-spacing compared to the original spacing of the layered graphite. When polymer chains are inserted into the graphite galleries, the adjacent platelets move away from each other along the c-axis, leading to a shift of the diffraction peak towards lower angles. According to Equation 2.1, an increase in the d-spacing results in a decrease in the angle 2θ . Hence, the presence of a Bragg peak at a greater distance (lower value of 2θ) implies that an intercalated nanocomposite structure is formed. On the other hand, the formation of an exfoliated structure leads to the complete loss in order of the graphene nanoplatelets, thus a complete disappearance of the Bragg peak occurs.

Figure 2.4 shows typical XRD patterns of pristine GO and poly(styrene-co-butyl acrylate)/GO (poly(St-co-BA)/GO) nanocomposites with different GO contents. The characteristic peak corresponding to the GO appears at around $2\theta = 11.3^\circ$, as shown in Figure 2.4 a. Only one broad diffraction peak appears at around $2\theta = 20^\circ$, relating to the diffraction peak of the poly(St-co-BA) copolymer in the nanocomposite (see Figure 2.4 b and c). The absence of the

characteristic peak of GO in the nanocomposite indicates that the graphene nanoplatelets in GO have been exfoliated.

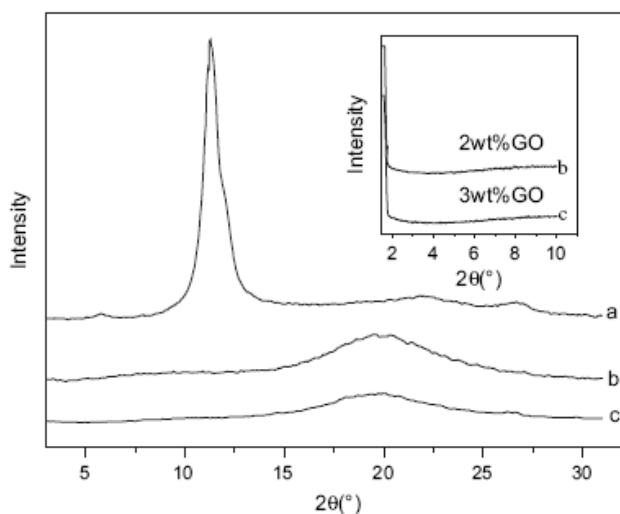


Figure 2.4: XRD patterns of: a) pristine GO; b) poly(St-co-BA)/GO nanocomposite with 2 wt% GO; and c) poly(St-co-BA)/GO nanocomposite with 3 wt% GO.⁹⁴

2.1.5.2 TEM analysis

TEM is a technique that can be visually used to see the morphology of the PGNs at the nanometer level. Most often TEM is used in combination with XRD analysis to determine the final structure and degree of graphite exfoliation in the nanocomposite. Figure 2.5 shows an example of a TEM image of a microtomed film of intercalated and exfoliated PGNs.

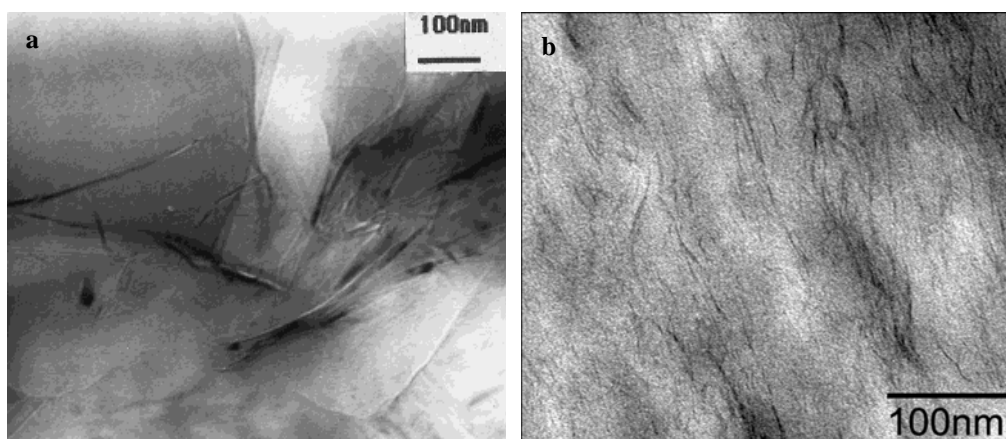


Figure 2.5: Examples of TEM images of a microtomed sample: a) intercalated poly(S-MMA)/graphite nanocomposite⁸ and b) exfoliated polyarylenesulfide/graphite nanocomposite.⁹⁵

Chapter 2: Historical and Theoretical Background

Contrast between the graphite nanosheets and the polymer domains is the result of the different path lengths and material densities of the constituting materials. This results in increased scattering of the incident electron beam from the graphite material, resulting in a darker region on the TEM images. As can be seen in Figure 2.5 a, the graphene nanoplatelets are still stacked in an ordered manner, indicating an intercalated structure. On the other hand, Figure 2.5 b shows that the graphene nanoplatelets are separated from each other, which results in an exfoliated morphology.

2.1.5.3 SEM analysis

In SEM analysis, a very fine electron incident beam is scanned across the sample surface. The scattered electrons are used to produce a signal, which is transformed to an image with great depth of field. SEM is not used as frequently as XRD and TEM for the characterization of PGNs; it is utilized as a complementary technique. When using SEM to determine the degree of exfoliation of the graphite in the final polymer nanocomposites great care must be exercised to identify the dispersed filler within the polymer matrix.⁷⁸ Stankovich et al.²⁸ used cross-sectional analysis by SEM to determine the dispersion of GO in a polymer matrix, which only showed stacks of graphene platelets within the polymer phase. In most cases the image will be related to the polymer region and the graphene platelets will not be seen in the final image. This is due to the graphene platelets being completely covered by the polymer matrix, which will be scanned by the SEM. However, SEM can give qualitative insight into the 3-D structure of graphite before adding to polymer. Figure 2.6 shows SEM image of graphite, showing graphene platelets in the micrometer size range with thicknesses in the nanometer range.

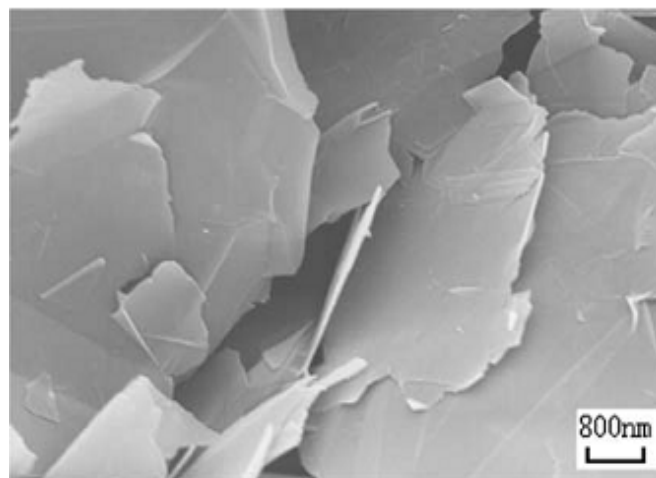


Figure 2.6: SEM image of graphite nanosheets.⁹⁶

2.1.5.4 Mechanical properties by DMA

Generally, the addition of graphite to polymers results in an enhancement of the mechanical properties of those polymers (discussed in Section 2.1.6.1). In DMA an oscillating force is applied to a sample while the material's response is recorded. It is an analytical technique that can be widely applied for the characterization of polymers and polymer nanocomposites. DMA measures the changes in mechanical behavior of a polymer sample as a function of temperature, time, frequency, stress and strain. Most commonly, the response of a polymer such as tendency to flow and the stiffness to cyclic deformation as a function of temperature is determined. There are three main parameters that are used to express DMA results:

- (i) The storage modulus (G'): This is a measure of the elastic response of the polymer to the deformation as a function of temperature or frequency.
- (ii) The loss modulus (G''): This can be used to measure the plastic response of the polymer as a function of temperature or frequency.
- (iii) $\tan \delta$: This parameter is used to measure the molecular mobility of polymers as a function of temperature. It is obtained from the ratio between the loss modulus and the storage modulus, where $\tan \delta = G''/G'$.

2.1.5.5 Thermal analysis by TGA

TGA measures the weight loss of a material due to the degradation of its organic volatile species as a function of temperature. Hence, TGA has been widely used to study the thermal stability of polymeric materials as a function of temperature. The analysis is usually carried out under an inert atmosphere (e.g., nitrogen), where the degradation of volatile functional groups takes place in the absence of oxygen. However, TGA can also be carried out in the presence of oxygen, where the oxidative degradation takes place as a function of temperature. Generally, the incorporation of graphite in the polymer matrix enhances its thermal stability by acting as a heat insulator and mass transport barrier to the volatile products generated during decomposition (discussed in Section 2.1.6.2).

2.1.6 Properties and applications of PGNs

In many circumstances, polymers fail to exhibit certain properties to satisfy the required conditions of the intended application. To enhance the functional performance of polymers,

one could consider the recent technology in reinforcement at the nanoscale. One such technology is the preparation of PGNs. These graphite-based polymer nanocomposites can offer many advanced and improved properties, such as excellent mechanical, electrical, barrier and thermal properties compared to pure polymers and at reasonable cost. The presence of graphite nanosheets in these nanocomposites may lead to a significant improvement in the properties of polymers, even with the addition of only a small weight fraction of the graphite nanofiller relative to polymers. These PGNs can be widely used in advanced technologies such as flame retardant materials, barrier coatings, and structural components for electronic devices. The properties and applications of PGNs are discussed in more details in the following sections.

2.1.6.1 Mechanical properties

The enhancement in mechanical properties of PGNs is caused by the strong interaction between polymer chains and graphene nanoplatelets, which have a high aspect ratio. This will lead to a significant increase in the mechanical properties of polymers in the presence of graphene, compared to pure polymers. The graphene nanoplatelets can be obtained through a process of oxidation and exfoliation. This enables polar and non-polar polymers to form intercalated or exfoliated nanocomposite systems, due to the larger c-axis spacing and the presence of various functional groups such as hydroxyl, carboxyl and epoxy, on the GO surface.^{16,17} The interaction between polymer and graphene layers could suppress the mobility of the polymer segments near the polymer-graphene interface, leading to improved mechanical properties of polymers.^{41,97}

2.1.6.2 Thermal stability and flame retardant properties

Graphite has been used with different polymers such as poly(acrylic ester), polyurethane (PU), poly(vinyl acetate) and poly(vinylidene dichloride) for the synthesis of nanocomposites with improved thermal properties.⁹⁸ The improvement in thermal stability of polymers in the presence of graphene can be attributed to the intercalation of polymer chains into the lamellae of graphite. The graphite nanosheets act as an insulator between the heat source and the surface area of the polymer where the combustion occurs.²⁴ This results in better thermal stability of polymers and hence they can be used, for instance, as flame retardant materials.^{13,14} The presence of graphene could also hinder the diffusion of volatile decomposition products within the nanocomposites by promoting char formation. The char

layer may act as a mass transport barrier slowing the escape of the volatile products generated as the polymer decomposes, resulting in better thermal stability.⁹⁴ It has been reported that the flame retardancy properties of PGNs are similar to those of PCNs, as examined by combustion calorimetry.²⁴

In a recent study, Thirumal et al.⁹⁹ investigated the effect of EG on the flame retardant properties of PU foam. They found that the flame retardant properties of the PU increased with increasing graphite loading and particle size. They attributed this to the presence of graphite particles, which resulted in more char residue, and thus better flame retardant properties were observed. This char formation protected the polymer surface by acting as a physical barrier, preventing more heat transfer. The char also prohibited the diffusion of air towards the polymer source, thus the fire can not spread further because of a lack of oxygen.

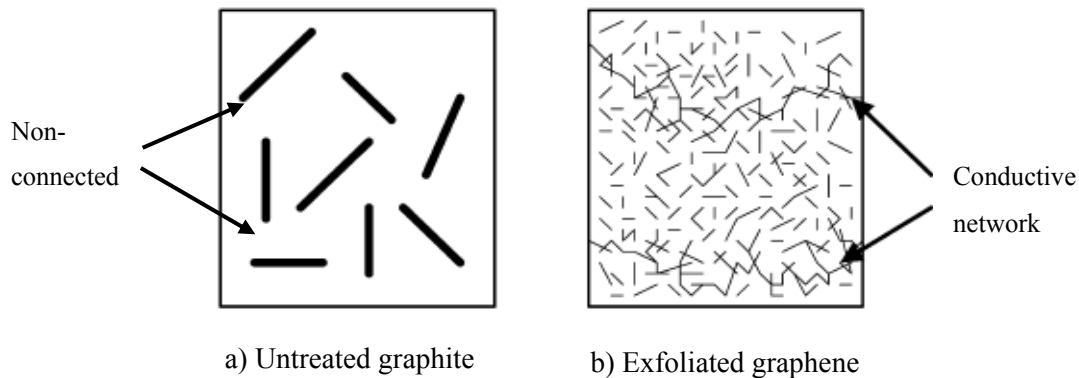
2.1.6.3 Electrical properties

Graphite possesses unique electrical properties, which makes it an attractive material for potential applications in electronic devices.¹⁰⁰⁻¹⁰² It has an electrical conductivity that is high along the graphene layers. Therefore, graphite can be used to enhance the electrical properties of insulating polymer materials. In recent years, graphene has been used for the synthesis of different conductive polymers, such as acrylic,^{90,103} polyester,²⁶ PU^{27,104} and natural rubbers.¹⁰⁵ These PGNs find many potential applications in advanced technologies, such as antistatic coatings,¹⁰⁶ electromagnetic shielding¹⁰⁷ and in secondary batteries.¹⁰⁸

The enhancement in electrical properties of the final nanocomposite, comprising conducting graphite particles, randomly distributed in an insulating polymer can be explained by the percolation theory. This theory is based on the so-called percolation threshold and involves the transition from a non-connected to a connected state. When the pristine graphite filler is dispersed in the polymer matrix the probability for graphite sheets to be in contact is small. However, when the graphite is well exfoliated into nanoscale layers the number and the aspect ratio of the graphene nanoplatelets are greatly increased. Thus, the probability of forming a conducting network is also greatly enhanced, which leads to a lower percolation threshold.

The resultant PGNs show electrical conductive behavior as a function of the filler content. At a critical value, a slight increase of the filler content leads to a sharp transition in the conductivity of the nanocomposite. Scheme 2.3 shows a schematic illustration of the effect of

the filler morphology on the electrical conductivity of PGNs. The solid lines represent the graphite sheets (Figure 2.3 a) and the dashed lines correspond to exfoliated graphene nanoplatelets in the nanocomposite.



Scheme 2.3: Schematic illustration of the effect of different graphite morphology on the conductive network formation in PGNs.¹⁰⁹

2.1.6.4 Barrier properties

Another important feature of graphite-based nanocomposites is their use as barrier coating materials. The nanolayers of graphite act as impermeable obstacles¹¹⁰ that provide longer diffusion paths across the polymer, resulting in improved barrier properties. This is due to the high number and aspect ratio of the graphene nanosheets provided as a result of exfoliation. Compared to the conventional fillers (Figure 2.7 a), the exfoliated graphene nanoplatelets provide a more torturous path through the polymer matrix (see Figure 2.7 b). Therefore, the presence of graphene decreases the permeability of low molecular weight molecules such as oxygen, nitrogen and water across a polymer matrix. This results in enhanced barrier performance for low molecular weight molecules such as gases through polymer nanocomposites.²⁶

In recent years, authors showed that graphite is the material of choice for applications of polymer nanocomposites with very low gas permeability. Kim et al.²⁷ studied the barrier properties of PU reinforced with GO and found that N₂ permeation of PU was significantly reduced. Using nanocomposite containing 3 wt% GO relative to polymer showed 90% decrease in N₂ permeability.

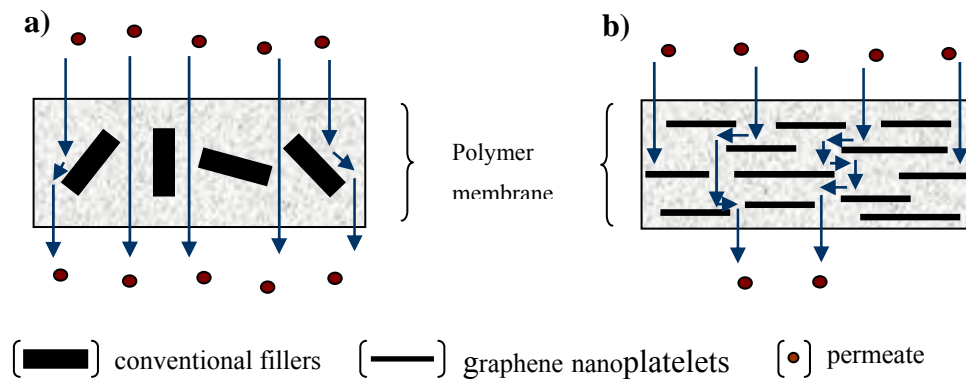


Figure 2.7: Permeation in polymer composites: a) conventional composites and b) formation of tortuous path in PGNs.

2.2 Miniemulsion polymerization

2.2.1 Introduction

Miniemulsion polymerization is a convenient one-step technique for the incorporation of solid supports and the polymerization of monomers with low water solubility.^{111,112} It offers several advantages over other dispersion polymerization techniques, such as small particle size of the final latex particles, efficient use of surfactant, production of latices with high solids content, and production of particles that are a 1:1 copy of the miniemulsion droplets.^{113,114} The latter can be attributed to the fact that the miniemulsion droplets are directly polymerized, thus the resulting polymer particles are often one-to-one copies of the monomer droplets.¹¹³

Miniemulsions contain submicron-size monomer droplets, ranging from 50 to 500 nm.¹¹⁵ The droplets are formed by shearing a pre-mixed system comprising water, monomer, surfactant and a hydrophobe (also referred to as a costabilizer). The surfactant prevents the droplets from coalescence, and the hydrophobe prevents Ostwald ripening. Coalescence occurs upon the collision of droplets while Ostwald ripening is caused by degradation of the droplets via diffusion. In a system susceptible to Ostwald ripening, larger monomer droplets will grow in size at the expense of the smaller ones due to the difference in the chemical potential between droplets of different radii.¹¹⁶ The low molecular weight molecules of the hydrophobe can diffuse only very slowly from one droplet to the other due to their highly hydrophobic nature, therefore they are trapped in the droplets. This will lead to the creation of an osmotic pressure in every droplet, which will suppress monomer diffusion from smaller to bigger droplets.

A well designed miniemulsion formulation would therefore greatly rely on a suitable choice of surfactant(s) and hydrophobe. The amount of surfactant used allows control over particle size of the final latex particles.¹¹⁷ An increase in the surfactant concentration will lead to a decrease in the particle size. In addition to a variation in surfactant concentration, the size of the droplets can be controlled through changes in the shear rate and time.¹¹⁸ Different surfactant/hydrophobe systems can be used for miniemulsion formulations. The most common model systems employ sodium dodecyl sulfate (SDS) in combination with cetyl alcohol (CA) or hexadecane (HD).

A characteristic feature of miniemulsion polymerization is that droplet nucleation is the predominant mechanism of particle formation.¹¹⁹ The nanometer-size monomer droplets formed by the application of high shear to the system have a sufficiently large surface area to effectively compete with the micelles or particles for radical capture.¹²⁰ The large droplet surface area is stabilized with the adsorption of an additional amount of surfactant from the water phase, which leads to a decrease in surfactant concentration in the water phase. Thus, there are usually no micelles present in a well prepared miniemulsion.

The first report on miniemulsion polymerization dates back to 1973, when Ugelstad et al.¹¹⁹ reported the polymerization of styrene (St) in the presence of a mixed emulsifier system of SDS and CA. For comparison, PS emulsion made with SDS alone was also prepared. Results showed that the prepared emulsion was unstable and phase separated within a few minutes when the stirring was stopped. On the other hand, when CA was used in addition to SDS, the stability of the PS emulsions was very good and the average droplet size was small. At that time the term miniemulsion had not been used, however, the polymerization features fit the general definition of miniemulsion polymerization—monomer droplets smaller than 1 μm were obtained by simple mixing of the monomer into an aqueous solution of a surfactant and a cosurfactant. The reduction in their average size makes the monomer droplets more competitive in capturing radicals generated in the aqueous phase, which provides the basis of miniemulsion polymerization, i.e., monomer droplet nucleation.

2.2.2 Miniemulsion vs. emulsion polymerization

Several authors have studied the differences between conventional emulsion and miniemulsion polymerization.^{121,122} The difference in size of the monomer droplets in emulsion and miniemulsion polymerization is the key factor to distinguish between the two

systems. The size of the dispersed droplets in miniemulsion is quite small (50–500 nm) relative to the size of monomer droplets in an emulsion system (1–100 μm).¹¹⁵ This significant difference in the droplet size is liable for the different mechanisms of particle nucleation operating in the two systems.

Emulsion polymerization normally consists of water-insoluble monomer(s), a dispersing medium (usually water), a suitable surfactant and a water-soluble initiator. The surfactant plays an important role in the stability, rheology, and control of particle size of the resulting latices. When the concentration of the surfactant is above its critical micelle concentration (cmc), the unabsorbed surfactant molecules remain in the aqueous phase and form micelles. The polymerization process commences with radicals, generated by the thermal decomposition (or otherwise) of the initiator, reacting with the monomer in the aqueous phase to form oligomeric radical chains.

In an emulsion system, there are three possible nucleation mechanisms for the growing oligomeric radical species: micellar, homogeneous (water phase), and (less often) droplet nucleation.¹²³ In homogenous nucleation, oligomers growing in the aqueous phase, begin to precipitate from solution as they reach a degree of polymerization that exceeds their solubility limit (critical length). The oligomeric radicals will then form precursor particles, which are stabilized by adsorbing surfactant molecules. These primary particles can then absorb monomer for further propagation, to form polymer particles. Droplet nucleation occurs when radicals formed in the aqueous phase enter monomer droplets and propagate to form polymer particles.

Micellar nucleation, on the other hand, occurs when sufficient surfactant is present in the system to exceed the cmc. As a result of Ostwald ripening in the emulsion system, monomer molecules tend to diffuse from smaller monomer droplets to larger ones to minimize the total interfacial energy of the system. The droplets are consequently large and the total interfacial area is unable to accommodate all of the surfactant molecules. The desorbed surfactant molecules remain in the aqueous phase and form micelles if the concentration of the surfactant is above the cmc. The hydrophobic tail of the aggregates will then be swollen by monomer, forming monomer-swollen micelles. Initiator radicals (or oligomeric radicals) generated in the aqueous phase can then enter the monomer-swollen micelles to form monomer-swollen polymeric particles. These swollen polymeric particles will grow further by propagation reactions until monomer and surfactant are depleted from unentered micelles.

All three of the above-mentioned mechanisms can occur in classical emulsion polymerization. However, due to the large size (small surface area) of the monomer droplets, they cannot effectively compete with micellar and homogeneous nucleation. Droplets merely act as reservoirs for monomer that diffuses through the water phase to the growing latex particles. Therefore, droplet nucleation is insignificant for most emulsion polymerizations. On the other hand, in miniemulsion polymerization, droplet nucleation is the predominant mechanism of particle formation due to the small size of monomer droplets and the presence of little or no micelles in the system.¹²⁴ These submicron droplets have a large interfacial area and are capable of capturing most of the oligomeric free radicals; thus the droplets become the locus of nucleation.

2.2.3 Miniemulsion formulations

A typical miniemulsion formulation includes water, a monomer (or monomer mixture), a surfactant, a hydrophobe and a suitable initiator system. Different monomers, with a wide range of water solubilities, including vinyl acetate (VAc),¹²⁵ MMA,^{126,127} n-butyl acrylate (BA)¹²⁸ and St,^{129,130} have been polymerized by means of miniemulsion polymerization. In other cases, formulations that contain more than one monomer have also been prepared, including miniemulsions in which small quantities of very water-soluble monomers, such as acrylic acid¹³¹ and methacrylic acid,¹³² have been used.

A very important factor for the formulation of a stable miniemulsion is the choice of an appropriate water-insoluble compound, or so-called hydrophobe. In most of the early work, authors investigated the miniemulsion polymerization of St stabilized with CA as a hydrophobe.¹¹⁴ It was found that although the nucleation period was rather long, most of the particles were nucleated at low conversion. As proposed by Landfester et al.,¹³³ the most efficient hydrophobes are very water-insoluble, surface-inactive reagents. The authors found that the predominant requirement for the hydrophobe is an extremely low water solubility (less than 10^{-7} mL mL⁻¹), independent of its chemical nature. It was also found that regardless of the amount and type of the hydrophobe, stable miniemulsions with similar structural characteristics were obtained.

The water-insoluble compound is usually a fatty alcohol or a long-chain alkane. The addition of the hydrophobe, such as a long-chain alkane (e.g., HD)^{134,135} or a long chain alcohol (e.g., CA),^{119,130} can efficiently retard the destabilization of the nanodroplets by Ostwald ripening

(discussed in Section 2.2.7). It should be noted that both linear and branched molecules can be used provided that they have very low water solubility. Other costabilizers that have been used include dodecyl mercaptan¹²⁷ or reactive alkyl methacrylates (e.g., dodecyl methacrylate).¹³⁶

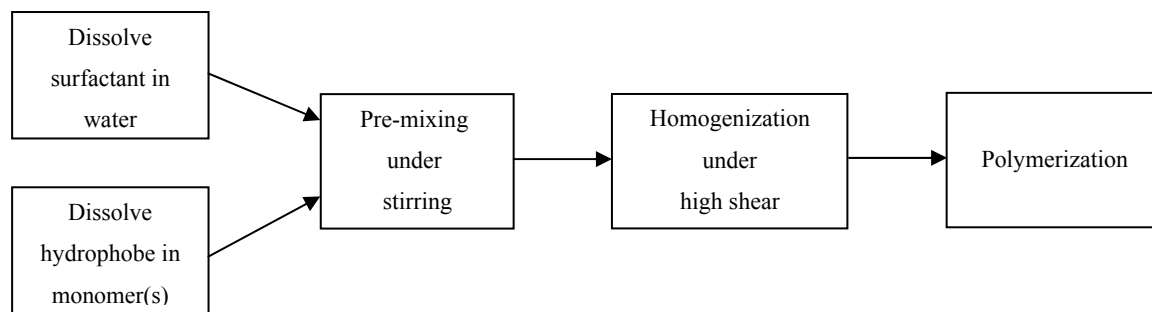
Another important formulation variable in miniemulsion polymerization is the use of an emulsifier or surfactant system to prevent the degradation of particles by collision (discussed in Section 2.2.7). For miniemulsion formulations, many different surfactants, including anionic,¹³⁰ cationic,¹³⁷ non-ionic,¹³⁸ non-reactive surfactants and reactive surfactants,¹³⁹ can be used. The surfactant provides stability against physical degradation (i.e., coalescence). This is due to the trend toward a minimal interfacial area between the dispersed phase and the dispersion medium. The surfactants used in miniemulsion polymerization should meet the same requirements as in conventional emulsion polymerization.¹⁴⁰ These requirements are the following: (i) their structure must have polar and non-polar groups, (ii) they must be more soluble in the aqueous phase than the oil phase so as to be readily available for adsorption on the oil droplet surface, (iii) they must adsorb strongly and not be easily displaced when two droplets collide, (iv) they must be effective at low concentrations, and (v) they should be relatively inexpensive, non-toxic and safe to handle.

2.2.4 Preparation of miniemulsions

In principle, miniemulsion preparation can be carried out by dissolving a suitable surfactant system in water and dissolving the hydrophobe in monomer (or monomer mixture), followed by premixing under stirring (see Scheme 2.4). The mixture is then subjected to a highly efficient homogenization process called miniemulsification. This can be achieved by using a high shear dispersion device to disperse the premixed solution into small droplets. Various homogenization techniques can be used for the preparation of stable miniemulsions. Stirring, used in the earlier work on miniemulsions,¹¹⁹ has now been replaced with high shear mechanical agitation and ultrasonication. The energy transferred by simple stirring is not sufficient to prepare small, well distributed particles.¹⁴¹ Therefore a much higher energy device such as a sonifier is required to create smaller droplets.

According to Asua,¹⁴⁰ the following devices are the most commonly used to achieve homogenization: rotor-stator devices, sonifiers and high-pressure homogenizers. Today miniemulsification by ultrasound, first reported in 1927,¹⁴² is most frequently used, especially

for small latex quantities. Rotor-stator devices, which rely on turbulence to produce the miniemulsion, are used to prepare large quantities of latex. High-pressure homogenizers such as a microfluidizer are also used to prepare such stable miniemulsions, and are upscalable.



Scheme 2.4: Schematic representation of miniemulsion preparation.

2.2.5 Initiators used in miniemulsions

In miniemulsions, polymerization can be initiated by using either a water-soluble or oil-soluble initiator. In the case of a water-soluble initiator polymerization commences in the aqueous phase; the initiator generates free radicals, by thermal decomposition, in the aqueous phase. This is similar to the case in conventional emulsion polymerization, where mainly water-soluble initiators are used. Polymerization involves the formation of oligomeric radicals, which will enter the monomer droplets when they reach a certain critical chain length. In this case, the initiator is added after the miniemulsification process takes place. Bechthold and Landfester¹⁴³ studied the miniemulsion polymerization of St using the water-soluble initiator, potassium persulfate (KPS). They found that the reaction rate was slightly increased by increasing the initiator concentration. However, increasing the initiator concentration caused a significant reduction of the average degree of polymerization.

On the other hand, an oil-soluble initiator can be mixed with the oil phase (monomer and hydrophobe) before premixing with the surfactant/water solution. Because of the small size of monomer droplets, radical recombination is then often a problem. Oil-soluble initiators are preferred when water-soluble monomers such as MMA and vinyl chloride are used. This is because nucleation can take place in the water phase (also referred to as secondary or homogeneous nucleation).¹⁴⁴ Oil-soluble initiators are also preferred when monomers with extremely low water solubility, such as lauryl methacrylate, need to be polymerized. Here the monomer concentration in the water phase is not high enough to frequently create oligomeric radicals which can enter the droplets.

The possibility of nucleation in the water phase can also be minimized by using a redox initiation system, which contains two components (e.g., $(\text{NH}_4)_2\text{S}_2\text{O}_8/\text{NaHSO}_3$). In this case one component is in the aqueous phase and the other is in the oil phase.¹⁴⁵ Hence, the initiation is restricted to the interfacial layer of monomer droplets with the water phase.

2.2.6 Properties of miniemulsions

The advantage of the miniemulsion polymerization technique is that it extends the possibilities of the widely applied emulsion polymerization technique. Polymerizations in miniemulsions, when carefully prepared, result in latex particles that have about the same size as the initial droplets. The particle size is established by controlling the energy produced by the shear source and the time under shear. Furthermore, particle size can be controlled by changing the surfactant type and concentration.¹⁴⁶

Another important feature of miniemulsion polymerization is the ability to produce high solids content latices with low viscosity. Latices with high solids content offer numerous advantages for most industrial applications, for example, lower shipping costs and less water to be removed from the latex. Ouzineb et al.¹⁴⁷ have investigated the use of miniemulsions to make high solids content, low viscosity latices using St and BA. Products with solids content > 70 wt% and viscosities as low as 350 mPa s at a shear rate of 20 s⁻¹ were obtained. Moreover, polydisperse latices show low viscosity because small particles fit within the voids of the array of the large particles. Polydisperse particles are often produced by miniemulsion polymerization.¹⁴⁸ Other advantages that miniemulsion polymerization offers over other polymerization techniques include the following:

- Copolymerization of monomers with different water solubilities is possible,¹⁴⁹
- Polymerization of very hydrophobic monomers, which often can be polymerized in emulsion polymerization with difficulty is possible,¹⁴⁹
- Polymer latices with better colloidal stability can be prepared,^{117,150}
- High solids content latices, with no coagulation, can be obtained.¹⁵¹

2.2.7 Miniemulsion stability

Miniemulsions are generally thermodynamically unstable and separate into two phases over a period of time.¹⁵² This is mainly because they include particles with very large interfaces. The

stability of miniemulsion droplets is affected by two distinct mechanisms, both of which are considered as major instability processes of an emulsion system. These are droplet coalescence and molecular diffusion degradation (Ostwald ripening). Therefore, to create a stable miniemulsion system, droplets must be stabilized against both Ostwald ripening and coalescence by collisions. Stabilization against Ostwald ripening can be achieved by the addition of a small amount of a third component which must be located in the dispersed phase. Coalescence can be prevented by the addition of appropriate surfactants, which provide electrostatic, steric or electrosteric stabilization to the droplets. The basic features of these two instability processes are as follows:

(1) Coalescence occurs when two droplets combine after they have collided, to form an aggregate. When the thin layer between these two neighbouring droplets is ruptured, the droplets form a new larger droplet, mixing their contents (see Figure 2.8). Thus coalescence is considered as an irreversible process unless shear is applied (e.g., in the initial shear process). The rate of coalescence is dependent on the droplet encounter rate (controlled by the droplet diffusion) and the properties of the droplets' surface.

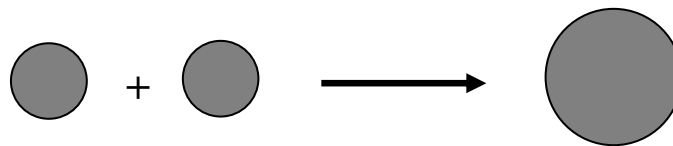


Figure 2.8: Coalescence of two droplets in miniemulsion.

(2) Ostwald ripening, as illustrated in Figure 2.9, involves the growth of the larger monomer droplets at the expense of the smaller droplets. This is due to the difference in the chemical potential between droplets having different radii.¹¹⁶ The growth of droplets occurs by molecular diffusion of monomers through the continuous phase, over time. In other words, Ostwald ripening is a growth mechanism, where small particles effectively are consumed by the larger particles.

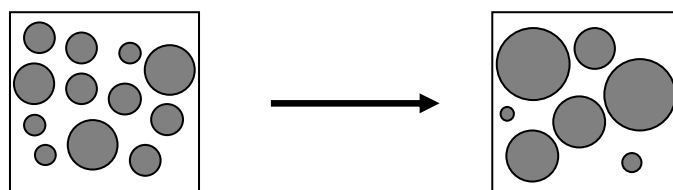


Figure 2.9: Ostwald ripening in miniemulsion.

2.3 Controlled/living radical polymerization (CLRP)

2.3.1 Introduction

Free radical polymerization is a chain addition reaction in which polymer chains are formed by monomer molecules adding to free radicals. The radicals are created by the thermal decomposition (or otherwise) of an initiator, usually organic peroxides or azo compounds. These free radicals have one unpaired electrons, which are highly reactive. Therefore, they tend to take part in addition reactions such as polymerization processes.¹⁵³ This polymerization is one of the most important and versatile methods used for the synthesis of high molecular weight polymers on a commercial scale.¹⁵⁴ It is a powerful and inexpensive technique that can be easily applied, in comparison to other polymerization methods. A wide range of monomers and functional groups, including methacrylates, styrenics, acrylamides, and butadiene, can be polymerized under different reaction conditions. Using this process, polymerizations such as bulk, solution, emulsion, miniemulsion, and suspension have been successfully implemented.¹⁵⁵

However, conventional free radical polymerization offers very little control over the macromolecular structure, such as the molecular weight distribution, composition and architecture of the polymers. This can be attributed to a constant radical generation followed by the occurrence of irreversible termination reactions throughout the polymerization process.^{156,157} In 1955, the first report of living polymerization by an anionic process was introduced by Szwarc.¹⁵⁸ The author referred to the polymers formed (i.e., PS) as ‘living polymers’ because they were able to grow whenever additional monomer was supplied.¹⁵⁹ This had a tremendous impact on polymer science, and several controlled radical polymerization techniques have since been reported. A detailed description of the mechanistic developments in the field of CLRP is given in a review by Braunecker and Matyjaszewski.¹⁵⁷

CLRP provides new synthesis methods that allow very precise control over the polymerization process while retaining much of the versatility of conventional free radical polymerization. It enables the synthesis and design of new polymer architectures with predictable molecular weights, controlled molecular weight distribution (i.e., low dispersity) and well defined end groups. The predication and control of the molecular weight is achieved through a complex series of reactions and intermediates. Under appropriate conditions, the termination reaction will be reduced and the polymerization will behave as a living system. In

a typical living polymerization, polymer chains must increase in molecular weight upon addition of new monomer units and the degree of polymerization should increase linearly with conversion.

2.3.2 Fundamentals of CLRP

In general, CLRP methods are based on the creation of a rapid equilibrium between the growing polymer radicals and dormant species. The irreversible chain termination reaction is suppressed by the presence of reagents that react with the propagating radicals in a activation/deactivation reaction (i.e., chain transfer process).¹⁶⁰ This allows the slow and simultaneous growth of all chains while keeping the concentration of radicals low enough to minimize termination. In the ideal case, the active growing polymer chains will continue growing as long as there is monomer present in the system. Only two processes, initiation and propagation, should occur, hence all growing polymer chains in the system should be active. Thus, all polymer chains, which were initiated at the beginning of the polymerization process, grow at the same rate, resulting in a better control of the polymerization.

The technique provides a simple method for the synthesis of advanced complex polymer architectures such as star, block and branched copolymers, which are more difficult to obtain by other synthetic methods.¹⁶¹ CLRP is generally more compatible with the functional groups of the monomers than classical living polymerization methods, and can be carried out in many solvents over a wide temperature range. Several fundamental characteristics for an ideal CLRP can be summarized below.¹⁶⁰

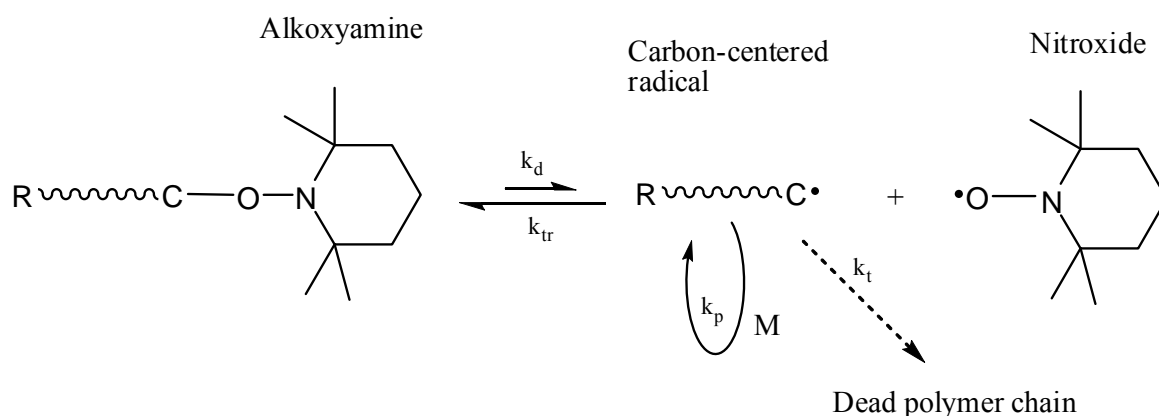
- Polymerization of monomers should proceed until all monomer molecules are consumed.
- The addition of new monomer results in the growth of the polymer chains without any new ones being initiated.
- During the polymerization process, the molar mass of polymers should be predictable.
- The number of living species must remain constant during the entire polymerization process and the molar mass should increase linearly with conversion.
- Polymers with narrow molecular weight distribution can be obtained.
- The end groups of the chain transfer compound are preserved at the ends of the resulting polymer chains.

2.3.3 Common CLRP techniques

Various free radical processes offering controlled growth of polymer chains have been developed. Many new techniques, including nitroxide-mediated polymerization (NMP), atom-transfer radical polymerization (ATRP) and reversible addition-fragmentation chain transfer (RAFT) mediated polymerization have recently emerged and are now available for the production of new polymers with well-defined structures. These methods are discussed in detail in the following sections, with emphasis on the RAFT method.

2.3.3.1 NMP

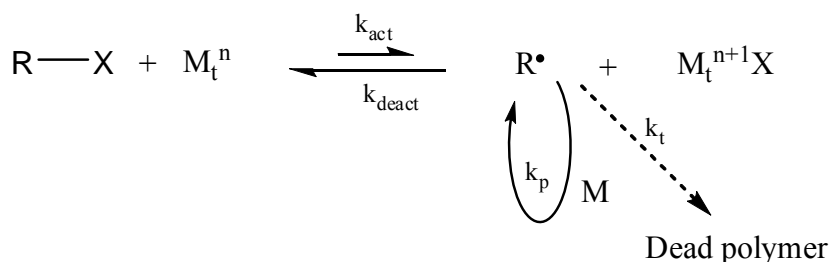
NMP, first introduced by Solomon and Rizzardo in the 1980s, is based on the reversible trapping of carbon-centered radicals by nitroxides.^{162,163} Scheme 2.5 shows a general mechanism of NMP method. At high temperature, the carbon-oxygen bond of the alkoxyamine species can be cleaved to form a nitroxide and a carbon-centered radical (i.e., equilibrium exists). The carbon-centered radical reacts with the monomer (M) units present to form propagating radicals. The radical can propagate or undergo a termination reaction until it is trapped by a nitroxide again. In an ideal case, the equilibrium lies greatly toward the alkoxyamine, resulting in a low concentration of radicals, and therefore minimizing the termination rate for the polymerization. There are some disadvantages of NMP, for example, the elevated reaction temperatures that are often required for polymerization (~ 120 °C) and the limited monomer range that can be polymerized in a controlled way.



Scheme 2.5: Nitroxide-mediated polymerization: k_d is the dissociation rate coefficient, k_{tr} is the trapping rate coefficient, k_p is the propagation rate coefficient and k_t is the termination rate coefficient.

2.3.3.2 ATRP

This technique was first independently reported by Wang and Matyjaszewski¹⁶⁴ and Kato et al.¹⁶⁵ in 1995. The process is based on a well known reaction in organic chemistry that is referred to as atom transfer radical addition. In this reaction, an organic radical is produced from an alkyl halide initiator (R-X), which can be transferred to a transition metal complex in a higher oxidation state. The radical can react with monomer to form polymer chains, which can be reversibly deactivated by transfer of the halogen back from the metal complex, or undergo termination or chain transfer reactions. If the correct halide is used, the exchange of the halogen atom between the alkyl group and the propagating radical polymer chain is fast and selective, resulting in a controlled polymerization. Scheme 2.6 illustrates the ATRP method.



Scheme 2.6: Atom transfer radical polymerization: M_t^n is a transition metal complex, k_{act} is the activation rate coefficient, k_{deact} is the deactivation rate coefficient, k_p is the propagation rate coefficient and k_t is the termination rate coefficient.

Although the range of monomer type in ATRP is broader than that in NMP, the contamination of the polymer with the metal catalyst is a major drawback of ATRP. Removal of the toxic transition metal from the final polymer is thus required. Halogens such as chlorine, bromine and iodine have been found to be suitable for such migration reaction with various transition metal systems for specific monomers. Transition metal systems used in ATRP include Cu(I)/Cu(II), Ru(II)/Ru(III), Fe(II)/Fe(III) and Ni(II)/Ni(III).

2.3.3.3 RAFT-mediated polymerization

Since its discovery in the late 1990s, the RAFT method has become one of the most effective and versatile methods of CLRP.^{156,166} As a CLRP technique, this process allows the construction of polymers having targeted molecular weights with very low dispersity.¹⁶⁷⁻¹⁶⁹ In

principle, the RAFT method operates via a degenerative transfer mechanism in which a thiocarbonylthio compound (e.g., dithioesters, xanthates, dithiocarbamates and trithiocarbonates) acts as a chain transfer agent.¹⁷⁰ Other thiocarbonylthio compounds such as phosphoryl dithioesters and dithiocarbazates have also been employed in RAFT polymerization.¹⁷¹ The preserved end groups of the RAFT agent can be reactivated, allowing the incorporation of additional monomer molecules to produce a variety of polymer architectures, including stars,¹⁷² grafts,¹⁷³ brushes and branches.¹⁷⁴

The key factor for a successful RAFT polymerization is the appropriate choice of the RAFT agent. This agent is a simple organic compound that possesses the thiocarbonylthio moiety (S=C–S) that imparts the living behavior to free radical polymerization. The general molecular structure of a RAFT agent is illustrated in Figure 2.10, where Z refers to the stabilizing group and R refers to the free radical homolytic leaving group. The Z group controls the reactivity of the C=S bond toward radical addition and fragmentation, and the R group is responsible for reinitiating the polymerization.

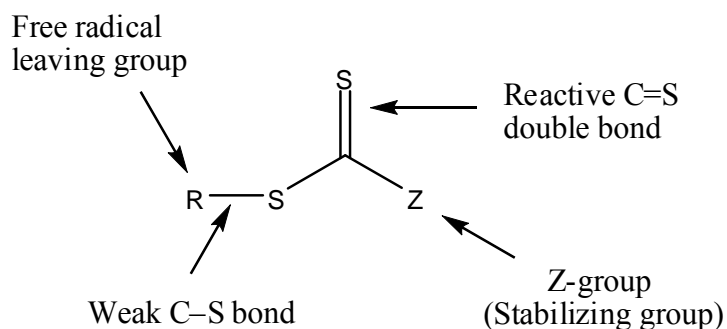
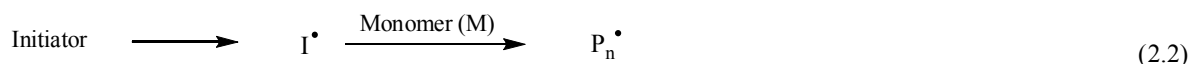
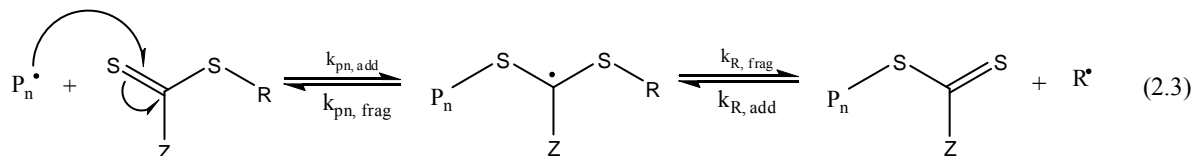
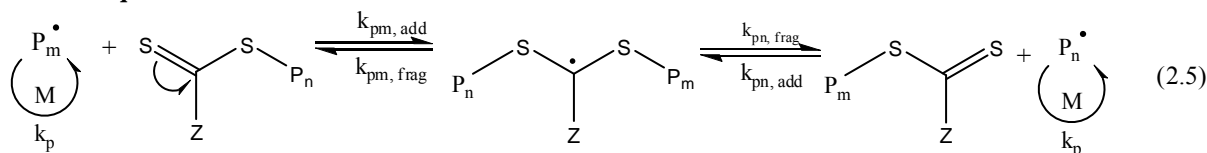


Figure 2.10: Basic structure of a typical RAFT agent.

Scheme 2.7 shows all the reactions involved in the RAFT process. The RAFT agent is added to the reaction medium in the presence of monomer (M) and radical initiator (I). Once the polymerization has commenced the initiator decomposes, generating free radicals, which can react with monomer to produce propagating radicals (P_n^\bullet) (Equation 2.2). The propagating radicals can react with the RAFT agent to give dormant chains, as shown in Equation 2.3. The leaving group radical then reacts with another monomer species, starting another active polymer chain (Equation 2.4). Equation 2.5 shows the main chain equilibrium reaction. This is the fundamental step in the RAFT process, which traps the majority of the active propagating species into the dormant thiocarbonyl compound. This limits the possibility of chain termination. By controlling the initiator to RAFT ratio, it is possible to produce polymer

Chapter 2: Historical and Theoretical Background

chains in a controlled manner with very narrow molecular weight distribution. The number of dead chains that are terminated by radical coupling (Equation 2.6) correspond to the amount of decomposed initiator and the living polymerization features will be observed.

Initiation**Reversible chain transfer****Reinitiation****Chain equilibrium****Termination****Scheme 2.7: The RAFT mechanism.**

The RAFT process has many advantages over other CLRP techniques (i.e., NMP and ATRP), such as its versatility towards different monomers and functional groups (e.g., methacrylates, acrylates and styrenics) as well as the suitability to a wide range of reaction conditions. NMP is usually carried out at a high temperature. The ATRP catalyst on the other hand tends to bind strongly to the functional groups in the monomers used. A major drawback of this contamination is that the removal of the toxic transition metal from the final polymer is necessary.

2.3.4 RAFT-mediated emulsion polymerization vs. miniemulsion polymerization

In the past, most research groups have focused on the RAFT method in homogeneous systems such as bulk¹⁷⁵ and solution¹⁷⁶ polymerization, where good understanding of polymerization mechanism has been achieved. As the CLRP in aqueous medium is industrially preferred,

applying the RAFT process in emulsion or miniemulsion systems using water as the medium will be most useful. If the RAFT mediated polymerization can be successfully carried out in aqueous systems, the application and versatility of this process will be greatly enhanced.

The use of RAFT mediated polymerization for the synthesis of polymer particles is, however, difficult to achieve by conventional emulsion polymerization, where colloidal instability is a major problem. This can be attributed to the poor transport of the RAFT agent from the monomer droplets to the polymer particles, which is necessary in such systems. This is due to the high hydrophobicity and low water solubility of most RAFT agents.^{166,177} In conventional emulsion systems, no transport of the fairly water insoluble RAFT components into micelles can take place, leading to phase separation (i.e., a RAFT rich and a polymer rich phase are observed). Thus, polymer latices with poor colloidal stability, loss of molecular weight control, slow polymerization rates and broad molecular weight distribution are obtained.^{178,179} However, miniemulsion polymerization, due to the initial dispersion of the hydrophobic components (RAFT agent and monomer), can be a powerful technique for the preparation of latex particles using RAFT mediated polymerization.¹⁸⁰

In comparison with emulsion polymerization, in miniemulsion polymerization most monomer droplets are, in principle, directly converted into particles, since the droplets are regarded as the locus of the initiation and propagation reaction.¹⁴⁶ Therefore, the transport of the monomer or other hydrophobic compounds from a reservoir to the polymerization locus, as in the case for emulsion polymerization, is unnecessary. This feature makes miniemulsion polymerization quite efficient as a convenient one-step nano-incorporation technique for hydrophobic compounds. In the miniemulsion process, the monomer droplets are directly polymerized, thus the resulting polymer particles are often one-to-one copies of the monomer droplets.¹¹³ The RAFT agent can be equally distributed in the droplets at the beginning of the polymerization (i.e., during miniemulsification process) and the transport of the RAFT agent is not required during the polymerization.

2.4 Barrier polymer coatings

2.4.1 Introduction

The use of polymers as barrier materials has become increasingly important due to the widespread use of polymeric films and rigid plastics for different applications, such as paints

Chapter 2: Historical and Theoretical Background

and coatings.^{181,182} The main purpose of using barrier polymers is to reduce the permeation of low molecular weight substances such as oxygen, water, and water vapor molecules. Barrier properties of polymers are determined by the rate of mass transport of these molecules through the polymer structure. The chemical nature of polymers is an important parameter that determines their ultimate barrier properties.

In general, barrier polymers can be defined as polymers that are able to restrict the passage of gases, vapors, and organic liquids through them. They are classified by the degree to which they restrict the passage of these gases and vapors (e.g., oxygen and moisture). The categories range from high barriers that exhibit low permeability, to low barriers that have high permeability.¹⁸³ On a molecular level, polymer chains must move aside to allow permeation. Therefore, the weaker the forces holding the polymer chains together, the more rapidly permeation will occur. These chain-to-chain interactions are determined partly by the chemical structure and nature of the polymer. On the other hand, hydrophobic polymers such as PS and poly(butyl acrylate) can reduce the permeation process of a low molecular weight compound, such as water, in the films made from them. This can be attributed to the high hydrophobic nature of these polymers.¹⁸⁴

The transport of low molecular weight molecules (permeate) such as gases and vapors through a polymer film is affected by the solubility of these molecules in the polymer and their diffusion coefficient in the polymer matrix.¹⁸⁵ The solubility is affected by the intermolecular forces between the polymer molecules and the permeate.¹⁸⁶ For example, films made from polar polymers such as those containing hydroxyl groups, e.g., poly(ethylene-co-vinyl alcohol), are excellent gas barriers but poor water and water vapor barriers.^{187,188} It is mainly the hydrogen bonds formed between the polar hydroxyl groups that explain the high cohesive energy density of the film and its good gas barrier properties in the anhydrous state. However, these polar groups are also at the origin of the hydrophilic character of the polymer at high relative humidity.¹⁸⁸ In contrast, non-polar hydrocarbon polymers such as PE have excellent water and water vapor barrier properties but poor gas barrier properties. The latter property improves as the density of the PE increases. In general, polymers must have the following properties in order to be used successfully as good barrier materials for coating applications:¹⁸⁹

- Close chain-to-chain packing ability to improve polymer crystallinity,
- Bonding or attraction between polymer chains,

- High chain stiffness to reduce diffusion,
- Inertness to the permeate, which means that polymers must not interact with the diffusing molecules,
- High glass transition temperature (at least higher than the service temperature).

2.4.2 Permeability of polymeric barrier coatings

The mechanism and transport behavior of gases and water molecules through polymer films and membranes have attracted attention in recent years.¹⁹⁰ Generally speaking, the term permeability is used to describe the penetration of low molecular weight substances through a barrier. Permeability can be defined as the transmission of a permeate through a resisting material. For polymer films, permeability to gases and vapors is often important.¹⁸³ Most often the gases or vapors of interest are water vapor, oxygen, carbon dioxide, and nitrogen. Knowledge of the permeability properties of polymer materials for these low molecular weight compounds could lead to their improved utilization. For a specific permeate, the chemical composition and physical properties of the polymeric membrane determine the permeation properties, according to the following relationship:¹⁸⁵

$$P = D \times S \quad (2.7)$$

where P is the permeability, and D and S are the diffusion and solubility coefficients respectively.

The diffusion coefficient (D) describes the ease with which the permeate moves in and through the polymer membrane while solubility (S) gives an indication on the polymer-permeate interaction.^{191,192} From Equation 2.7 one can see that permeability can be greatly influenced by the diffusion and solubility coefficients. A low permeability may result from a low diffusion coefficient or a low solubility coefficient, or both. These factors in turn can be greatly influenced by the chemical and physical structure of the polymer in use. In this regard, it is very important to investigate the relationship between the chemical and physical properties and the gas transport behavior, to explain the permeability behavior of polymeric materials and coated polymeric films. One example is the permeation of water and water vapor through polymer films. Polymer films are often characterized in terms of their moisture vapor transmission rate (MVTR), that is, a measure of the passage of water in gaseous form through the film.¹⁹³

It is generally believed that permeability through a polymer membrane depends on interactions between the polymer material and permeate molecules. Permeation, as shown in Figure 2.11, is a multistep process,¹⁹⁴ which includes:

- Adsorption
- Solution (thermodynamic process)
- Diffusion (kinetic process)
- Desorption

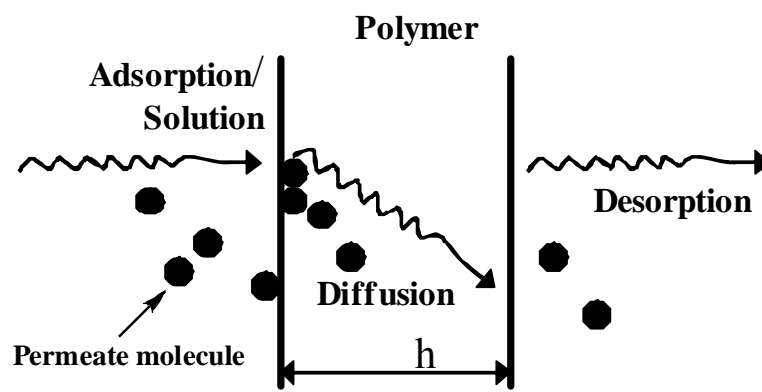


Figure 2.11: Permeation process in a polymer film of thickness h .

The transport properties of diffusing molecules through a polymer membrane are affected by other factors such as the presence of fillers in the polymer matrix. The transport of water and gases in polymers filled with clay has been studied, and a reduction in permeability in PCNs compared to neat polymer has been reported.^{195,196} However, the transport of water and water vapor in PGNs has not been investigated. The incorporation of nanolayered material such as graphite nanosheets into polymers can significantly reduce the permeation of water relative to the neat polymer. The addition of hydrophobic graphene nanosheets to a polymer matrix will result in a reduction of the water solubility, hence decreasing the polymer permeability. In addition, a percolating network of graphene nanoplatelets can provide a tortuous path which inhibits the diffusion of water, resulting in reduced permeability. The water molecules must maneuver around the impermeable 2-D graphene nanoplatelets, resulting in reduced permeability.

2.4.3 Effect of temperature and humidity on permeability

Permeability is affected by several physical properties, such as humidity and temperature.¹⁹⁷ Many polymers, particularly those having polar groups, can absorb moisture from the atmosphere or from a liquid in contact with the polymer. Also, if such a polymer is in contact with a humid environment it absorbs water. This has the effect of swelling or plasticizing the polymer. Plasticization occurs when the polymer/water interactions are strong.¹⁹⁸ Plasticization increases polymer chain mobility and, in doing so, it increases the rate of permeate transport in the material and reduces the barrier properties of the polymer. The ability of different polymers to absorb water from a humid environment depends on the type of polymer. For instance, water does not affect the permeabilities of some non-polar polymers, including polyolefins, vinylidene chloride copolymers and acrylonitrile copolymers.¹⁸⁵ In other polar polymers, including ethylene-vinyl alcohol copolymers and most polyamides, the permeability increases with increasing relative humidity. Permeability often also varies with temperature according to the Arrhenius equation:¹⁹⁷

$$P = P_o \exp (-E_p / RT) \quad (2.8)$$

where P_o is a constant, E_p is the activation energy for permeation, R is the gas constant, and T is the absolute temperature.

The temperature at which the barrier polymer is used can therefore also be of great importance. For instance, if the polymer has a T_g higher than the application temperature, the polymer will be in its glassy state, and the segments will have little mobility. Thus, a diffusing molecule will have a much more tortuous path through the polymer, leading to a less permeable material. If the polymer has a T_g lower than the application temperature, the polymer will be in its rubbery state, leading to a more permeable material. Therefore, the recommended temperature of use will be below the T_g of the polymer, and the polymer will consequently have improved barrier properties.¹⁹⁹

2.5 References

- (1) Usuki, A.; Kojima, Y.; Kawasumi, M.; Okada, A.; Fukushima, Y.; Kurauchi, T.; Kamigaito, O. *Journal of Materials Research* **1993**, 8, 1179-1184.
- (2) Hussain, F.; Hojjati, M.; Okamoto, M.; Gorga, R. E. *Journal of Composite Materials* **2006**, 40 (17), 1511-1575.
- (3) Chen, Z.; Gong, K. *Journal of Applied Polymer Science* **2002**, 84 (8), 1499-1503.
- (4) Alexander, B. M.; Jeffrey, W. G. *Journal of Applied Polymer Science* **2003**, 87 (8), 1329-1338.
- (5) Naoki, H.; Hirotaka, O.; Arimitsu, U. *Journal of Applied Polymer Science* **2004**, 93 (2), 758-764.
- (6) Chen, G.; Weng, W.; Wu, D.; Wu, C.; Lu, J.; Wang, P.; Chen, X. *Carbon* **2004**, 42 (4), 753-759.
- (7) Tryba, B.; Morawski, A. W.; Inagaki, M. *Carbon* **2005**, 43 (11), 2417-2419.
- (8) Guo-Hua, C.; Da-Jun, W.; Wen-Gui, W.; Wen-Li, Y. *Journal of Applied Polymer Science* **2001**, 82 (10), 2506-2513.
- (9) Xu, J.; Hu, Y.; Song, L.; Wang, Q.; Fan, W. *Materials Research Bulletin* **2001**, 36 (10), 1833-1836.
- (10) Ding, R.; Hu, Y.; Gui, Z.; Zong, R.; Chen, Z.; Fan, W. *Polymer Degradation and Stability* **2003**, 81 (3), 473-476.
- (11) Geim, A. K.; Novoselov, K. S. *Nature Materials* **2007**, 6 (3), 183-191.
- (12) Park, S.; Ruoff, R. S. *Nature Nanotechnology* **2009**, 4 (4), 217-224.
- (13) Wang, Z.; Han, E.; Ke, W. *Corrosion Science* **2007**, 49 (5), 2237-2253.
- (14) Higginbotham, A. L.; Lomeda, J. R.; Morgan, A. B.; Tour, J. M. *ACS Applied Materials & Interfaces* **2009**, 1 (10), 2256-2261.
- (15) Viculis, L. M.; Mack, J. J.; Mayer, O. M.; Hahn, H. T.; Kaner, R. B. *Journal of Materials Chemistry* **2005**, 15, 974-978.
- (16) Lerf, A.; He, H.; Forster, M.; Klinowski, J. *The Journal of Physical Chemistry B* **1998**, 102 (23), 4477-4482.
- (17) Hontoria-Lucas, C.; López-Peinado, A. J.; López-González, J. d. D.; Rojas-Cervantes, M. L.; Martín-Aranda, R. M. *Carbon* **1995**, 33 (11), 1585-1592.
- (18) Chen, G.-H.; Wu, D.-J.; Weng, W.-G.; Yan, W.-L. *Polymer Engineering & Science* **2001**, 41 (12), 2148-2154.
- (19) Titelman, G. I.; Gelman, V.; Bron, S.; Khalfin, R. L.; Cohen, Y.; Bianco-Peled, H. *Carbon* **2005**, 43 (3), 641-649.
- (20) Szabó, T.; Tombácz, E.; Illés, E.; Dékány, I. *Carbon* **2006**, 44 (3), 537-545.
- (21) Paredes, J. I.; Villar-Rodil, S.; Martínez-Alonso, A.; Tascon, J. M. D. *Langmuir* **2008**, 24 (19), 10560-10564.

Chapter 2: Historical and Theoretical Background

- (22) Lv, C.; Xue, Q.; Xia, D.; Ma, M.; Xie, J.; Chen, H. *The Journal of Physical Chemistry C* **2010**, 114 (14), 6588-6594.
- (23) Strawhecker, K. E.; Manias, E. Nanocomposites based on water soluble polymers and unmodified smectite clays. In *Polymer Nanocomposites*, 2nd edition; Mai, Y.-W.; Yu, Z.-Z., Eds.; Woodhead Publishing: New York, 2006; Vol. 8, pp 206-233.
- (24) Jianqi, W.; Zhidong, H. *Polymers for Advanced Technologies* **2006**, 17 (4), 335-340.
- (25) Okamoto, M. Polymer/clay nanocomposites. In *Encyclopedia of Nanoscience and Nanotechnology*, 1st edition; Nalwa, H. S., Ed.; American Scientific Publishers: California, 2004; Vol. 8, pp 791-843.
- (26) Kim, H.; Macosko, C. W. *Macromolecules* **2008**, 41 (9), 3317-3327.
- (27) Kim, H.; Miura, Y.; Macosko, C. W. *Chemistry of Materials* **2010**, 22 (11), 3441-3450.
- (28) Stankovich, S.; Dikin, D. A.; Dommett, G. H. B.; Kohlhaas, K. M.; Zimney, E. J.; Stach, E. A.; Piner, R. D.; Nguyen, S. T.; Ruoff, R. S. *Nature* **2006**, 442 (7100), 282-286.
- (29) Wissler, M. *Journal of Power Sources* **2006**, 156 (2), 142-150.
- (30) IUPAC Compendium of Chemical Terminology, Blackwell Scientific Publications, 2nd edition; 1977.
- (31) Pierson, H. O., *Handbook of Carbon, Graphite, Diamond and Fullerenes*. 2nd edition; Noyes Publications: New Jersey, 1993; Vol. 10, pp 226-243.
- (32) Ragan, S. *Journal of Materials Science* **1983**, 18, 3161-3176.
- (33) Pierson, H. O., *Handbook of Carbon, Graphite, Diamond and Fullerenes*. 2nd edition; Noyes Publications: New Jersey, 1993; Vol. 4, pp 70-86.
- (34) Cong, C.; Yu, T.; Sato, K.; Shang, J.; Saito, R.; Dresselhaus, G. F.; Dresselhaus, M. S. *ACS Nano* **2011**, 5 (11), 8760-8768.
- (35) Gopakumar, T. G.; Page, D. J. Y. S. *Polymer Engineering and Science* **2004**, 44 (6), 1162-1169.
- (36) Dresselhaus, M. S.; Dresselhaus, G. *Advances in Physics* **1981**, 30 (2), 139-326.
- (37) Kamimuro, H. *Physics Today* **1987**, 40 (12), 64-71.
- (38) Hummers, W. S.; Offeman, R. E. *Journal of the American Chemical Society* **1958**, 80, 1339.
- (39) Lee, C.; Wei, X.; Kysar, J. W.; Hone, J. *Science* **2008**, 321 (5887), 385-388.
- (40) Velasco-Santos, C.; Martinez-Hernandez, A. L.; Castano, V. M. *Composite Interfaces* **2005**, 11 (8/9), 567-586.
- (41) Donghwan, C.; Sangyeob, L.; Gyeongmo, Y.; Hiroyuki, F.; Lawrence, T. D. *Macromolecular Materials and Engineering* **2005**, 290 (3), 179-187.
- (42) Fukushima, H.; Drzal, L. T., A Carbon Nanotube Alternative: Graphite Nanoplatelets as Reinforcements for Polymers. In *ANTEC 2003 Plastics: Annual Technical Conference, Volume 2: Materials*, Society of Plastics Engineers: 2003; pp 2230-2234.
- (43) Kalaitzidou, K.; Fukushima, H.; Drzal, L. T., Mechanical and Electrical Properties of Exfoliated Graphite-Platelet Polypropylene Nanocomposites. In *ANTEC 2004 Plastics:*

Chapter 2: Historical and Theoretical Background

- Annual Technical Conference, Volume 2: Materials*, Society of Plastics Engineers: 2004; pp 1533-1537.
- (44) Chung, D. *Journal of Materials Science* **1987**, 22 (12), 4190-4198.
- (45) Gomez-Navarro, C.; Weitz, R. T.; Bittner, A. M.; Scolari, M.; Mews, A.; Burghard, M.; Kern, K. *Nano Letters* **2007**, 7 (11), 3499-3503.
- (46) Yu, A.; Ramesh, P.; Itkis, M. E.; Bekyarova, E.; Haddon, R. C. *The Journal of Physical Chemistry C* **2007**, 111 (21), 7565-7569.
- (47) Balandin, A. A.; Ghosh, S.; Bao, W.; Calizo, I.; Teweldebrhan, D.; Miao, F.; Lau, C. N. *Nano Letters* **2008**, 8 (3), 902-907.
- (48) Pierson, H. O., *Handbook of Carbon, Graphite, Diamond and Fullerenes*. 2nd edition; Noyes Publications: New Jersey, 1993; Vol. 3, pp 43-69.
- (49) Toyoda, M.; Inagaki, M. *Carbon* **2000**, 38 (2), 199-210.
- (50) Toyoda, M.; Moriya, K.; Aizawa, J. I.; Konno, H.; Inagaki, M. *Desalination* **2000**, 128 (3), 205-211.
- (51) Lavrakas, V. *Journal of Chemical Education* **1957**, 34 (5), 240-241.
- (52) Schniepp, H. C.; Li, J.-L.; McAllister, M. J.; Sai, H.; Herrera-Alonso, M.; Adamson, D. H.; Prud'homme, R. K.; Car, R.; Saville, D. A.; Aksay, I. A. *The Journal of Physical Chemistry B* **2006**, 110 (17), 8535-8539.
- (53) Jeong, H.-K.; Lee, Y. P.; Lahaye, R. J. W. E.; Park, M.-H.; An, K. H.; Kim, I. J.; Yang, C.-W.; Park, C. Y.; Ruoff, R. S.; Lee, Y. H. *Journal of the American Chemical Society* **2008**, 130 (4), 1362-1366.
- (54) Stankovich, S.; Piner, R. D.; Chen, X.; Wu, N.; Nguyen, S. T.; Ruoff, R. S. *Journal of Materials Chemistry* **2006**, 16 (2), 155-158.
- (55) Zhang, W.; He, W.; Jing, X. *The Journal of Physical Chemistry B* **2010**, 114 (32), 10368-10373.
- (56) Wang, G.; Yang, J.; Park, J.; Gou, X.; Wang, B.; Liu, H.; Yao, J. *The Journal of Physical Chemistry C* **2008**, 112 (22), 8192-8195.
- (57) Bourlinos, A. B.; Georgakilas, V.; Zboril, R.; Steriotis, T. A.; Stubos, A. K. *Small* **2009**, 5 (16), 1841-1845.
- (58) Zhang, Z.; Lerner, M. M. *Chemistry of Materials* **1996**, 8 (1), 257-263.
- (59) Falcao, E. H. L.; Blair, R. G.; Mack, J. J.; Viculis, L. M.; Kwon, C.-W.; Bendikov, M.; Kaner, R. B.; Dunn, B. S.; Wudl, F. *Carbon* **2007**, 45 (6), 1367-1369.
- (60) Kim, H.; Abdala, A. A.; Macosko, C. W. *Macromolecules* **2010**, 43 (16), 6515-6530.
- (61) Gilje, S.; Han, S.; Wang, M.; Wang, K. L.; Kaner, R. B. *Nano Letters* **2007**, 7 (11), 3394-3398.
- (62) Liang, X.; Chang, A. S. P.; Zhang, Y.; Harteneck, B. D.; Choo, H.; Olynick, D. L.; Cabrini, S. *Nano Letters* **2008**, 9 (1), 467-472.

Chapter 2: Historical and Theoretical Background

- (63) Hernandez, Y.; Nicolosi, V.; Lotya, M.; Blighe, F. M.; Sun, Z.; De, S.; McGovern, I. T.; Holland, B.; Byrne, M.; Gun'Ko, Y. K.; Boland, J. J.; Niraj, P.; Duesberg, G.; Krishnamurthy, S.; Goodhue, R.; Hutchison, J.; Scardaci, V.; Ferrari, A. C.; Coleman, J. N. *Nature Nanotechnology* **2008**, 3 (9), 563-568.
- (64) Biswas, S.; Drzal, L. T. *Nano Letters* **2008**, 9 (1), 167-172.
- (65) Kim, K. S.; Zhao, Y.; Jang, H.; Lee, S. Y.; Kim, J. M.; Kim, K. S.; Ahn, J.-H.; Kim, P.; Choi, J.-Y.; Hong, B. H. *Nature* **2009**, 457 (7230), 706-710.
- (66) Reina, A.; Jia, X.; Ho, J.; Nezich, D.; Son, H.; Bulovic, V.; Dresselhaus, M. S.; Kong, J. *Nano Letters* **2008**, 9 (1), 30-35.
- (67) Paci, J. T.; Belytschko, T.; Schatz, G. C. *The Journal of Physical Chemistry C* **2007**, 111 (49), 18099-18111.
- (68) Boukhalov, D. W.; Katsnelson, M. I. *Journal of the American Chemical Society* **2008**, 130 (32), 10697-10701.
- (69) Lahaye, R. J. W. E.; Jeong, H. K.; Park, C. Y.; Lee, Y. H. *Physical Review B* **2009**, 79 (12), 125435.
- (70) Szabo, T.; Berkesi, O.; Forgo, P.; Josepovits, K.; Sanakis, Y.; Petridis, D.; Dekany, I. *Chemistry of Materials* **2006**, 18 (11), 2740-2749.
- (71) Cai, W.; Piner, R. D.; Stadermann, F. J.; Park, S.; Shaibat, M. A.; Ishii, Y.; Yang, D.; Velamakanni, A.; An, S. J.; Stoller, M.; An, J.; Chen, D.; Ruoff, R. S. *Science* **2008**, 321 (5897), 1815-1817.
- (72) Gao, W.; Alemany, L. B.; Ci, L.; Ajayan, P. M. *Nature Chemistry* **2009**, 1 (5), 403-408.
- (73) Mkhoyan, K. A.; Contryman, A. W.; Silcox, J.; Stewart, D. A.; Eda, G.; Mattevi, C.; Miller, S.; Chhowalla, M. *Nano Letters* **2009**, 9 (3), 1058-1063.
- (74) He, H.; Klinowski, J.; Forster, M.; Lerf, A. *Chemical Physics Letters* **1998**, 287 (1-2), 53-56.
- (75) He, H.; Riedl, T.; Lerf, A.; Klinowski, J. *The Journal of Physical Chemistry* **1996**, 100 (51), 19954-19958.
- (76) Li, J.-L.; Kudin, K. N.; McAllister, M. J.; Prud'homme, R. K.; Aksay, I. A.; Car, R. *Physical Review Letters* **2006**, 96 (17), 176101.
- (77) Buchsteiner, A.; Lerf, A.; Pieper, J. *The Journal of Physical Chemistry B* **2006**, 110 (45), 22328-22338.
- (78) Potts, J. R.; Dreyer, D. R.; Bielawski, C. W.; Ruoff, R. S. *Polymer* **2011**, 52 (1), 5-25.
- (79) Hirata, M.; Gotou, T.; Horiuchi, S.; Fujiwara, M.; Ohba, M. *Carbon* **2004**, 42 (14), 2929-2937.
- (80) Hirata, M.; Gotou, T.; Ohba, M. *Carbon* **2005**, 43 (3), 503-510.
- (81) Meng, Y. Polymer/graphite nanocomposites. In *Polymer Nanocomposites*, 2nd edition; Mai, Y.-W.; Yu, Z.-Z., Eds.; Woodhead Publishing: Cambridge, 2006; Vol. 19, pp 510-539.
- (82) Zheng, W.; Wong, S.-C.; Sue, H.-J. *Polymer* **2002**, 73 (25), 6767-6773.
- (83) Zheng, W.; Wong, S.-C. *Composites Science and Technology* **2003**, 63 (2), 225-235.

Chapter 2: Historical and Theoretical Background

- (84) Xu, J.; Hu, Y.; Song, L.; Wang, Q.; Fan, W.; Liao, G.; Chen, Z. *Polymer Degradation and Stability* **2001**, 73 (1), 29-31.
- (85) Jing-Wei, S.; Xiao-Mei, C.; Wen-Yi, H. *Journal of Applied Polymer Science* **2003**, 88 (7), 1864-1869.
- (86) Krupa, I.; Chodák, I. *European Polymer Journal* **2001**, 37 (11), 2159-2168.
- (87) Wenge, Z.; Xuehong, L.; Shing-Chung, W. *Journal of Applied Polymer Science* **2004**, 91 (5), 2781-2788.
- (88) Kalaitzidou, K.; Fukushima, H.; Drzal, L. T. *Carbon* **2007**, 45 (7), 1446-1452.
- (89) Liu, P.-G.; Xiao, P.; Xiao, M.; Gong, K.-c. *Chinese Journal of Polymer Science* **2000**, 18 (5), 413-418.
- (90) Wang, W.-P.; Pan, C.-Y. *Polymer Engineering and Science* **2004**, 44 (12), 2335-2339.
- (91) Yasmin, A.; Luo, J.-J.; Daniel, I. M. *Composites Science and Technology* **2006**, 66 (9), 1182-1189.
- (92) Mack, J. J.; Viculis, L. M.; Ali, A.; Luoh, R.; Yang, G.; Hahn, H. T.; Ko, F. K.; Kaner, R. B. *Advanced Materials* **2005**, 17 (1), 77-80.
- (93) Bragg, W. L. *Proceedings of the Cambridge Philosophical Society* **1913**, 17, 43-57.
- (94) Zhang, R.; Hu, Y.; Xu, J.; Fan, W.; Chen, Z. *Polymer Degradation and Stability* **2004**, 85 (1), 583-588.
- (95) Du, X.; Yu, Z.-Z.; Dasari, A.; Ma, J.; Mo, M.; Meng, Y.; Mai, Y.-W. *Chemistry of Materials* **2008**, 20 (6), 2066-2068.
- (96) Chen, G.; Lu, J.; Wu, D. *Journal of Materials Science* **2005**, 40 (18), 5041-5043.
- (97) Yang, J.; Tian, M.; Jia, Q.-X.; Shi, J.-H.; Zhang, L.-Q.; Lim, S.-H.; Yu, Z.-Z.; Mai, Y.-W. *Acta Materialia* **2007**, 55 (18), 6372-6382.
- (98) Le-Bras, M.; Wilkie, C.; Bourbigot, S.; Duquesne, S.; Jama, C., *Fire Retardancy of Polymers: New Application of Mineral Fillers*. 2nd edition; Royal Society of Chemistry: Cambridge, 2005; pp 161-176.
- (99) Thirumal, M.; Khastgir, D.; Singha, N. K.; Manjunath, B. S.; Naik, Y. P. *Journal of Applied Polymer Science* **2008**, 110 (5), 2586-2594.
- (100) Berger, C.; Song, Z.; Li, X.; Wu, X.; Brown, N.; Naud, C.; Mayou, D.; Li, T.; Hass, J.; Marchenkov, A. N.; Conrad, E. H.; First, P. N.; de Heer, W. A. *Science* **2006**, 312 (5777), 1191-1196.
- (101) Zhou, S. Y.; Gweon, G. H.; Fedorov, A. V.; First, P. N.; de Heer, W. A.; Lee, D. H.; Guinea, F.; Castro Neto, A. H.; Lanzara, A. *Nature Materials* **2007**, 6 (10), 770-775.
- (102) Chen, Z.; Lin, Y.-M.; Rooks, M. J.; Avouris, P. *Physica E* **2007**, 40 (2), 228-232.
- (103) Jang, J. Y.; Kim, M. S.; Jeong, H. M.; Shin, C. M. *Composites Science and Technology* **2009**, 69 (2), 186-191.
- (104) Nguyen, D. A.; Lee, Y. R.; Raghu, A. V.; Jeong, H. M.; Shin, C. M.; Kim, B. K. *Polymer International* **2009**, 58 (4), 412-417.

Chapter 2: Historical and Theoretical Background

- (105) Prud'homme, R. K.; Ozbas, B.; Aksay, I. A.; Register, R. A.; Adamson, D. H. W. O. Patent 2008045778 A1. 2008.
- (106) Lettow, J. S.; Aksay, I. A.; Korkut, S.; Chiang, K. S. U.S. Patent 20070092432 A1. 2009.
- (107) Liang, J.; Wang, Y.; Huang, Y.; Ma, Y.; Liu, Z.; Cai, J.; Zhang, C.; Gao, H.; Chen, Y. *Carbon* **2009**, 47 (3), 922-925.
- (108) Cassagneau, T.; Fendler, J. H. *Advanced Materials* **1998**, 10 (11), 877-881.
- (109) Wenge, Z.; Shing-Chung, W.; Sue, H.-J. *Polymer* **2002**, 73, 6767-6773.
- (110) Bunch, J. S.; Verbridge, S. S.; Alden, J. S.; van der Zande, A. M.; Parpia, J. M.; Craighead, H. G.; McEuen, P. L. *Nano Letters* **2008**, 8 (8), 2458-2462.
- (111) Al-Ghamdi, G. H.; Sudol, E. D.; Dimonie, V. L.; El-Aasser, M. S. *Journal of Applied Polymer Science* **2006**, 101 (5), 3479-3486.
- (112) López-Martínez, E. I.; Márquez-Lucero, A.; Hernández-Escobar, C. A.; Flores-Gallardo, S. G.; Ibarra-Gómez, R.; Yacamán, M. J.; Zaragoza-Contreras, E. A. *Journal of Polymer Science: Part B: Polymer Physics* **2007**, 45 (5), 511-518.
- (113) Landfester, K.; Bechthold, N.; Förster, S.; Antonietti, M. *Macromolecular Rapid Communications* **1999**, 20 (2), 81-84.
- (114) Miller, C.; Sudol, E.; Silebi, C.; El-Aasser, M. *Journal of Polymer Science Part A: Polymer Chemistry* **1995**, 33, 1391-1408.
- (115) Sudol, E.; El-Aasser, M. Miniemulsion Polymerization. In *Emulsion Polymerization and Emulsion Polymers*, Lovell, P.; El-Aasser, M., Eds.; John Wiley & Sons Ltd.: New York, 1997; pp 699-722.
- (116) Soma, J.; Papadopoulos, K. *Journal of Colloid and Interface Science* **1996**, 181, 225-231.
- (117) Antonietti, M.; Landfester, K. *Progress in Polymer Science* **2002**, 27, 689-757.
- (118) Rodriguez, V.; El-Aasser, M.; Asua, J.; Silebi, C. *Journal of Polymer Science Part A: Polymer Chemistry* **1989**, 27, 3659-3671.
- (119) Ugelstad, J.; El-Aasser, M.; Vanderhoff, J. *Journal of Polymer Science: Polymer Letters Edition* **1973**, 11, 503-513.
- (120) Hansen, F.; Ugelstad, J. *Journal of Polymer Science: Polymer Chemistry Edition* **1979**, 17, 3069-3082.
- (121) Kim, N.; Sudol, E.; Dimonie, V.; El-Aasser, M. *Macromolecules* **2004**, 37, 2427-2433.
- (122) Aizpurua, I.; Barandiaran, M. *Polymer* **1999**, 40, 4105-4115.
- (123) El-Aasser, M.; Sudol, E. Features of Emulsion Polymerization. In *Emulsion Polymerization and Emulsion Polymers*, 2nd edition; Lovell, P.; El-Aasser, M., Eds.; John Wiley & Sons Ltd: New York, 1997; pp 37-58.
- (124) Schork, F.; Poehlein, G.; Wang, S.; Reimers, J.; Rodrigues, J.; Samer, C. *Colloid and Surfaces A: Physicochemical and Engineering Aspects* **1999**, 153, 39-45.
- (125) Wang, S.; Schork, F. *Journal of Applied Polymer Science* **1994**, 54, 2157-2164.
- (126) Reimers, J.; Schork, F. *Journal of Applied Polymer Science* **1996**, 59, 1833-1841.

Chapter 2: Historical and Theoretical Background

- (127) Mouran, D.; Reimers, J.; Schork, F. *Journal of Applied Polymer Science* **1996**, 34, 1073-1083.
- (128) Tang, P.; Sudol, E.; Adams, M.; El-Aasser, M.; Asua, J. *Journal of Applied Polymer Science* **1991**, 42, 2019-28.
- (129) Alduncin, J.; Forcada, J.; Asua, J. *Macromolecules* **1994**, 27, 2256-2261.
- (130) Choi, Y.; El-Aasser, M.; Sudol, E.; Vanderhoff, J. *Journal of Polymer Science: Polymer Chemistry Edition* **1985**, 23, 2973-2987.
- (131) Unzue, M.; Asua, J. *Journal of Applied Polymer Science* **1993**, 49, 81-90.
- (132) Masa, J.; Arbin, L.; Asua, J. *Journal of Applied Polymer Science* **1993**, 48, 205-213.
- (133) Landfester, K.; Bechthold, N.; Tiarks, F.; Antonietti, M. *Macromolecules* **1999**, 32, 5222-5228.
- (134) Lim, M.-S.; Chen, H. *Journal of Polymer Science Part A: Polymer Chemistry* **2000**, 38 (10), 1818-1827.
- (135) Delgado, J.; El-Aasser, M.; Vanderhoff, J. *Journal of Polymer Science Part A: Polymer Chemistry* **1986**, 24, 861-874.
- (136) Chern, C.; Chen, T. *Colloid and Polymer Science* **1997**, 275, 546 - 554
- (137) Landfester, K.; Betchthold, N.; Tiarks, F.; Antonietti, M. *Macromolecules* **1999**, 32, 2679-2683.
- (138) Chern, C.; Liou, Y. *Polymer* **1999**, 40, 3763-3772.
- (139) Kitzmiller, E.; Miller, C.; Sudol, E.; El-Aasser, M. *Macromolecules Symposia* **1995**, 92, 157-168.
- (140) Asua, J. *Progress in Polymer Science* **2002**, 27, 1283-1346.
- (141) Abismail, B.; Canselier, J.; Wilhelm, A.; Delmas, H.; Gourdon, C. *Ultrasonics Sonochemistry* **1999**, 6, 75-83.
- (142) Wood, R.; Loomis, A. *Philosophical Magazine* **1927**, 4, 417.
- (143) Bechthold, N.; Landfester, K. *Macromolecules* **2000**, 33, 4682-4689.
- (144) Saethre, B.; Mork, P.; Ugelstad, J. *Journal of Polymer Science Part A: Polymer Chemistry* **1995**, 33, 2951-2959.
- (145) Wang, C.; Yu, N.; Chen, C.; Kuo, J. *Journal of Applied Polymer Science* **1996**, 60, 493-501.
- (146) Antonietti, M.; Landfester, K. *Progress in Polymer Science* **2002**, 27 (4), 689-757.
- (147) Ouzineb, K.; Graillat, C.; Mckenna, T. *Journal of Applied Polymer Science* **2005**, 97, 745-752.
- (148) Erdem, B.; Sudol, E.; Dimonie, V.; El-Aasser, M. *Journal of Polymer Science Part A: Polymer Chemistry* **2000**, 38, 4431-4440.
- (149) Wu, X. Q.; Schork, F. J. *Industrial & Engineering Chemistry Research* **2000**, 39 (8), 2855-2865.
- (150) Schork, F.; Luo, Y.; Smulders, W.; Russum, J.; Butte, A.; Fontenot, K. *Advances in Polymer Science* **2005**, 175, 129-255.

Chapter 2: Historical and Theoretical Background

- (151) Schellenberg, C.; Akari, S.; Regenbrecht, M.; Tauer, K.; Petrat, F.; Antonietti, M. *Langmuir* **1999**, 15, 1283-1290.
- (152) Katsumoto, Y.; Ushiki, H.; Mendiboure, B.; Graciaa, A.; Lachaise, J. *Colloid and Polymer Science* **2000**, 278, 905-909.
- (153) Morrison, R.; Boyd, R., *Organic Chemistry*. 3rd edition; Allyn and Bacon: New York, 1973; pp 46-50.
- (154) Moad, G.; Solomon, D. H., *The Chemistry of Free Radical Polymerization*. 2nd edition; Pergamon: Oxford, 1995.
- (155) Van Herk, A. M.; Monteiro, M. Heterogeneous Systems. In *Handbook of Radical Polymerization*, 2nd edition; Matyjaszewski, K.; Thomas, P. D., Eds.; John Wiley & Sons, Inc.: New Jersey, 2003; Vol. 6, pp 301-331.
- (156) Moad, G.; Rizzardo, E.; Thang, S. H. *Australian Journal of Chemistry* **2005**, 58 (6), 379-410.
- (157) Braunecker, W. A.; Matyjaszewski, K. *Progress in Polymer Science* **2007**, 32 (1), 93-146.
- (158) Szwarc, M. *Nature* **1956**, 178 (4543), 1168-1169.
- (159) Szwarc, M. *Journal of Polymer Science Part A: Polymer Chemistry* **1998**, 36 (1), IX-XV.
- (160) Matyjaszewski, K. General Concepts and History of Living Radical Polymerization. In *Handbook of Radical Polymerization*, 2nd edition; Matyjaszewski, K.; Thomas, P. D., Eds.; John Wiley & Sons, Inc.: New Jersey, 2003; Vol. 8, pp 361-406.
- (161) Ganou, Y.; Taton, D. Macromolecular Engineering by Controlled/Living Radical Polymerization. In *Handbook of Radical Polymerization*, 2nd edition; Matyjaszewski, K.; Davis, T. P., Eds.; John Wiley & Sons, Inc.: New Jersey, 2003; Vol. 14, pp 775-844.
- (162) Solomon, D. H.; Rizzardo, E.; Caciolo, P. U. S Patent 4, 581, 429. 1986.
- (163) Solomon, D. H. *Journal of Polymer Science Part A: Polymer Chemistry* **2005**, 43 (23), 5748-5764.
- (164) Wang, J.-S.; Matyjaszewski, K. *Journal of the American Chemical Society* **1995**, 117 (20), 5614-5615.
- (165) Kato, M.; Kamigaito, M.; Sawamoto, M.; Higashimura, T. *Macromolecules* **1995**, 28 (5), 1721-1723.
- (166) Moad, G.; Chiefari, J.; Chong; Krstina, J.; Mayadunne, R. T.; Postma, A.; Rizzardo, E.; Thang, S. H. *Polymer International* **2000**, 49 (9), 993-1001.
- (167) McCormick, C. L.; Lowe, A. B. *Accounts of Chemical Research* **2004**, 37 (5), 312-325.
- (168) Yin, X.; Hoffman, A. S.; Stayton, P. S. *Biomacromolecules* **2006**, 7 (5), 1381-1385.
- (169) Millard, P. E.; Barner, L.; Stenzel, M. H.; Davis, T. P.; Barner-Kowollik, C.; Müller, A. H. E. *Macromolecular Rapid Communications* **2006**, 27 (11), 821-828.
- (170) Chiefari, J.; Rizzardo, E. Control of Free-Radical Polymerization by Chain Transfer Methods. In *Handbook of Radical Polymerization*, 2nd edition; Matyjaszewski, K.; Thomas, P. D., Eds.; John Wiley & Sons, Inc.: New Jersey, 2003; pp 629-690.

Chapter 2: Historical and Theoretical Background

- (171) Chiefari, J.; Chong, Y. K.; Ercole, F.; Krstina, J.; Jeffery, J.; Le, T. P. T.; Mayadunne, R. T. A.; Meijs, G. F.; Moad, C. L.; Moad, G.; Rizzardo, E.; Thang, S. H. *Macromolecules* **1998**, 31 (16), 5559-5562.
- (172) Boschmann, D.; Vana, P. *Macromolecules* **2007**, 40 (8), 2683-2693.
- (173) Zhao, Y.; Perrier, S. *Macromolecular Symposia* **2007**, 248 (1), 94-103.
- (174) Vogt, A. P.; Gondi, S. R.; Sumerlin, B. S. *Australian Journal of Chemistry* **2007**, 60 (6), 396-399.
- (175) Lee, J. M.; Kim, O. H.; Shim, S. E.; Lee, B. H.; Choe, S. *Macromolecular Research* **2005**, 13 (3), 236-242.
- (176) Lowe, A. B.; McCormick, C. L. *Progress in Polymer Science* **2007**, 32 (3), 283-351.
- (177) Rizzardo, E.; Chen, M.; Chong, B.; Moad, G.; Skidmore, M.; Thang, S. H. *Macromolecular Symposium* **2007**, 248, 104-116.
- (178) Monteiro, M. J.; Hodgson, M.; De Brouwer, H. *Journal of Polymer Science Part A: Polymer Chemistry* **2000**, 38 (21), 3864-3874.
- (179) Monteiro, M. J.; de Barbeyrac, J. *Macromolecules* **2001**, 34 (13), 4416-4423.
- (180) Zhou, X.; Ni, P.; Yu, Z. *Polymer* **2007**, 48 (21), 6262-6271.
- (181) Doren, K.; Freitag, W.; Stoye, D., *Water-borne Coatings: The Environmentally-Friendly Alternative*. Hanser: Munich, 1994.
- (182) Stoye, D.; Freitag, W., *Paints, Coatings and Solvents*. 2nd edition; Wiley-VCH: Weinheim, 1998.
- (183) Combellick, W. Barrier Polymers. In *Encyclopedia of Polymer Science and Engineering*, Mark, H.; Bikales, N.; Overberger, C.; Menges, G., Eds.; John Wiley & Sons, Inc.: New York, 1985; Vol. 2, pp 176-192.
- (184) Vandezande, G.; Smith, O.; Bassett, D. Vinyl Acetate Polymerization. In *Emulsion Polymerization and Emulsion Polymers*, Lovell, P.; El-Aasser, M., Eds.; John Wiley & Sons Ltd.: New York, 1997; pp 593-587.
- (185) Delassus, P. Barrier Polymers. In *The Wiley Encyclopedia of Packaging Technology*, 2nd edition; Brody, A.; Marsh, K., Eds.; John Wiley & Sons, Inc.: New York, 1997; pp 71-77.
- (186) Mills, N., *Plastics: Microstructure, Properties and Applications*. Edward Arnold Ltd.: Amsterdam, 1986; pp 225-226.
- (187) Zhang, Z.; Britt, I. J.; Tung, M. A. *Journal of Applied Polymer Science* **2001**, 82 (8), 1866-1872.
- (188) Zhang, Z.; Britt, I. J.; Tung, M. A. *Journal of Polymer Science Part B: Polymer Physics* **1999**, 37 (7), 691-699.
- (189) Sangaj, N.; Malshe, V. *Progress in Organic Coatings* **2004**, 50, 28-39.
- (190) Mogri, Z.; Paul, D. *Polymer* **2001**, 42, 7765-7780.
- (191) Comyn, J., *Polymer Permeability*. Elsevier Applied Science Publishers: New York, 1986.
- (192) Crank, J., *Diffusion in Polymers*. Academic Press: London and New York, 1968.

Chapter 2: Historical and Theoretical Background

- (193) Hu, Y.; Topolkaraev, V.; Hiltner, A.; Baer, E. *Journal of Applied Polymer Science* **2001**, 81 (7), 1624-1633.
- (194) Besenhard, J. O.; Winter, M.; Yang, J.; Biberacher, W. *Journal of Power Sources* **1995**, 54 (2), 228-231.
- (195) Gorrasi, G.; Tortora, M.; Vittoria, V.; Kaempfer, D.; Mulhaupt, R. *Polymer* **2003**, 44 (13), 3679-3685.
- (196) Kumar, S. A.; Yuelong, H.; Yumei, D.; Le, Y.; Kumaran, M. G.; Thomas, S. *Industrial & Engineering Chemistry Research* **2008**, 47 (14), 4898-4904.
- (197) DeLassus, P., Barrier Polymers. In *Encyclopedia of Chemical Technology*, Howe-Grant, M., Ed. John Wiley & Sons, Inc.: New York, 1992; Vol. 3, pp 931-962.
- (198) Stacey, R.; Mary, E. *Polymer* **2004**, 45, 2641-2649.
- (199) Alentiev, A.; Drioli, E.; Gokzhaev, M.; Golemme, G.; Ilinich, O.; Lapkin, A.; Volkov, V.; Yampolskii, Y. *Journal of Membrane Science* **1998**, 138, 99-107.

POLY(STYRENE-CO-BUTYL ACRYLATE)/GRAPHITE NANOCOMPOSITES USING GRAPHITE OXIDE

The work described in this chapter has been submitted to be published in the following paper:

Hussein M. Etmimi and Ronald D. Sanderson, *In situ* intercalation of graphite nanosheets in the synthesis of polymer/graphite oxide nanocomposites using miniemulsion polymerization, submitted to **Polymer** (March, 2012).

Abstract

Poly (styrene-co-butyl acrylate) (poly(St-co-BA)) nanocomposite latices based on graphite oxide (GO) were synthesized using the miniemulsion polymerization process. GO, of various loadings, was dispersed in styrene and n-butyl acrylate monomers and the resultant mixture emulsified in the presence of a hydrophobe (hexadecane) and a surfactant (sodium dodecylbenzene sulfonate) into miniemulsions. The stable miniemulsions thus obtained were polymerized to yield poly(St-co-BA)/GO nanocomposite latices. The focus of this study was to investigate the suitability of miniemulsion polymerization for the synthesis of nanocomposites based on graphite with intercalated or exfoliated structure in a one-step nano-incorporation technique. The morphology and nanostructure (i.e., whether conventional, intercalated or exfoliated) of the synthesized nanocomposite were investigated by transmission electron microscopy (TEM) and X-ray diffraction (XRD) to determine the structure of the nanocomposites. TEM was used to determine the nanocomposite morphology by directly visualizing the latex particles and their films at the nanometer level. XRD was used to confirm the structure of the nanocomposites, i.e., intercalation and/or exfoliation of GO nanosheets within the polymer matrix. The molecular weight of the polymer in the nanocomposites was determined by size exclusion chromatography (SEC). Differential scanning calorimetry (DSC) was used to determine the glass transition temperature (T_g) of poly(St-co-BA) in the nanocomposites. TEM and XRD indicated that the nanocomposites exhibited mainly an intercalated morphology, irrespective of the GO filler loading. SEC showed that the GO concentration had no significant effect on the molecular weight of the polymer in the nanocomposites. DSC showed that all nanocomposites made with various loadings of GO exhibited one T_g , corresponding to poly(St-co-BA).

3.1 Introduction

Recent rapid growth in nanoscience has led to the preparation of polymer nanocomposites with enhanced properties compared to pure polymers. Currently, one of the most advanced research areas of nanotechnology focuses on the inclusion of nanoparticle fillers into polymers in order to enhance the functional and physical properties of polymers. Some of the nanoparticles used to date include nanofibers, silica nanoparticles, carbon nanotubes (CNTs), clays and graphite.¹ Perhaps the most studied is the use of clay, due to its ease of modification and availability. However, because of its unique properties, graphite has become the material of choice in the field of nanoscience and nanotechnology in recent years.^{2,3} Not only do graphite nanosheets provide most of the advantages offered by the nanometer-size fillers but they can be incorporated in both hydrophilic and hydrophobic polymers.⁴⁻⁶ Moreover, graphite is naturally available and thus its use is generally cost effective. The low cost of this material, together with its good mechanical, thermal and barrier properties, offer new possibilities for material development of polymer nanocomposites using graphite nanoparticles.

The properties of polymer nanocomposites based on graphite strongly depend on how well the graphite nanosheets are dispersed in the final nanocomposites.⁷ The preparation of polymer/graphite nanocomposites (PGNs) based on parent graphite is difficult to achieve. Most monomers and polymers can not be easily intercalated between graphene nanosheets in the pristine graphite. This is mainly because there are no reactive groups on the surface of pristine natural graphite. Therefore, natural graphite lacks both the space and affinity for polymer molecules (or monomers) to be intercalated into its galleries. Furthermore, the graphene layers are bound together by Van der Waals forces, which make the interlayer distance in graphite very narrow. However, the synthesis of graphite oxide (GO) from natural graphite creates many oxygen functionalities on its surface, which could greatly facilitate the interaction of monomer and polymer molecules into graphite galleries.⁸ Therefore, GO has been widely used instead of pristine graphite in the synthesis of polymer nanocomposites.⁹

GO is prepared by the oxidation of pristine natural graphite using a strong oxidizing agent such as potassium permanganate in the presence of concentrated mineral acids (e.g., H₂SO₄ or HNO₃). The oxidation of graphite is currently considered one of the most promising methods for the large scale production of graphene nanoplatelets, which can be obtained by exfoliating the GO. The oxidation leaves many new oxygen-containing groups such as epoxide, hydroxyl

and carboxyl groups on the graphene surface. These oxygen groups significantly increase the compatibility between the graphene nanoplatelets in GO and polymers. Therefore, GO can be intercalated by various monomers or polymers to prepare different polymer/GO nanocomposites with improved properties.^{8,9}

There are mainly three methods available for the synthesis of GO, those of Hummers and Offeman,¹⁰ Staudenmaier¹¹ and Brodie.¹² In the Hummers method, H₂SO₄ and KMnO₄ are used as the mineral acid and the oxidizing agent, respectively. In the Staudenmaier and Brodie methods HNO₃ and KClO₃ (or NaClO₃) are used as the acid and oxidizing agent, respectively. In general, these methods achieve similar levels of oxidation, with carbon to oxygen ratios of about 2:1.

Miniemulsion polymerization is well known to be an effective nano-incorporation polymerization method. Various polymer composites based on filler materials such as clay¹³ and CNTs¹⁴ have been successfully prepared using the miniemulsion technique. Miniemulsion offers many advantages over other polymerization methods: it is environmentally friendly, latices with high solids content and high conversion can be obtained, polymers with high molar masses can be prepared, high rates of polymerization are achieved, during polymerization the viscosity remains low, and it is compatible with highly hydrophobic monomers. The advantages of miniemulsion polymerization make it attractive to be used for the synthesis of PGNs.

In this process, the oil phase, which consists of the monomers and the hydrophobe, is dispersed in the water phase, which contains the surfactant, by a high shear device such as a sonicator.¹⁵ The initial dispersion of the graphite nanosheets within the monomer droplets can be achieved by using the high shear device during the miniemulsification process. The use of the high shear device will lead to the exfoliation of graphene nanoplatelets, which is followed by the *in situ* polymerization of monomers in the presence of these exfoliated graphite nanosheets.

3.2 Formation of PGNs

Many studies have focused on understanding the formation of polymer nanocomposites based on graphite. According to the degree of graphite dispersion, the structure of these nanocomposites can be varied to a large extent. Three different morphologies, conventional,

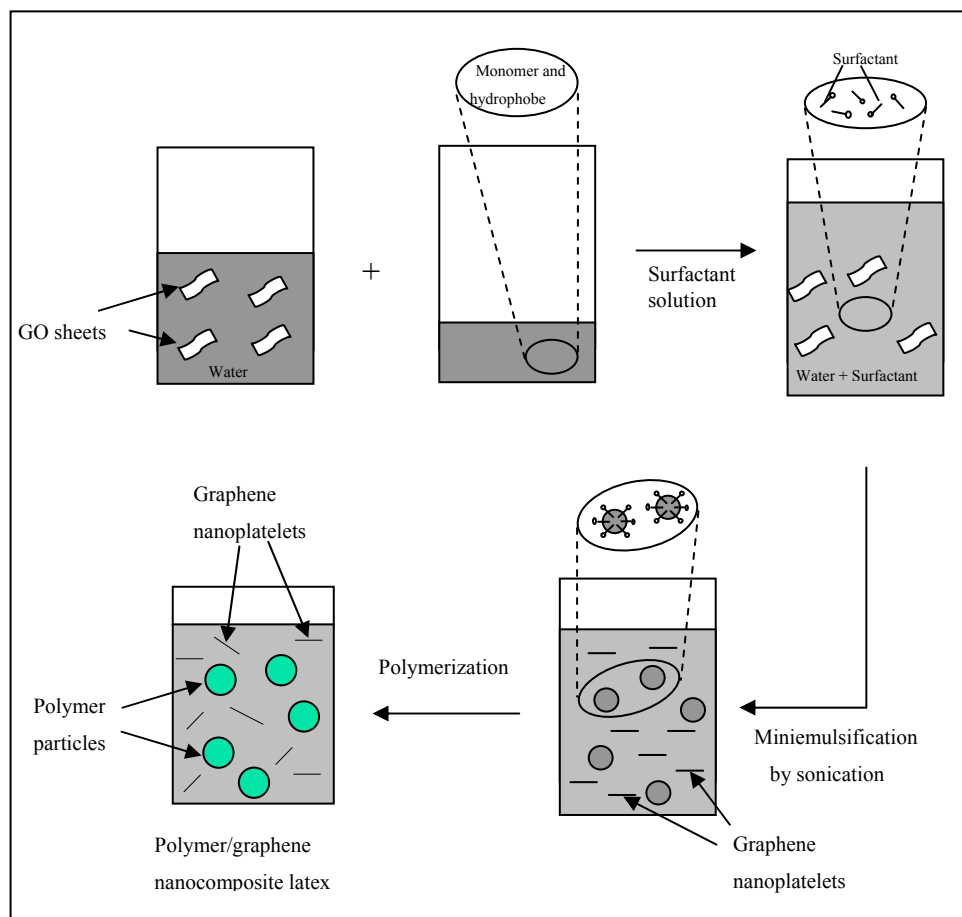
intercalated and exfoliated can be obtained.⁷ These morphologies and structures were discussed in detail in Section 2.1.4.

Various techniques have been used to prepare PGNs: solution mixing (also called exfoliation-adsorption), melt mixing (melt intercalative and/or exfoliation process) and *in situ* methods,^{7,9} of which the most common are solution and melt mixing. These processes were probably the first general methods used to prepare polymer composites based on graphite. The solution process generally involves the mixing of colloidal suspensions of graphite or graphite derivatives, such as GO, with the desired polymer by simple stirring or shear mixing.^{4,5} The resulting composite can be precipitated using a non-solvent for the polymer, which can be then removed by filtration and evaporation.

In melt mixing, the graphite filler and the polymer are mixed in the molten state under high shear conditions. Because there is no solvent used, melt mixing is often considered more economical and is more compatible with many current industrial practices.¹⁶ However, studies suggest that this method does not provide the same level of dispersion of the filler as solvent methods or *in situ* polymerization.¹⁷

PGNs can be also prepared by *in situ* methods, which involve mixing the graphite based fillers with monomer (or monomer mixture), followed by a polymerization process.^{9,18} The same method has been widely used for the synthesis of polymer-clay nanocomposites (PCNs).¹⁹ In recent years, the technique has been successfully applied to polymer composites based on graphite.²⁰ The resulting nanocomposites will have a high level of dispersion of graphite nanosheets, without a prior exfoliation step being required.

In this study, miniemulsion polymerization has been successfully used for the synthesis of polymer nanocomposites based on GO. A schematic representation of the formation of PGNs by miniemulsion polymerization is shown in Scheme 3.1. The GO nanosheets can be added to a mixture of monomer and a hydrophobe for swelling. Surfactant solution is then added, followed by the emulsification process by sonication. The sonication step (i.e., miniemulsification) will lead to the exfoliation of GO nanosheets to thinner graphene nanoplatelets. Upon polymerization, these graphene nanoplatelets will be finely distributed within the polymer matrix, resulting in an intercalated or exfoliated polymer nanocomposite system.



Scheme 3.1: The formation of polymer nanocomposite latices based on GO using miniemulsion polymerization.

This chapter focuses on the synthesis and characterization of poly(styrene-co-butyl acrylate) poly(St-co-BA) nanocomposites using GO in miniemulsion polymerization. The emphasis is on determining the suitability of miniemulsion polymerization for the synthesis of polymer nanocomposite latices based on graphite in a convenient one-step nano-incorporation technique. It is shown that the intercalation of graphene within a polymer matrix will be achieved *in situ* during the miniemulsion process without a prior exfoliation step.

3.3 Experimental

The materials and methods used in the synthesis of the poly(styrene-co-butyl acrylate)/GO (poly(St-co-BA)/GO) nanocomposites and neat poly(St-co-BA) are now described.

3.3.1 Materials

Styrene (St) (99%, Aldrich) and n-butyl acrylate (BA) (99%, Aldrich) were purified by washing with aqueous 0.3 M KOH, followed by distillation at 40 °C under reduced pressure. Sodium dodecylbenzene sulfonate (SDBS) (99%, Fluka) and hexadecane (HD) (99%, Sigma-Aldrich) were used as received. 2,2'-Azobis(isobutyronitrile) (AIBN) (98%) was obtained from Aldrich and purified by recrystallization from methanol. Potassium permanganate (KMnO₄) (99%), sodium nitrate (NaNO₃) (99%) and hydrogen peroxide (H₂O₂) (30%) were obtained from Sigma-Aldrich and used as received. Sulfuric acid (H₂SO₄) (98.08%, Merck) was also used as received. Natural graphite (99.5%) was obtained from Graphit Kropfmühl AG (Hauzenberg, Germany) and used without any further purification. Distilled deionized (DDI) water was obtained from a Millipore Milli-Q water purification system. GO was prepared as described in literature.¹⁰

3.3.2 Preparation of GO from natural graphite

The preparation of GO was done by treating the natural graphite powder with potassium permanganate in the presence of sulfuric acid, following the method of Hummers et al.¹⁰ A mixture of 10 g of powdered flake graphite and 5 g of sodium nitrate was stirred into 230 mL of 98% sulfuric acid. The ingredients were mixed in a 1.5 L jar that was cooled to 0 °C in an ice bath as a safety measure. While maintaining vigorous agitation, 30 g of potassium permanganate was added to the suspension. The rate of addition was carefully controlled to prevent the temperature of the suspension from exceeding 20 °C. The ice bath was then removed and the temperature of the suspension brought to 35 °C, where it was maintained for 30 min. As the reaction progressed, the mixture gradually thickened. After 15 min, the mixture became pasty, with a brownish gray color. After 30 min, 460 mL of water was slowly stirred into the paste, causing a violent reaction and an increase in temperature to 98 °C. The diluted suspension was maintained at this temperature for 15 min. The suspension was then further diluted with ~ 420 mL of warm water and 3% hydrogen peroxide to reduce the residual permanganate and manganese dioxide to colorless soluble manganese sulfate. Upon treatment with the peroxide, the suspension turned bright yellow. The suspension was filtered and a yellow-brown filter cake was obtained. The filtering was conducted while the suspension was still warm to avoid precipitation of the slightly soluble salt of mellitic acid formed as a side reaction. The final solid containing the GO was obtained by centrifugation.

3.3.3 Miniemulsion copolymerization of St and BA in the presence of GO

The following miniemulsion polymerization procedure for the synthesis of poly(St-co-BA)/GO nanocomposite latices was carried out. The GO was dispersed in DDI water by sonication using a Vibracell VCX 750 ultrasonicator (Sonics & Materials Inc.) for 10 min. The sonicator was set at 80% amplitude and a pulse rate of 2.0 sec (energy = ~ 70 kJ). St and BA monomers, HD and AIBN were stirred for 30 min and then added to the GO solution. Surfactant solution (2% SDBS relative to monomer) was added and the mixture was sonicated for 15 min to obtain the miniemulsion latex. A three-neck round-bottomed flask containing the resultant miniemulsion was immersed in an oil bath at room temperature. The content of the flask was purged with nitrogen for 15 min before increasing the temperature to 75 °C to start the polymerization. The reaction was carried out for 6 h under a nitrogen atmosphere, after which it was cooled to room temperature to stop the polymerization.

A similar procedure was followed for the synthesis of a poly(St-co-BA) reference without GO. The oil phase, consisting of St and BA monomers, AIBN (0.009 g) and HD were mixed with an aqueous solution of SDBS for 30 min. The mixture was then sonicated under the same conditions used for the synthesis of poly(St-co-BA)/GO nanocomposites for 15 min to afford the miniemulsion latex. A three-neck round-bottomed flask containing the resultant miniemulsion latex was immersed in an oil bath at room temperature, which was then purged with nitrogen for 15 min. The temperature was increased to 75 °C to start the polymerization and the reaction was carried out for 6 h under a nitrogen atmosphere. The various formulations used for the synthesis of poly(St-co-BA)/GO nanocomposites and the poly(St-co-BA) reference are tabulated in Table 3.1.

Table 3.1: Formulations used in the miniemulsion polymerizations for the preparation of Poly(St-co-BA) and Poly(St-co-BA)/GO nanocomposite latices

Nanocomposite	GO (g)	St (g)	BA (g)	SDBS (g)/10 g DDI water	HD (g)	DDI water (g)
P(St-co-BA)	-	2.71	2.31	0.102	0.077	50.08
P(St-co-BA)/GO-1	0.05	2.71	2.30	0.101	0.066	50.10
P(St-co-BA)/GO-2	0.10	2.71	2.30	0.103	0.067	50.60
P(St-co-BA)/GO-3	0.15	2.70	2.30	0.100	0.070	50.50
P(St-co-BA)/GO-4	0.20	2.73	2.36	0.107	0.075	50.40
P(St-co-BA)/GO-5	0.25	2.72	2.31	0.105	0.066	50.10
P(St-co-BA)/GO-6	0.30	2.70	2.31	0.105	0.071	50.40

3.3.4 Characterization and analytical techniques

Various analytical techniques were used to characterize the GO samples and the poly(St-co-BA)/GO nanocomposites. Nanocomposite samples were obtained from the latices by precipitation. The latex (3 mL) was treated with concentrated hydrochloric acid, the precipitate was washed several times with methanol, then with DDI water, and finally dried at 40 °C under reduced pressure. The analytical instrumentation and procedures used were as follows:

3.3.4.1 Monomer conversion

The monomer conversion in all experiments was determined gravimetrically. Samples were taken from the reaction vessel over time in order to determine the monomer conversion. Monomer conversion was calculated and plotted vs. time for all experiments.

3.3.4.2 Transmission electron microscopy (TEM)

TEM was used to directly visualize the morphology of the poly(St-co-BA)/GO nanocomposites at the nanometer level. Bright-field TEM images were recorded using a LEO 912 Omega TEM instrument (Zeiss, Germany), at an accelerating voltage of 120 kV. Prior to analysis, miniemulsion samples were diluted with DDI water (0.05%) and placed on 300-mesh copper grids, which were then transferred to the TEM apparatus. The average particle size of the synthesized latices was determined using computer software, ImageJ (NIH, USA). A portion of the poly(St-co-BA)/GO miniemulsion latices was dried, then embedded in an epoxy resin, and cured at 60 °C for 24 h. The embedded samples were then ultra-microtomed with a diamond knife on a Reichert Ultracut S ultramicrotome, at room temperature. This resulted in sections with a nominal thickness of approximately 100 nm. The sections were collected on a water surface and transferred to 300-mesh copper grids at room temperature, which were then transferred to the TEM apparatus. TEM was also used to observe the graphite nanosheets after modification (i.e., oxidation process). GO (0.1 g) was dispersed in DDI water (50 g) by sonication. The GO samples were diluted with DDI water (0.05%) and placed on 300-mesh grids for analysis. The average particle size and galleries spacing were calculated using computer software (Image J).

3.3.4.3 Dynamic light scattering (DLS)

DLS was used to determine the particle size of the prepared latices. The measurements were carried out using a Zetasizer ZS 90 (Malvern Instruments, United Kingdom) apparatus equipped with a 4 mW He-Ne laser, operating at a wavelength of 633.0 nm. Miniemulsion samples were first diluted with DDI water before they were analyzed; a drop of the latex was diluted in DDI water (~ 4 mL). The instrument was first calibrated with a nano-standard solution with a particle size of 220 nm, before a latex sample was run. The scattered light was detected at an angle of 90° and the final particle size was obtained from three measurements, each comprising 10–15 sub-runs. The particle size was calculated via a CONTIN analysis and presented as the Z-average particle size (Z_{avg}).

3.3.4.4 Fourier-transform infrared (FT-IR) spectroscopy

FT-IR spectra were obtained using a Nexus 470 FT-IR spectrophotometer (Thermo Nicolet, USA), and recorded by averaging 32 scans. All spectra were acquired from 450 to 4000 cm^{-1} by using an attenuated total reflectance unit at a resolution of 4 cm^{-1} .

3.3.4.5 Nuclear magnetic resonance (NMR) spectroscopy

^1H NMR spectroscopy was performed at 20 °C using a Varian VXR-Unity 300 MHz instrument. Nanocomposite samples (30 mg) were dissolved in 2 mL of deuterated chloroform (CDCl_3) by stirring overnight. All chemical shifts are reported in ppm downfield from tetramethylsilane, which was used as an internal standard ($\delta = 0$ ppm).

3.3.4.6 X-ray diffraction (XRD)

XRD patterns were obtained using a X'Pert PRO multi-purpose diffractometer (PANalytical B.V., The Netherlands) equipped with a Cu K (alpha) sealed tube X-ray source (wavelength 1.514 Å). X'Celerator in Bragg-Brentano mode was used as the detector for all analyses.

3.3.4.7 Differential scanning calorimetry (DSC)

DSC was used for the measurement of temperatures and heat flows associated with the phase transitions of the polymer in the nanocomposites. Measurements were carried out on a Q 100 DSC instrument (TA Instruments, USA). The analysis was done by heating samples of less than 10 mg from -40 °C to 250 °C at a heating rate of 10 °C/min, which were then cooled

from 250 °C to -40 °C, followed by a second heating step. All measurements were conducted under a nitrogen atmosphere, and at a purge gas flow rate of 50 mL/min. The DSC curves were obtained from the second heat cycle.

3.3.4.8 Scanning electron microscope (SEM)

SEM was used to observe the nanostructure of graphite flakes before and after the oxidation. Imaging of the samples was accomplished using a field emission gun SEM instrument (FEI Nova NanoSEM) equipped with an Oxford X-Max EDS detector (University of Cape Town). The graphite samples were carefully mounted on the top of the SEM tub with double-sided carbon tape. The samples were then coated with a thin layer of gold in order to make the sample surface electrically conducting. Images were recorded between 500× and 10000× magnification, at 7 kV voltage, with a working distance of ~ 13 mm.

3.3.4.9 Thermogravimetric analysis (TGA)

TGA measurements were carried out on a Q500 thermogravimetric analyzer (TA Instruments, USA). Sample sizes of less than 15 mg were used for all analyses. Analyses were carried out from ambient temperature to 600 °C, at a heating rate of 20 °C/min, under a nitrogen atmosphere (nitrogen purged at a flow rate of 50 mL/min).

3.3.4.10 Size exclusion chromatography (SEC)

SEC was carried out using a Waters 610 Fluid Unit, Waters 410 Differential Refractometer at 30 °C, Waters 717plus Autosampler and Waters 600E System Controller (run by Millennium 32 V3.05 software). Tetrahydrofuran (THF) (HPLC grade), sparged with IR grade helium, was used as an eluent at a flow rate of 1 mL/min. Two PLgel 5- μ m Mixed-C columns and a PLgel 5- μ m guard pre-column were used. The column oven was kept at 35 °C and the injection volume was 100 μ l. The system was calibrated with narrow PS standards (5 mg/mL THF), ranging from 2 500 to 898 000 g mol⁻¹. The nanocomposite samples were dissolved in THF (5 mg/mL) over a period of 24 h and then filtered through a 0.45 μ m nylon filter. All molar mass data are reported as equivalent to the linear PS standards.

3.4 Results and discussion

3.4.1 Characterization of GO

3.4.1.1 FT-IR analysis

The chemical changes occurring upon the treatment of graphite with potassium permanganate in the presence of sulfuric acid were detected by FT-IR spectroscopy. Similar results recorded for the FT-IR spectra of GO films have been found in literature.^{21,22} Figure 3.1 shows the FT-IR spectra for the natural graphite and its oxidized form (GO). The assignment of the main FT-IR peaks of GO films and their comparison with data found in the literature are summarized in Table 3.2. Compared with the pristine graphite (Figure 3.1 a), the FTIR spectra of GO (Figure 3.1 b) clearly shows the characteristic peaks of GO such as the stretching vibration of hydroxyl group (-OH), the stretching vibration of C=O from carbonyl and carboxylic groups, the vibration of O-H and the vibration of C-O centered at 3288, 1715, 1384 and 1041 cm^{-1} , respectively.²¹

The peaks at 2158 and 1615 cm^{-1} in Figure 3.1 b are attributed to carbon dioxide and the deformation vibration of water molecules in the sample, respectively.^{21,23} The appearance of these oxygen-containing functional groups suggests that successful oxidation of the graphite was achieved. Furthermore, the C=C bonds were not detected (see Figure 3.1 b), most probably due to the strong oxidant KMnO_4 used. This indicates the complete oxidation of natural graphite. The peaks at 1658 and 1540 cm^{-1} correspond to the stretching of C=C bonds of natural graphite.²¹

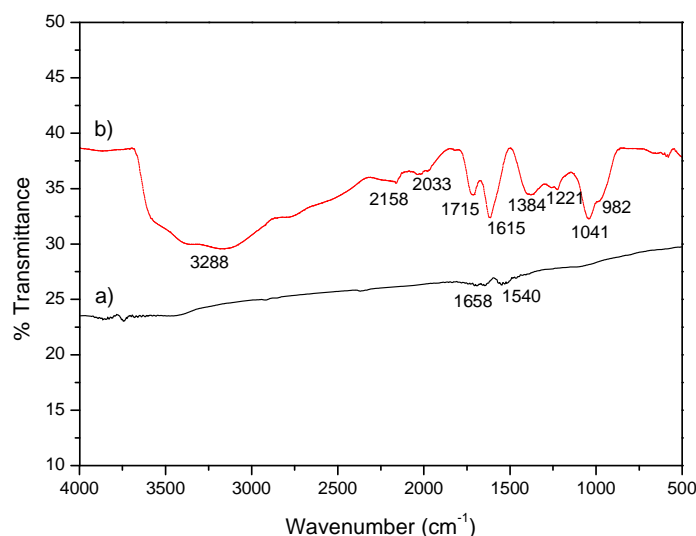


Figure 3.1: FT-IR spectrum of (a) natural graphite and (b) its oxidized form (GO).

Table 3.2: Assignment of the main FT-IR peaks of GO films and their comparison with data in the literature.

Functional group	Titelman et al. ²¹ (cm ⁻¹)	Paredes et al. ²² (cm ⁻¹)	This study (cm ⁻¹)
The stretching vibration of hydroxyl groups	3391	3430	3288
The stretching vibration of carboxyl groups on the edges of the layer planes or conjugated carbonyl groups	1731	1726	1715
The deformation vibration of water molecules	1622	1666	1615
The stretching vibrations of C=C bonds from unoxidized graphitic domains	absent	1588	absent
The vibration of O–H	1361	absent	1384
The vibration of covalent sulfates	1225	1226*	1221
The vibration of C–O	1053	1103	1041
Epoxy group	987	absent	982

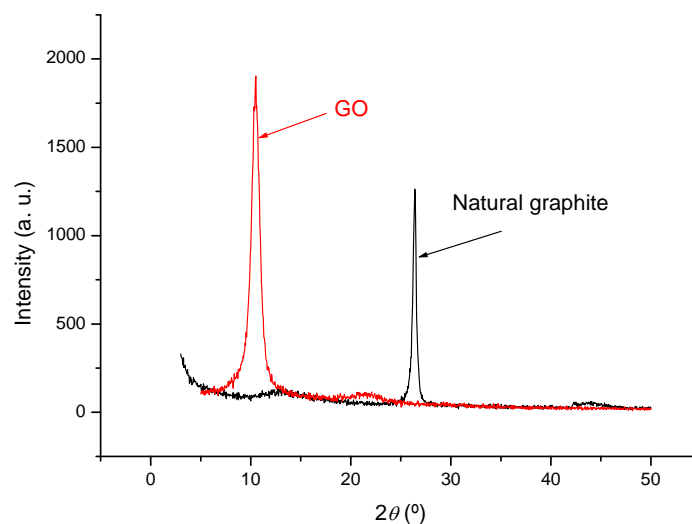
* They attributed this to C–OH stretching vibrations

3.4.1.2 XRD measurements

Functionalization of graphite is expected to modify the average interlayer distance (commonly known as d-spacing) of stacked graphene. Figure 3.2 shows the XRD pattern for natural graphite and GO. An increase in the d-spacing between graphite sheets was observed. For pristine graphite, a sharp reflection peak at $2\theta = 26.4^\circ$ in the XRD scattering pattern, originating from the interlayer (002) spacing ($d = 0.34$ nm), is observed. Upon oxidation, the characteristic peak of natural graphite at $2\theta = 26.4^\circ$ could no longer be detected and the GO exhibited only one peak at a lower 2θ value of 10.5° . This indicates that the interlayer distance between neighboring graphene layers in GO has increased (they are ~ 0.84 nm apart), because of the intercalation by oxygen-containing groups and moisture.²⁴ The fact that the XRD pattern for GO exhibited only one peak suggests that a highly oxidized GO sample was synthesized. The average d-spacing of natural graphite and GO were calculated using the Bragg law and are listed in Table 3.3.

Table 3.3: The average interlayer distances of natural graphite and GO

XRD data	Graphite	GO
2θ (°)	26.4	10.5
d-spacing (nm)	0.34	0.84

**Figure 3.2: XRD results of natural graphite and its oxidized form (GO).**

3.4.1.3 Thermal analysis by TGA

TGA measures the weight loss of a material due to the presence of volatile groups as a function of temperature. The loss in weight is attributed to the thermal degradation of functional species as the temperature increases. Figure 3.3 shows the TGA plot of natural graphite and its oxidized form (GO). GO differs from pristine graphite in that it has many polar functional groups on its surface. Hence, GO is thermally less stable than natural graphite. This is shown in the onset and maximum degradation temperatures of natural graphite and GO samples in Figure 3.3. One can see that graphite is thermally stable over the temperature range up to 600 °C, while GO shows a three-step degradation pathway.

This is in agreement with previous reports in the literature for GO,^{22,25,26} which indicate that the main weight loss of $\sim 30\%$ takes place around 200 °C. This is attributed to the decomposition of labile oxygen-containing functional groups present in the GO, giving rise to CO, CO₂, H₂O and carbon.^{27,28} There is also a mass loss of about 15% below 100 °C, which can be attributed to the removal of adsorbed water. The slower steady weight loss ($\sim 10\%$) over the temperature range 300–600 °C can be assigned to the removal of more stable oxygen functionalities on GO.²²

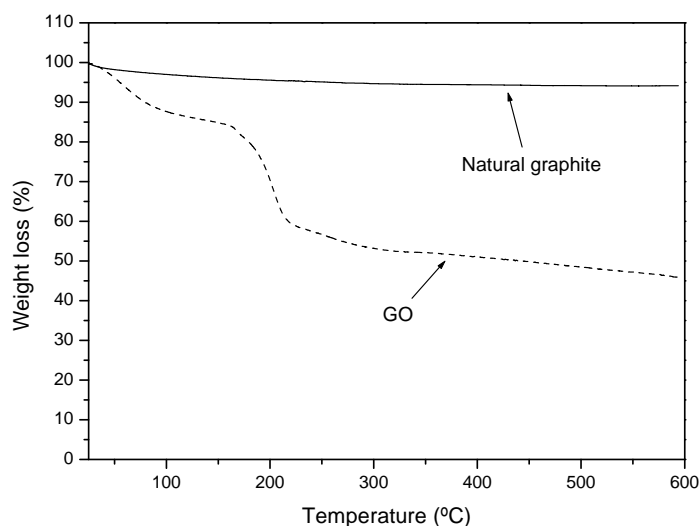


Figure 3.3: TGA thermograms of natural graphite and GO.

3.4.1.4 Thermal analysis by DSC

Figure 3.4 shows the DSC curves of pristine graphite and GO samples obtained under N_2 atmosphere. The GO sample shows one exothermic peak at 220 °C, which is caused by the decomposition of the organic groups on the GO sheets. Jimenez²⁹ showed that the thermal decomposition of GO under inert atmosphere results in the formation of new compounds, including CO , CO_2 and H_2O . No exothermic peak was observed for the pristine graphite sample because there are no functional groups on its surface. This indicates that the natural graphite has been successfully oxidized and functionalized with oxygen-containing groups such as epoxy, $-OH$ and $-COOH$, as determined by FT-IR previously.

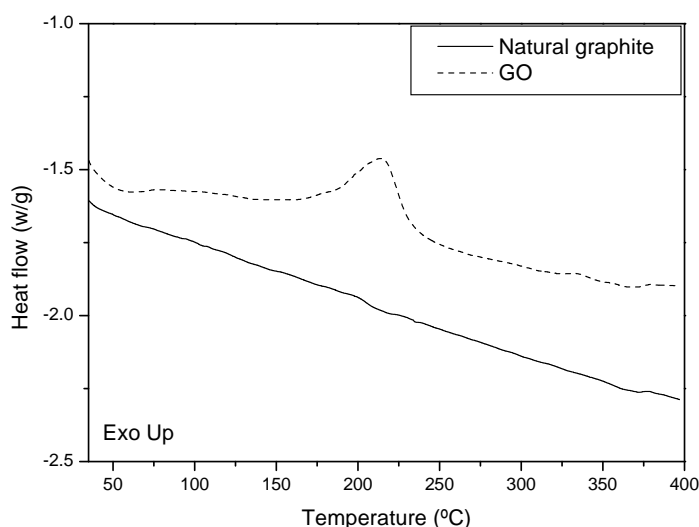


Figure 3.4: DSC curves of graphite and GO.

3.4.1.5 Nanostructure of GO by SEM and TEM

The dispersion of pristine natural graphite within a polymer matrix is very difficult due to the close packing of the graphene layers. Figure 3.5 shows SEM images of the natural graphite flakes, showing graphite particles with sizes in the micrometer range. The graphene sheets within pristine graphite have dimensions on the order of 5–10 μm in length and 500 nm in thickness. However, after oxidation the particle size of the graphite sheets is reduced considerably due to the effect of the oxidation process. The size of GO nanosheets has been reduced to nanometer scale (see Figure 3.6). From XRD analysis (Figure 3.2 and Table 3.3), it can be seen that the interlayer spacing between graphene nanoplatelets has increased considerably for GO. The natural graphite resulted in an intense d_{002} diffraction peak indicating that the graphene layers are arranged in an ordered structure with 0.34 nm spacing. On the other hand, GO exhibited one peak at lower 2θ of 10.5° with interlayer distance of 0.84 nm).

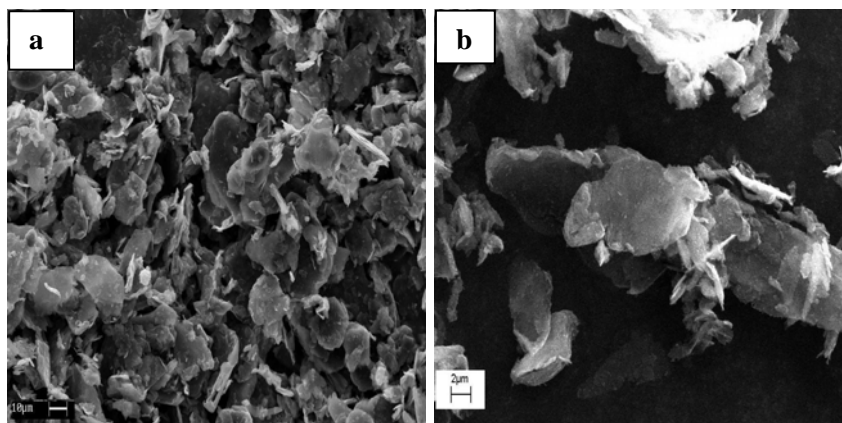


Figure 3.5: SEM images of natural graphite: a) at low magnification and b) at high magnification.

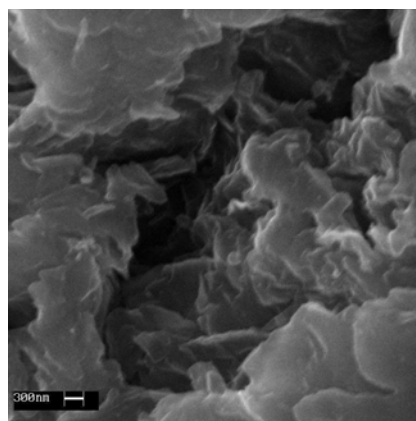


Figure 3.6: SEM images of GO at high magnification.

The GO nanosheets were also observed by TEM (dispersed in water) at the nanometer level (see Figure 3.7). The TEM images clearly show that the thick graphite sheets consist of thinner nanosheets, with sizes in the nanometer level.

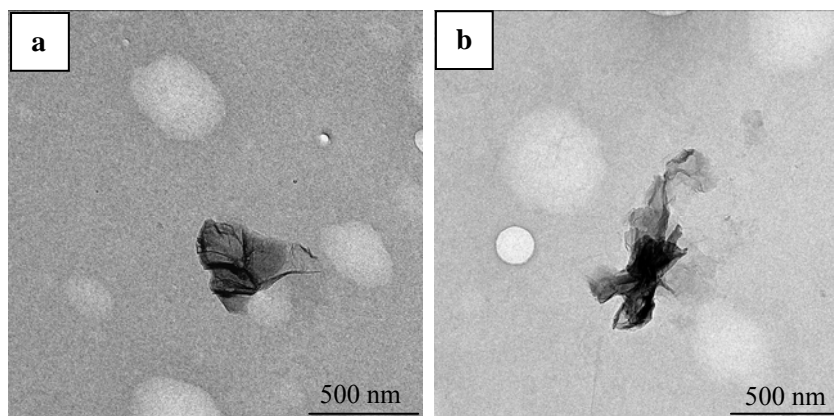


Figure 3.7: TEM images showing a) thinner nanosheets of GO and b) different area of the same sample of GO.

3.4.2 Characterization of the nanocomposite latices

3.4.2.1 Monomer conversion and latex stability

Figure 3.8 shows the monomer conversion of the miniemulsion polymerization of St and BA in the presence of different quantities of GO. For comparison, monomer conversion for St and BA monomers in the absence of GO is also shown in Figure 3.8. AIBN was used as the initiator and the polymerization was carried out at 75 °C. All latices prepared were stable and polymerization reactions proceeded with high final monomer conversions (70–98%). Moreover, it is noted that all reactions had similar polymerization rates and there was no significant effect of GO loading on the rate of polymerization. This findings are similar to those of other researchers, who investigated the effect of other filler content, such as clay, on the monomer conversion in the preparation of PCNs. Moraes et al.³⁰ observed no difference in conversion with an increase in clay loading after they investigated the synthesis of poly(St-co-BA) via miniemulsion polymerization.

Figure 3.9 shows digital photographs of the latices that were prepared using different GO contents (1 and 5 wt%). A photograph of the poly(St-co-BA) latex that was made without GO (Figure 3.9 a) is also shown for comparison. The color of the latices varied from white for the latex made with no GO to light blue for the latex made with 1 wt% GO. The latex made with

higher loading of GO (5 wt%) exhibited a dark gray color (see Figure 3.9 c). The images were taken ~ 5 months after the latices were prepared. The images clearly show that all latices were stable, even after a long period of time.

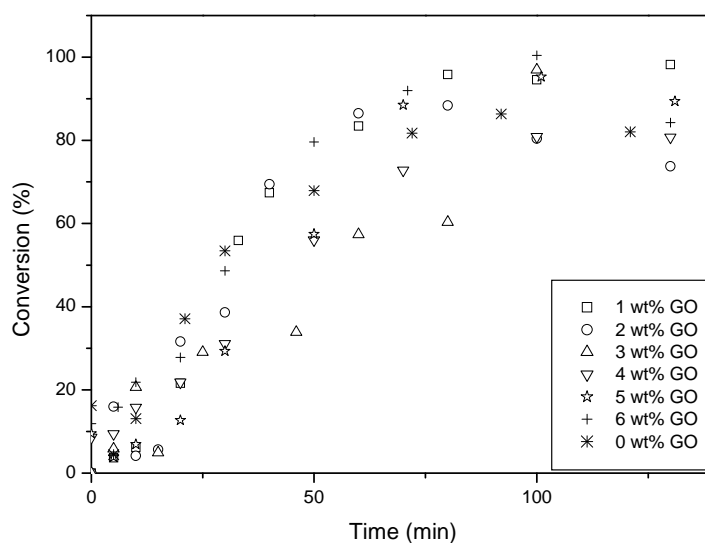


Figure 3.8: Monomer conversion of the miniemulsion polymerization of St and BA in the presence of different GO content (0–6 wt%).

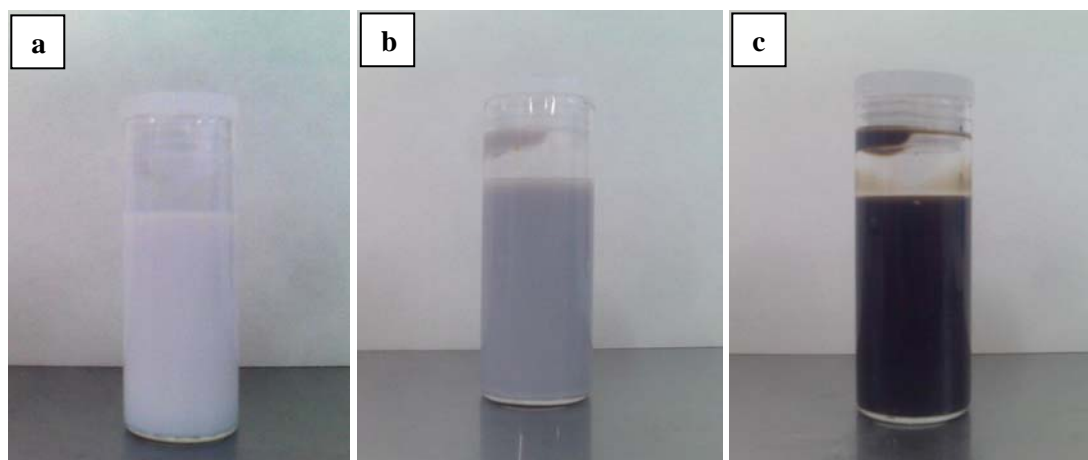


Figure 3.9: Digital photographs showing poly(St-co-BA) miniemulsion latices: a) latex without GO, b) latex containing 1 wt% GO and c) latex containing 5 wt% GO.

3.4.2.2 FT-IR analysis of nanocomposites

Although FT-IR spectroscopy is the most widely used technique in the characterization of polymers, the use of this technique for the analysis of polymer nanocomposites can be very difficult.³¹ In the case of polymer nanocomposites made with GO the analysis is complicated due to the presence of the GO particles in the nanocomposite. Table 3.4 shows the main absorption bands that can be seen in the FT-IR spectra of GO, pure poly(St-co-BA) and

poly(*St-co-BA*)/GO nanocomposites. The actual FT-IR spectra of pure poly(*St-co-BA*) and poly(*St-co-BA*)/GO nanocomposites (containing 1 and 5 wt% GO) are shown in Appendix A.

Evidence of the formation of poly(*St-co-BA*)/GO nanocomposites was obtained by comparing the FT-IR main absorption bands of pure poly(*St-co-BA*) with that of poly(*St-co-BA*)/GO nanocomposites. The vibration bands at 3000–3600, 1715 and 1047 cm^{-1} are associated with –OH, C=O and C–O of GO, respectively.²¹ The adsorption bands at 1727 cm^{-1} and the bands in the range 3090–3026 cm^{-1} are associated with C=O and hydrogen atoms attached to aromatic groups (Ar–H) of poly(*St-co-BA*), respectively.³² It can be seen that all the components of the nanocomposite materials were present in the final product. All the expected bands of GO and poly(*St-co-BA*) are seen in the FT-IR spectrum of the poly(*St-co-BA*)/GO nanocomposites, confirming the formation of poly(*St-co-BA*) nanocomposites containing GO.

Table 3.4: FT-IR data of GO, poly(*St-co-BA*) and poly(*St-co-BA*)/GO nanocomposites

Functional group	GO (cm^{-1})	Poly(<i>St-co-BA</i>) (cm^{-1})	Poly(<i>St-co-BA</i>)/GO nanocomposite (cm^{-1})
–OH	3000–3600	-	3000–3600
C=O	1715	-	1728
C–O	1047	-	1061
>C–C<	-	1022, 753	1022, 754
C–H	-	2920, 2847	2926, 2851
C=O	-	1727	1732
Ar–H	-	3090, 3061, 3026	3069, 3030
–CH ₂ –	-	1492, 1448	1496, 1447

3.4.2.3 Chemical composition of poly(*St-BA*) nanocomposites as determined by NMR spectroscopy

The polymerization of *St* and *BA* was carried out in the presence of GO. Poly(*St-co-BA*) reference without GO was also prepared under similar conditions to those employed for the synthesis of the nanocomposites. The composition of the poly(*St-co-BA*) and poly(*St-co-BA*)/GO nanocomposites was analyzed using ¹H NMR spectroscopy. The ¹H NMR spectra of pure poly(*St-co-BA*) and poly(*St-co-BA*) in the nanocomposites (synthesized at different GO loadings) are shown in Figure 3.10. The peaks at 6.71 and 7.26 ppm are due to the resonance

of aromatic protons of the phenyl groups from St units, while the peak at 0.88 ppm is due to the methyl group of the BA units.³³ The copolymer composition was calculated from the area of the peaks of St and BA units based on the following equation:

$$\text{PS\%} = \frac{A/n}{A/n + B/m} \times 100 \quad (3.1)$$

where: PS% is the percentage of PS in the copolymer, A and B are the integrated area of St and BA, while n and m are the numbers of protons in the integrated peaks of St and BA, respectively. The amount of St and BA in the nanocomposites as calculated from Equation 3.1 is tabulated in Table 3.5. The ¹H NMR spectra of pure poly(St-co-BA) and poly(St-co-BA) in the nanocomposites (synthesized at different GO loadings) showing all the integrated peaks are shown in Appendix B. The composition of all nanocomposites is very close to the amounts of St and BA (54.1 wt% St and 45.9 wt% BA) that were added to the initial formulation.

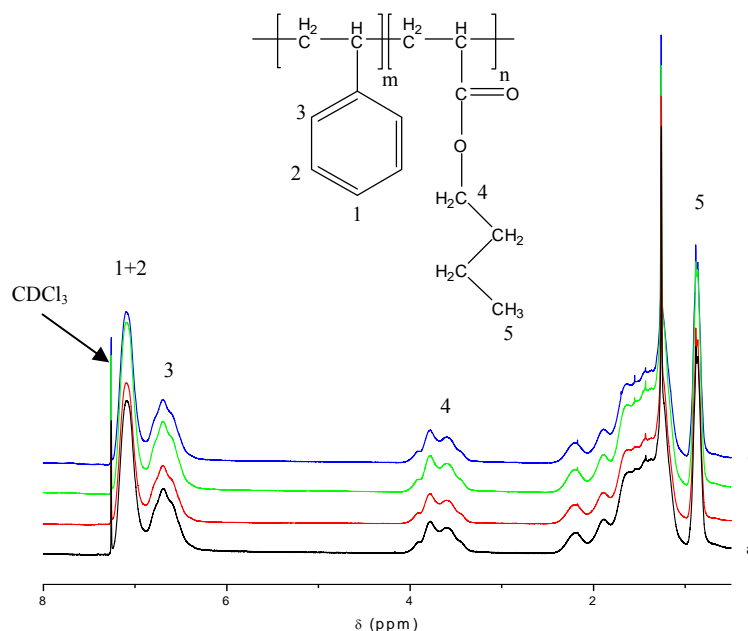


Figure 3.10: ¹H NMR spectra of poly(St-co-BA) nanocomposites with different GO content: a) 0 wt% GO, b) 1 wt% GO, c) 3 wt% GO and d) 5 wt% GO.

Table 3.5: The amount of St and BA in the nanocomposites as calculated from ^1H NMR

Nanocomposite	GO content (wt%)	St%	BA%
P(St-co-BA)	0	54.0	46.0
P(St-co-BA)/GO-1	1	53.0	47.0
P(St-co-BA)/GO-3	3	53.3	46.7
P(St-co-BA)/GO-5	5	54.0	46.0

3.4.2.4 Effect of GO loading on molecular weight of poly(St-co-BA)

Table 3.6 tabulates the molecular weights (weight average molecular weight, \bar{M}_w and number average molecular weight, \bar{M}_n) and dispersity (\mathcal{D}) of the poly(St-co-BA) reference and poly(St-co-BA)/GO nanocomposites prepared using different quantities of GO. Table 3.6 shows that all the synthesized polymers have relatively high molecular weights. This is common for polymers prepared by miniemulsion polymerization and can be attributed to the limitation of diffusion of propagating species during the polymerization step (i.e., confinement effect).³⁴ The viscosity inside the polymer particles increases as the polymerization progresses, therefore the movement of propagating species will become extremely slow, leading to reduced termination.

Table 3.6: \bar{M}_n , \bar{M}_w and \mathcal{D} of poly(St-co-BA) nanocomposites prepared using different quantities of GO (0–6 wt%)

Nanocomposite	GO content (wt%)	\bar{M}_n (g/mol)	\bar{M}_w (g/mol)	\mathcal{D}
P(St-co-BA)	0	7.10×10^5	1.53×10^6	2.16
P(St-co-BA)/GO-1	1	6.62×10^5	1.54×10^6	2.33
P(St-co-BA)/GO-2	2	7.22×10^5	1.63×10^6	2.26
P(St-co-BA)/GO-3	3	9.13×10^5	1.81×10^6	2.00
P(St-co-BA)/GO-4	4	6.10×10^5	1.41×10^6	2.32
P(St-co-BA)/GO-5	5	8.08×10^5	1.79×10^6	2.22
P(St-co-BA)/GO-6	6	7.65×10^5	1.62×10^6	2.12

No significant effect of the GO concentration on the molar mass of the polymer in the nanocomposites was observed. As the GO loading increased, the nanocomposites had similar molecular weights. Increasing the GO content also had no effect on the \mathcal{D} values, which

remained effectively constant with different GO loadings. The similarities between the polymers synthesized in the presence of different GO loadings is important since this implies that any changes in the nanocomposite properties are due to the GO content and not fundamentally due to differences in the polymer matrix.

3.4.3 Nanocomposite morphology

3.4.3.1 XRD analysis

Figure 3.11 shows XRD patterns of poly(St-co-BA) nanocomposites made with different quantities of GO relative to monomer. XRD proved that the final structure of the nanocomposites is influenced by the GO filler content in the nanocomposites. The structure of the nanocomposites changed significantly when the amount of GO in the nanocomposite increased. Therefore, nanocomposites made with different GO loadings have different XRD patterns depending on the quantity of GO incorporated into the sample. However, the nanostructure showed mainly an intercalated morphology, as revealed by the XRD results in Figure 3.11. This is evident from the appearance of a broad peak at a 2θ value between 7 and 10° . The broad peak at $2\theta = 20^\circ$ observed in the XRD scattering pattern corresponds to poly(St-co-BA) (amorphous halo) in the nanocomposites.³⁵

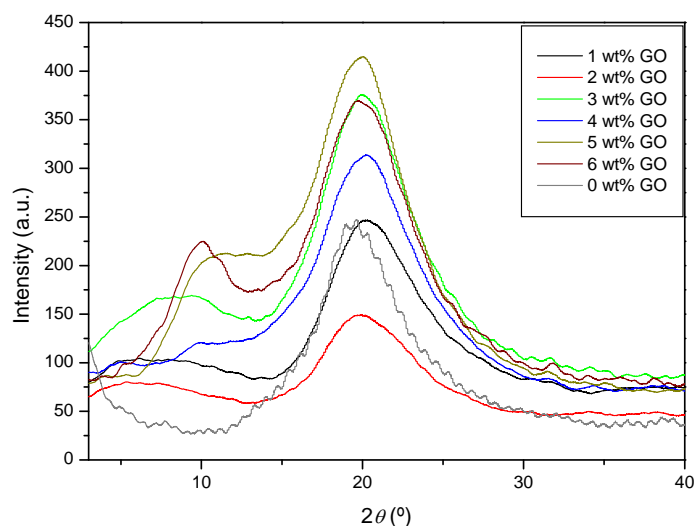


Figure 3.11: XRD patterns of neat poly(St-co-BA) (0 wt% GO) and poly(St-co-BA)/GO nanocomposites made with different quantities of GO (1–6 wt%).

XRD indicates that in all nanocomposites, the graphene nanoplatelets in GO have been intercalated by the polymer molecules. The broad peak at $2\theta = 6\text{--}8^\circ$ appearing for the

nanocomposites at relatively low GO content (1–4 wt%) indicated that an intercalated structure was obtained. The average interlayer distances of the GO in these nanocomposites are in the range 1.1–1.5 nm, which is greater than that of the pure GO (0.84 nm). However, in the case of nanocomposites with relatively higher GO content (5 and 6 wt%) a more defined peak appeared at $2\theta = 10^\circ$, corresponding to an intercalated structure with more graphene order. The interlayer distance of GO in these nanocomposite measured about 0.88 nm, which is also greater than that for pure GO. This indicates that the nanocomposites prepared with lower GO content had more intercalated structure (less graphene order). This can be explained by the fact that when the GO content is high (i.e., 5 and 6 wt%), the GO nanosheets tend to recombine in stacks of GO, leading to more ordered material (less broad XRD peak).

3.4.3.2 TEM analysis

TEM was used to observe the morphology of the synthesized poly(St-co-BA)/GO nanocomposites at the nanometer level. The TEM images in Figure 3.12 show the poly(St-co-BA)/GO latices containing 1 and 2 wt% GO relative to monomer. The images show polymer particles with sizes ranging from 60 to 100 nm, which is in the typical range of a miniemulsion polymerization (50–500 nm). The particle size distribution is narrow, which is an indication that no secondary particle nucleation occurred during the polymerization. The GO nanosheets could not be seen in the TEM images in Figure 3.12, except few areas where GO nanosheets are seen around the polymer particles. The absence of the graphene sheets in the latex suggests that most of these GO nanosheets were encapsulated in the polymer particles. However, a few GO nanosheets were unable to enter the polymer particles and bridged the particles in the so-called linked particle formation.

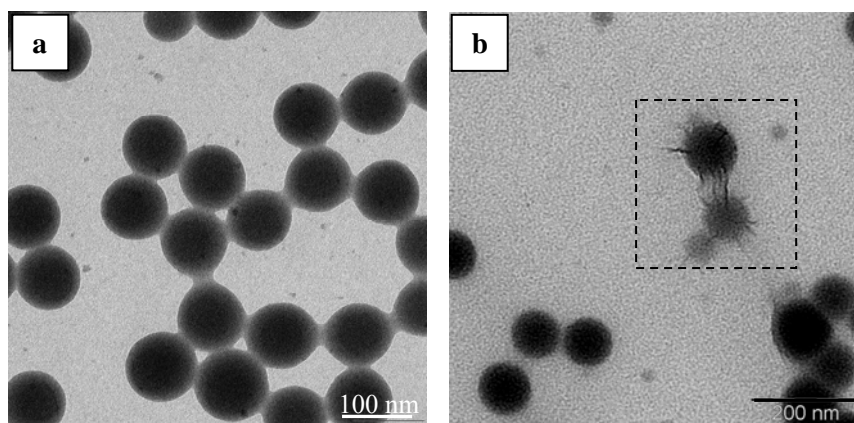


Figure 3.12: TEM images of poly(St-co-BA)/GO nanocomposite latices made with a) 1 and b) 2 wt% GO relative to monomer.

Figure 3.13 shows lattices that were made with higher GO concentration relative to monomer, i.e., 4 and 5 wt% GO. The TEM images show that the lattices had relatively broad particle size distribution and more small particles started to appear at higher GO concentrations. These small particles are most likely caused by secondary nucleation, which will result in the formation of polymer particles with different sizes.³⁶ It can also be seen that some of the polymer particles are partially deformed due to the film drying that occurred during the TEM analysis. The observed particle deformation most probably occurred during the sample preparation due to the low T_g of the poly(St-co-BA) copolymer. This could also be caused by melting of the copolymer under the electron beam of the TEM instrument.³⁷ Polymer particles can undergo radiation beam damage or melting when exposed to the high energy electron beam of TEM.^{38,39}

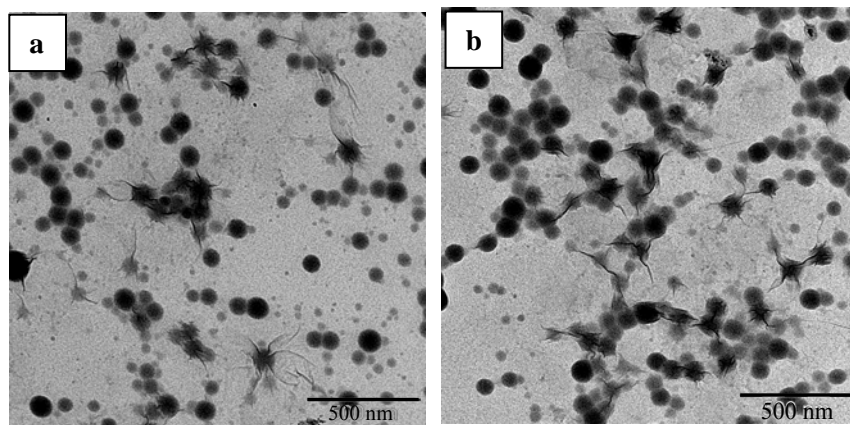


Figure 3.13: TEM images of poly(St-co-BA)/GO nanocomposite lattices made with a) 4 and b) 5 wt% GO.

The GO nanosheets are seen in the TEM images as dark lines attached to the polymer particles (see Figure 3.13). The larger amount of GO nanosheets will result in more aggregates of GO nanosheets. These aggregated GO sheets will not be able to enter the particles, so they will be distributed around the polymer particles. The polymer particles tend to link together to house the GO aggregates as shown in Figure 3.13. The GO nanosheets form the link between these miniemulsion particles, leading to the formation of linked polymer particles. These morphologies could have a significant effect on the overall stability of the synthesized lattices. In recent studies, clay has been successfully used as a stabilizer of polymer particles. Bon and Colver⁴⁰ investigated the use of clay particles as a stabilizer for a variety of hydrophobic monomers (i.e., styrene, lauryl (meth) acrylate, butyl (meth)acrylate, octyl acrylate, and 2-ethyl hexyl acrylate) synthesized via miniemulsion polymerization. The study showed that the clay-stabilized miniemulsion polymerization yielded armored lattices, in which the surface of

the particles was covered with clay discs. The GO nanosheets could have the same effect on the stability of polymer particles, resulting in stable polymer particles.

Table 3.7 shows the particle size analysis of the latices made with different GO concentrations, as measured by DLS. Changing the amount of GO did not significantly affect the average particle size of the synthesized latex particles. This is to be expected since most of the GO nanosheets are distributed outside the polymer particles. Therefore, an increase in the GO loading will not have any significant effect on the size of the synthesized polymer particles.

Table 3.7: Average particle size of nanocomposite latices made with different quantities of GO (0–6 wt%) obtained from DLS

Nanocomposite	GO loading (wt%)	Average particle size (nm)
P(St-co-BA)	0	73
P(St-co-BA)/GO-1	1	62
P(St-co-BA)/GO-2	2	69
P(St-co-BA)/GO-3	3	72
P(St-co-BA)/GO-4	4	74
P(St-co-BA)/GO-5	5	71
P(St-co-BA)/GO-6	6	72

TEM results for the microtomed films cast from the nanocomposite latices indicated that the nanocomposite films had an intercalated morphology (in agreement with XRD analysis). Figures 3.14 and 3.15 show the TEM images of the dried films obtained from the latices, which contain 1 and 2 wt%, and 3 and 4 wt% GO relative to monomer, respectively. The dark lines represent the GO nanosheets and the polymer matrix appears as relatively bright domains. In some areas the GO dispersed as thin layers of graphene nanoplatelets in the polymer matrix, leading to the formation of a highly intercalated structure.

However, most of the films exhibited stacking of graphene nanoplatelets, which indicates that the GO did not disperse very well in the polymer system. This suggests that the nanocomposites exhibited mainly intercalated morphology at GO loading of 1–4 wt%. (in agreement with XRD results in Figure 3.11).

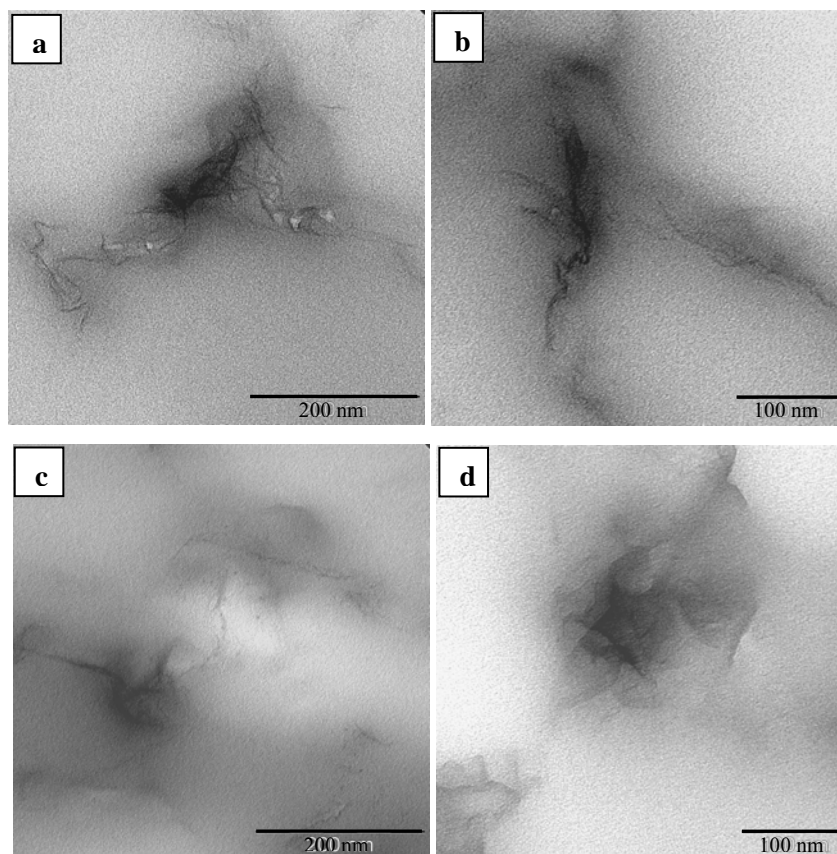


Figure 3.14: TEM images of poly(St-co-BA)/GO nanocomposites at different magnifications: a) and b) 1 wt% GO loading, and c) and d) 2 wt% GO loading.

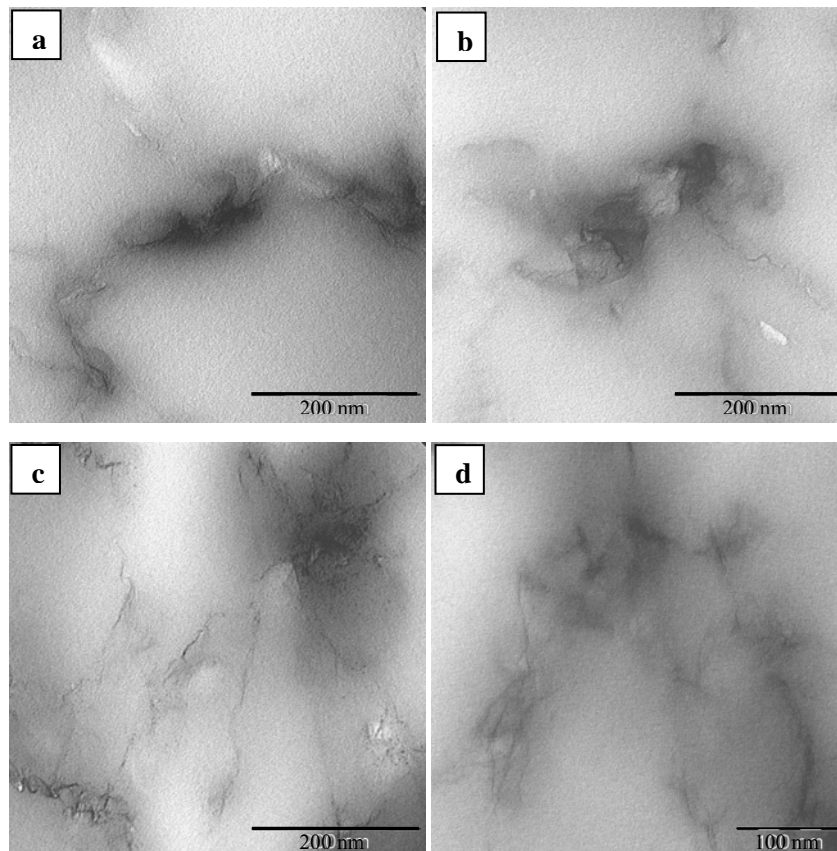


Figure 3.15: TEM images of poly(St-co-BA)/GO nanocomposites at different magnifications: a) and b) 3 wt% GO loading, and c) and d) 4 wt% GO loading.

The TEM images of poly(St-co-BA)/GO nanocomposites made with 5 and 6 wt% GO content are shown in Figure 3.16. The images indicate that most of the graphene nanoplatelets in GO stacked in an orderly manner, which exhibited a more defined intercalated morphology. The lighter areas are representative of the polymer, while the darker areas represent the dense stacks of graphene nanoplatelets in GO. This is also evident from the results of XRD analysis of these nanocomposites, which showed a less broad peak (see Figure 3.11, 5 and 6 wt% GO).

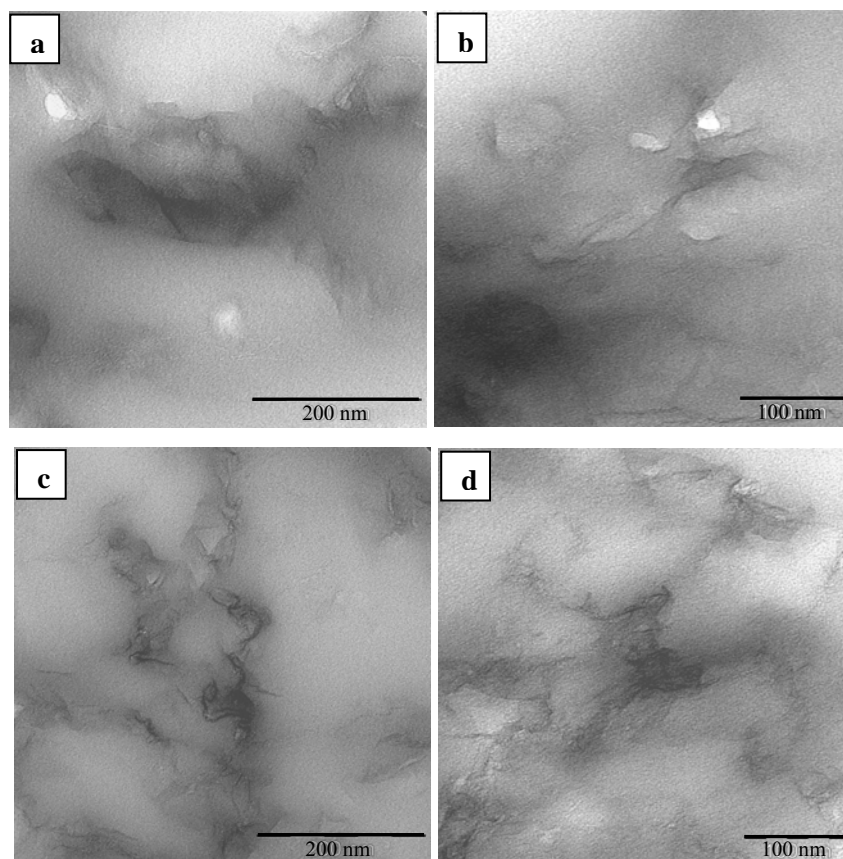


Figure 3.16: TEM images of poly(St-co-BA)/GO nanocomposites at different magnifications: a) and b) 5 wt% GO loading, and c) and d) 6 wt% GO loading.

3.4.3.4 The amount of GO incorporated in the nanocomposites as determined by TGA

Figure 3.17 displays the TGA weight loss curves of poly(St-co-BA) and the poly(St-co-BA)/GO nanocomposites made with different GO concentrations. There is no significant weight loss of the pure poly(St-co-BA) copolymer below 380 °C. The thermal degradation of neat poly(St-co-BA) copolymer only occurs in one step above 380 °C. On the other hand, in the TGA of poly(St-co-BA)/GO nanocomposites there is an obvious weight loss stage between 190 and 380 °C, which can be attributed to GO. The decomposition behavior of GO is shown as an insertion in Figure 3.17. The GO alone starts to decompose at about 160 °C

and its residue at 550 °C is about 47 wt%. The weight loss of GO between 30 and 100 °C corresponds to the removal of water from the interlayers of graphene. The weight loss of GO in the temperature range 190–600 °C is attributed to the decomposition of oxygen-containing groups of GO.²²

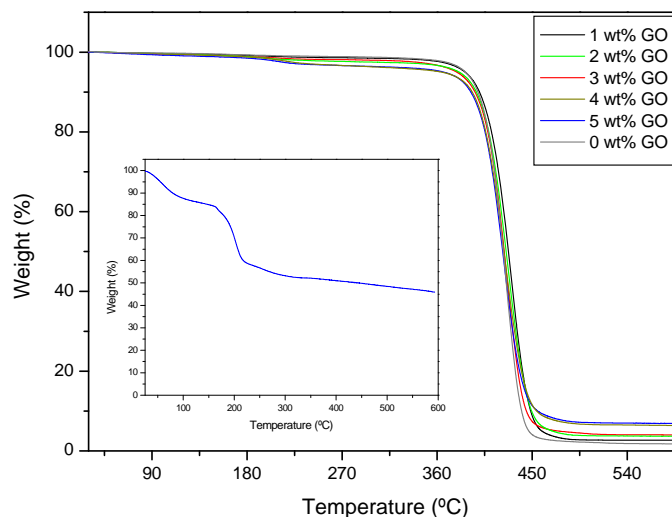


Figure 3.17: TGA thermograms of Poly(*St-co-BA*)/GO nanocomposites made with different quantities of GO. The insertion shows the TGA thermogram of GO.

The weight percentage of GO in a sample was determined from the residual weight difference between the neat poly(*St-co-BA*) copolymer and the poly(*St-co-BA*)/GO nanocomposites containing different contents of GO at 550 °C.⁴¹ Table 3.8 summarizes the TGA data of the neat poly(*St-co-BA*) and the poly(*St-co-BA*)/GO nanocomposites, as determined by TGA. Results showed that at 550 °C, when the residue of pure copolymer is 1.80%, the charred residue of the nanocomposites is increased at increasing GO loadings. This indicates that introducing GO into the nanocomposites enhances the formation of char on the surface of the polymer. Consequently, it reduces the rate of decomposition of the nanocomposites. The nanocomposite containing 1 wt% GO has a weight loss of 97%, while the nanocomposite which contains 5 wt% GO exhibited less weight loss of 93%.

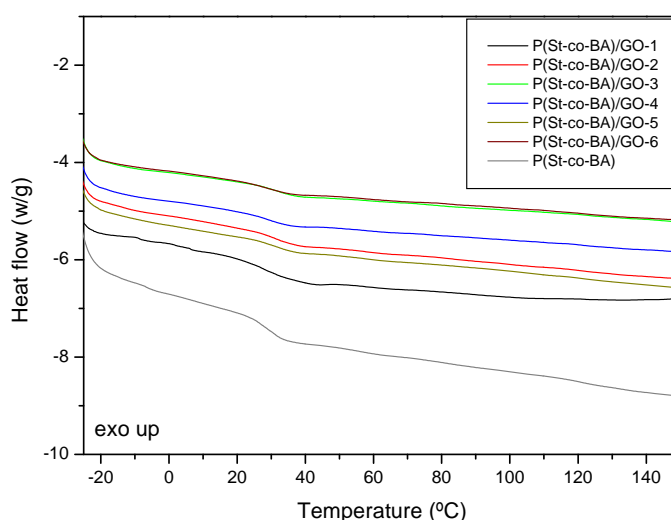
The amount of GO char (i.e., wt%) in the nanocomposites was found to be slightly lower than the nominal GO amount that was added. This was attributed to the fact the GO nanosheets, which were incorporated in the nanocomposites are highly oxidized, as indicated by FT-IR analysis (see Figures 3.1). As shown in Figure 3.17, the GO loses ~ 50% of its weight at 550 °C, which is attributed to the degradation of its oxygen-containing groups.²² The GO will, therefore, ‘burn’ at high temperature, leading to the observed difference in char residue.

Table 3.8: The initial GO content added and the quantities of GO in the nanocomposites determined from TGA analysis

Nanocomposite	Nominal GO added (wt%)	Weight loss at 550 °C (%)	Char (%)	Actual GO content (wt%)
P(St-co-BA)	-	98.20	1.8	-
P(St-co-BA)/GO-1	1	97.35	2.65	0.85
P(St-co-BA)/GO-2	2	96.27	3.73	1.93
P(St-co-BA)/GO-3	3	95.92	4.08	2.30
P(St-co-BA)/GO-4	4	95.82	4.20	2.50
P(St-co-BA)/GO-5	5	93.57	6.43	4.63

3.4.3.5 Glass transition temperature of poly(St-co-BA) in the nanocomposites as determined by DSC

The DSC second heating curves of all synthesized poly(St-co-BA) nanocomposites are shown in Figure 3.18. All nanocomposites exhibited one T_g , which corresponds to the T_g of the poly(St-co-BA) copolymer made without GO. This suggests that all the monomers are incorporated in the copolymer and no homopolymerization of St or BA occurred. The T_g of all nanocomposites containing different GO loadings are summarized in Table 3.9.

**Figure 3.18: DSC thermograms of poly(St-co-BA) reference and poly(St-co-BA)/GO nanocomposites with different GO content (1–6 wt%).**

As the amount of GO was increased, no significant change in the T_g of the polymer in the nanocomposites was observed. This was attributed to the fact that the obtained nanocomposites had only intercalated morphologies. The GO nanosheets are arranged in stacks of graphene nanoplatelets and not totally distributed in the nanocomposites.⁴² Wang and Pan⁴³ reported that the intercalation of monomer, followed by *in situ* polymerization, occurred during the emulsion polymerization of methyl methacrylate in the presence of GO. The authors observed that the mechanical properties of the composites decreased as the content of GO increased. They attributed this phenomenon to the fact that the obtained composites had only intercalated structure.

Table 3.9: T_g of poly(*St-co-BA*) and poly(*St-co-BA*)/GO nanocomposites prepared with different GO content (1–6 wt%).

Nanocomposite	GO content (wt%)	T_g (°C)
P(<i>St-co-BA</i>)	-	31.0
P(<i>St-co-BA</i>)/GO-1	1	29.0
P(<i>St-co-BA</i>)/GO-2	2	31.0
P(<i>St-co-BA</i>)/GO-3	3	32.0
P(<i>St-co-BA</i>)/GO-4	4	28.0
P(<i>St-co-BA</i>)/GO-5	5	29.0
P(<i>St-co-BA</i>)/GO-6	6	27.0

3.5 Conclusion

Poly(*St-co-BA*) nanocomposite lattices containing intercalated graphite nanosheets were successfully synthesized using miniemulsion polymerization as a one-step nano-incorporation technique. Graphite was functionalized by oxidation to obtain graphite oxide (GO). GO nanosheets were intercalated during the miniemulsification step followed by miniemulsion polymerization of *St* and *BA*. The polymerization proceeded to relatively high monomer conversion and produced stable nanocomposite lattices. This is new in terms of the combination of miniemulsion polymerization and graphene nanoplatelets obtained from GO.

FT-IR results confirmed the formation of poly(*St-co-BA*)/GO nanocomposites with various quantities of GO (1–6 wt%). The chemical composition of the nanocomposites was studied by NMR spectroscopy. The degree of graphene dispersion was determined by XRD and TEM.

TEM was used to directly visualize the particles at the nanometer level to obtain their particle morphology and size. XRD indicated the formation of intercalated nanocomposites irrespective of the amount of GO relative to monomer. Examination of the nanocomposites by TEM proved the formation of an intercalated morphology. Particle size was also measured using DLS, the results of which showed good agreement with TEM analysis. Results showed that GO loading had no effect on the size of the latex particles produced. DSC showed that the poly(St-co-BA) copolymer in the nanocomposites exhibited a similar T_g , which was not a function of GO loading.

3.6 References

- (1) Mai, Y.-W.; Yu, Z.-Z., *Polymer Nanocomposites*. 2nd edition; Woodhead Publishing: Cambridge, 2006.
- (2) Stankovich, S.; Dikin, D. A.; Dommett, G. H. B.; Kohlhaas, K. M.; Zimney, E. J.; Stach, E. A.; Piner, R. D.; Nguyen, S. T.; Ruoff, R. S. *Nature* **2006**, 442 (7100), 282-286.
- (3) Geim, A. K.; Novoselov, K. S. *Nature Materials* **2007**, 6 (3), 183-191.
- (4) Zheng, W.; Wong, S.-C. *Composites Science and Technology* **2003**, 63 (2), 225-235.
- (5) Zheng, W.; Wong, S.-C.; Sue, H.-J. *Polymer* **2002**, 73 (25), 6767-6773.
- (6) Xu, J.; Hu, Y.; Song, L.; Wang, Q.; Fan, W.; Liao, G.; Chen, Z. *Polymer Degradation and Stability* **2001**, 73 (1), 29-31.
- (7) Meng, Y. Polymer/graphite nanocomposites. In *Polymer Nanocomposites*, 2nd edition; Mai, Y.-W.; Yu, Z.-Z., Eds.; Woodhead Publishing: Cambridge, 2006; Vol. 19, pp 510-539.
- (8) Kim, H.; Abdala, A. A.; Macosko, C. W. *Macromolecules* **2010**, 43 (16), 6515-6530.
- (9) Potts, J. R.; Dreyer, D. R.; Bielawski, C. W.; Ruoff, R. S. *Polymer* **2011**, 52 (1), 5-25.
- (10) Hummers, W. S.; Offeman, R. E. *Journal of the American Chemical Society* **1958**, 80, 1339.
- (11) Staudenmaier, L. *Berichte der Deutschen Chemischen Gesellschaft* **1898**, 31, 1481-1487.
- (12) Brodie, B. C. *Philosophical Transactions of the Royal Society of London, Series A* **1859**, 149, 249-259.
- (13) Samakande, A.; Sanderson, R. D.; Hartmann, P. C. *Journal of Polymer Science Part A: Polymer Chemistry* **2008**, 46 (21), 7114-7126.
- (14) Lu, H. F.; Fei, B.; Xin, J. H.; Wang, R. H.; Li, L.; Guan, W. C. *Carbon* **2007**, 45 (5), 936-942.
- (15) Sudol, E.; El-Aasser, M. Miniemulsion Polymerization. In *Emulsion Polymerization and Emulsion Polymers*, Lovell, P.; El-Aasser, M., Eds.; John Wiley & Sons Ltd.: New York, 1997; pp 699-722.
- (16) Paul, D. R.; Robeson, L. M. *Polymer* **2008**, 49 (15), 3187-3204.
- (17) Kim, H.; Miura, Y.; Macosko, C. W. *Chemistry of Materials* **2010**, 22 (11), 3441-3450.

- (18) Lee, Y. R.; Raghu, A. V.; Jeong, H. M.; Kim, B. K. *Macromolecular Chemistry and Physics* **2009**, 210 (15), 1247-1254.
- (19) Sinha Ray, S.; Okamoto, M. *Progress in Polymer Science* **2003**, 28 (11), 1539-1641.
- (20) Fim, F. d. C.; Guterres, J. M.; Basso, N. R. S.; Galland, G. B. *Journal of Polymer Science Part A: Polymer Chemistry* **2010**, 48 (3), 692-698.
- (21) Titelman, G. I.; Gelman, V.; Bron, S.; Khalfin, R. L.; Cohen, Y.; Bianco-Peled, H. *Carbon* **2005**, 43 (3), 641-649.
- (22) Paredes, J. I.; Villar-Rodil, S.; Martinez-Alonso, A.; Tascon, J. M. D. *Langmuir* **2008**, 24 (19), 10560-10564.
- (23) Uhl, F. M.; Wilkie, C. A. *Polymer Degradation and Stability* **2004**, 84 (2), 215-226.
- (24) Hontoria-Lucas, C.; López-Peinado, A. J.; López-González, J. d. D.; Rojas-Cervantes, M. L.; Martín-Aranda, R. M. *Carbon* **1995**, 33 (11), 1585-1592.
- (25) Stankovich, S.; Dikin, D. A.; Piner, R. D.; Kohlhaas, K. A.; Kleinhammes, A.; Jia, Y.; Wu, Y.; Nguyen, S. T.; Ruoff, R. S. *Carbon* **2007**, 45 (7), 1558-1565.
- (26) Becerril, H. A.; Mao, J.; Liu, Z.; Stoltenberg, R. M.; Bao, Z.; Chen, Y. *ACS Nano* **2008**, 2 (3), 463-470.
- (27) Wang, G.; Yang, Z.; Li, X.; Li, C. *Carbon* **2005**, 43 (12), 2564-2570.
- (28) Lurf, A.; He, H.; Forster, M.; Klinowski, J. *The Journal of Physical Chemistry B* **1998**, 102 (23), 4477-4482.
- (29) Jimenez, P. S. V. *Materials Research Bulletin* **1987**, 22 (5), 601-608.
- (30) Moraes, R. P.; Santos, A. M.; Oliveira, P. C.; Souza, F. C. T.; do Amaral, M.; Valera, T. S.; Demarquette, N. R. *Macromolecular Symposia* **2006**, 245-246 (1), 106-115.
- (31) Young, R. J., *Introduction to Polymers*. 2nd edition; Chapman and Hall Ltd: London, 1981; pp 138-140.
- (32) Zou, M.; Wang, S.; Zhang, Z.; Ge, X. *European Polymer Journal* **2005**, 41 (11), 2602-2613.
- (33) You, B.; Wen, N.; Cao, Y.; Zhou, S.; Wu, L. *Polymer International* **2009**, 58 (5), 519-529.
- (34) Crespy, D.; Landfester, K. *Beilstein Journal of Organic Chemistry* **2010**, 6, 1132-1148.
- (35) Zhang, R.; Hu, Y.; Xu, J.; Fan, W.; Chen, Z. *Polymer Degradation and Stability* **2004**, 85 (1), 583-588.
- (36) Saethre, B.; Mork, P. C.; Ugelstad, J. *Journal of Polymer Science Part A: Polymer Chemistry* **1995**, 33 (17), 2951-2959.
- (37) Tiarks, F.; Landfester, K.; Antonietti, M. *Langmuir* **2001**, 17, 908-918.
- (38) Chen, Y.; Dimonie, V.; El-Aasser, M. *Macromolecules* **1991**, 24 (13), 3779-3787.
- (39) Dimonie, V.; Daniels, E.; Shaffer, O.; El-Aasser, M. Control of Particle Morphology. In *Emulsion Polymerization and Emulsion Polymers*, Lovell, P.; El-Aasser, M., Eds.; John Wiley and Sons Ltd.: New York, 1997; pp 293-326.
- (40) Bon, S. A. F.; Colver, P. J. *Langmuir* **2007**, 23 (16), 8316-8322.

Chapter 3: Poly(Styrene-co-butyl acrylate)/graphite oxide nanocomposites

- (41) Greesh, N.; Hartmann, P. C.; Cloete, V.; Sanderson, R. D. *Journal of Colloid and Interface Science* **2008**, 319 (1), 2-11.
- (42) Donghwan, C.; Sangyeob, L.; Gyeongmo, Y.; Hiroyuki, F.; Lawrence, T. D. *Macromolecular Materials and Engineering* **2005**, 290 (3), 179-187.
- (43) Wang, W.-P.; Pan, C.-Y. *Polymer Engineering and Science* **2004**, 44 (12), 2335-2339.

POLY(STYRENE-CO-BUTYL ACRYLATE)/GRAPHITE NANOCOMPOSITES USING FUNCTIONALIZED GRAPHITE OXIDE

The work described in this chapter has been published in the following paper:

Hussein M. Etmimi and Ronald D. Sanderson, New approach to the synthesis of exfoliated polymer/graphite nanocomposites by miniemulsion polymerization using functionalized graphene, **Macromolecules**, Vol. 44 (21), 8504–8515 (2011) (DOI: 10.1021/ma2003008)

Abstract

A new method is described for the synthesis of exfoliated polymer nanocomposites made with modified graphite oxide (GO) using a miniemulsion polymerization technique. GO was synthesized and then modified with a reactive surfactant, 2-acrylamido-2-methyl-1-propane sulfonic acid (AMPS), which widened the gap between the graphene layers and facilitated monomer intercalation into the GO nanogalleries. The AMPS-modified GO was emulsified in the presence of styrene and n-butyl acrylate monomers, a surfactant (sodium dodecylbenzene sulfonate), and a hydrophobe (hexadecane). The stable miniemulsions were polymerized to afford encapsulated poly(styrene-co-butyl acrylate) (poly(St-co-BA))/GO nanocomposite latex particles. The exfoliated structure of the nanocomposites was confirmed by X-ray diffraction (XRD) and transmission electron microscopy (TEM). TEM revealed that GO nanosheets were largely exfoliated (about 2–5 nm thick) in the resultant films obtained from the synthesized nanocomposite latices. Examination of the nanostructure of the obtained nanocomposites by XRD analysis confirmed the formation of exfoliated GO nanoplatelets. The thermal stability and mechanical properties of the nanocomposites were evaluated by thermogravimetric analysis (TGA) and dynamic mechanical analysis (DMA). TGA showed that all the prepared nanocomposites exhibited enhanced thermal stability relative to the neat poly(St-co-BA) copolymer. DMA also revealed that the glass transition temperature of poly(St-co-BA) in the nanocomposites increased significantly in the presence of modified GO relative to the pure copolymer. Furthermore, the nanocomposites had improved storage and loss modulus only at relatively high GO content (i.e., 5 and 6 wt% relative to monomer).

4.1 Introduction

Graphite is naturally abundant and well known to be a layered material with unique and unusual properties.^{1,2} It is a pseudo-two-dimensional solid with sp^2 -hybridized carbon atoms arranged in a hexagonal pattern within each layer. These layers, known as graphene,³ are organized in the ABAB alternating stacking sequence, with strong covalent bonding between the carbon atoms in the same graphene layers. Thus, cleavage of the bonds between the carbon atoms among these layers is very difficult. This results in graphene nanoplatelets having very high strength as well as good mechanical properties in the same plane.^{4,5} On the contrary, the weak van der Waals interactions acting between the graphene layers makes the cleavage of bonds between these layers very easy. Therefore, graphite can be converted into high aspect ratio (length-to-thickness ratio) reinforcement platelets with nanometer-scale thickness through a process of intercalation and exfoliation.⁶

Pristine unmodified graphite cannot be easily dispersed in a polymer matrix.⁷ Thus, there are very few reports of polymer nanocomposites based on pristine natural graphite.⁸ This is because there are no reactive groups on the natural graphene layers, which makes it difficult for organic molecules or monomers to be loaded on its surface. In addition, graphene layers lack the affinity and space for hydrophilic or hydrophobic molecules and polymers to intercalate into its galleries. Hence, pristine graphite is usually functionalized and exfoliated in order to be used for the synthesis of polymer nanocomposites.^{3,9} Oxidation of graphite followed by exfoliation, either by rapid thermal expansion¹⁰ or by ultrasonic dispersion,¹¹ is one approach that can be used to obtain functionalized and exfoliated graphite sheets. The first synthesis of such modified graphite sheets was described by Brodie in 1859.¹² Today there are three main methods for the preparation of graphite oxide (GO) from natural graphite – as described by Brodie,¹² Staudenmaier¹³ and, more recently, Hummers and Offeman.¹⁴ Each method is based on the oxidation of graphite in the presence of a strong concentrated mineral acid (e.g., sulfuric acid) and strong oxidizing agent (e.g., potassium permanganate).

The oxidation chemistry of graphite is similar to that used to functionalize carbon nanotubes (CNTs) and results in a variety of oxygen-containing functionalities (e.g., epoxide, $-OH$ and $-COOH$), at different sites on the graphite surface.⁹ It is generally believed that the epoxide and hydroxyl functional groups are located in the basal planes of the graphene sheets, while the edges of these sheets are functionalized with carbonyl and carboxyl groups.¹⁵⁻¹⁸ After oxidation, GO still possesses a layered structure, but it is much lighter in color than pristine

graphite due to the loss of electronic conjugation during the oxidation step. The oxygen-containing functionalities alter the chemistry of the graphite sheets and render them hydrophilic, thus facilitating their hydration and exfoliation in aqueous media.¹⁹ As a result, GO easily forms stable colloidal dispersions of thin graphene oxide nanoplatelets in water.²⁰⁻²² The nanometer-scale sheets and galleries in the final GO, caused by the exfoliation process, as well as the oxygen groups on the edges and borders of sheets (generated by chemical oxidation), create favorable conditions that allow for suitable polymers (water soluble polymers) to intercalate and form polymer/GO nanocomposites.²³ However, water insoluble (hydrophobic) monomers or polymers such as polystyrene (PS) and poly(methyl methacrylate) (PMMA) cannot be easily intercalated between GO layers.²⁴ This is because the GO nanosheets are hydrophilic,¹⁹ and therefore incompatible with hydrophobic monomers or polymers.²⁵ Thus, the compatibility between the GO nanosheets and the monomers or polymers selected for use needs be enhanced.

In a recent study, Hu et al.²⁶ reported the use of GO for the synthesis of PS nanocomposites by *in situ* emulsion polymerization. The authors showed that this could be a promising route for the production of composite materials based on graphite with improved thermal stability. However, during the synthesis procedure the GO was reduced to graphite using hydrazine hydrate, which decreased the hydrophilic nature of graphite sheets, leading to better compatibility with monomer. In another study, Wang and Pan²⁴ reported that the intercalation of monomer, followed by *in situ* polymerization, occurred during the emulsion polymerization of methyl methacrylate in the presence of GO. The authors observed that the mechanical properties of the composites (i.e., notched Izod impact strength and tensile strength) decreased as the content of GO increased from 1 to 8 wt%. They attributed this phenomenon to the low compatibility of GO with PMMA, which resulted in composites with intercalated structure. They also showed that the amount of PMMA that grafted onto GO was very small, and the surface properties of GO were little improved.

Graphite-derived materials such as GO have been widely used as fillers for the preparation of polymer nanocomposites to improve their mechanical, thermal and electrical properties.^{25,27-29} Methods such as solution blending,³⁰ exfoliation–adsorption,³¹ melt intercalation,³² and *in situ* intercalation³³ polymerization have been used to prepare such nanocomposites. However, there are still many challenges (e.g., the preparation method) that must be addressed before such nanocomposites can reach their full potential. Although significant success has been achieved in the preparation of polymer/graphite nanocomposites (PGNs) using *in situ*

polymerization of the monomer in the presence of graphite,^{28,33,34} there are only few reports on the preparation of these nanocomposites in emulsion systems. In particular, the use of miniemulsion polymerization has not been investigated for the synthesis of such nanocomposites.

Miniemulsion polymerization can be a very useful method for the preparation of latex particles on nanoscale made with nanofiller materials such as graphite. This is due to the initial dispersion of the polymerization reaction components, which can be directly polymerized into polymer particles. In the miniemulsion process, the oil phase, which consists of the monomer and the filler, can be dispersed in the water phase by a high-shear device such as a sonicator. This will lead to the formation of monomer droplets containing the nanofiller particles and stabilized by the surfactant and the hydrophobe from which polymer particles will develop during the polymerization step.³⁵ In various studies, miniemulsion polymerization was successfully used for the incorporation of filler compounds such as clay³⁵ and CNTs³⁶ within a polymer matrix. These studies showed that miniemulsion could be used as an effective method for the synthesis of polymer nanocomposites with improved properties.

In an emulsion system there are three possible nucleation mechanisms for the growing oligomeric radical species: micellar, homogeneous (water phase) and, less often, droplet nucleation.³⁷ Droplet nucleation occurs when radicals formed in the aqueous phase enter monomer droplets and propagate to form polymer particles. In miniemulsion polymerization, droplet nucleation is the predominant mechanism of particle formation due to the small size of the monomer droplets and the presence of few or no micelles in the system.³⁸ These submicron droplets have a large interfacial area and are capable of capturing most of the oligomeric free radicals – thus the droplets become the locus of nucleation. The incorporation of nanofiller materials is much easier in miniemulsion polymerization than in conventional emulsion polymerization because the need of mass transport through the water phase is minimized by droplet nucleation.

In several studies authors have focused on investigating the intercalation of clay with reactive surfactants (known as surfmers), such as 2-acrylamido-2-methyl-1-propane sulfonic acid (AMPS), to prepare polymer-clay nanocomposites (PCNs).³⁹⁻⁴¹ The use of this compound as a clay modifier seems to play a major role in achieving successful exfoliation of clay in the synthesized PCNs. Xu et al.³⁹ used AMPS as a clay modifier in the synthesis of exfoliated

poly(styrene-co-methyl methacrylate)/clay nanocomposites using emulsion polymerization. They found that AMPS has the ability to increase the interlayer spacing between clay layers from 1.17 nm in pristine clay up to 2.1 nm, depending on the AMPS/clay ratio used. They also found that AMPS can accelerate the insertion of comonomers into clay layers, resulting in PCNs with exfoliated structures.

It is believed that the interaction of AMPS with clay occurs by adsorption of AMPS on the surface of the clay by formation of hydrogen bonds between the sulfate and amido groups of AMPS with the hydroxyl groups on the clay surface.⁴² The same concept can be applied to GO, since GO has a larger c-axis spacing compared to the pristine graphite, and polar groups such as hydroxyl and carboxylic groups on its surface. Thus the intercalation of AMPS into GO particles becomes possible via the formation of hydrogen bonds between the functional groups of AMPS and GO. The chemical structure of AMPS is shown in Appendix C.

Here we report a new method for the synthesis of exfoliated poly(styrene-co-butyl acrylate) (poly(St-co-BA)) nanocomposites based on modified GO using the miniemulsion technique. First, the GO nanosheets were modified with the reactive surfactant, AMPS. The resultant modified GOs were then used in the synthesis of poly(St-co-BA) nanocomposites using *in situ* miniemulsion polymerization to promote the intercalation of water insoluble monomers, styrene (St) and n-butyl acrylate (BA), within layered GO. We intend to show that AMPS can intercalate into the GO galleries and lead to an increase in the interlayer spacing (commonly known as the d-spacing) between graphene oxide nanosheets in GO. Furthermore, due to its polymerizable groups, AMPS can take part in the polymerization of St and BA, and thus provide the exfoliation driving force for the formation of nanocomposites with exfoliated structure.

To the best of our knowledge, this is the first report on the modification of GO with a surfmer such as AMPS, and the subsequent use of the modified GOs in the miniemulsion polymerization of St and BA monomers. The treatment of GO with organic modifiers such as AMPS could lead to the synthesis of chemically modified GO derivatives possessing improved properties. The modification with AMPS will alter the intercalation behavior of GO and allow for the complete exfoliation of GO into individual graphene oxide nanoplatelets in polymer systems. The use of miniemulsions will also allow the formation of polymer particles, containing the modified GO nanosheets, which can be polymerized in a convenient one-step process.

4.2 Methods: Experimental and characterization

4.2.1 Materials

Styrene (99%, Aldrich) and n-butyl acrylate (99%, Aldrich) were purified by washing with aqueous 0.3 M KOH, followed by distillation at 40 °C under reduced pressure. Sodium dodecylbenzene sulfonate (SDBS) (99%, Fluka), 2-acrylamido-2-methyl-1-propane sulfonic acid (99%, Aldrich) and hexadecane (HD) (99%, Sigma-Aldrich) were used as received. Potassium persulfate (KPS) was obtained from Aldrich and purified by recrystallization from methanol. Potassium permanganate (99%), sodium nitrate (99%) and hydrogen peroxide (30%) were obtained from Sigma-Aldrich and used as received. Sulfuric acid (98.08%, Merck) was used as received. Distilled and deionized (DDI) water was obtained from a Millipore Milli-Q water purification system. Natural graphite (99.5%) was obtained from Graphit Kropfmühl AG (Hauzenberg, Germany) and used without any further purification. GO was prepared as described in the literature, with some modification.¹⁴

4.2.2 Preparation of GO

GO was prepared by treating the natural graphite with potassium permanganate in the presence of sulfuric acid, following the method of Hummers and Offeman.¹⁴ Flake graphite (10 g) and sodium nitrate (5 g) were stirred into 98% sulfuric acid (230 mL). As a safety measure, the ingredients were mixed in a 1.5 L flask that was previously cooled to 0 °C in an ice bath. Potassium permanganate (30 g) was slowly added to the suspension, while maintaining vigorous agitation, taking care not to allow the temperature of the suspension to exceed 20 °C. The ice bath was then removed and the temperature of the suspension brought to 35 °C, where it was maintained for 30 min. The mixture gradually thickened as the reaction progressed and after 30 min the mixture became pasty, with a brownish gray color. DDI water (460 mL) was then slowly stirred into the paste, causing a violent reaction and an increase in temperature to 100 °C. The diluted suspension was maintained at this temperature for 15 min. The suspension was then further diluted with warm water (~ 420 mL) and hydrogen peroxide (3%) (100 mL) to reduce the residual permanganate and manganese dioxide to colorless soluble manganese sulfate. Upon treatment with the peroxide, the suspension turned bright yellow. Filtration afforded a yellow-brown filter cake. The GO was washed several times with DDI water until neutrality. The final solid containing the GO platelets was obtained by centrifugation.

4.2.3 Modification of GO with AMPS

GO was treated with AMPS as follows: GO (0.5 g) was introduced to a 250 mL flask containing DDI water (150 g). The mixture was stirred at room temperature for 15 min, after which it was sonicated using a Vibracell VCX 750 ultrasonicator (Sonics & Materials, USA) for a further 15 min. This was done in order to achieve complete dispersion of GO nanosheets in water. AMPS was added to the mixture (20 wt% relative to GO), which was then stirred for a further 24 h at room temperature. The treatment was repeated with various quantities of AMPS: 40, 60 and 80 wt% relative to GO.

4.2.4 Typical preparation of poly(St-co-BA)/GO using miniemulsion polymerization

The AMPS treated GO (AMPS-GO) (modified with 40 wt% AMPS) was added to the monomer mixture (St and BA) and the mixture stirred for 1 h to allow effective swelling of GO with the monomers. Surfactant (~ 2 wt% SDBS relative to monomer) and HD were added and the mixture was stirred for a further 30 min. The mixture was sonicated using a Vibracell VCX 750 ultrasonicator (Sonics & Materials, USA) for 10 min, to obtain the miniemulsion latex. The sonicator amplitude was set at 80% and the pulse rate was set at 2 sec. The average energy expended was ~ 67 kJ. A three-neck round-bottomed flask containing the resultant miniemulsion latex was then immersed in an oil bath at room temperature. KPS (0.008 g) was added and the contents of the flask nitrogen purged for 15 min before increasing the temperature to 70 °C to initiate the polymerization. The reaction was carried out for 4 h under a nitrogen atmosphere, after which it was cooled to room temperature to stop the polymerization.

A similar procedure was followed for the synthesis of a poly(St-co-BA) reference made without GO by miniemulsion polymerization. The oil phase, consisting of St and BA monomers, and HD, was mixed with an aqueous solution of SDBS for 30 min. The mixture was then sonicated under the same conditions used for the synthesis of poly(St-co-BA)/GO nanocomposites for 15 min to afford the miniemulsion latex. KPS (0.008 g) was added and the temperature was increased to 70 °C to initiate the polymerization. The reaction was carried out for 4 h under a nitrogen atmosphere. The various formulations used for the polymerization of poly(St-co-BA)/GO nanocomposites and the poly(St-co-BA) reference are tabulated in Table 4.1.

Table 4.1: Quantities of reagents and monomers used in the miniemulsion polymerizations

Nanocomposite	AMPS-GO (g)	St (g)	BA (g)	SDBS (g)	HD (g)
P(St-co-BA)	-	4.51	0.51	0.102	0.022
P(St-co-BA)/GO-1	0.05	4.51	0.50	0.105	0.023
P(St-co-BA)/GO-2	0.10	4.50	0.52	0.101	0.022
P(St-co-BA)/GO-3	0.15	4.56	0.44	0.102	0.024
P(St-co-BA)/GO-4	0.20	4.51	0.50	0.105	0.023
P(St-co-BA)/GO-5	0.25	4.50	0.51	0.104	0.022
P(St-co-BA)/GO-6	0.30	4.50	0.52	0.101	0.022

4.2.5 Analytical techniques

Various analytical techniques were used to characterize the GO samples and the poly(St-co-BA)/GO nanocomposites (i.e., powders). Nanocomposite samples were obtained from the latices by precipitation. The latex (3 mL) was treated with concentrated hydrochloric acid. The precipitate was washed several times with methanol, then with DDI water, and finally dried at 40 °C under reduced pressure. The analytical instrumentation and procedures used were as follows:

4.2.5.1 Transmission electron microscopy (TEM)

TEM was used to directly visualize the morphology of the GO particles in poly(St-co-BA)/GO nanocomposites at the nanometer level. Bright field TEM images were recorded using a LEO 912 Omega TEM instrument (Zeiss, Germany), at an accelerating voltage of 120 kV. Prior to analysis the miniemulsion samples were diluted with DDI water (0.05%) and placed on 300-mesh copper grids, which were then transferred to the transmission electron microscope. Portions of the poly(St-co-BA)/GO nanocomposite miniemulsion samples were dried, embedded in epoxy resin, and then cured for 24 h at 60 °C. The embedded samples were ultra-microtomed with a diamond knife on a Reichert Ultracut S ultra-microtome, at room temperature. This resulted in sections with a nominal thickness of approximately 100 nm. The sections were transferred from water to 300-mesh copper grids, which were then transferred to the TEM apparatus for analysis. TEM was also used to visualize the GO particles. GO (0.1 g) was dispersed in DDI water (50 g) by sonication. The GO samples were diluted with DDI water (0.05%) and placed on 300-mesh grids for analysis. The average

particle sizes and gallery spacing were calculated using computer software, ImageJ (NIH, USA).

4.2.5.2 Scanning electron microscopy (SEM)

The microstructure of the graphite flakes and sheets before and after the oxidation was observed using a scanning electron microscope (Leo 1430 VP, Germany). Samples were carefully mounted on the top of the sample holder, which was then coated with a single layer of gold in order to make the sample surface electrically conducting. The holder was loaded into the chamber of the SEM instrument and images were recorded at between 500× and 40000× magnification, at 7 kV voltage and a distance of ~ 11mm.

4.2.5.3 Thermogravimetric analysis (TGA)

TGA measurements were carried out on a Q500 thermogravimetric analyzer (TA Instruments, USA). Sample sizes of less than 15 mg were used for all analyses. Analyses were carried out from ambient temperature to 900 °C, at a heating rate of 20 °C/min, under a nitrogen atmosphere (nitrogen purged at a flow rate of 50 mL/min).

4.2.5.4 Fourier-transform infrared (FT-IR) spectroscopy

FT-IR spectra were obtained using a Nexus 470 FT-IR spectrophotometer (Thermo Nicolet, USA), and recorded by averaging 32 scans. All spectra were acquired over the 450 to 4000 cm^{-1} wavenumber range by using an attenuated total reflectance unit at a resolution of 4 cm^{-1} .

4.2.5.5 Size exclusion chromatography (SEC)

SEC analyses were carried out using a 610 Fluid Unit, a 410 Differential Refractometer at 30 °C and a 717 plus Autosampler (Waters, USA). A 600E System Controller, run by Millennium 32 V3.05 software, was used in all analyses. Tetrahydrofuran (THF; HPLC grade), sparged with helium (IR grade), was used as the eluent, at a flow rate of 1 mL/min. Two PLgel 5 μm mixed-C columns and a PLgel 5 μm guard pre-column were used. The column temperature was 35 °C and the injection volume was 100 μL . The system was calibrated with narrow PS standards (5 mg/mL THF), ranging from 2.5×10^3 to 8.9×10^4 g mol^{-1} . The nanocomposite

samples were dissolved in THF (5 mg/mL) over a period of 24 h and then filtered through a 0.45 μm nylon filter.

4.2.5.6 X-ray diffraction (XRD)

XRD patterns were obtained using a X'Pert PRO multi-purpose diffractometer (PANalytical B.V., The Netherlands) equipped with a CuK (α) sealed tube X-ray source (wavelength 1.514 \AA). X'Celerator in Bragg-Brentano mode was used as the detector throughout.

4.2.5.7 Dynamic mechanical analysis (DMA)

DMA analysis of the poly(St-co-BA)/GO films was carried out using a Physica MCR 501 rheometer apparatus (Anton Paar, Germany). Parallel-plate geometry (25 mm diameter), with a 1-mm gap distance, and a constant strain of 0.1% was used. All measurements were carried out from 180 to 40 $^{\circ}\text{C}$, at a cooling rate of -5 $^{\circ}\text{C}$, an oscillation frequency of 1 Hz, and a normal force of 5 N. The nanocomposite films were prepared by pressing the composite samples into thin discs (25 mm) using a hydraulic press machine at 120 $^{\circ}\text{C}$.

4.3 Results and discussion

4.3.1 Preparation of GO

Figure 4.1 shows the FT-IR spectra of the pristine natural graphite (Figure 4.1 a) and its oxidized form (GO) (Figure 4.1 b). In Figure 1a the peaks at 1658 and 1540 cm^{-1} correspond to the stretching of C=C bonds in the benzene ring of graphene.²² Figure 4.1 b shows the characteristic peaks of GO, such as the stretching vibration of the hydroxyl groups ($-\text{OH}$), the stretching vibration of the carboxyl groups ($-\text{COOH}$), the vibration of O-H, the vibration of C-O, and the vibration of epoxy groups, centered at 3393, 1718 and 1630, 1390, 1054 and 845 cm^{-1} , respectively.²² The peaks at 2347 and 1630 cm^{-1} can be attributed to carbon dioxide and the deformation vibration of water molecules in the sample, respectively.^{22,43} The appearance of these oxygen-containing functional groups indicates that oxidation of the natural graphite was achieved. Indications of the C=C bond were not found in the GO spectrum, which shows that complete oxidation was achieved, due to the strong KMnO_4 oxidant used.

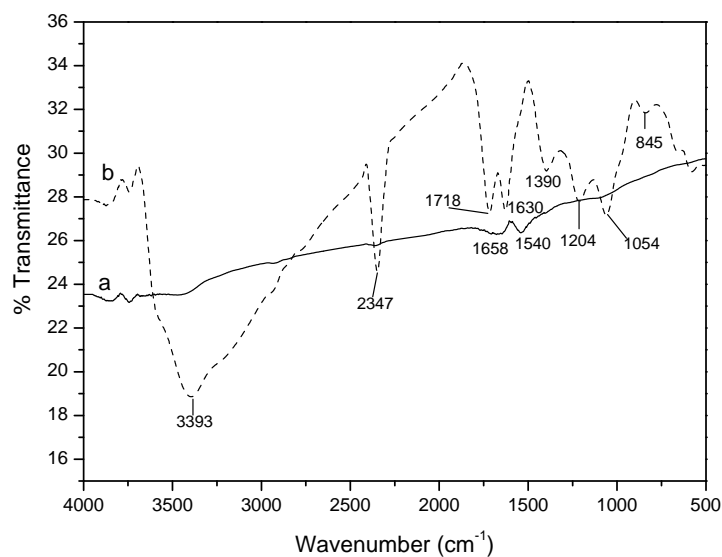


Figure 4.1: FT-IR spectra of a) pristine natural graphite and b) its oxidized form (GO).

4.3.2 Characterization of GO

4.3.2.1 Interlayer spacing of GO as determined by XRD

The oxidation of graphite is expected to increase the interlayer distance (d-spacing) of stacked graphene nanoplatelets.²⁴ XRD was used to determine the d-spacing between the graphene nanoplatelets in natural graphite before and after oxidation. Results showed an increase in the d-spacing between graphene nanoplatelets after oxidation. In the case of pristine graphite, there is a sharp reflection peak at $2\theta = 26.4^\circ$ in the XRD scattering pattern due to the interlayer (002) spacing ($d = 0.34$ nm).^{44,45} The XRD results of pristine natural graphite and its oxidized form (GO) are shown in Figure 4.2.

Upon oxidation, the characteristic peak of graphite could not be detected; the GO exhibited only one peak at a lower 2θ value = 12° . This indicates that the interlayer distance between neighboring graphene oxide layers in GO had increased (layers are now ~ 0.74 nm apart), because of the intercalation by functional groups and moisture.¹⁷ The fact that the XRD pattern of GO exhibited only one peak also suggests that a highly oxidized GO sample had been synthesized (in agreement with FT-IR results).

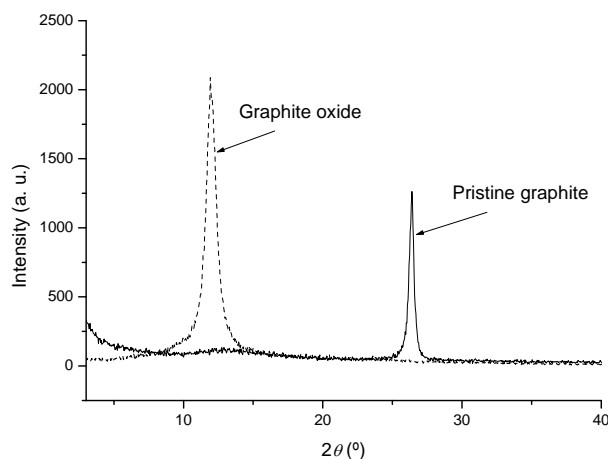


Figure 4.2: XRD curves of pristine natural graphite and GO.

4.3.2.2 Nanostructure of GO as determined by SEM and TEM

SEM was used to visualize the graphite particles before and after oxidation. Results are shown in Figures 4.3 and 4.4. The original graphite particles have a plate-like shape, with average sizes of 1–10 μm and thickness of 50–200 nm (see Figure 4.3). Each flake consists of multiple layers of graphene nanoplatelets with aspect ratios of about 20–50. The layers of graphite can be expanded a few hundred times during oxidation, as reported in the literature.⁴⁶ The SEM images of dried GO films show that a continuous film-like structure is formed by elimination of water (see Figure 4.4 a). This might be due to the plate-like nanostructure – which could be very desirable for the construction of high quality films. Furthermore, due to the presence of the oxygen-containing functional groups on the surface, GO nanosheets can interact with each other by hydrogen bonding, resulting in the formation of a film structure.

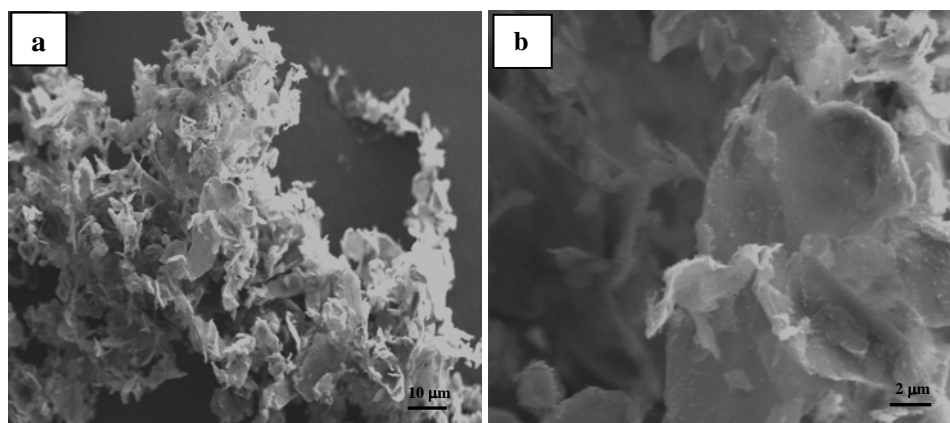


Figure 4.3: SEM images of natural graphite: a) at low magnification and b) at higher magnification.

The GO structure is basically parallel boards, which collapse and deform during the drying process, resulting in many pores of different sizes, ranging from 300 to 800 nm. This can be seen in Figure 4.4 b, where a higher magnification SEM image of a GO surface is presented. The thickness of the graphite nanosheets in GO is in the micrometer range, as evident in the SEM image in Figure 4.4 c.

According to the microstructure of graphite, the thickness of sheets in intercalated graphite (i.e., GO) may be as thin as a single carbon layer when the graphite is fully exfoliated. The structure of graphite, consisting of graphite nanosheets and graphene nanolayers (nanoplatelets), is illustrated in Figure 4.5. Figure 4.5 a shows that the graphite flakes consist of graphite sheets, which are normally < 100 nm in thickness. Each graphite sheet can be further divided into aggregates of a number of graphite nanosheets, 2–8 nm thick (see Figure 4.5 b). These graphite nanosheets are composed of graphene nanoplatelets, which can be as thin as one carbon atom layer thick (Figure 4.5 c).⁴⁷

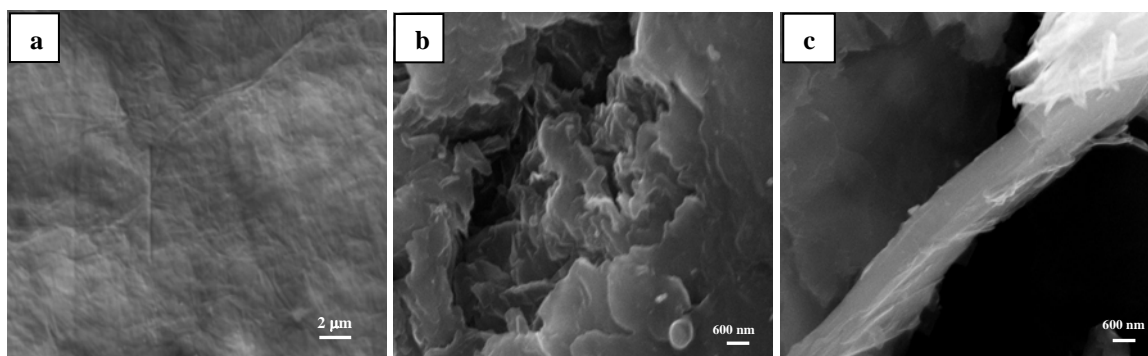


Figure 4.4: SEM images of GO: a) at low magnification, and b) and c) at higher magnification.

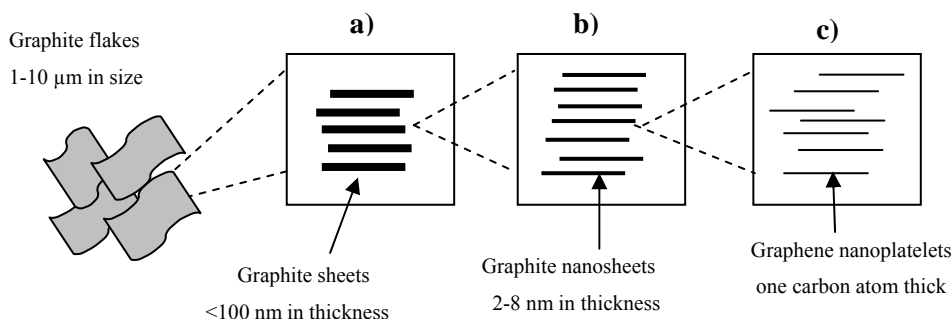


Figure 4.5: Microstructure of the graphite flakes and graphite nanosheets consisting of graphene nanoplatelets.

TEM was used to observe the GO nanosheets (dispersed in water) at the nanometer level (see Figure 4.6). The TEM images clearly show that the thick graphite sheets consist of thinner nanosheets, 2–5 nm thick, and the gallery spacing between these nanosheets is about 5–10 nm (Figure 4.6 b). The reason why SEM images showed GO sheet with a thickness of $\sim 1 \mu\text{m}$, as shown in Figure 4.4 c, is possibly the stacking and combining of graphene nanoplatelets on the surface during the drying process.

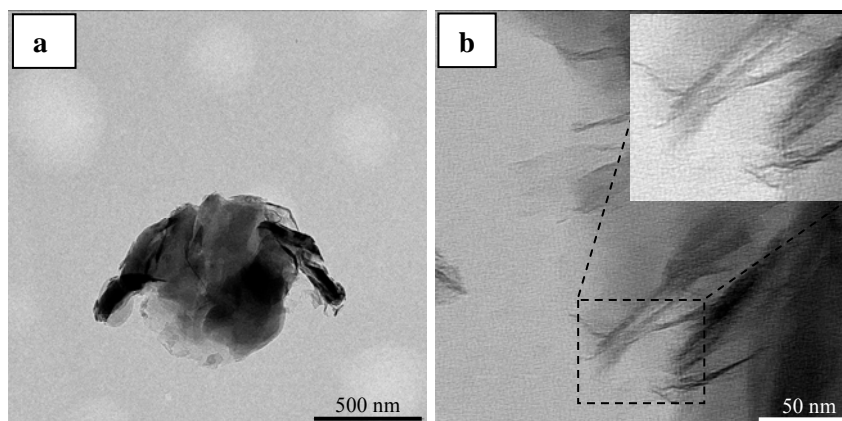


Figure 4.6: TEM images showing thinner sheets inside GO: a) low magnification image and b) higher magnification image.

4.3.2.3 The organization of AMPS in the GO galleries

Changes in the interlayer distance of GO can be caused by the intercalation of organic compounds. A change in the d-spacing of graphite as a function of the incorporation of different organic compounds has been reported elsewhere.⁴⁸⁻⁵⁰ The d-spacing is calculated according to Bragg's law⁵¹ (see equation 4.1):

$$2d \sin\theta = n\lambda \quad (4.1)$$

where d is the distance between two diffractive lattice planes of graphite, θ is the measured diffraction angle, n is the order of interference, and λ is the wavelength of X-ray radiation used in the diffraction experiment.

Figure 4.7 shows the XRD spectra of pure GO and the GOs modified with different quantities of AMPS. Table 4.2 tabulates the d-spacing calculated from the GO peaks in the XRD spectra. The interlayer spacing of GO increased from 0 to 20% and 20 to 40% AMPS concentration, but remained steady thereafter. It reached a maximum of about 0.80 nm when

$\geq 40\%$ AMPS was used. This was rather surprising, because more AMPS molecules should lead to an increase in the interlayer spacing of GO. This could be explained by the fact that there are a limited number of functional groups on the surface of GO that could interact with the AMPS molecules. It could also be attributed to the nature of AMPS molecules and their arrangement inside the galleries of GO. This behavior has been reported previously for other fillers, such as clay, modified with AMPS.⁴² The AMPS molecules could adopt different conformations inside the GO galleries as the AMPS concentration changes, resulting in different d-spacings. The AMPS molecules are thought to lie either parallel to the host layers, forming mono- or bi-layers, or radiate away from the surface, forming extended (paraffin-type) mono- or bi-molecular arrangements.⁵²

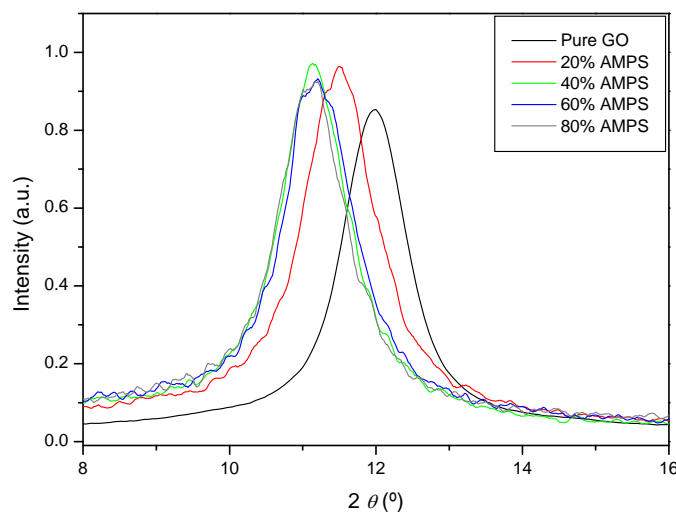


Figure 4.7: XRD patterns of GO and GOs modified with different quantities of AMPS.

The increase in the interlayer spacing of modified GO relative to pure GO confirmed the insertion of AMPS between GO nanosheets, not only the presence of AMPS on the external surface of the GO. The AMPS molecules can interact with GO both via their amido and sulfate groups. These groups can form hydrogen bonds with the functional groups of GO. This is in agreement with the findings of Liu et al.,³³ after they investigated the synthesis of poly(vinyl acetate)-intercalated GO by *in situ* intercalative polymerization. They prepared a graphite intercalation compound in which GO was intercalated with n-octanol. They attributed the interaction of GO by n-octanol to the formation of hydrogen bonds between the hydroxyl groups of the n-octanol and the other polar groups of the GO.

Greesh et al.⁴² investigated the adsorption mechanism of AMPS and other related compounds into the galleries of montmorillonite clay. They found that the interaction of AMPS with clay

occurs by adsorption of AMPS on the edges and the surfaces of the clay galleries. The formation of hydrogen bonds between the sulfate and amido groups of AMPS with the hydroxyl groups and water molecules adsorbed on the clay surface leads to an increase in the basal spacing of the clay. The intercalation of AMPS inside the GO galleries could be similar to that occurring in clay particles because the GO has many functional groups, such as hydroxyl and carboxyl, present on its surface.^{9,22} The sulfate and amido groups of AMPS can interact with the hydroxyl and carboxyl groups present on the GO.

Table 4.2: Interlayer distance (d-spacing) of GO and GOs modified with different amounts of AMPS

Sample code	AMPS (wt%)	2θ (°)	d-spacing (nm)
GO	0	12.00	0.74
AMPS-GO-1	20	11.50	0.77
AMPS-GO-2	40	11.14	0.80
AMPS-GO-3	60	11.16	0.79
AMPS-GO-4	80	11.12	0.80

4.3.3 Characterization of poly(St-co-BA)/GO nanocomposites

4.3.3.1 Determination of morphology by TEM

TEM was used to visually detect the latex particles that were synthesized and to determine the morphology of the films that were prepared from these latices. Figure 4.8 shows TEM images of the nanocomposite prepared using 1 wt% GO relative to monomer. The particle size distribution is fairly narrow and there are many GO nanosheets outside the polymer particles, as can be seen in Figure 4.8 a. This suggests that most of the GO sheets have not been encapsulated by the copolymer shell. This is to be expected because of the hydrophilic nature of the GO, which prefers to be in the water phase. The unmodified GO sheets contain a number of stacked graphene nanoplatelets with relatively small d-spacing (see Figure 4.7 and Table 4.2). These stacked nanosheets are large in size compared to the polymer particles and thus they are unable to enter the polymer particles.

The GO nanosheets can also be seen in a TEM image of the dried film that was embedded into the epoxy resin (Figure 4.8 b). Most of the GO nanosheets are mainly of intercalated morphology, with the exception of some areas that contain few exfoliated graphene

nanoplatelets. The stacking of graphene indicates that the GO did not disperse very well in the polymer matrix, leading to the formation of an intercalated structure. However, when GO was modified with AMPS the GO nanosheets could not be seen in the TEM images (see Figure 4.9 a). This absence of GO sheets in the latex suggests that all the modified GO nanosheets were encapsulated in the copolymer particles. The modification of GO with AMPS increased the gap between the graphene nanoplatelets, resulting in largely exfoliated GO (the nanoplatelets are smaller in size due to exfoliation). These nanoplatelets can easily enter the polymer latex particles to form the core domain.

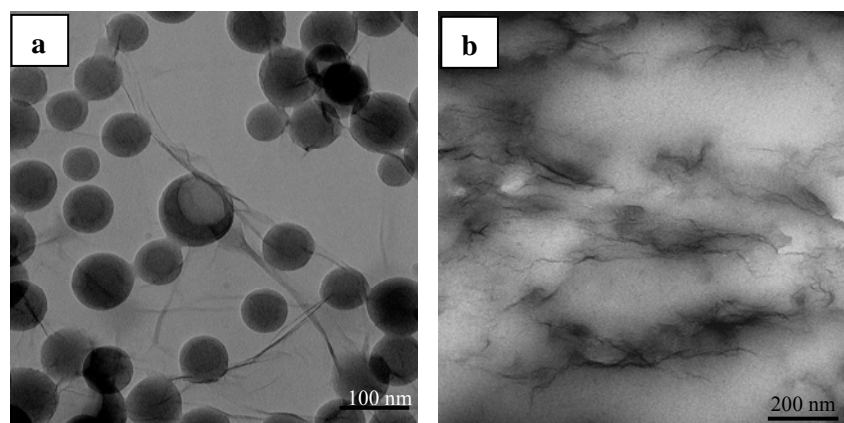


Figure 4.8: TEM images of poly(St-co-BA)/GO nanocomposite latex made with 1 wt% GO relative to monomer: a) latex particles and b) a microtomed film cast from the same latex.

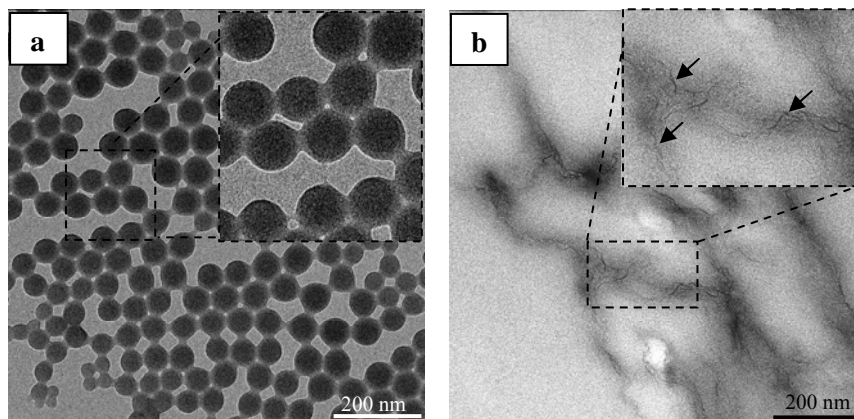


Figure 4.9: TEM images of poly(St-co-BA)/GO nanocomposite prepared using 1 wt% AMPS-modified GO: a) latex particles and b) a microtomed film cast from the same latex.

The TEM image in Figure 4.9 a also shows that a miniemulsion with good particle size distribution was obtained. The dark core domains inside the particles can be attributed to the presence of modified GO nanosheets inside the copolymer shell layer. AMPS could also alter

the chemistry of GO, resulting in modified GO with increased hydrophobicity, and allowing for better compatibility between GO and hydrophobic monomers (St and BA). Furthermore, the TEM images of the microtomed films that were prepared from the latex show that the AMPS-modified GO platelets were mostly of exfoliated structure. Figure 4.9 b shows very thin graphene nanoplatelets, about 2–5 nm thick, which correspond to ~ 2–5 layers stacking.⁵³ This indicates that most of the AMPS-GO nanosheets dispersed as a thin layer, which means that the graphene platelets are mostly exfoliated in the polymer matrix. This is due to the effect of AMPS, which widened the d-spacing of GO and facilitated the intercalation of monomer into the GO nanogalleries, resulting in an exfoliated structure.

Recently, Stankovich et al.⁵⁴ reported that the treatment of GO with organic isocyanates resulted in a new class of functionalized GO materials that had reduced hydrophilic properties. The authors showed that, in contrast to the unmodified (as-prepared) GO, the modified GO does not disperse in water. However, it can be dispersed and readily exfoliate in polar aprotic solvents such as N,N'-dimethylformamide, N-methylpyrrolidone and dimethyl sulfoxide to form stable colloidal dispersions. In the current study, the effect of AMPS on the properties of GO could provide the driving force to allow better intercalation of the monomer in the GO nanogalleries. It should be noted here that in all nanocomposites the GO was modified with 40% AMPS. XRD showed that the highest change in the d-spacing of GO was obtained when 40% AMPS relative to GO was used. Any further increase in AMPS concentration did not change the d-spacing compared to the GO modified with 40% AMPS (see Figure 4.7). The presence of an excess amount of AMPS could have an effect on the polymerization rate,³⁹ and therefore the minimum amount of AMPS that led to a significant change in the d-spacing of GO was used (i.e., 40%).

4.3.3.2 Determination of nanocomposite structure by XRD

Figure 4.10 shows the XRD results of poly(St-co-BA)/GO nanocomposites prepared with different amounts of AMPS-modified GO. For comparison, XRD results of a poly(St-co-BA) reference are also included in Figure 4.10. The nanostructure ranged from intercalated to largely exfoliated morphology, depending on the amount of modified GO used. The broad peak at $2\theta = 10^\circ$ observed in the XRD scattering pattern corresponds to GO while the peak at $2\theta = 20^\circ$ is due to the poly(St-co-BA) copolymer.⁵⁵ The average interlayer distance of the GO in the nanocomposites was 0.84 nm, which is greater than that of the as-prepared GO (0.74

nm) and AMPS-modified GO (0.80 nm). This indicates that AMPS plays a very important role in the intercalation process of GO by the polymer during polymerization.

Figure 4.10 shows that at AMPS-GO loadings of 1–4 wt% in the nanocomposite, the system resulted in mainly intercalated structure. This is indicated by a broad peak that emerged at a 2θ value of approximately 10° , which is lower than that of GO and AMPS-GO (see XRD results in Figure 4.7). In the case that an intercalated morphology is formed, few polymer chains can penetrate between the GO nanogalleries, thus the interlayer distance is increased. This leads to a shift of the diffraction peak towards lower angle values in the XRD pattern.⁵⁶ However, when the AMPS-GO loading was relatively high (5–6 wt%) the nanostructure showed more exfoliated morphology, indicated by a less defined peak.⁵⁷ Similar results were obtained for polymer composites made with other filler materials such as clay,⁴¹ which were attributed to thermodynamic effects. In the presence of high filler content, the filler particles are very close to each other, and any particle movements can generate energy by friction. This energy could lead to a free movement of other filler particles, resulting in a random orientation of these particles (i.e., a less defined peak in the XRD will be observed).⁶⁵

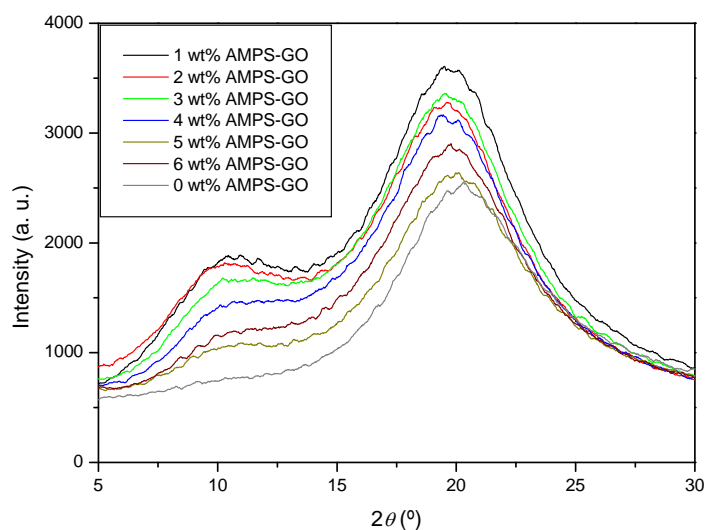


Figure 4.10: XRD results of poly(St-co-BA)/GO nanocomposites made with different amounts of AMPS-modified GO.

4.3.3.3 Mechanical properties of the poly(St-co-BA)/GO nanocomposites

The mechanical properties of poly(St-co-BA)/GO nanocomposites were determined by DMA. Measurements were performed on the dried films prepared from the poly(St-co-BA)/GO latices containing 0–6 wt% GO relative to monomer. DMA analysis showed that the

nanocomposites with high GO content had enhanced storage and loss modulus in the glassy state relative to the neat poly(St-co-BA) reference (see Figure 4.11). At AMPS-GO loadings of 1–4 wt% relative to monomer the storage and loss modulus of the nanocomposites was lower than that of the poly(St-co-BA) reference (2.5×10^8 and 9.0×10^6 Pa, respectively).

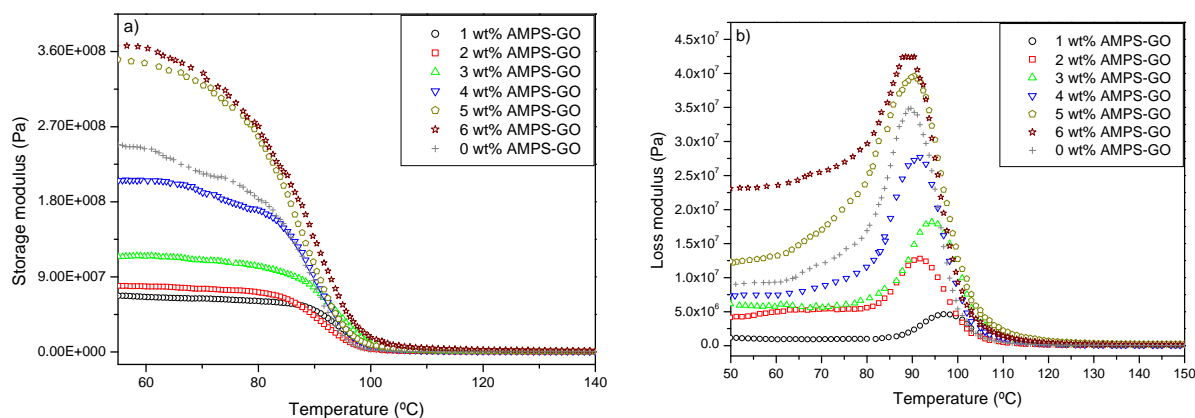


Figure 4.11: Mechanical properties as a function of temperature of poly(St-co-BA)/GO nanocomposites, at AMPS-GO loadings of 0–6 wt%: a) storage modulus and b) loss modulus.

Nanocomposite samples with higher filler content (5 and 6 wt%) had higher storage and loss modulus values than the poly(St-co-BA) reference. Furthermore, it was noted that the storage and loss modulus of poly(St-co-BA)/GO nanocomposites increased with increasing AMPS-GO content in the sample. As indicated by the XRD results in Figure 4.10, when the AMPS-GO loading increased the degree of graphene exfoliation was enhanced significantly. This resulted in the formation of polymer nanocomposites with improved mechanical properties (i.e., improved storage and loss modulus).

The glass transition temperature (T_g) of the polymer in a nanocomposite was determined from the onset temperature of the $\tan \delta$ curve in the DMA scan. The variation of $\tan \delta$ of the poly(St-co-BA)/GO nanocomposites with temperature is shown in Appendix D. It was noticed that the area of the $\tan \delta$ peak of the nanocomposite is smaller than that of the neat poly(St-co-BA) copolymer. This was due to the incorporation of polymer chains inside the graphite galleries, which led to reduced damping.⁵⁸ Table 4.3 shows the T_g values of all nanocomposites synthesized with different AMPS-GO content (0–6 wt%). The T_g of poly(St-co-BA) was enhanced in the presence of AMPS-modified GO relative to nanocomposites made with 0 wt% GO.

The increase in T_g was not a function of AMPS-GO content in the nanocomposites. This was rather surprising, because an increase in graphite content is expected to result in nanocomposites with increased T_g values. This behavior was attributed to the change in molecular weight of the polymer chains caused by the presence of graphite. This can be seen in Table 4.4, which tabulates the molecular weights (weight average molecular weight, \bar{M}_w and number average molecular weight, \bar{M}_n) and dispersity (\mathcal{D}) of the poly(St-co-BA) reference and poly(St-co-BA)/GO nanocomposites prepared using different quantities of AMPS-GO. As the AMPS-GO loading increased, the molecular weight of the copolymer decreased markedly, especially in the case of 2, 5 and 6 wt% AMPS-GO loadings. Furthermore, the \mathcal{D} of poly(St-co-BA) copolymer was slightly affected by the change in AMPS-GO concentration. The low molecular weight polymer chains may act as plasticizer and cause the T_g of the polymer in the nanocomposite to decrease.⁵⁹ This plasticization effect could counteract the effect of AMPS-GO on the polymer chain movements, resulting in less improvement in the T_g .

Table 4.3: T_g of poly(St-co-BA)/GO nanocomposites, at AMPS-GO loadings of 0–6 wt%

Nanocomposite	AMPS-GO content (wt%)	T_g (°C)
P(St-co-BA)	0	87.0
P(St-co-BA)/GO-1	1	94.5
P(St-co-BA)/GO-2	2	89.0
P(St-co-BA)/GO-3	3	92.0
P(St-co-BA)/GO-4	4	89.0
P(St-co-BA)/GO-5	5	88.0
P(St-co-BA)/GO-6	6	89.0

Similar results were observed for polymer nanocomposites made with other fillers, such as clay. Greesh et al.⁶⁰ observed that clay loading had a significant effect on the molecular weight of poly(St-co-BA) nanocomposites prepared by emulsion polymerization. They found that the molecular weight of poly(St-co-BA) decreased as the clay concentration increased in the nanocomposites. They attributed these results to the presence of clay particles, which may hinder the growth of polymer chains, resulting in a decreased molecular weight as the clay concentration increases. Due to the dispersion of the filler particles in the monomer phase the viscosity increases, thus the movement and diffusivity of the monomers, initiators and free radicals may all be retarded. Therefore, the probability of chain propagation, chain transfer and termination decreases with increasing filler content.⁶¹

Table 4.4: \bar{M}_n , \bar{M}_w and \bar{D} of the poly(St-co-BA) reference and poly(St-co-BA)/GO nanocomposites prepared using different quantities of AMPS-GO (0–6 wt%)

Nanocomposite	AMPS-GO content (wt%)	\bar{M}_n (g/mol)	\bar{M}_w (g/mol)	\bar{D}
P(St-co-BA)	0	7.1×10^5	1.5×10^6	2.1
P(St-co-BA)/GO-1	1	5.2×10^5	1.6×10^6	3.2
P(St-co-BA)/GO-2	2	4.0×10^5	1.3×10^6	3.3
P(St-co-BA)/GO-3	3	3.6×10^5	1.2×10^6	3.4
P(St-co-BA)/GO-4	4	3.6×10^5	1.1×10^6	3.2
P(St-co-BA)/GO-5	5	2.6×10^5	8.4×10^5	3.2
P(St-co-BA)/GO-6	6	2.7×10^5	7.7×10^5	2.8

The improvement in mechanical properties of poly(St-co-BA) in the presence of AMPS-modified GO is because of the fine dispersion of the nanosheets and strong interaction between the polar groups of poly(St-co-BA) and the polar groups of GO. These GO nanoplatelets have a high aspect ratio (due to the high exfoliation of GO nanosheets), which greatly restricts the mobility of the polymer chain segments near the polymer–graphite interface, resulting in higher storage and loss modulus, and T_g values.^{58,62} Furthermore, the modification of GO with AMPS widened the interlayer spacing between the graphene layers in GO and facilitated the intercalation of monomers into the GO nanogalleries. This led to the formation of poly(St-co-BA) nanocomposites with exfoliated structure, leading to enhanced mechanical properties.

The effect of GO modification with AMPS can be seen in Figure 4.12, which shows the mechanical properties (storage and loss modulus) of nanocomposite samples made with AMPS-modified GO and unmodified GO. The mechanical properties are significantly improved in nanocomposites made with AMPS-modified GO, compared to those made with the neat GO. The storage modulus increased from 3.5×10^7 to about 6.7×10^7 Pa, while the loss modulus increased from 1.0×10^6 to about 4.3×10^6 Pa. This indicates that the improvement in mechanical properties is due to the modification of GO with AMPS, which resulted in largely exfoliated graphene nanosheets dispersed in the polymer matrix.

Table 4.3 shows that the highest T_g of poly(St-co-BA) is observed when the filler loading is 1 wt%. This seems to be the threshold at which the best interaction between the graphite

nanosheets and the polymer occurs. It should be noted here that the storage and loss modulus values were not the highest when 1 wt% AMPS-GO loading was used. This can be attributed to the changes in mechanical behavior of a polymer sample as a function of temperature. The storage and loss modulus are a measure of the elastic and plastic response of a polymer to the deformation as a function of temperature. On the other hand, the T_g is used to measure the molecular mobility of polymers as a function of temperature. The intercalation with even small amounts of the filler nanosheets will lead to a restricted mobility of polymer chains, resulting in higher T_g .

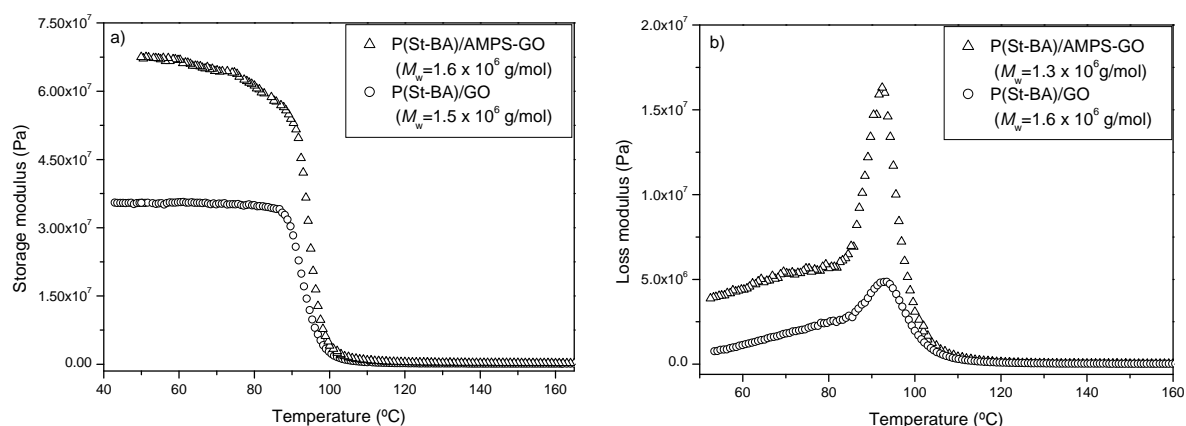


Figure 4.12: Mechanical properties as a function of temperature of poly(St-co-BA) nanocomposites made with AMPS-GO and GO: a) storage modulus (1 wt% filler loading) and b) loss modulus (2 wt% filler loading).

4.3.3.4 Thermal stability of poly(St-co-BA)/GO nanocomposites

Yet another enhanced property that PGNs exhibit is their increased thermal stability compared to neat polymers.^{63,64} Our results showed that the thermal stability of poly(St-co-BA)/GO nanocomposites was improved, relative to neat poly(St-co-BA) copolymer. The TGA thermograms of poly(St-co-BA)/GO nanocomposites prepared with different quantities of modified GOs are shown in Figure 4.13. Table 4.5 tabulates the thermogravimetric data, including T_{10} and T_{90} of degradation. T_{10} is the onset temperature at which 10% mass loss of the nanocomposite occurs and T_{90} is the temperature at which 90% mass loss occurs. The remaining fraction of non-volatile material left at 850 °C, called char, is also shown in Table 4.5. The poly(St-co-BA) copolymer does not contain any volatile products below 395 °C, however, the main chain of poly(St-co-BA) decomposes at around 400 °C.

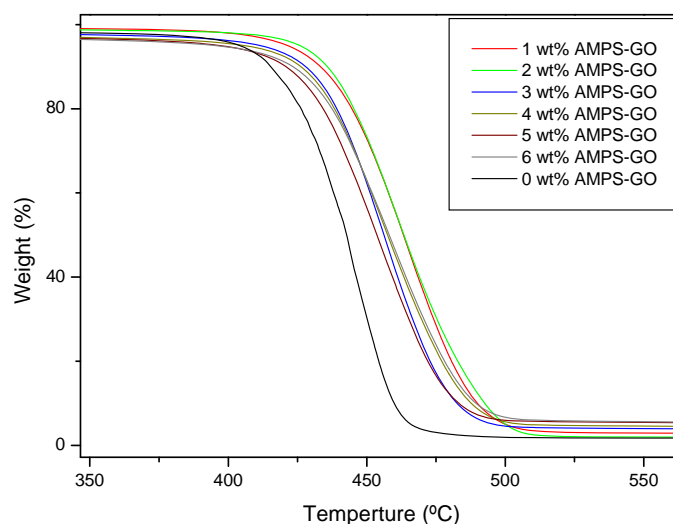


Figure 4.13: TGA curves of poly(St-co-BA) nanocomposites prepared using various amounts of AMPS-GO (1–6 wt %).

Table 4.5: Thermogravimetric properties of poly(St-co-BA) and its nanocomposites made with different concentrations of AMPS-GO (0–6 wt%)

Nanocomposite	AMPS-GO loading (wt%)	T _{10%} (°C)	T _{90%} (°C)	Char (%)
P(St-co-BA)	0	415.0	459.5	0.24
P(St-co-BA)/GO-1	1	433.5	490.0	1.09
P(St-co-BA)/GO-2	2	435.5	492.5	1.71
P(St-co-BA)/GO-3	3	428.0	483.0	2.15
P(St-co-BA)/GO-4	4	426.0	487.5	2.69
P(St-co-BA)/GO-5	5	421.0	483.0	4.10
P(St-co-BA)/GO-6	6	423.0	489.0	4.15

Table 4.5 shows that all nanocomposites synthesized with AMPS-modified GO are more thermally stable relative to the neat poly(St-co-BA) copolymer. At AMPS-GO loading of only 1–2 wt% relative to monomer the temperature of degradation of the nanocomposite increased, relative to pure polymer. The T₁₀ of all the synthesized nanocomposite increased by 6–20.5 °C compared to pure poly(St-co-BA) copolymer and T₉₀ increased by about 23.5–33.0 °C. This clearly shows that the thermal stability of poly(St-co-BA) increases in the presence of AMPS-GO. However, a further increase in AMPS-GO loading did not result in any improvement of thermal stability relative to the cases of 1–2 wt% loadings.

Moreover, the increase in AMPS-GO content above 2% in the nanocomposites generally resulted in a slight decrease in the thermal stability of the nanocomposites. This can be explained by the effect of AMPS-GO loading on the molecular weight of the copolymer, as indicated in Table 4.4. As the AMPS-GO content increased in the nanocomposite there was a significant decrease in the molecular weight of the copolymer. The change in molecular weight may counteract the effect of the increase in filler loading on the thermal stability of the nanocomposites. Samakande et al.⁶⁵ observed the same effect of the filler content on the thermal stability of PS made with clay nanoparticles.

The TGA data in Table 4.5 also show that at 850 °C, when the residue of pure copolymer is 0.24%, the charred residue of the nanocomposites is increased at increasing AMPS-GO loadings. These results indicate that introducing AMPS-modified GO into the nanocomposites enhances the formation of char on the surface of the polymer and, consequently, reduces the rate of decomposition.⁵⁶ It should be noted here that at AMPS-GO loading of 3–6 wt% the char was significantly lower than the nominal amount of modified GO that was added. This is because the graphene nanoplatelets (in AMPS-GO) in these nanocomposites are largely exfoliated. We hypothesize that the exfoliated nanoplatelets (especially the single sheets) will not form char as the stacked graphene sheets do. The exfoliated GO nanosheets will ‘burn’ more easily than the intercalated or less exfoliated ones. Therefore, a significant difference between the nominal and the actual char content of GO will be observed. The difference in char content could be the reason why some nanocomposites did not exhibit increased thermal stability relative to the case of nanocomposites with 1–2 wt% filler loadings. It should be also noted that at 6 wt% AMPS-GO loading the char content is similar to that of the 5 wt% AMPS-GO loading sample (see Table 4.5); subsequently, these nanocomposites exhibit similar T_g values of 89 and 88 °C, respectively.

TGA results also proved that there is a significant enhancement in thermal stability of the nanocomposites when the GO was modified with AMPS. Figure 4.14 shows the thermal properties of nanocomposite samples made with AMPS-modified GO and unmodified GO. For comparison, the TGA curve of the poly(St-co-BA) reference is also shown in Figure 4.14. It is clear that the thermal stability is significantly improved in nanocomposites made with AMPS-modified GO, compared to those made with the neat GO. At a filler loading of 1 wt%, the T_{10} and T_{90} increased from 421.5 to 433.5 °C and 486.0 to 490.0 °C, respectively. Similarly, at filler loading of 2%, the T_{10} and T_{90} increased from 426.0 to 436.0 °C and 487.0 to 493.0 °C, respectively. This indicates that AMPS plays a very significant role in the

exfoliation of GO in the polymer matrix, which results in largely exfoliated nanocomposites with improved thermal stability.

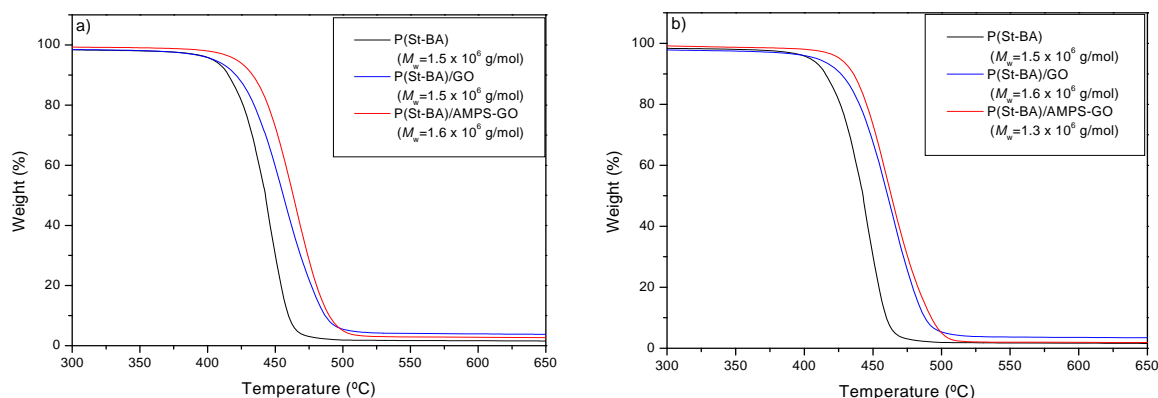


Figure 4.14: Thermal properties as a function of temperature of poly(St-co-BA) nanocomposites made with AMPS-GO and GO: a) 1 wt% AMPS-GO and GO loading and b) 2 wt% AMPS-GO and GO loading.

4.4 Conclusion

A novel method was demonstrated for the preparation of exfoliated poly(St-co-BA) nanocomposites by miniemulsion polymerization using functionalized GO. The synthesis was carried out by first mixing the GO with AMPS, followed by miniemulsification in the presence of St and BA monomers. The polymerization resulted in encapsulated GO nanosheets in poly(St-co-BA) particles and the nanocomposites were exfoliated during polymerization. TEM showed that the graphene nanoplatelets in GO were exfoliated (~ 2 – 5 layers thick) in the films obtained from the synthesized nanocomposite latices. TEM also revealed that dispersion of GO nanosheets covered with a copolymer layer in an encapsulated structure, with good particle size distribution, was achieved.

The exfoliated structure in the nanocomposites was confirmed by XRD measurements. The nanocomposites had structures ranging from intercalated to largely exfoliated, and the degree of graphene exfoliation was enhanced as the AMPS-modified GO loading increased. The modification of GO with AMPS broadened the gap between the graphene layers and facilitated the intercalation of monomers into the GO nanogalleries. This provided the needed exfoliation driving force for the formation of poly(St-co-BA) nanocomposites with exfoliated structure. The use of miniemulsion as the *in situ* polymerization method promoted the intercalation of St and BA monomers into the modified GO layers.

TGA and DMA analyses indicated that polymer nanocomposites prepared with AMPS-modified GO had better thermal and mechanical properties relative to the neat copolymer. Furthermore, the use of AMPS-GO led to the synthesis of nanocomposites with better properties compared to those synthesized with unmodified GO (i.e., as-prepared GO). DMA proved that the mechanical properties of poly(St-co-BA), namely storage and loss modulus, increased in the presence of AMPS-GO, as a function of filler loading. Moreover, all nanocomposites made with AMPS-GO had T_g values higher than that of the neat poly(St-co-BA) copolymer. However, the increase in the T_g of the copolymer was not a function of filler content. This was attributed to the effect of AMPS-GO concentration on the molecular weight of the copolymer, which showed a significant decrease as the filler content increased. TGA results also indicated that all the prepared nanocomposites exhibited enhanced thermal stability in the presence of AMPS-GO compared to the neat copolymer. The thermal decomposition of all nanocomposites shifted to higher temperature in the presence of AMPS-modified GO relative to the neat copolymer.

4.5 References

- (1) Stankovich, S.; Dikin, D. A.; Dommett, G. H.; Kohlhaas, K. M.; Zimmney, E. J.; Stach, E. A.; Piner, R. D.; Nguyen, S. T.; Ruoff, R. S. *Nature* **2006**, 442, 282-286.
- (2) Geim, A. K.; Novoselov, K. S. *Nature Materials* **2007**, 6 (3), 183-191.
- (3) Dreyer, D. R.; Ruoff, R. S.; Bielawski, C. W. *Angewandte Chemie International Edition* **2010**, 49 (49), 9336-9344.
- (4) Lee, C.; Wei, X.; Kysar, J. W.; Hone, J. *Science* **2008**, 321 (5887), 385-388.
- (5) Velasco-Santos, C.; Martinez-Hernandez, A. L.; Castano, V. M. *Composite Interfaces* **2005**, 11 (8/9), 567-586.
- (6) Viculis, L. M.; Mack, J. J.; Mayer, O. M.; Hahn, H. T.; Kaner, R. B. *Journal of Materials Chemistry* **2005**, 15, 974-978.
- (7) Kim, H.; Abdala, A. A.; Macosko, C. W. *Macromolecules* **2010**, 43 (16), 6515-6530.
- (8) Wakabayashi, K.; Pierre, C.; Dikin, D. A.; Ruoff, R. S.; Ramanathan, T.; Brinson, L. C.; Torkelson, J. M. *Macromolecules* **2008**, 41 (6), 1905-1908.
- (9) Dreyer, D. R.; Park, S.; Bielawski, C. W.; Ruoff, R. S. *Chemical Society Reviews* **2010**, 39 (1), 228-240.
- (10) Schniepp, H. C.; Li, J.-L.; McAllister, M. J.; Sai, H.; Herrera-Alonso, M.; Adamson, D. H.; Prud'homme, R. K.; Car, R.; Saville, D. A.; Aksay, I. A. *The Journal of Physical Chemistry B* **2006**, 110 (17), 8535-8539.
- (11) Stankovich, S.; Piner, R. D.; Chen, X.; Wu, N.; Nguyen, S. T.; Ruoff, R. S. *Journal of Materials Chemistry* **2006**, 16 (2), 155-158.

- (12) Brodie, B. C. *Philosophical Transactions of the Royal Society of London, Series A* **1859**, 149, 249-259.
- (13) Staudenmaier, L. *Berichte der Deutschen Chemischen Gesellschaft* **1898**, 31, 1481-1487.
- (14) Hummers, W. S.; Offeman, R. E. *Journal of the American Chemical Society* **1958**, 80, 1339.
- (15) Lerf, A.; He, H.; Forster, M.; Klinowski, J. *The Journal of Physical Chemistry B* **1998**, 102 (23), 4477-4482.
- (16) He, H.; Klinowski, J.; Forster, M.; Lerf, A. *Chemical Physics Letters* **1998**, 287 (1-2), 53-56.
- (17) Hontoria-Lucas, C.; López-Peinado, A. J.; López-González, J. d. D.; Rojas-Cervantes, M. L.; Martín-Aranda, R. M. *Carbon* **1995**, 33 (11), 1585-1592.
- (18) He, H.; Riedl, T.; Lerf, A.; Klinowski, J. *The Journal of Physical Chemistry* **1996**, 100 (51), 19954-19958.
- (19) Szabó, T.; Szeri, A.; Dékány, I. *Carbon* **2005**, 43 (1), 87-94.
- (20) Hirata, M.; Gotou, T.; Horiuchi, S.; Fujiwara, M.; Ohba, M. *Carbon* **2004**, 42 (14), 2929-2937.
- (21) Hirata, M.; Gotou, T.; Ohba, M. *Carbon* **2005**, 43 (3), 503-510.
- (22) Titelman, G. I.; Gelman, V.; Bron, S.; Khalfin, R. L.; Cohen, Y.; Bianco-Peled, H. *Carbon* **2005**, 43 (3), 641-649.
- (23) Putz, K. W.; Compton, O. C.; Palmeri, M. J.; Nguyen, S. T.; Brinson, L. C. *Advanced Functional Materials* **2010**, 20 (19), 3322-3329.
- (24) Wang, W.-P.; Pan, C.-Y. *Polymer Engineering and Science* **2004**, 44 (12), 2335-2339.
- (25) Potts, J. R.; Dreyer, D. R.; Bielawski, C. W.; Ruoff, R. S. *Polymer* **2011**, 52 (1), 5-25.
- (26) Hu, H.; Wang, X.; Wang, J.; Wan, L.; Liu, F.; Zheng, H.; Chen, R.; Xu, C. *Chemical Physics Letters* **2010**, 484 (4-6), 247-253.
- (27) Savoskin, M. V.; Yaroshenko, A. P.; Whyman, G. E.; Mysyk, R. D. *Journal of Physics and Chemistry of Solids* **2006**, 67, 1127-1131.
- (28) Du, X. S.; Xiao, M.; Meng, Y. Z. *Journal of Polymer Science Part B: Polymer Physics* **2004**, 42, 1972-1978.
- (29) Kim, T. Y.; Lee, H. W.; Stoller, M.; Dreyer, D. R.; Bielawski, C. W.; Ruoff, R. S.; Suh, K. S. *ACS Nano* **2011**, 5 (1), 436-442.
- (30) Zheng, W.; Wong, S.-C. *Composites Science and Technology* **2003**, 63 (2), 225-235.
- (31) Jing-Wei, S.; Xiao-Mei, C.; Wen-Yi, H. *Journal of Applied Polymer Science* **2003**, 88 (7), 1864-1869.
- (32) Wenge, Z.; Xuehong, L.; Shing-Chung, W. *Journal of Applied Polymer Science* **2004**, 91 (5), 2781-2788.
- (33) Liu, P.-G.; Xiao, P.; Xiao, M.; Gong, K.-c. *Chinese Journal of Polymer Science* **2000**, 18 (5), 413-418.
- (34) Zheng, G.; Wu, J.; Wang, W.; Pan, C. *Carbon* **2004**, 42, 2839-2847.

- (35) Samakande, A.; Sanderson, R. D.; Hartmann, P. C. *Journal of Polymer Science Part A: Polymer Chemistry* **2008**, 46 (21), 7114-7126.
- (36) Lu, H. F.; Fei, B.; Xin, J. H.; Wang, R. H.; Li, L.; Guan, W. C. *Carbon* **2007**, 45 (5), 936-942.
- (37) El-Aasser, M.; Sudol, E. Features of Emulsion Polymerization. In *Emulsion Polymerization and Emulsion Polymers*, 2nd edition; Lovell, P.; El-Aasser, M., Eds.; John Wiley & Sons Ltd: New York, 1997; pp 37-58.
- (38) Schork, F.; Poehlein, G.; Wang, S.; Reimers, J.; Rodrigues, J.; Samer, C. *Colloid and Surfaces A: Physicochemical and Engineering Aspects* **1999**, 153, 39-45.
- (39) Xu, M.; Choi, Y. S.; Kim, Y. K.; Wang, K. H.; Chung, I. J. *Polymer* **2003**, 44 (20), 6387-6395.
- (40) Choi, Y. S.; Ham, H. T.; Chung, I. J. *Polymer* **2003**, 44 (26), 8147-8154.
- (41) Choi, Y. S.; Ham, H. T.; Chung, I. J. *Chemistry of Materials* **2004**, 16 (13), 2522-2529.
- (42) Greesh, N.; Hartmann, P. C.; Cloete, V.; Sanderson, R. D. *Journal of Colloid and Interface Science* **2008**, 319 (1), 2-11.
- (43) Uhl, F. M.; Wilkie, C. A. *Polymer Degradation and Stability* **2004**, 84 (2), 215-226.
- (44) Uhl, F. M.; Yao, Q.; Nakajima, H.; Manias, E.; Wilkie, C. A. *Polymer Degradation and Stability* **2005**, 89 (1), 70-84.
- (45) Wang, W. P.; Liu, Y.; Li, X. X.; You, Y. Z. *Journal of Applied Polymer Science* **2006**, 100 (2), 1427-1431.
- (46) Chung, D. *Journal of Materials Science* **1987**, 22 (12), 4190-4198.
- (47) Mai, Y.-W.; Yu, Z.-Z., *Polymer Nanocomposites*. 2nd edition; Woodhead Publishing: Cambridge, 2006; Vol. 19, pp 510-533.
- (48) Bourlinos, A. B.; Gournis, D.; Petridis, D.; Szabo, T.; Szeri, A.; Dekany, I. *Langmuir* **2003**, 19 (15), 6050-6055.
- (49) Nethravathi, C.; Rajamathi, M. *Carbon* **2006**, 44 (13), 2635-2641.
- (50) Bhinde, T.; Clarke, S. M.; Phillips, T. K.; Arnold, T.; Parker, J. E. *Langmuir* **2010**, 26 (11), 8201-8206.
- (51) Bragg, W. L. *Proceedings of the Cambridge Philosophical Society* **1913**, 17, 43-57.
- (52) Vaia, R. A.; Teukolsky, R. K.; Giannelis, E. P. *Chemistry of Materials* **1994**, 6 (7), 1017-1022.
- (53) Choi, K. S.; Liu, F.; Choi, J. S.; Seo, T. S. *Langmuir* **2010**, 26 (15), 12902-12908.
- (54) Stankovich, S.; Piner, R. D.; Nguyen, S. T.; Ruoff, R. S. *Carbon* **2006**, 44 (15), 3342-3347.
- (55) Zhang, R.; Hu, Y.; Xu, J.; Fan, W.; Chen, Z. *Polymer Degradation and Stability* **2004**, 85 (1), 583-588.
- (56) Ding, R.; Hu, Y.; Gui, Z.; Zong, R.; Chen, Z.; Fan, W. *Polymer Degradation and Stability* **2003**, 81 (3), 473-476.
- (57) Meng, Y. Polymer/graphite nanocomposites. In *Polymer Nanocomposites*, 2nd edition; Mai, Y.-W.; Yu, Z.-Z., Eds.; Woodhead Publishing: Cambridge, 2006; Vol. 19, pp 510-539.

Chapter 4: Poly(styrene-co-butyl acrylate) nanocomposites using functionalized graphite oxide

- (58) Yang, J.; Tian, M.; Jia, Q.-X.; Shi, J.-H.; Zhang, L.-Q.; Lim, S.-H.; Yu, Z.-Z.; Mai, Y.-W. *Acta Materialia* **2007**, 55 (18), 6372-6382.
- (59) Wang, C.; Wang, Q.; Chen, X. *Macromolecular Materials and Engineering* **2005**, 290 (9), 920-926.
- (60) Greesh, N.; Hartmann, P. C.; Sanderson, R. D. *Macromolecular Materials and Engineering* **2009**, 294 (3), 206-212.
- (61) Zhong, Y.; Zhu, Z.; Wang, S.-Q. *Polymer* **2005**, 46 (9), 3006-3013.
- (62) Donghwan, C.; Sangyeob, L.; Gyeongmo, Y.; Hiroyuki, F.; Lawrence, T. D. *Macromolecular Materials and Engineering* **2005**, 290 (3), 179-187.
- (63) Xiao, M.; Sun, L.; Liu, J.; Li, Y.; Gong, K. *Polymer* **2002**, 43 (8), 2245-2248.
- (64) Uhl, F. M.; Wilkie, C. A. *Polymer Degradation and Stability* **2002**, 76 (1), 111-122.
- (65) Samakande, A.; Sanderson, R. D.; Hartmann, P. C. *European Polymer Journal* **2009**, 45 (3), 649-657.

POLYSTYRENE/GRAPHITE NANOCOMPOSITES VIA SURFACE RAFT-MEDIATED POLYMERIZATION

The work described in this chapter has been published in the following paper:

Hussein M. Etmimi, Matthew P. Tonge and Ronald D. Sanderson, Synthesis and Characterization of Polystyrene-Graphite Nanocomposites via Surface RAFT-Mediated Miniemulsion Polymerization, **Journal of Polymer Science Part A: Polymer Chemistry**, Vol. 49, 1621–1632 (2011) (DOI: 10.1002/pola.24586)

Abstract

Graphite oxide (GO) was prepared and immobilized with dodecyl isobutyric acid trithiocarbonate (DIBTC) RAFT agent. The hydroxyl groups of GO were attached to the DIBTC RAFT agent through an esterification process. The resultant modified GO was used for the preparation of polystyrene/graphite nanocomposites in miniemulsion polymerization. The RAFT-grafted GO (GO-DIBTC), at various loadings, was dispersed in styrene monomer and the resultant mixtures sonicated in the presence of a surfactant (sodium dodecylbenzene sulfonate) and a hydrophobe (hexadecane) to form miniemulsions. The stable miniemulsions thus obtained were polymerized using azobis(isobutyronitrile) as the initiator to yield encapsulated polystyrene-graphite oxide (PS-GO) nanocomposites. The molar mass and dispersity of PS in the nanocomposites depended on the amount of RAFT-grafted GO in the system, in accordance with the features of the RAFT polymerization method. The PS-GO nanocomposites were of exfoliated morphology, as confirmed by X-ray diffraction and transmission electron microscopy measurements. The thermal stability and mechanical properties of the PS-GO nanocomposites were better than those of the neat PS polymer. Furthermore, the mechanical properties were dependent on the modified GO content (i.e., the amount of RAFT-grafted GO).

5.1 Introduction

Graphite is a pseudo-two-dimensional solid, which has a layered nanostructure. Due to its unique properties it can be used for the preparation of polymer nanocomposites with enhanced properties.¹⁻³ Graphite consists of a flat monolayer of carbon atoms, arranged in a planar ring system in six-atom hexagonal cells, known as graphene. These carbon atoms are tightly held together by covalent bonds on each graphene layer plane. The carbon atoms positioned in adjacent planes are bound by weak van der Waals forces. Due to there being no reactive groups on the graphite sheets and the high crystal lattice energy, graphite can not be easily dispersed in any polar or non-polar media. This makes it very difficult for a monomer or polymer to be loaded onto its surface. However, subjection of graphite flakes to oxidation under strong acidic conditions (e.g., H₂SO₄/HNO₃) leads to the formation of its oxidized form, referred to as graphite oxide (GO). This enables hydrophilic monomers (water soluble monomers) to form intercalated or exfoliated nanocomposite systems, due to the large interlayer spacing between GO nanosheets and the presence of various functional groups such as hydroxyl, carbonyl and epoxy on the GO surface.^{4,5} However, water insoluble (hydrophobic) monomers or polymers cannot be easily intercalated between GO layers. This is because the GO nanosheets are hydrophilic and therefore incompatible with hydrophobic monomers or polymers. Thus the compatibility between the GO nanosheets and the monomers or polymers selected for use needs to be improved.

In recent years, various studies have focused on the synthesis of polymer/graphite nanocomposites (PGNs) using chemically modified GO.^{6,7} Modification of GO sheets is expected to play a vital role in tailoring the structure and properties of GO, and improving the solubility and compatibility of GO sheets in polymer systems. The functionalization of GO will also enable us to prepare novel PGNs with enhanced functional properties. In 2010, Pramoda et al.⁸ reported the synthesis of poly(methyl methacrylate) (PMMA)/graphite nanocomposites using the *in situ* polymerization of methylmethacrylate (MMA) monomer in the presence of modified GO. First, the GO was functionalized with octadecylamine, and then reacted with methacryloyl chloride to incorporate polymerizable groups at the graphene nanoplatelets. The modified GO was then employed in the polymerization of MMA to obtain covalently bonded PMMA-graphite nanocomposites. The authors indicated that the thus obtained nanocomposites showed a significant enhancement in thermal and mechanical properties compared with neat PMMA. With only 0.5 wt% graphite content, the glass transition temperature (T_g) increased from 119 °C for neat PMMA to 131 °C for the

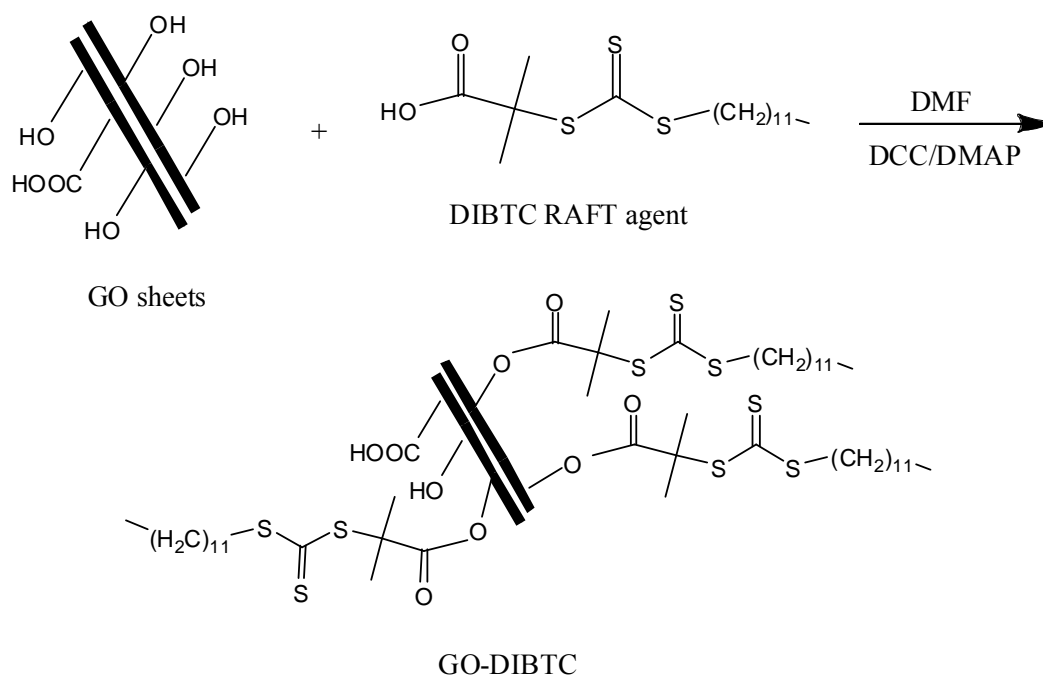
PMMA/graphite nanocomposite and the respective storage modulus increased from 1.29 to 2 GPa.

In the last decade, the use of solid supports in controlled/living radical polymerization (CLRP) has attracted much attention in the field of nanoscience and nanotechnology.⁹ This is due to the many advantages that CLRP offers over other polymerization techniques. These include: precise control over molecular architecture, the wide range of monomers that can be used, and the simple reaction conditions required. Various controlled polymerization methods such as nitroxide-mediated polymerization (NMP),^{10,11} atom transfer radical polymerization (ATRP),^{12,13} and reversible addition-fragmentation chain transfer (RAFT)¹⁴⁻¹⁸ are available, and have been widely applied to graft polymeric chains onto solid supports.

Since its discovery in the late 1990s,¹⁹ the RAFT method has become one of the most effective and versatile methods of CLRP.²⁰ The method operates via a degenerative transfer mechanism in which a thiocarbonylthio compound acts as a chain transfer agent. Its suitability over a wide range of reaction conditions required for the RAFT process and its versatility for use with different monomers make this method among the most useful of all the controlled polymerization techniques for designing molecular architectures.^{21,22} Thus, a combination of the RAFT process and graphite nanosheets for the synthesis of PGNs is expected to allow the preparation of tailor-made polymer nanocomposites with enhanced properties.

In the past, most researchers have focused mainly on the synthesis and characterization of PGNs using conventional free radical polymerization.³ Only a few articles on the use of CLRP, such as the RAFT method, focus on the use of clay^{23,24} and carbon nanotubes.^{25,26} In this study we report, for the first time, on the use of graphite-anchored RAFT agent in miniemulsion polymerization of Styrene (St). We intend to show that the RAFT agent is successfully attached to the surface of GO sheets via an esterification reaction. This led to an increase in the hydrophobic nature of the GO nanosheets, subsequently leading to better compatibility between GO and the water insoluble monomer, St. We also hypothesize that the use of an anchored RAFT agent will result in controlled living radical polymer growth from the graphite surface. This will lead to polymer nanocomposites with polymer chains attached to the GO nanosheets. Using the newly prepared RAFT-grafted GO (i.e., GO-dodecyl isobutyric acid trithiocarbonate (GO-DIBTC)), polystyrene (PS) nanocomposites with improved properties were prepared. To date, there are no reports in the open literature on the preparation or use of RAFT agents anchored onto graphene platelets.

The attachment of the RAFT agent to a solid support can be performed using either the R-group or the Z-group approach. In the R-group approach, the RAFT agent is attached to the solid support via the leaving and re-initiating R-group. In the Z-group approach, the RAFT agent is attached to the solid support through the stabilizing Z-group. Recently, Stenzel et al.²⁷ showed that in the R-group approach attachment via the R-group will lead to detachment of the RAFT agent during the polymerization, which may result in the loss of immobilized functionalities. In the Z-group approach these side reactions can be prevented, and controlled growth of polymer chains can be achieved.²⁸ In this study, however, a RAFT agent that has a carboxylic end group in the re-initiating group (R) was used. The RAFT agent that was successfully anchored onto the GO surface controlled the polymerization of St. Scheme 5.1 presents the overall synthesis route for the preparation of RAFT-immobilized GO nanosheets.



Scheme 5.1: The overall synthesis route for the preparation of RAFT-immobilized GO nanosheets (DMF: N,N-dimethylformamide, DCC: 1,3-dicyclohexyl carbodiimide, DMAP: 4-dimethylaminopyridine).

Miniemulsion is a convenient one-step technique that can be used for the incorporation of nanolayered filler materials such as clay²³ and carbon nanotubes²⁹ in polymer matrices. In the miniemulsion process, the oil phase, which consists of the monomer and the filler, can be dispersed in the water phase by a high-shear device such as a sonicator. This will lead to the formation of monomer droplets containing the filler particles, and stabilized by the surfactant and the hydrophobe, from which polymer particles will develop during the polymerization

step.²³ In this study, RAFT-grafted GO was dispersed in water in the presence of St monomer, a surfactant and a hydrophobe, to form miniemulsions. The obtained miniemulsions were polymerized to afford polystyrene-graphite oxide (PS-GO) nanocomposites in a controlled manner.

5.2 Experimental

5.2.1 Chemicals

Styrene (99%, Aldrich) was purified by washing with aqueous 0.3 M KOH, followed by distillation at 40 °C under reduced pressure. Hexadecane (HD) (99%, Sigma-Aldrich), acetone (99%, Aldrich), chloroform (98%, Aldrich), isopropanol (99%, Aldrich), hexane (95%, Aldrich), 1-dodecanthiol (97%, Aldrich), tricaprlyl methyl ammonium chloride (Aliquot 336) (Acros), carbon disulfide (99.9%, Aldrich), 1,3-dicyclohexyl carbodiimide (DCC) (99%, Aldrich) and 4-dimethylamino pyridine (DMAP) (98%, Aldrich) were all used as received, without any further purification. 2,2'-Azobis(isobutyronitrile) (AIBN) (98%, Aldrich) was purified by recrystallization from methanol. Sodium dodecylbenzene sulfonate (SDBS) (99%, Fluka), hydrochloric acid (32%, Merck), sodium hydroxide (97%, Merck), potassium hydroxide (84%, Merck), *N,N*-dimethylformamide (DMF) (99%, Fluka) and dichloromethane (DCM) (99%, Fluka) were also used without any further purification. Potassium permanganate (99%), sodium nitrate (99%) and hydrogen peroxide (30%) were obtained from Sigma-Aldrich and used as received. Sulfuric acid (98.08%, Merck) was also used as received. Natural graphite (99.5%) was obtained from Graphit Kropfmühl AG (Hauzenberg, Germany) and used without any further purification. GO was prepared as described in the literature.³⁰ Distilled and deionized (DDI) water was obtained from a Millipore Milli-Q water purification system.

5.2.2 Analytical techniques

Size exclusion chromatography (SEC) was carried out using a Waters 610 Fluid Unit, Waters 410 Differential Refractometer at 30 °C, Waters 717plus Autosampler and Waters 600E System Controller (run by Millennium 32 V3.05 software). Tetrahydrofuran (THF) (HPLC grade), sparged with IR grade helium, was used as an eluent at a flow rate of 1 mL/min. Two PLgel 5- μ m Mixed-C columns and a PLgel 5- μ m guard pre-column were used. The column

oven was kept at 35 °C and the injection volume was 100 μL . The system was calibrated with narrow PS standards (5 mg/mL THF), ranging from 2 500 to 898 000 g mol^{-1} .

Prior to SEC analysis, 3 mL of each latex was precipitated with concentrated hydrochloric acid, the precipitate was washed several times with methanol, then with DDI water, and finally dried at 40 °C under reduced pressure. The PS chains were cleaved from the GO nanosheets at the ester bond under basic conditions. Typically, the dried nanocomposite sample (0.1 g) was dispersed in 40 mL 1M KOH/ethanol and THF solution (1:4) and stirred for 48 h. The dried samples were then dissolved in THF (5 mg/mL) for 24 h and filtered through a 0.45- μm nylon filter. SEC analysis, using THF as mobile phase and an initial polymer concentration of 5 mg/mL, was performed on the polymer solutions.

Transmission electron microscopy (TEM) was used to directly visualize the morphology of the PS-GO nanocomposites at the nanometer level. Bright-field TEM images were recorded using a LEO 912 transmission electron microscope, at an accelerating voltage of 120 kV. Prior to analysis, miniemulsion samples were diluted with DDI water (0.05%) and placed on 300-mesh copper grids, which were then transferred to the TEM apparatus. The average particle size of the synthesized latices was determined using computer software (Image J). A portion of the PS-GO miniemulsion latices was dried, then embedded in an epoxy resin, and cured at 60 °C for 24 h. The embedded samples were then ultra-microtomed with a diamond knife on a Reichert Ultracut S ultramicrotome, at room temperature. This resulted in sections with a nominal thickness of approximately 100 nm. The sections were collected on a water surface and transferred to 300-mesh copper grids at room temperature, which were then transferred to the TEM apparatus.

Thermogravimetric analysis (TGA) measurements were done on a TA Instruments Q500 thermogravimetric analyzer. Sample weights of 10–15 mg were used for all analyses. Analyses were carried out from ambient temperature to 600 °C, using a heating rate of 20 °C/min. All TGA analyses were carried out under a nitrogen atmosphere: nitrogen was purged at a flow rate of 50 mL/min.

Nuclear magnetic resonance (NMR) spectroscopy was performed at 20 °C using a Varian VXR-Unity 300 MHz.

Dynamic light scattering (DLS) was used to determine the average particle size of the prepared latices. The measurements were carried out using a Zetasizer ZS 90 (Malvern Instruments, United Kingdom) apparatus equipped with a 4 mW He-Ne laser, operating at a wavelength of 633.0 nm. Miniemulsion samples were first diluted with DDI water before they were analyzed; a drop of the latex was diluted in DDI water (~ 4 mL). The instrument was first calibrated with a nano-standard solution with a particle size of 220 nm, before a latex sample was run. The scattered light was detected at an angle of 90° and the final particle size was obtained from three measurements, each comprising 10 sub-runs. The droplet size was calculated via a CONTIN analysis and presented as the Z-average particle size (Z_{avg}).

Fourier-transform infrared (FT-IR) spectroscopy was carried out on a Nexus 470 FT-IR instrument (Thermo Nicolet, USA), by averaging 32 scans. All spectra were acquired over the 450 to 4000 cm^{-1} wavenumber range with a resolution of 4 cm^{-1} .

X-ray diffraction (XRD) patterns were obtained using a PANalytical X'Pert PRO Multi-Purpose Diffractometer equipped with a CuK (alpha) sealed tube X-ray source (wavelength 1.514 Å). X'Celerator in Bragg-Brentano mode was used as the detector for all analyses.

Dynamic mechanical analysis (DMA) of the PS-GO films was carried out using a Physica MCR 501 Rheometer apparatus (Anton Paar, Germany). Parallel-plate geometry (25 mm in diameter) with a 1-mm gap distance and a constant strain of 0.1% was used. All measurements were carried out from 140 to 80 °C, at a cooling rate of -5 °C, an oscillation frequency of 1 Hz, and a normal force of 5 N. In the case of PS reference, the measurements were carried out from 140 to 50 °C under the same conditions. The nanocomposite films were prepared by pressing the composite samples into thin discs (25 mm) using a hydraulic press machine at 120 °C.

Ultraviolet (UV) absorption spectra were recorded using a 1-cm path length quartz cuvette, with DCM as the reference, on a Perkin Elmer Lambda 20 UV spectrophotometer.

5.2.3 Preparation of GO

The preparation of GO was carried out by treating the natural graphite with potassium permanganate in the presence of sulfuric acid, following the method of Hummers and Offeman,³⁰ with some modification. In brief, powdered flake graphite (1 g) and sodium nitrate

(0.5 g) were stirred into 98% sulfuric acid (23 mL). As a safety measure, the ingredients were mixed in a 150 mL conical flask that had been cooled to 0 °C in an ice bath. Potassium permanganate (3 g) was then added to the suspension. The rate of addition was carefully controlled to prevent the temperature of the suspension from exceeding 20 °C. The ice bath was then removed and the temperature of the suspension brought to 35 °C, where it was maintained for 30 min.

The mixture gradually thickened as the reaction progressed and after 15 min the mixture became pasty, with a brownish gray color. After 30 min, water (46 mL) was slowly stirred into the paste, causing a violent reaction and an increase in temperature to 100 °C. The diluted suspension was then maintained at this temperature for 15 min. The suspension was then further diluted with warm water (42 mL), after which 3% hydrogen peroxide (10 mL) was added to reduce the residual permanganate and manganese dioxide to colorless soluble manganese sulfate. The solid product containing the GO nanosheets was obtained by centrifugation. The final solid was then washed five times with DDI water until neutrality (pH ~ 7), to yield brown GO (1.2 g).

5.2.4 Synthesis of DIBTC RAFT agent

DIBTC was synthesized according to the method of Lai et al.³¹ 1-dodecanthiol (8.0 g, 0.04 mol), acetone (20.1 g, ~ 6x molar excess) and a phase transfer catalyst Aliquot 336 (0.65 g, 0.0016 mol) were mixed in a reaction vessel, which was previously cooled to ~ 0 °C in an ice bath. Sodium hydroxide solution (50%; 3.5 g, 0.043 mol) was added dropwise over 20 min and the reaction mixture stirred for a further 15 min. This was followed by the dropwise addition of a carbon disulfide solution (3.1 g, 0.041 mol) in acetone (4.0 g, 0.069 mol) over 20 min. The viscosity of the reaction mixture increased and the product changed from an opaque milky white color to a bright transparent yellow color. After 10 min, chloroform (7.0 g, 0.06 mol) was added to the solution in one portion, followed by the dropwise addition of a second quantity of sodium hydroxide (50%; 16.0 g, 0.2 mol) over 30 min.

The content of the reaction vessel was stirred at room temperature overnight under reflux. The mixture was then poured into a large beaker and stirred at high revolutions (600 rpm). DDI water (60 mL) was added to the reaction mixture, which was then acidified with hydrochloric acid (33%; 10.0 mL). The reaction was stirred vigorously to evaporate any remaining acetone.

The product congealed, and the solid product was collected by filtration, using a Buchner funnel. The solid was stirred in excess isopropanol for 30 min. The isopropanol solution containing crystalline S,S'-bis(1-dodecyl) trithiocarbonate was concentrated and the final product was recrystallized from hexane to yield S-1-dodecyl-S'-(isobutyric acid) trithiocarbonate; purity 98% by NMR. ¹H-NMR (300 MHz, (DMSO-*d*₆) δ (ppm): 0.85 (t, *J* = 7.02 Hz, 3H) (CH₃-CH₂-); 1.24–1.34, m, 20H (CH₃-CH₂-CH₂-); 1.62, s, 6H (CH₃-); 3.3 (t, *J* = 7.42 Hz, 2H) (-CH₂-S); 13.05, s, 1H (-OH). ¹³C-NMR (75 MHz, CDCl₃) δ (ppm): 220.78 (C=S), 178.75 (C=O), 55.58 (C), 37.05 (C-S), 31.90 1C (-CH₂-CH₂-CH₂-), 27.81–29.62, 8C (-CH₂-CH₂-CH₂-), 25.21, 2C (CH₃)₂, 22.68, 1C (CH₃-CH₂-CH₂-), 14.11, 1C (CH₃-CH₂-). The ¹H-NMR and ¹³C-NMR spectra are shown in Appendix E.

5.2.5 Immobilization of the DIBTC RAFT agent on the GO surface

Graphite oxide (0.2 g) was stirred in DMF (100 mL) for 15 min, after which it was sonicated for a further 15 min using a Vibracell VCX 750 ultrasonicator (Sonics & Materials Inc.). The sonicator amplitude was set at 90% and the pulse rate was set at 2 s. The sonication was done to allow effective dispersion of the GO sheets in the solvent DMF. DIBTC RAFT agent (0.5 g) was then added and the resultant mixture stirred for 5 min at room temperature. After DCC (0.5 g) and DMAP (0.1 g) were added to the solution, the mixture was stirred at room temperature for 24 h under reflux. The solvent was then removed under reduced pressure and the solid was washed with DCM four times (until the washings were free of the RAFT agent, as determined by UV analysis) to remove the unattached RAFT agent. The resultant product was then dried at 40 °C under vacuum overnight to yield the RAFT agent-immobilized GO (0.25 g).

5.2.6 Synthesis of PS-GO nanocomposites by RAFT-mediated miniemulsion polymerization

Predetermined quantities of RAFT-grafted GO (GO-DIBTC) were stirred in DDI water (~ 50 g) for 15 min. The mixture was sonicated using a Vibracell VCX 750 ultrasonicator (Sonics & Materials Inc.) for 15 min to disperse the GO sheets to small nanoplatelets. AIBN, St and HD (oil phase) were added and the mixture was stirred for a further 15 min, after which it was sonicated for another 15 min to allow effective swelling of the GO-DIBTC nanoplatelets by the monomer. An aqueous solution of SDBS was added to the oil phase and the mixture stirred for a further 1 h to obtain a pre-mini-emulsion. The pre-mini-emulsion was

then sonicated for 15 min, in a water-jacketed vessel. The sonicator was set at 80% amplitude, a pulse rate of 2 s, and a cut-off temperature of 40 °C to prevent polymerization during the sonication step. The average energy expended was approximately 67 kJ. A three-neck round-bottom flask containing the resultant miniemulsion was immersed in an oil bath. The content of the flask was then nitrogen purged for 15 min before the temperature was raised to 75 °C to start the polymerization. The reaction was carried out for 10 h under a nitrogen atmosphere, after which it was cooled to room temperature to stop the polymerization.

A similar procedure was used for the synthesis of the PS reference by miniemulsion polymerization. The oil phase, consisting of St, AIBN, DIBTC and HD was mixed with an aqueous solution of SDBS for 30 min. The mixture was then sonicated under the same conditions for 15 min to obtain the miniemulsion. The polymerization was started at 75 °C and carried out for 10 h under a nitrogen atmosphere. The formulations used for the polymerization of PS-GO nanocomposites and the PS reference are tabulated in Table 5.1.

Table 5.1: Miniemulsion formulations used for the preparation of PS-GO nanocomposites and the PS reference

Nano-composite	DIBTC (g)	GO-DIBTC (g)	St (g)	AIBN (g)	SDBS/10 g of DDI water (g)	HD (g)	DDI water (g)
PS-Standard	0.0085	-	3.05	0.0052	0.060	0.15	50.18
PS-GO-1	-	0.030	3.01	0.0083	0.060	0.10	51.13
PS-GO-2	-	0.060	3.02	0.0080	0.060	0.10	50.17
PS-GO-3	-	0.091	3.06	0.0082	0.061	0.11	50.82
PS-GO-4	-	0.112	3.01	0.0080	0.062	0.12	50.30
PS-GO-5	-	0.137	3.08	0.0084	0.060	0.12	50.42
PS-GO-6	-	0.170	3.06	0.0080	0.060	0.11	50.13
PS-GO-7	-	0.204	3.01	0.0081	0.062	0.14	50.23

5.3 Results and discussion

5.3.1 Nanostructure of GO by TEM

TEM was used to visually observe the graphite sheets before and after modification in order to determine their particle size and morphology. Figure 5.1 shows the TEM images of pristine natural graphite dispersed in DDI water. As can be seen in Figure 5.1, the dimensions of the flakes of natural graphite are in the micrometer range. These flakes consist of graphite

nanosheets, which are normally less than 100 nm in thickness.³² Figure 5.2 shows the TEM images of the GO, dispersed in aqueous solution of SDBS (3% relative to GO) by sonication. The TEM images in Figure 5.2 a clearly show that the GO consisted of small aggregates of graphite nanosheets with sizes < 200 nm. These graphite aggregates contain smaller GO nanoplatelets 2–5 nm in size (see Figure 5.2 b).

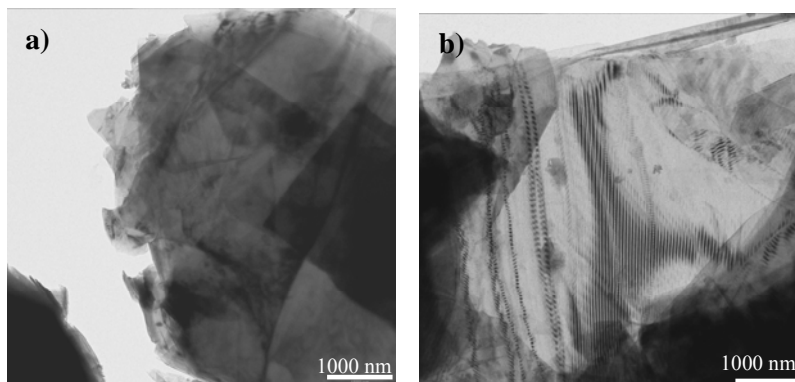


Figure 5.1: TEM images of natural graphite showing different areas of the same graphite sample.

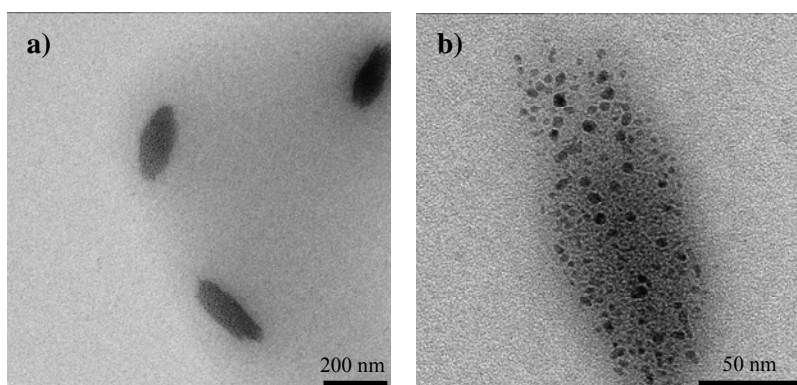


Figure 5.2: TEM images of GO dispersed in aqueous solution of SDBS: a) low magnification image and b) higher magnification image.

5.3.2 Immobilization of RAFT agent onto GO surfaces

In 2002, Lai et al.³¹ reported on the synthesis and use of a trithiocarbonate (i.e., DIBTC) as the RAFT agent in the controlled free radical polymerization of St. Their results showed that trithiocarbonate is an excellent RAFT agent for the living radical polymerization of St. Because the carbon attached to the labile sulfur atom is tertiary, this RAFT agent has extremely high chain-transfer efficiency and control over radical polymerization. PS with narrow molecular weight distribution and predictable molecular weight was obtained. Therefore, attempts were made to immobilize trithiocarbonate DIBTC RAFT agent onto a GO surface in order to prepare PS-grafted GOs.

After treatment of natural graphite with potassium permanganate in the presence of sulfuric acid, graphite was functionalized with hydroxyl groups.⁴ The RAFT agent immobilized GO (i.e., GO-DIBTC) was prepared by the reaction of hydroxyl functionalized GO (GO-OH) with the RAFT agent DIBTC in the presence of DCC and DMAP (see Scheme 5.1). In order to remove the unattached RAFT agent from the graphite surface, the GO-DIBTC sample was washed with DCM solvent. The procedure was repeated until the washing solvent was free of RAFT agent, as confirmed by measuring the UV absorbance of the washing solvent. It is well known that the thiocarbonyl moiety (C=S) has an absorption maximum at about 320 nm: λ_{\max} 320 nm (C=S, π - π^*). Figure 5.3 shows the change in UV absorbance of the solvent after washing as a function of the number of washes. After four washes the washing solvent was free of the RAFT agent, indicating that all unattached RAFT agent was removed from the GO-DIBTC sample.

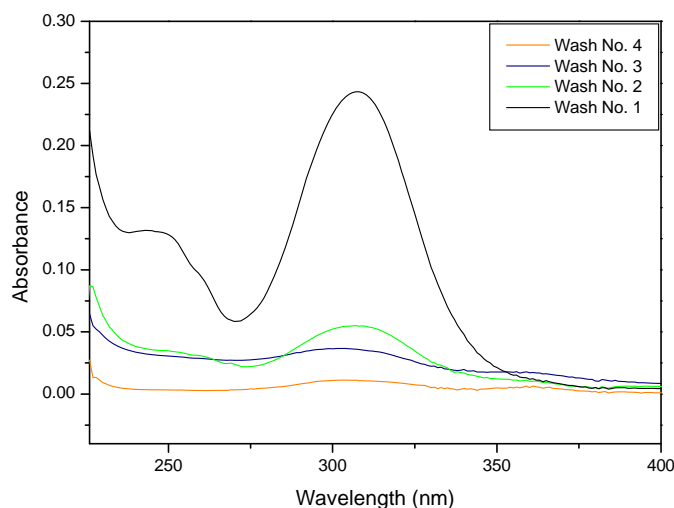


Figure 5.3: UV spectrum of GO-DIBTC product after successive washings with DCM.

The GO-DIBTC product was then characterized by FT-IR (KBr discs). The amount of GO sample added to the KBr had to be strictly controlled because the black GO can absorb most of the infrared rays if too high concentration of GO is used. Compared with the FT-IR spectrum of crude GO (Figure 5.4 b), the FT-IR spectrum of GO-DIBTC (Figure 5.4 c) shows the characteristic peaks of the DIBTC RAFT agent, such as C–H, C=O, C–S and C=S stretching vibrations, centered at 2921 and 2853, 1701, 815 and 1069 cm^{-1} , respectively (see Figure 5.4 a). Using this information, and knowing that all free RAFT was removed, it was concluded that the RAFT agent is covalently bound to the surface of the GO.

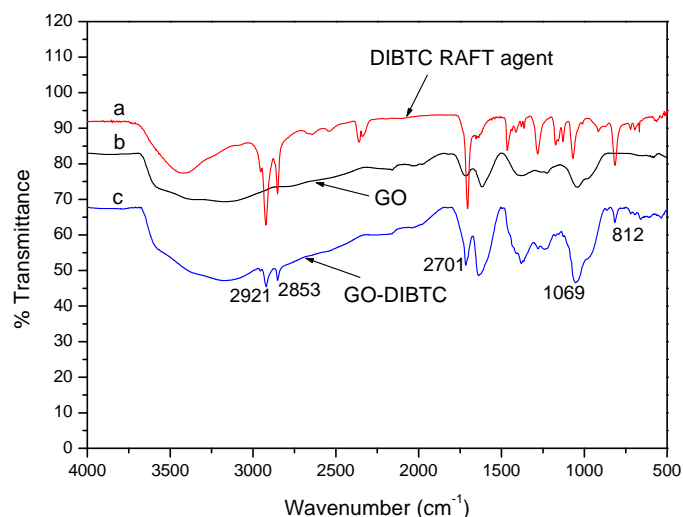


Figure 5.4: FT-IR spectra of (a) DIBTC RAFT agent, (b) GO and (c) GO-DIBTC.

Dispersion of GO into St monomer was very difficult to achieve, even after stirring the mixture overnight. This can be attributed to the hydrophilic nature of GO, which can not be easily dispersed in hydrophobic monomers such as St. However, dispersion of GO-DIBTC into St was very easy, even when a large amount of GO-DIBTC relative to monomer was used. Figure 5.5 shows digital images of the GO and the RAFT-grafted GO dispersed in St monomer. It is apparent that GO is insoluble in St, and there was much sedimentation of GO at the bottom of the vial (see Figure 5.5 a). However, as shown in Figure 5.5 b, the RAFT-functionalized GO is soluble in St – it forms a homogeneous solution (no sedimentation observed). The anchored RAFT agent led to an increase in the hydrophobic character of the GO nanosheets, subsequently leading to better compatibility between GO and the water insoluble monomer St.

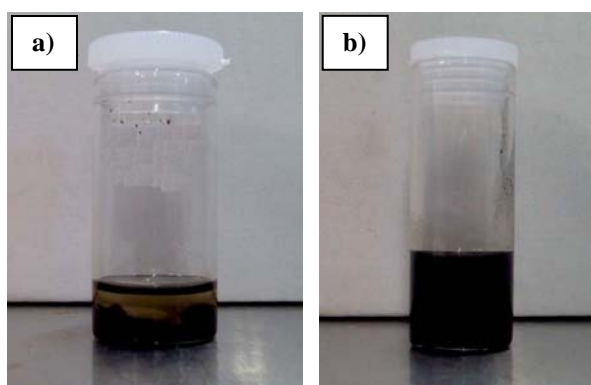


Figure 5.5: Digital photographs of GO and GO-DIBTC dispersed in St monomer: (a) 1 wt% GO relative to monomer and (b) 5 wt% GO-DIBTC relative to monomer.

The quantity of DIBTC RAFT agent in a sample was determined by using the residual weight difference between DIBTC-functionalized GO and the neat GO. TGA showed 82.5% weight loss at 500 °C for GO-DIBTC and 50.5% weight loss for GO (see Figure 5.6). As can be seen in Figure 5.6, the RAFT agent was totally lost at 500 °C (~ 0% weight was observed). This 32% difference in weight loss is due to the DIBTC RAFT agent, which was grafted onto the GO sheets.

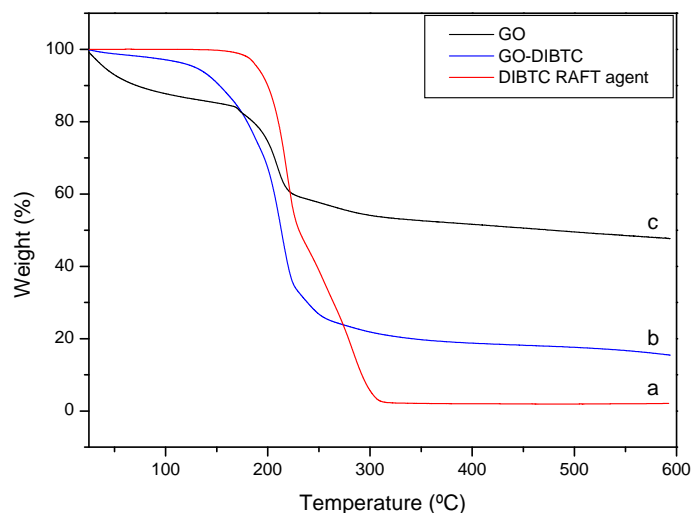


Figure 5.6: TGA curves of (a) DIBTC RAFT agent, (b) GO-DIBTC and (c) GO.

5.3.3 Characterization of PS-GO nanocomposites

5.3.3.1 SEC analysis

Styrene was polymerized using AIBN as initiator and DIBTC RAFT agent that was attached to the GO sheets as chain transfer agent. The PS-GO nanocomposite was obtained from the latex by precipitation in methanol. After washing and drying the final nanocomposite product, a gray powder was obtained. Table 5.2 summarizes the molecular weights (weight average molecular weight, \bar{M}_w and number average molecular weight, \bar{M}_n) and dispersity (\mathcal{D}) values of PS in the nanocomposites prepared with different quantities of GO-DIBTC. An increase in GO-DIBTC loading resulted in a decrease in the molar masses of the PS chains. This was expected, because the concentration of the RAFT agent increases with an increase in the amount of RAFT-modified GO incorporated into the polymer nanocomposites. It is well known that an increase in the RAFT agent concentration results in a decrease in the molar mass of polymers.^{33,34}

From Table 5.2, it can be seen that the best control was achieved with 7 wt% GO-DIBTC loading, which seems to be the threshold concentration at which good control begins to be observed. The higher \bar{D} values recorded at low GO-DIBTC content may be attributed to the fact that the system is highly heterogeneous. In this system the monomer is emulsified in the water phase and the modified GO, on which the RAFT agent is attached, is suspended in the monomer phase. Thus the RAFT agent is not homogeneously distributed in the monomer phase, resulting in regions of low and high RAFT agent concentration. Therefore, the probability of a growing polymeric radical to encounter a RAFT molecule, and thus control of polymerization, increases with an increase in GO-DIBTC concentration (i.e., an increase in RAFT agent concentration).

Table 5.2: Molar masses and \bar{D} of the PS-GO nanocomposites and PS reference

Nanocomposite	GO-DIBTC relative to monomer (wt%)	\bar{M}_n (g/mol)	\bar{M}_w (g/mol)	\bar{D}
PS	-	96700	162600	1.68
PS-GO-1	1	177400	287700	1.62
PS-GO-2	2	116600	185000	1.58
PS-GO-3	3	74600	106800	1.43
PS-GO-4	4	84600	126400	1.49
PS-GO-5	5	61700	87900	1.42
PS-GO-6	6	71100	93900	1.32
PS-GO-7	7	53600	67500	1.26

Furthermore, at lower GO-DIBTC loadings the number of GO-DIBTC particles might vary from one polymer particle to another, leading to different target chain lengths, and thus higher \bar{D} is observed. In addition, it was observed that at low GO-DIBTC loading (i.e., low RAFT concentration) polymer chains with high \bar{M}_n were obtained (see Table 5.2). This could result in a larger \bar{D} value due to the effect of the more newly formed PS chains from AIBN. As the concentration of RAFT-grafted GO increases, such variation is expected to be smaller, resulting in lower \bar{D} values.

5.3.3.2 TEM analysis

TEM was also used to visualize the latex particles and to determine the morphology of the films that were prepared from the obtained latices. Figure 5.7 shows TEM images of the latex

particles prepared using 4 and 5 wt% GO-DIBTC relative to the monomer. Individual polymer particles with diameters ranging from 150 to 180 nm were obtained. The particle size distribution is fairly narrow, which is an indication that little to no secondary particle nucleation occurred during the polymerization process. The lighter areas are representative of the polymer shell, while the darker areas represent the core modified GO. This is due to the difference in contrast between the core and the shell domains as a result of the different path lengths and material densities of the constituent materials. This resulted in increased scattering of the incident electron beam from the core material (GO), resulting in a darker region in the TEM images. The GO nanoplatelets, which have smaller particle dimensions (see Figure 5.2) could be incorporated into the polymer particles. This is due to the effect of the DIBTC RAFT agent, which made GO more hydrophobic, allowing for better compatibility between the monomer and the GO nanosheets. As indicated in Figure 5.5, GO is hydrophilic and does not mix with monomer (St), while GO-DIBTC is hydrophobic and disperses in monomer.

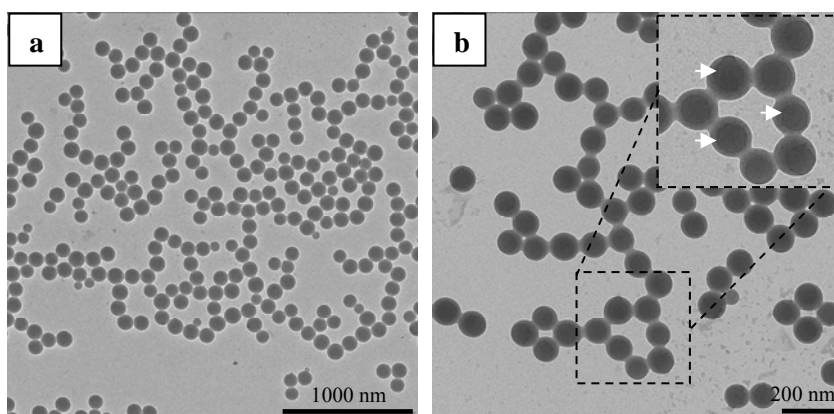


Figure 5.7: TEM images of PS-GO nanocomposite latex particles made with different amounts of GO-DIBTC: (a) 5 wt% GO-DIBTC (at low magnification) and (b) 4 wt% GO-DIBTC (at higher magnification).

The GO nanosheets can also be seen in the TEM images of the dried film that was embedded into epoxy resin. Figure 5.8 a and b show TEM images of films made with 3 and 5 wt% of GO-DIBTC relative to monomer, respectively. Most of the graphene nanoplatelets were of exfoliated morphology, with the exception of some areas that contained a few intercalated GO nanosheets (in agreement with the XRD measurements).

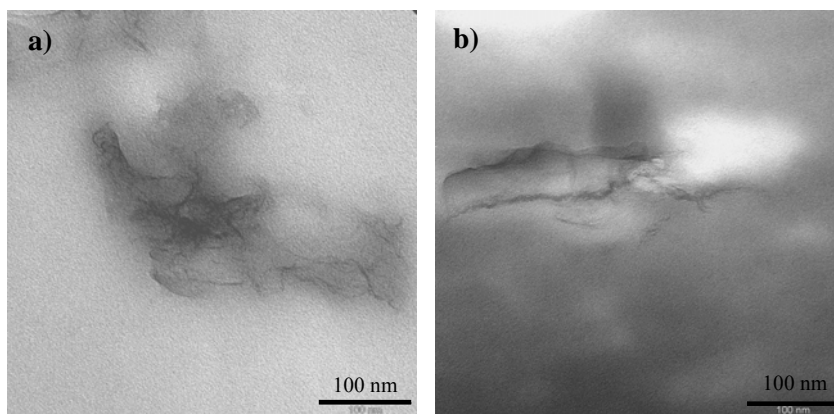


Figure 5.8: TEM images of microtomed films cast from PS-GO nanocomposite latices prepared with different amount of GO-DIBTC: (a) 3 wt% GO-DIBTC, and (b) 5 wt% GO-DIBTC.

5.3.3.3 XRD analysis

The XRD patterns of PS-GO nanocomposites with different GO-DIBTC loadings are shown in Figure 5.9. The measurements were performed on nanocomposites containing 1, 5 and 7 wt% GO-DIBTC relative to monomer. Complete exfoliation of the GO sheets was obtained (no diffraction peak of GO nanoplates was observed). The absence of the characteristic peak of GO suggested that the layered GO had been exfoliated in the nanocomposites.³⁵ The broad peak observed at a 2θ value of 20° is due to PS, as reported in literature.³⁶

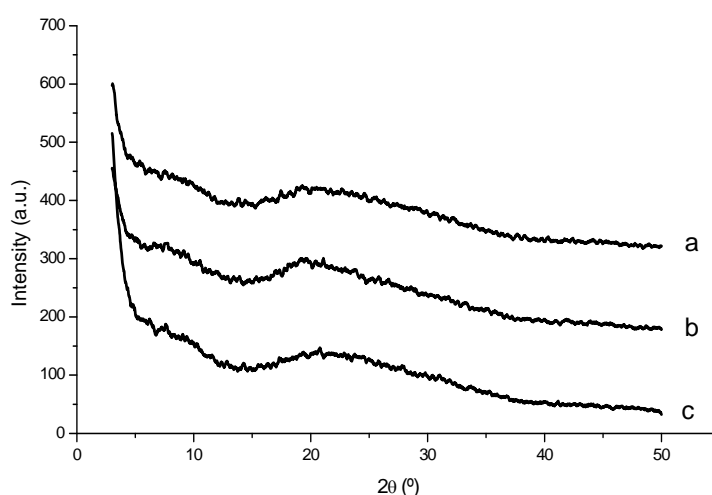


Figure 5.9: XRD results of PS-GO nanocomposites with different GO-DIBTC loadings: (a) 1 wt% GO-DIBTC, (b) 5 wt% GO-DIBTC and (c) 7 wt% GO-DIBTC.

5.3.3.4 Particle size measurements

The average particle size of the PS-GO miniemulsion latices increased as the GO-DIBTC loading increased. An increase in modified GO content implies that more space is required to accommodate the nanosheets within the polymer particles. The increased particle size might also be due to the increase in hydrophilic content due to the GO sheets. Figure 5.10 shows the evolution of particles size as the GO-DIBTC content increases, as measured by DLS. Latex particles with sizes ranging from 125 to 160 nm were observed (in agreement with TEM results).

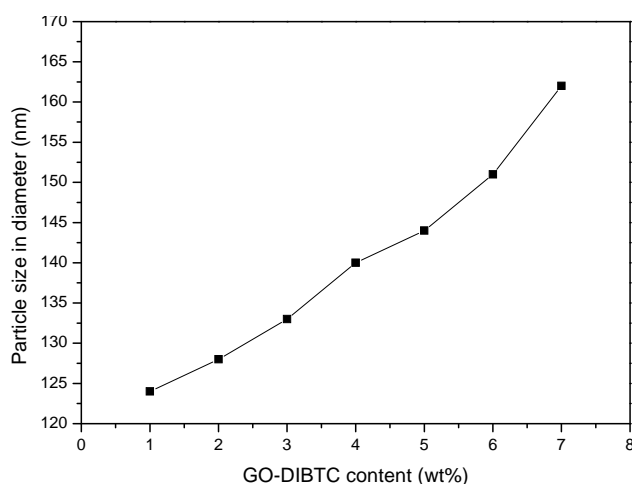


Figure 5.10: Evolution of particle size vs. DIBTC-grafted-GO loading.

5.3.3.5 Thermal stability

Another enhanced property that PGNs may exhibit is their increased thermal stability.^{36,37} Our results also showed that the thermal stability of PS-GO nanocomposites is improved relative to neat PS. Figure 5.11 shows the TGA thermograms of PS-GO nanocomposites prepared with different quantities of GO-DIBTC. For comparison, a TGA thermogram of a PS reference is also shown. It can be seen that PS does not contain any volatile products below 300 °C; however, the main chain of PS decomposes at around 300 °C.

The onset temperature of degradation for the PS in the nanocomposites increased noticeably in the presence of GO and all synthesized nanocomposites are more thermally stable relative to the neat PS. This indicates that the incorporation of GO into the PS leads to better thermal stability of the polymer. However, the results indicate that improvement in thermal stability is not simply a function of GO-DIBTC loading (see Figure 5.11). This was attributed to the effect of GO-DIBTC concentration in the molar masses of the PS in the nanocomposite. It

was found that the molar masses of the polymer in the nanocomposites decreased markedly as the RAFT-functionalized graphite loading increased (see Table 5.2). The effect of this change in molar mass could counteract the effect of the increased graphite content on the thermal stability.

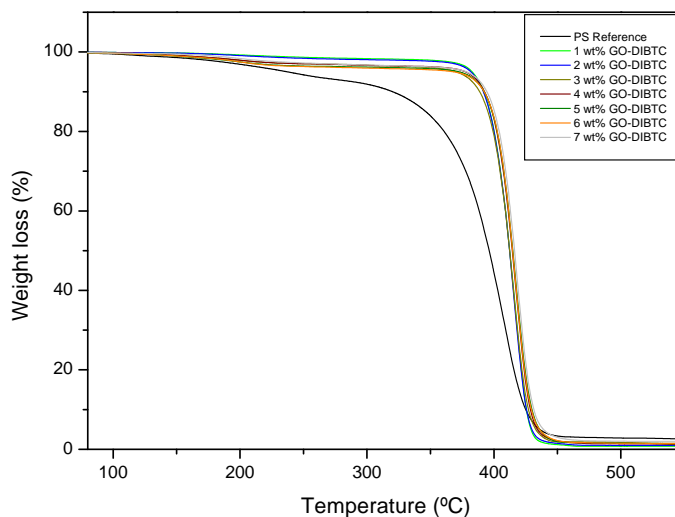


Figure 5.11: TGA thermograms of PS-GO nanocomposites and a PS reference.

The improvement in thermal stability of PS in the presence of GO can be attributed to the intercalation of PS into the lamellae of graphite. The PS chains are trapped between the graphene nanoplatelets in GO, which may act as an insulator between the heat source and the surface area of polymer, where the combustion occurs.³⁸ The presence of graphene nanoplatelets may also hinder the diffusion of volatile decomposition products within the nanocomposites by promoting char formation. The char formed layer act as a mass transport barrier that retards the escape of the volatile products generated as the PS decomposes.³⁵ The enhancement of the nanocomposites' thermal stability has also been attributed to the movement restriction of the polymer chains inside the graphite nanogalleries.³⁵

5.3.3.6 Mechanical properties

The mechanical properties of the PS-GO nanocomposites were evaluated by DMA. DMA measurements were performed on dried films prepared from the PS-GO latex composites containing 1, 2, 3 and 6 wt% GO-DIBTC relative to monomer. Results showed that the nanocomposites with high GO-DIBTC content had enhanced storage and loss modulus in the glassy state relative to the neat PS reference (see Figures 5.12 and 5.13).

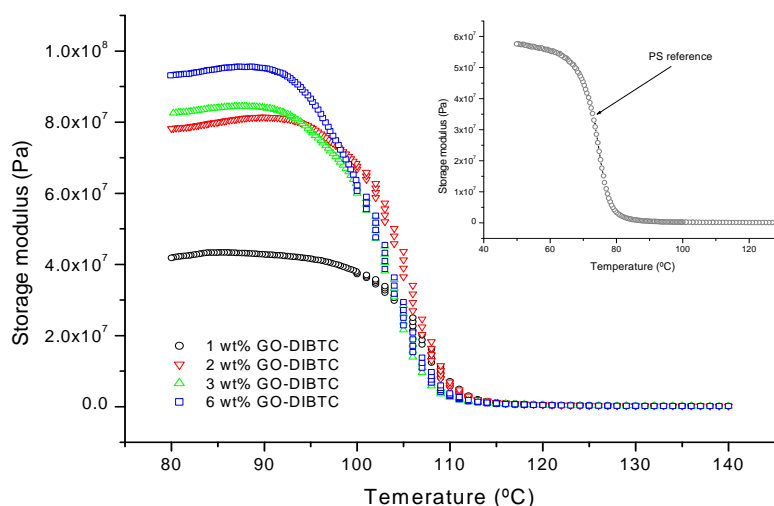


Figure 5.12: Storage modulus as function of temperature of PS-GO nanocomposites at GO-DIBTC loadings of 1, 2, 3 and 6 wt%. The insertion shows the storage modulus of PS reference.

At modified GO loadings of 1 wt% relative to monomer, the storage modulus of the nanocomposite was lower than that of the PS reference (5.7×10^7 Pa). However, samples with higher GO-DIBTC content (2–6 wt%) had storage modulus values higher than that of the pure PS. Furthermore, at low GO-DIBTC content (1–3 wt%) the loss modulus of the nanocomposites was lower than that of the PS reference (1.6×10^7 Pa).

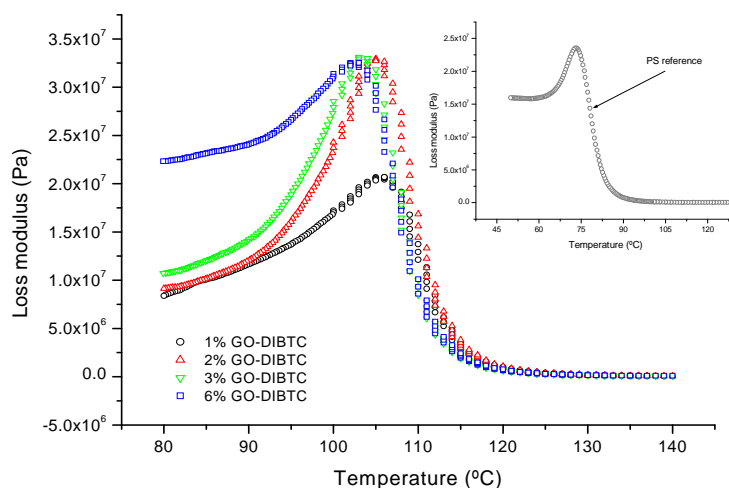


Figure 5.13: Loss modulus as function of temperature of PS-GO nanocomposites, at GO-DIBTC loadings of 1, 2, 3 and 6 wt%. The insertion shows the loss modulus of PS reference.

However, when the modified GO content reached 6 wt% relative to monomer the loss modulus was higher than that of the pure PS standard (see Figure 5.13). Results also showed

that the modulus was simply a function of filler content in the nanocomposite. Both the storage and the loss modulus of PS-GO nanocomposites increase with increasing modified GO content in the sample. The enhancement in storage and loss modulus is caused by the strong interaction between polymer chains and GO nanoplatelets, which have a high aspect ratio. This results in a decrease in the polymer segments' mobility near the polymer-graphite interface, leading to a higher modulus.^{39,40}

The T_g of the PS polymer in the nanocomposite was determined from the onset temperature of the $\tan \delta$ curve in the DMA scan. Figure 5.14 shows the variation of $\tan \delta$ of the PS-GO nanocomposites with temperature. Table 5.3 shows the T_g of PS-GO nanocomposites containing different loading of GO-DIBTC. A shift of the $\tan \delta$ peaks of the nanocomposites to higher temperatures relative to the PS reference was recorded. This indicates that the PS-GO nanocomposites have higher T_g values, ranging from 101 to 105 °C, compared to the value of the pure PS ($T_g = 74$ °C) (see Table 5.3). This was due to restricted chain mobility of the polymer caused by the presence of GO nanosheets.

However, as the modified GO (GO-DIBTC) loading increased, a slight shift of the $\tan \delta$ peaks to lower temperatures (lower T_g values) was recorded. This was attributed to the change in molar masses of the PS in the nanocomposites prepared with different quantities of modified GO (i.e., GO-DIBTC). It was shown in Table 5.2 that an increase in the RAFT-functionalized GO loading resulted in a significant decrease in the molar mass of the PS chains. This led to a significant decrease in the T_g of PS in the nanocomposites. It is well known that T_g increases with increasing \bar{M}_n , which can be attributed to a reduction in the relative number of polymer chain ends.⁴¹

Table 5.3: T_g values of PS-GO nanocomposites and PS reference obtained from the onset temperature of the $\tan \delta$ curve in the DMA scan

Nanocomposite	GO-DIBTC content relative to monomer (wt%)	T_g (°C)
PS	0	74
PS-GO-1	1	105
PS-GO-2	2	103
PS-GO-3	3	102
PS-GO-6	6	101

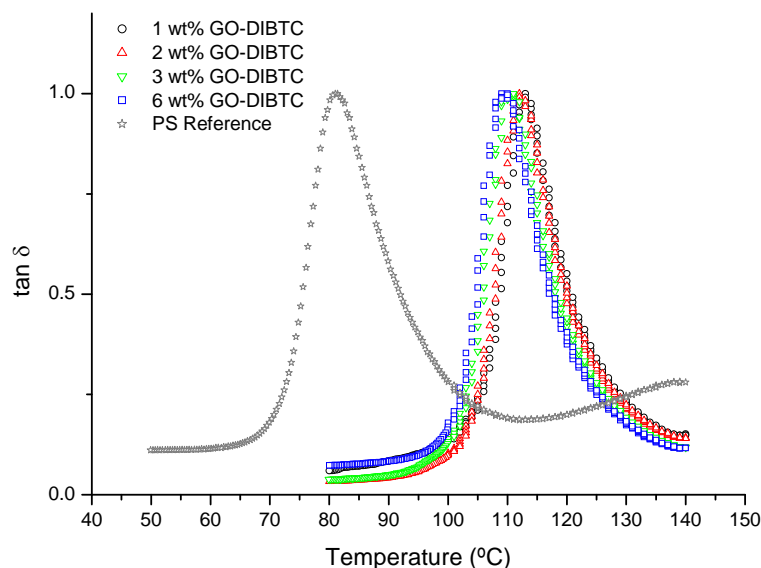


Figure 5.14: Tan δ as a function of temperature of PS-GO nanocomposites at GO-DIBTC loadings of 1, 2, 3 and 6 wt%.

5.4 Conclusion

RAFT-mediated miniemulsion polymerization was used to control the grafting of St from a GO surface. The DIBTC RAFT agent that was successfully anchored onto the GO surface controlled the polymerization of St. The hydroxyl groups of GO, created by the oxidation of graphite, were attached to the RAFT agent by means of an esterification reaction. The RAFT-grafted GO (GO-DIBTC) was dispersed in the monomer and the resultant mixtures sonicated in the presence of a surfactant and a hydrophobe, to form miniemulsions. The miniemulsion polymerization resulted in PS-GO nanocomposites with core-shell morphology. The hydrophobic nature of the RAFT agent led to the formation of monomer droplets that contained the modified graphite particles, which were stabilized by the surfactant, and from which polymer particles developed during the polymerization step.

The molar mass and dispersity of PS in the nanocomposites decreased markedly as the RAFT-functionalized GO concentration increased, as expected for RAFT-mediated polymerization. TEM observations showed that the PS-GO nanocomposites had exfoliated morphology, even at relatively high graphite loadings. TGA results indicated that all PS-GO nanocomposites had higher thermal stabilities than the neat PS. However, it was found that

the thermal stability of the PS-GO nanocomposites is not a function of graphite concentration (i.e., GO-DIBTC). An increase in modified GO content did not have any effect on the thermal stability of the obtained nanocomposites. This was attributed to the effect of RAFT-grafted GO on the molar masses of the PS, which decreased significantly as the amount of GO-DIBTC in the nanocomposites increased. Furthermore, the mechanical properties (i.e., storage and loss modulus) of the nanocomposites improved significantly as the amount of modified GO increased, as measured by DMA. The storage and loss modulus of the nanocomposites were higher than those of the neat PS when the GO loadings reached 3% and 6%, respectively. However, as the RAFT-modified GO content increased in the sample, a shift of the $\tan \delta$ peaks to lower temperatures (i.e., lower T_g values) was recorded. This was attributed to the change in molar masses of the PS chains in the nanocomposites.

5.5 References

- (1) Liu, J.; Yang, W.; Tao, L.; Li, D.; Boyer, C.; Davis, T. P. *Journal of Polymer Science Part A: Polymer Chemistry* **2010**, 48 (2), 425-433.
- (2) Fim, F. d. C.; Guterres, J. M.; Basso, N. R. S.; Galland, G. B. *Journal of Polymer Science Part A: Polymer Chemistry* **2010**, 48 (3), 692-698.
- (3) Kim, H.; Abdala, A. A.; Macosko, C. W. *Macromolecules* **2010**, 43 (16), 6515-6530.
- (4) Hontoria-Lucas, C.; López-Peinado, A. J.; López-González, J. d. D.; Rojas-Cervantes, M. L.; Martín-Aranda, R. M. *Carbon* **1995**, 33 (11), 1585-1592.
- (5) Lurf, A.; He, H.; Forster, M.; Klinowski, J. *The Journal of Physical Chemistry B* **1998**, 102 (23), 4477-4482.
- (6) Zhang, B.; Chen, Y.; Zhuang, X.; Liu, G.; Yu, B.; Kang, E.-T.; Zhu, J.; Li, Y. *Journal of Polymer Science Part A: Polymer Chemistry* **2010**, 48 (12), 2642-2649.
- (7) Liu, J.; Tao, L.; Yang, W.; Li, D.; Boyer, C.; Wuhrer, R.; Braet, F.; Davis, T. P. *Langmuir* **2010**, 26 (12), 10068-10075.
- (8) Pramoda, K. P.; Hussain, H.; Koh, H. M.; Tan, H. R.; He, C. B. *Journal of Polymer Science Part A: Polymer Chemistry* **2010**, 48 (19), 4262-4267.
- (9) Braunecker, W. A.; Matyjaszewski, K. *Progress in Polymer Science* **2007**, 32 (1), 93-146.
- (10) Li, D.; Sheng, X.; Zhao, B. *Journal of the American Chemical Society* **2005**, 127 (17), 6248-6256.
- (11) Bartholome, C.; Beyou, E.; Bourgeat-Lami, E.; Chaumont, P.; Lefebvre, F.; Zydowicz, N. *Macromolecules* **2005**, 38 (4), 1099-1106.
- (12) Ohno, K.; Morinaga, T.; Koh, K.; Tsujii, Y.; Fukuda, T. *Macromolecules* **2005**, 38 (6), 2137-2142.

- (13) Maud, S.; Gwenaëlle, G.; Julien, B.; Bernadette, C.; Cédric, B.; David, G.; Clément, S. *Macromolecular Rapid Communications* **2006**, 27 (6), 393-398.
- (14) Tsujii, Y.; Ejaz, M.; Sato, K.; Goto, A.; Fukuda, T. *Macromolecules* **2001**, 34 (26), 8872-8878.
- (15) Li, C.; Benicewicz, B. C. *Macromolecules* **2005**, 38 (14), 5929-5936.
- (16) Li, C.; Han, J.; Ryu, C. Y.; Benicewicz, B. C. *Macromolecules* **2006**, 39 (9), 3175-3183.
- (17) Sumerlin, B. S.; Lowe, A. B.; Stroud, P. A.; Zhang, P.; Urban, M. W.; McCormick, C. L. *Langmuir* **2003**, 19 (14), 5559-5562.
- (18) Hernández-Guerrero, M.; Davis, T. P.; Barner-Kowollik, C.; Stenzel, M. H. *European Polymer Journal* **2005**, 41 (10), 2264-2277.
- (19) Le, T. P.; Moad, G.; Rizzardo, E.; Thang, S. H. PCT Int. Appl. WO 9801478 A1 980115.
- (20) Chiefari, J.; Chong, Y. K.; Ercole, F.; Krstina, J.; Jeffery, J.; Le, T. P. T.; Mayadunne, R. T. A.; Meijs, G. F.; Moad, C. L.; Moad, G.; Rizzardo, E.; Thang, S. H. *Macromolecules* **1998**, 31 (16), 5559-5562.
- (21) Rizzardo, E.; Chen, M.; Chong, B.; Moad, G.; Skidmore, M.; Thang, S. H. *Macromolecular Symposium* **2007**, 248, 104-116.
- (22) Perrier, S.; Takolpuckdee, P. *Journal of Polymer Science Part A: Polymer Chemistry* **2005**, 43 (22), 5347-5393.
- (23) Samakande, A.; Sanderson, R. D.; Hartmann, P. C. *Journal of Polymer Science Part A: Polymer Chemistry* **2008**, 46 (21), 7114-7126.
- (24) Samakande, A.; Sanderson, R. D.; Hartmann, P. C. *European Polymer Journal* **2009**, 45 (3), 649-657.
- (25) Wang, G.-J.; Huang, S.-Z.; Wang, Y.; Liu, L.; Qiu, J.; Li, Y. *Polymer* **2007**, 48 (3), 728-733.
- (26) Pei, X.; Hao, J.; Liu, W. *The Journal of Physical Chemistry C* **2007**, 111 (7), 2947-2952.
- (27) Martina, H. S.; Thomas, P. D. *Journal of Polymer Science Part A: Polymer Chemistry* **2002**, 40 (24), 4498-4512.
- (28) Martina, H. S.; Ling, Z.; Wilhelm, T. S. H. *Macromolecular Rapid Communications* **2006**, 27 (14), 1121-1126.
- (29) Lu, H. F.; Fei, B.; Xin, J. H.; Wang, R. H.; Li, L.; Guan, W. C. *Carbon* **2007**, 45 (5), 936-942.
- (30) Hummers, W. S.; Offeman, R. E. *Journal of the American Chemical Society* **1958**, 80, 1339.
- (31) Lai, J. T.; Filla, D.; Shea, R. *Macromolecules* **2002**, 35 (18), 6754-6756.
- (32) Mai, Y.-W.; Yu, Z.-Z., *Polymer Nanocomposites*. 2nd edition; Woodhead Publishing: Cambridge, 2006; Vol. 19, pp 510-533.
- (33) Lowe, A. B.; McCormick, C. L. *Progress in Polymer Science* **2007**, 32 (3), 283-351.
- (34) Postma, A.; Davis, T. P.; Li, G.; Moad, G.; O'Shea, M. S. *Macromolecules* **2006**, 39 (16), 5307-5318.
- (35) Zhang, R.; Hu, Y.; Xu, J.; Fan, W.; Chen, Z. *Polymer Degradation and Stability* **2004**, 85 (1), 583-588.

Chapter 5: Polystyrene/graphite nanocomposites via surface RAFT-mediated polymerization

- (36) Uhl, F. M.; Wilkie, C. A. *Polymer Degradation and Stability* **2002**, 76 (1), 111-122.
- (37) Xiao, M.; Sun, L.; Liu, J.; Li, Y.; Gong, K. *Polymer* **2002**, 43 (8), 2245-2248.
- (38) Jianqi, W.; Zhidong, H. *Polymers for Advanced Technologies* **2006**, 17 (4), 335-340.
- (39) Yang, J.; Tian, M.; Jia, Q.-X.; Shi, J.-H.; Zhang, L.-Q.; Lim, S.-H.; Yu, Z.-Z.; Mai, Y.-W. *Acta Materialia* **2007**, 55 (18), 6372-6382.
- (40) Donghwan, C.; Sangyeob, L.; Gyeongmo, Y.; Hiroyuki, F.; Lawrence, T. D. *Macromolecular Materials and Engineering* **2005**, 290 (3), 179-187.
- (41) Cown, J. M. G. *European Polymer Journal* **1975**, 11 (4), 297-300.

WATER BARRIER PROPERTIES OF POLYMER/GRAPHITE NANOCOMPOSITES

The work described in this chapter has been submitted to be published in the following paper:

Hussein M. Etmimi and Ronald D. Sanderson, Polymer/graphite nanocomposites: effect of reducing the functional groups of graphite oxide on water barrier properties, submitted to **Macromolecular Materials and Engineering** (March, 2012)

Abstract

Water barrier properties (water resistance) of poly(styrene-co-butyl acrylate)/graphite oxide (poly(St-co-BA)/GO) nanocomposites were studied using hydrophobicity and permeability analysis. The hydrophobicity of the synthesized nanocomposites was studied using contact angle measurements, while water permeability was obtained by measuring the moisture vapor transmission rate (MVTR). The nanocomposite latices were treated with hydrazine hydrate in order to reduce the functional groups on graphite oxide (GO). Results showed that nanocomposites containing the reduced-GO (RGO) had better water resistance and barrier properties compared to those made with unreduced GO (i.e., as-prepared GO). The nanocomposites containing RGO had higher hydrophobicity and lower water uptake and MVTR compared to those made with as-prepared GO. The nanolayered graphene nanoplatelets in GO and RGO resulted in lower water permeation in the final films compared to pure polymer. The highly hydrophobic nature of the RGO exhibited lower water solubility, which resulted in films with lower MVTR values compared to those made with as-prepared GO.

6.1 Introduction

Polymer emulsions and miniemulsions are well established and extensively used for barrier coating formulations.^{1,2} They can be applied to numerous surfaces to reduce the unwanted penetration and interactions of different liquids (e.g., water) and gases (e.g., oxygen and carbon dioxide).³ Coating is generally defined as the process by which a uniform layer is applied across a substrate. The most common reason for applying these barrier coatings to a permeable material is to reduce the permeation rate of water and water vapor.⁴

In fact, most polymers are not absolute barriers against water vapor, gases and organic substances. Filler materials in the form of nanoplatelets are usually added to polymers to produce polymer nanocomposites with enhanced barrier properties. The nanolayered filler platelets, which have high aspect ratios, could lead to increased barrier performance of polymers.⁵ This can be attributed to a tortuous path model, where the filler particles act as physical barrier for the diffusing molecules because they are impermeable.^{6,7}

For a specific permeate, the chemical composition and physical properties of the polymeric membrane determine the permeation properties, according to the following relationship:⁸

$$P = D \times S \quad (6.1)$$

where P is the permeability, and D and S are the diffusion and solubility coefficients respectively.

The diffusion coefficient (D) describes the ease with which the permeate moves in and through the polymeric membrane while the solubility (S) gives an indication on the polymer-permeate interaction.^{9,10} Equation 6.1 shows that the permeability can be greatly influenced by both the diffusion and the solubility coefficients. A low permeability may result from a low diffusion coefficient or a low solubility coefficient, or both. These coefficients can, in turn, be greatly influenced by the chemical and physical structure of the polymer in use. In this regard, it is very important to investigate the relationship between the polymer structure and the permeation behavior, to explain the permeability of polymeric materials. One example of this is the permeation of water vapor through polymer and polymer nanocomposite films. These films are often characterized in terms of their moisture vapor transmission rate (MVTR), that is, a measure of the passage of water in gaseous form through the film.

The incorporation of graphene into polymers can significantly reduce the permeation of low molecular weight molecules (e.g., N₂, O₂ and water) relative to the neat polymers. This can be attributed to the tortuous path introduced by the graphene platelets, which are impermeable to the permeate, so that the permeate travels a longer distance in graphene-filled polymers than in neat polymers. In addition to diffusion, the permeate solubility is of a great importance. Solubility of the permeate in polymer/graphite nanocomposites (PGNs) can be markedly influenced by the presence of graphene particles in the nanocomposite. If the graphene particles are hydrophobic then low water permeability is expected due to the decrease of the solubility coefficient, as anticipated from Equation 6.1.

Therefore, graphite can be successfully used with polymers to produce latex formulations that can be used as barrier coatings. The key factor for the synthesis of these nanocomposites is the degree of exfoliation of the graphite into individual platelets, thereby maximum barrier improvements can be achieved. The resultant percolating network of the exfoliated graphite filler platelets can provide a tortuous path that inhibits molecular diffusion through the polymer matrix, thus resulting in significantly reduced permeability.

Nielsen¹¹ proposed the tortuous path model to predict the minimum permeability that can be expected for a polymer filled with plate-like particles. This model assumes that the filler particles are impermeable to the diffusing permeate and that the plates are oriented parallel to the surface of the polymer films, perpendicular to the direction of diffusion. Recently, Bunch et al.¹² showed that a membrane of monolayer graphene nanoplatelets is impermeable to all standard gas molecules. By applying a pressure difference across the graphene membrane, the authors showed that graphene nanoplatelets can provide a unique separation barrier between two distinct regions that is only one atom thick. Several authors have investigated the permeation properties of polymers made with graphite and graphite-derived materials.¹³⁻¹⁶ Gas permeability data of graphene-based polymer nanocomposites that appear in the literature are summarized in Table 6.1.

Kim et al.¹⁵ showed that graphene nanoplatelets exfoliated from graphite oxide (GO) can be successfully used for the preparation of polymer nanocomposites with enhanced gas barrier performance at low filler loading. The authors synthesized polyurethane (PU) nanocomposites using three different methods of dispersion: solvent blending, *in situ* polymerization and melt compounding. The graphene nanoplatelets were obtained from two different processes: chemical modification to produce isocyanate-treated GO (iGO) and thermal exfoliation to

obtain thermally-exfoliated GO (TEGO). The authors showed that N₂ permeability was markedly reduced, demonstrating that exfoliated graphene can be used as diffusion barriers in polymeric membranes. The synthesized composites exhibited 99% and 81% reduction in N₂ permeability with 3.7 wt% loading of iGO and TEGO, respectively. The authors attributed this to the high aspect ratio of the exfoliated graphene platelets used.

Table 6.1: Gas permeability of graphene-based nanocomposites¹⁷

Polymer ^a	Graphite type ^b	Processing method	Permeate	Reduction in permeability (%)	Graphene (wt%)	Ref	
PEN	TRG	melt	hydrogen	44	1.8	16	
PC	TRG	melt	helium	32	1.6	17	
			nitrogen	39	1.6		
TRU	TRG	melt	nitrogen	52	1.6	18	
				solvent	81		1.6
				<i>in situ</i> polymerization	71		1.5
	iGO	solvent	94–99	1.6			
	GO	<i>in situ</i> polymerization	62	1.5			
Natural rubber	TRG	melt/solvent/oligomer polymerization	air	60	1.7	19	
PS-PI-PS				~ 80	2.2		
PDMS				~ 80	2.2		

^a PEN: poly(ethylene naphthalate); PC: polycarbonate; TRU: thermoplastic polyurethane; PS-PI-PS: poly(styrene-co-isoprene-co-styrene); PDMS: polydimethylsiloxane.

^b TRG: thermally-reduced graphene; GO: graphite oxide; iGO: isocyanate-treated GO.

Other authors found a 20% reduction in O₂ permeability for polypropylene (PP) with 6.5 wt% exfoliated graphene nanoplatelets¹⁸ and a 39% reduction in the N₂ permeability of a polycarbonate composite made with thermally expanded GO at approximately 3.5 wt% content.¹⁴ In a comparative study, polystyrene (PS) nanocomposites made with chemically modified graphene were reported to show a lower O₂ permeability than PS nanocomposites made with exfoliated clay at equivalent loadings.¹⁹ At 0.02 vol% clay content, the PS

nanocomposite showed permeability similar to that of pristine PS. On the other hand, the PS nanocomposite made with graphene exhibited 20% less permeability than that of the pristine PS at the same concentration (0.02 vol%). The authors attributed these results to the hydrophilicity of the clay surface, along with difficulties in exfoliating clay aggregates during the preparation process. Contrary, the modified graphene nanosheets were shown to have a high aspect ratio and they do not agglomerate when processed into nanocomposites.²⁰ As a result, these graphene nanoplatelets can be used to significantly decrease the permeability of polymer nanocomposites, leading to improved barrier properties.

The water permeability of PGNs has, however, not been investigated. The aim of this study was to determine the water resistance and barrier properties of PGNs to water and water vapor. The synthesized PGNs films were tested for their hydrophobicity and permeability against water and water vapor molecules. The incorporation of graphene nanoplatelets within the polymer matrix was achieved using miniemulsion polymerization. The influence of the graphene filler on the hydrophobicity of the final films was studied through static contact angle measurements. The permeability of the nanocomposites was studied by using MVTR, which gives the amount of water passage through the nanocomposite film in 24 h. Water uptake was also used to gather information about the water affinity of the synthesized nanocomposite films. Conductivity measurements were used to obtain information about surfactant migration, which can directly affect the water permeation properties of the final films.

6.2 Experimental

The materials and methods used to prepare poly(styrene-co-butyl acrylate)/GO (poly(St-co-BA)/GO) latices are now described. The poly(St-co-BA) nanocomposites containing the RGO were obtained by reducing the GO in the latices by using hydrazine hydrate as the reducing agent.

6.2.1 Materials

Styrene (St) (99%, Aldrich) and n-butyl acrylate (BA) (99%, Aldrich) were purified by washing with aqueous 0.3 M KOH, followed by distillation at 40 °C under reduced pressure. Sodium dodecylbenzene sulfonate (SDBS) (99%, Fluka) and hexadecane (HD) (99%, Sigma-Aldrich) were used as received. 2,2'-Azobis(isobutyronitrile) (AIBN) (98%) was obtained

from Aldrich and purified by recrystallization from methanol. Hydrazine hydrate (50–60%) was obtained from Alderich. Distilled and deionized (DDI) water was obtained from a Millipore Milli-Q water purification system. GO was prepared as described in Chapter 3.²¹

6.2.2 Synthesis of poly(St-co-BA)/GO nanocomposite latices

The following miniemulsion polymerization procedure was followed for the synthesis of poly(St-co-BA)/GO nanocomposite latices. The GO was dispersed in DDI water by sonication for 10 min to disperse the GO nanosheets in water. The sonicator was set at 80% amplitude and a pulse rate of 2.0 sec. The average energy expended was approximately 69 kJ. St and BA monomers, hexadecane and AIBN were stirred for 30 min and added to the GO solution. An aqueous surfactant solution (2 wt% SDBS relative to monomer) was added and the mixture was sonicated for 15 min to obtain the miniemulsion latex. A three-neck round-bottomed flask containing the resultant miniemulsion latex was then immersed in an oil bath at room temperature. The content of the flask was nitrogen purged for 15 min before increasing the temperature to 75 °C to initiate the polymerization. The reaction was carried out for 6 h under a nitrogen atmosphere, after which it was cooled to room temperature to stop the polymerization.

A similar procedure was followed for the synthesis of a poly(St-co-BA) reference without GO, by miniemulsion polymerization. The oil phase, consisting of St and BA monomers, AIBN (0.009 g) and HD (0.066 g), was mixed with an aqueous solution of SDBS (0.10 g) for 30 min. The mixture was then sonicated under the same conditions used for the synthesis of poly(St-co-BA)/GO nanocomposites for 15 min to afford the miniemulsion latex. A three-neck round-bottomed flask containing the resultant miniemulsion latex was then immersed in an oil bath at room temperature. The content of the flask was nitrogen purged for 15 min. The temperature of the oil bath was increased to 75 °C to initiate the polymerization and the reaction was carried out for 6 h under a nitrogen atmosphere. The various formulations used for the synthesis of poly(St-co-BA)/GO nanocomposites and the poly(St-co-BA) reference are tabulated in Table 6.2.

6.2.3 Reduction of GO in the nanocomposite latices with hydrazine hydrate

In practice, the reduction of water-dispersed GO nanosheets results in a gradual decrease in their hydrophilic character, which eventually leads to their irreversible agglomeration and precipitation. However, stable aqueous dispersions of RGO nanoplates can be obtained if the

reduction is carried out in the presence of a surfactant.²² The poly(St-co-BA)/GO nanocomposite dispersion, which contain ~ 2 wt% SDBS, was treated with hydrazine hydrate to reduce the oxygen-containing functional groups in GO. The procedure was as follows: the latex (15 mL) was loaded to a 250-mL round-bottom flask and hydrazine hydrate (1 mL) was added. The solution was heated in an oil bath at 100 °C with a water-cooled condenser for 24 h. As the reduction proceeded, the blue-gray color of the latex eventually turned to black. The black color of the latices suggests a partial re-graphitization of the GO, as described in the literature.²³

Table 6.2: Formulations used in the miniemulsion polymerization reactions

Nanocomposite	GO (g)	St (g)	BA (g)	DDI water (g)
P(St-co-BA)	-	2.71	2.31	50.08
P(St-co-BA)/GO-1	0.05	2.71	2.30	50.10
P(St-co-BA)/GO-2	0.10	2.71	2.30	50.60
P(St-co-BA)/GO-3	0.15	2.70	2.30	50.50
P(St-co-BA)/GO-4	0.20	2.73	2.36	50.40
P(St-co-BA)/GO-5	0.25	2.72	2.31	50.10
P(St-co-BA)/GO-6	0.30	2.70	2.31	50.40

6.2.4 Analyses

Various analytical methods were used to characterize the resultant nanocomposite films for their barrier performance. The methods that were used, and their purpose, are listed below.

- Size exclusion chromatography (SEC) was used to determine the molar mass of poly(St-co-BA) in the nanocomposites after removal of graphite by filtration.
- Static contact angles were used to determine the hydrophobicity of the surface of the final nanocomposite films.
- MVTR tests were used to measure the permeation properties of the final nanocomposite films.
- Water uptake measurements were used to determine the water affinity of the resultant nanocomposite films.
- Conductivity measurements were used to obtain information about surfactant migration in the final nanocomposite films.

6.2.4.1 SEC analysis

SEC analyses were carried out using a 610 Fluid Unit, a 410 Differential Refractometer at 30 °C and a 717 plus Autosampler (Waters, USA). A 600E System Controller, run by Millennium 32 V3.05 software, was used for all analyses. Tetrahydrofuran (THF; HPLC grade), sparged with helium (IR grade), was used as the eluent, at a flow rate of 1 mL/min. Two PLgel 5 μm mixed-C columns and a PLgel 5 μm guard pre-column were used. The column temperature was 35 °C and the injection volume was 100 μL . The system was calibrated with narrow PS standards (5 mg/mL THF), ranging from 2.5×10^3 to 8.9×10^4 g mol^{-1} . The nanocomposite samples were dissolved in THF (5 mg/mL) over a period of 24 h and then filtered through a 0.45 μm nylon filter.

6.2.4.2 Hydrophobicity

The hydrophobicity of the nanocomposite films was determined from static contact angle measurements. Static contact angle measurements were made using a stereomicroscope (Nikon SMZ-2T, Japan), connected to a camera. A 1 μL drop of DDI water was placed on the flat surface of a nanocomposite film. The films were prepared by drying ~ 3 mL of the latex in an aluminum pan for 24 h at a temperature of about 100 °C. A photograph of each drop was then taken with computer software (Scion Image). The contact angle (θ) of the water droplet with the surface of the film was then measured and reported (see Figure 6.1). The contact angle for each sample was based on the average of contact angle of 10 drops of water.

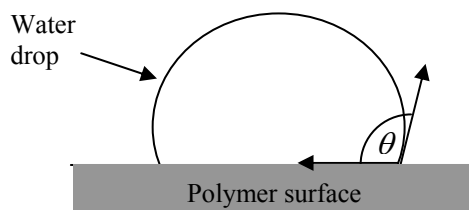


Figure 6.1: Static contact angle of a water drop on a polymer surface.

6.2.4.3 MVTR test

MVTR determines the amount of moisture vapor that passes through a film in 24 h under specified conditions of relative humidity and temperature. The following apparatus and procedure were used.

a) Apparatus:

- Humidity cabinet set at 30 °C and 85% relative humidity
- Moisture resistant glass vessel of 84 mm diameter, open at the top, and equipped with a screw-on open lid with a rubber seal
- A balance (accurate to four decimal places)
- Silica gel with a color indicator

b) Procedure:

Films made from the synthesized PGNs latices were coated on a porous support (standard paperboard) and their MVTR values were determined using a Heraeus Votsch humidity cabinet, type VTRK 300. The measurements were performed at 30 °C and 85% relative humidity. The coatings were applied to the paperboard by means of a coating machine using a K-bar, which gives a film thickness of 125 µm, and. The coating was then dried at a temperature of about 100–110 °C for 1–2 min. The coated paperboard was characterized by determining the MVTR, as follows:

- Silica gel was dried in an oven at 110 °C for 2 h
- 100 g of the dried silica gel was added to the glass vessel
- A round disc sample was cut and fitted in the lid of the vessel
- The lid with the sample was screwed onto the vessel
- The vessel was weighed and the weight was recorded (A)
- The sample was left in the humidity cabinet for 24 h at 30 °C and 85% relative humidity
- The vessel was weighed again after 24 h and the weight was recorded (B).
- The open area of the vessel was calculated in m²
- The MVTR was calculated by means of the following equation:

$$MVTR = \frac{B - A}{Area} \quad (6.2)$$

MVTR: measured in g/m²/24 h

A: Weight of jar prior 24 h exposure (g)

B: Weight of jar after 24 h exposure (g)

Area: Area of the circle (m²)

6.2.4.4 Conductivity and water uptake measurements

Films with similar surface areas (10 cm²) were placed in DDI water. Films were prepared by drying ~ 3 mL of the latex on a glass slide at 100 °C for 24 h. Conductivity and water uptake (w.u.) of the films were measured. DDI water, with an electrical conductivity of ~ 1.0 μS/cm, was used for all measurements.

Conductivity was measured for each film after a period of two weeks with a Cond 730 inoLab WTW Series conductimeter.

Water uptake is defined as the weight increase relative to the initial mass of the film after a period of two weeks:

$$\text{Water uptake} = \frac{m_2 - m_1}{m_1} \times 100 \quad (6.3)$$

where m_1 and m_2 are the film weight before and after immersing into water, respectively.

6.3 Results and discussion

6.3.1 SEC analysis

The molecular weight of the polymer in the nanocomposite was expected to have a large impact on the permeation of water vapor molecules through the final nanocomposite films. As indicated earlier, the permeation rate of water vapor through polymer membranes is a function of both the solubility of the vapor as well as its rate of diffusion through a polymer. The solubility coefficient is influenced by the interaction between polymer chains, and hence, the molecular weight of the polymer.²⁴ Longer polymer chains result in greater chain entanglement, reducing the chain mobility, and resulting in reduced diffusion and consequently lower permeability through the polymer. Therefore, higher molecular weight polymer chains will result in films with more chain entanglements, leading to lower water penetration through the film.

The molecular weight could also have a big impact on the water uptake and surfactant migration in the film. Films with fewer voids are formed when higher molecular weight polymers are used as membranes, leading to films with lower water uptake (high barrier properties).²⁵ Chain entanglements observed with higher molecular weight polymers could

also lead to a significant reduction in the migration of surfactant towards the film surfaces. Figure 6.2 shows the effect of GO loading on the molecular weight of poly(St-co-BA) in the nanocomposites.

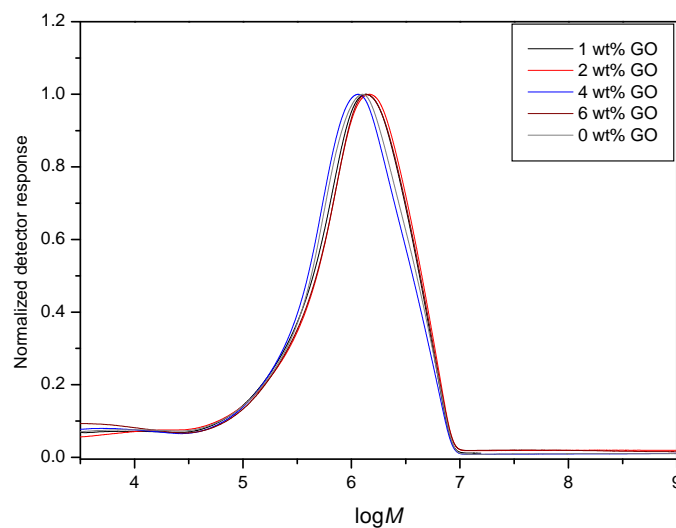


Figure 6.2: Effect of GO loading on the Molecular weight of poly(St-co-BA).

No significant effect of the GO concentration on the molecular weight of the polymer in the nanocomposites was observed. The similarities in the molecular weights of the nanocomposites prepared with different GO content are important. This implies that any changes in the barrier properties (i.e., hydrophobicity, water uptake and MVTR) of the nanocomposites are due to the GO loading and not fundamentally due to differences in the polymer matrix.

6.3.2 Hydrophobicity as determined by contact angle measurements

The hydrophobicity of poly(St-co-BA) nanocomposite films was studied using static contact angle measurements. The contact angle of water droplets on solid surfaces (e.g., polymers) will greatly depend on the hydrophilic or hydrophobic nature of the solid material (see Figure 6.3). If the water is very strongly attracted to the surface, such as the case for highly hydrophilic polymers, the droplet will completely spread out on the solid surface. Therefore, highly hydrophilic surfaces will exhibit contact angles of 0–30°. ²⁶ On the other hand, less hydrophilic surfaces will have a contact angle up to 90° and hydrophobic surfaces will exhibit a higher contact angle ($\theta > 90^\circ$). ²⁶

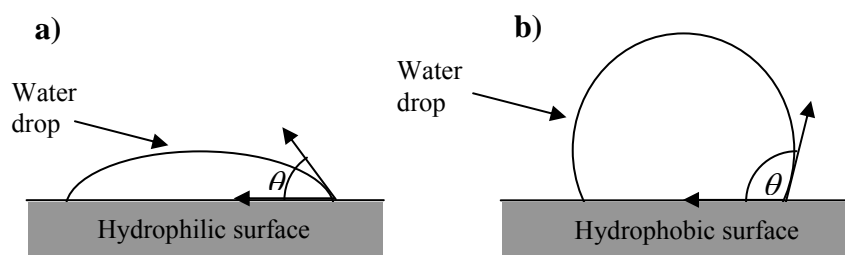


Figure 6.3: Static contact angle of a water drop on a solid surface: a) hydrophilic surface ($\theta = 0\text{--}30^\circ$) and b) hydrophobic surface ($\theta \geq 90^\circ$).

In this study, contact angle measurements showed that the hydrophobicity of the films' surface was improved significantly by reducing the functional groups on GO. Figure 6.4 shows the digital images of water droplets on different films that contain GO and RGO. The film containing RGO (Figure 6.4 b) exhibited a static contact angle $\theta = 100^\circ$ compared to $\theta = 67^\circ$ for a film made with unmodified GO (i.e., as-prepared GO) (see Figure 6.4 a). It should be noted here that the poly(St-co-BA) reference film made with no GO exhibited a static contact angle $\theta = 65^\circ$, which is slightly lower than that of nanocomposite films made with GO. The static contact angle of the poly(St-co-BA) reference film made with no GO is shown in Figure 6.5. The use of RGO nanosheets resulted in more hydrophobic polymer films, whereby a water droplet remained on its surface, with a contact angle $\theta > 90^\circ$.²⁷

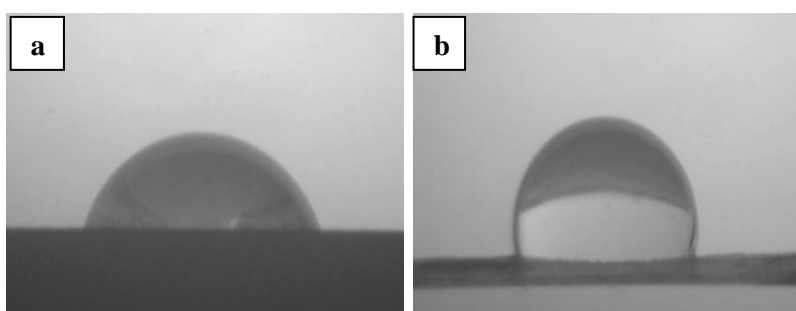


Figure 6.4: Static contact angle of nanocomposite films: a) 2 wt% GO ($\theta = 67^\circ$) and b) 2 wt% RGO ($\theta = 100^\circ$).

Table 6.3 shows the average contact angles of the films prepared using different quantities of GOs (unmodified GO and RGO). The average contact angle for each sample was based on the images of 10 drops of water. Films made with RGO had a higher contact angle, indicating that the films were hydrophobic. This was attributed to the hydrophobic character of the RGO nanosheets, which enhanced the hydrophobic nature of the final nanocomposite films. As

indicated from the FT-IR results in Figure 6.6, the functional groups on GO were reduced, which gave the graphene nanosheets a hydrophobic nature. The absorbance peak at 3100–3600 cm^{-1} corresponds to the stretching vibration of hydroxyl groups on the GO. The absence of this peak in the FT-IR spectra of the RGO in the nanocomposites indicates that the hydroxyl groups on GO had been reduced. However, due to the presence of polymer molecules, the assignment of other functional groups such as carboxyl was not possible.

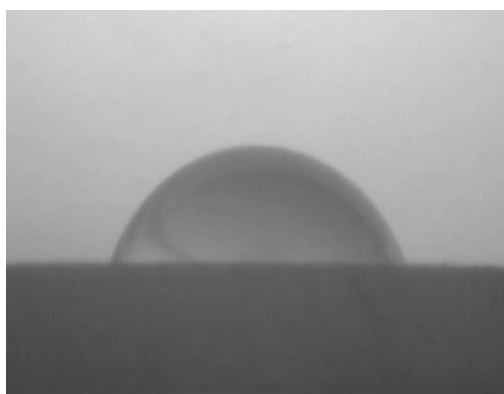


Figure 6.5: Static contact angle of a poly(St-co-BA) reference film made with no GO ($\theta = 65^\circ$).

Table 6.3: Static contact angles of the poly(St-co-BA) films prepared using different quantities of GO and RGO

Sample code	Graphite content (wt%)	GO (θ°)	RGO (θ°)
Film 1	1	65	93
Film 2	2	64	91
Film 3	3	66	92
Film 4	4	64	92
Film 5	5	65	92
Film 6	6	66	91

The oxygen groups on the GO surface have high affinity for water due to the possibility of hydrogen bonding. The polar nature of water molecules enables the formation of hydrogen bonds and to interact strongly with polar groups of the GO. The hydrophobicity of the films' surface remained largely unaffected by the increased amount of GO (i.e., similar contact angles were observed for different GO content). The fact that an increase in the GO amount had no effect on the static contact angle of the films indicates that a substantial fraction of GO

migrated to the surface of the films. This means that surface characteristics were dominated mostly by the GO, leading to surfaces with similar hydrophobicity.

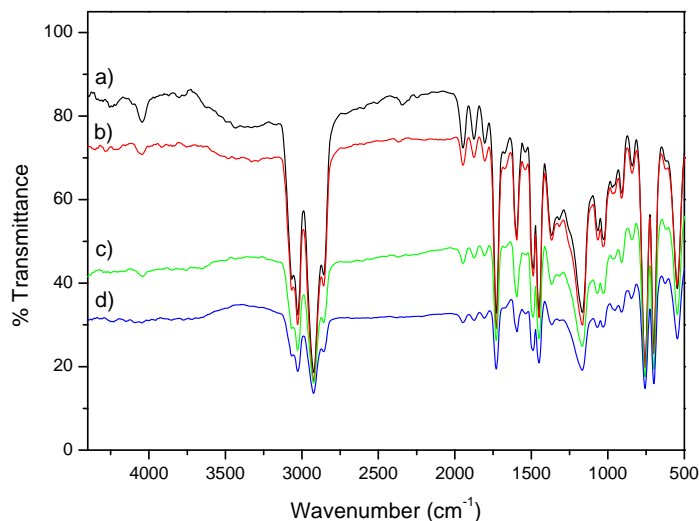


Figure 6.6: FT-IR spectra of poly(St-co-BA)/GO nanocomposites: a) 1 wt% GO, b) 2 wt% GO, c) 1 wt% RGO and d) 2 wt% RGO.

6.3.3 Permeability studies using MVTR measurements

Adding the graphene nanoplatelets to polymer films was expected to have a two-fold effect: (1) the water solubility in the resulting polymer films was expected to change significantly with adding graphene nanoplatelets according to the hydrophilic or hydrophobic nature of the graphene derivative used and (2) water diffusion in the final films was expected to be reduced by the addition of these impermeable graphene nanoplatelets. The graphene will provide longer diffusion paths across the polymer, thus increasing the final barrier properties of the film. Low solubility and/or diffusion coefficients of water molecules in the final films will lead to low water permeability (i.e., low MVTR value).⁸

The permeability of poly(St-co-BA) nanocomposite films was studied using MVTR analysis. Figure 6.7 shows MVTR results for poly(St-co-BA)/GO films made with different quantities of GO and RGO. The addition of graphene generally decreased the permeability of water through the nanocomposite films compared to pure polymer. Most of the synthesized nanocomposite exhibited lower MVTR values than that of the neat polymer (MVTR = 950 g/m²/24 h). This was attributed to the presence of graphene nanoplatelets, which resulted in lower water diffusion leading to lower water permeability. The nanolayered graphene act as impermeable obstacles, which led to lower water diffusion in the films.¹² This can be attributed to the high number and aspect ratio of the graphene nanoplatelets as a result of

exfoliation of GO. This results in enhanced barrier performance for water moisture transmission through polymer membranes.¹³ Figure 6.7 also shows that as the amount of GO and RGO in the latex increases, the permeation of water vapor molecules decreases noticeably. A greater number of graphene nanoplatelets will provide a more torturous path through the polymer membrane, resulting in better barrier properties.

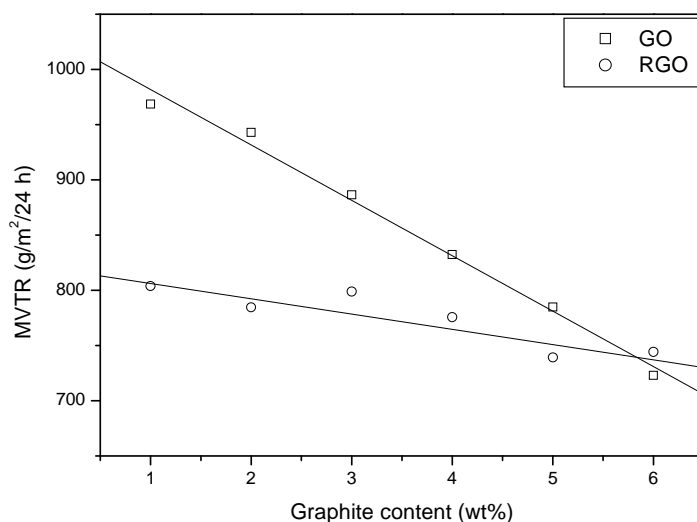


Figure 6.7: MVTR vs. GO and RGO content (wt%) for poly(St-co-BA) nanocomposite films.

Besides the diffusion factor, the effect of the graphite content on the permeation of water molecules in the nanocomposite films can be caused by the solubility factor. This can be seen in Figure 6.7, which reveals that the nanocomposites containing RGO generally exhibited lower MVTR than that of unmodified GO. This was attributed to the more hydrophobic character of the RGO due to the low water affinity of its nanosheets (see contact angle measurements). The hydrophobic structure of the RGO nanosheets will result in a significant reduction in the solubility coefficient, while the presence of nanolayers introduced by graphene will generally lead to a large decrease in the diffusion coefficient. Thus, water permeation through the nanocomposite film was decreased significantly when the RGO was used, as a result of the combined effect of a reduction of both diffusion and solubility coefficients, as expected from Equation 6.1.

On the contrary, the nanocomposite films made with GO had the highest MVTR values. This was attributed to the high water affinity of GO nanosheets, which resulted in higher MVTR values. Due to the presence of oxygen-containing functionalities (i.e., polar groups) such as hydroxyl and carboxyl groups, the GO is more hydrophilic. It can, therefore, interact with

water molecules via hydrogen bonding and readily disperses in water.²⁸ The solubility effect will counteract the effect of diffusion, leading to higher permeability.

6.3.4 Water uptake measurements

Water uptake measurements were used to gather information about the water affinity of the nanocomposite films. Results showed that the water uptake of the films decreased noticeably when RGO was used, compared to films containing unmodified GO (see Figure 6.8). The films containing the as-prepared GO had a higher water uptake, as a function of GO loading. This is due to the high water affinity of GO, caused by the presence of oxygen functionalities (in agreement with contact angle measurements). However, water uptake was similar for all films made with different quantities of RGO. For films containing the same amount of the filler (3 wt%), water uptake was ~ 15% for the film made with as-prepared GO, while it was ~ 0.03% for films made with RGO. This was expected, since the RGO has a hydrophobic structure that can greatly increase the water resistance of the polymer nanocomposite. The presence of a substantial amount of hydrophobic graphene nanoplatelets in the film resulted in a smaller fraction of available sites for water absorption, leading to a lower final water uptake. These findings are in agreement with those of Despond et al.,²⁹ where the addition of a hydrophobic material such as wax greatly decreased the water uptake of a permeable material (e.g., paper).

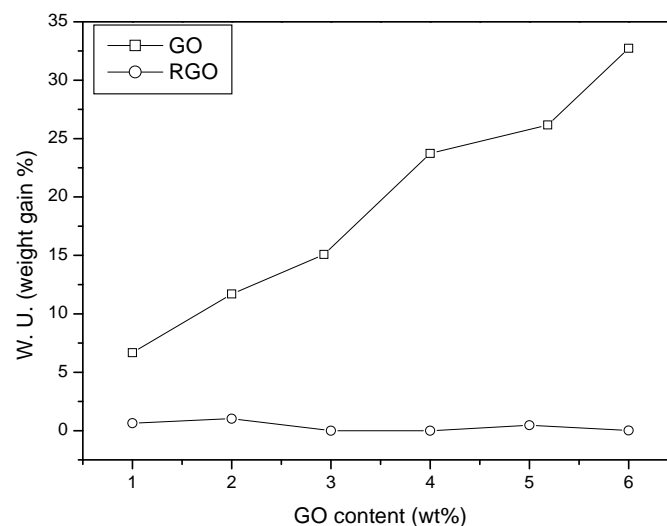


Figure 6.8: Water uptake vs. GO and RGO content (wt%) for poly(St-co-BA) nanocomposite films.

6.3.5 Conductivity measurements

Conductivity measurements were used to obtain information about surfactant migration towards the film surface during or after the film formation process. This will provide a good indication of the water permeation behavior in the final polymer films. High surfactant migration will lead to polymer films with poor barrier properties, while low surfactant migration will result in films with better barrier properties. Although surfactant molecules prevent aggregation of latex particles upon synthesis and storage, their presence in a polymer film (upon the evaporation of the water from the latex) is disadvantageous in terms of the barrier properties of the final film. It has been reported that when latices are used as film-forming polymers, the surfactant can migrate to the film/air interface, creating a separate phase, which increases penetration of water in the film.^{30,31}

The migration of surfactants has been observed in several polymer latex systems in which surfactant was exuded to film/air and film/substrate interfaces with passing time.^{32,33} Major drawbacks are the water affinity of the surfactants and their ability to migrate to the surface of the film, leaving behind grooves and pores in the film structure. Water can diffuse through the polymer or penetrate through defects, pores or channels present inside the film.³⁴ Therefore, higher surfactant migration in films may result in higher water permeability in the film by the creation of new paths for water penetration. On immersion into water, the surfactant will be washed out, leading to an increase of the conductivity of water in which a film was immersed. By measuring the increase in conductivity of water with time, one can get an indication of surfactant migration.

In this study, conductivity results showed that that films made with RGO had very low conductivity (low surfactant migration) compared to those made with as-prepared GO. This indicates that films containing RGO will have better barrier properties than those made with as-prepared GO. Figure 6.9 shows the evolution of the conductivity of the water in which different films prepared from different GOs and RGOs were immersed (DDI water with a conductivity of $\sim 1.1 \mu\text{S}/\text{cm}$ was used). The water in which the films containing the RGO were immersed had relatively low conductivity compared to those made with as-prepared GO. This indicates that surfactant migration decreased notably when RGO was used. This is because surfactant migration to the surface is hindered by the presence of hydrophobic graphene (RGO) in the nanocomposite. On the other hand, when as-prepared GO was used

the water conductivity in which the film was immersed increased significantly, indicating that more surfactant migration towards the film surface was taking place.

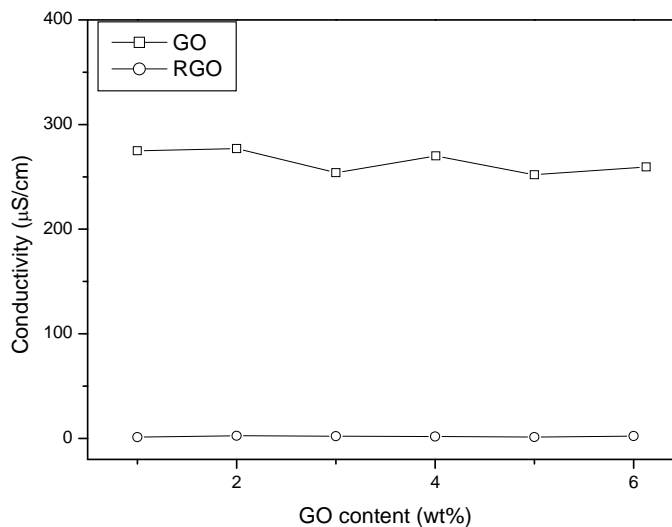


Figure 6.9: Water conductivity vs. GO and RGO content (wt%) for poly(St-co-BA) nanocomposite films.

Figure 6.9 also shows that films made with RGO had very low surfactant migration, indicated by very low conductivity values (close to the value of pure DDI water). This is because of the low water affinity of RGO, which prevents surfactant molecules from migrating to the films' surface due to the high hydrophobicity of RGO. On the other hand, the unmodified GO has a very hydrophilic nature, which results in surfactant migration towards the film surface, leading to higher water conductivity. Furthermore, in most cases water conductivity was independent of the change in the amount of GO and RGO used in the miniemulsion formulation (see Figure 6.8). This is because the same amount of surfactant was used in the initial latex formulation, therefore similar conductivity values were obtained.

6.4 Conclusion

The water resistance of poly(St-co-BA) nanocomposite films containing GO and RGO was studied. The hydrophobicity of the films (cast from the nanocomposite latices) was determined using contact angle measurements. Nanocomposite latices made with GO were obtained by miniemulsion polymerization. The GO in the nanocomposite latices was reduced by using hydrazine hydrate. The barrier properties were evaluated using water uptake and MVTR analyses. The effect of reducing the functional groups on GO was investigated and results compared to those of composites made with unreduced GO (as-prepared).

FT-IR results indicated that the amount of oxygenated groups (e.g., –OH) were reduced in the nanocomposites. Permeability analysis showed that water sensitivity of the final films was greatly affected by the type of GO used in the miniemulsion formulation. The use of RGO led to the formation of films with good water resistance and barrier properties relative to the films made with as-prepared GO. Lower water uptake and MVTR were observed when the RGO was used. The hydrophobicity of the surface of the nanocomposite films increased when the polar groups of GO in the latices was reduced. This was attributed to the higher hydrophobicity of the graphene nanoplatelets in RGO. The nanolayered structure of graphene led to low water diffusion through the film. The highly hydrophobic RGO also resulted in a reduction of the water solubility in the polymer film. Thus, lower MVTR of the films made with RGO nanosheets were observed as a result of the combined effect of a reduction of solubility and diffusion coefficients.

On the contrary, the use of as-prepared GO led to the preparation of nanocomposite films with poor barrier properties. Films made with unmodified GO resulted in low water resistance properties (i.e., relatively high water uptake) compared to the films made with RGO. Conductivity measurements were used to gather information about surfactant migration, which is directly related to barrier properties of the final films. The use of GO resulted in higher surfactant migration towards the film-air interface resulting in poor barrier properties. On the other hand, films made with RGO resulted in less surfactant migration, leading to good barrier properties.

6.5 References

- (1) Ghosh, S., *Functional Coatings: By Polymer Microencapsulation*. Wiley-VCH: Weinheim, 2006.
- (2) Doren, K.; Freitag, W.; Stoye, D., *Water-borne Coatings: The Environmentally-Friendly Alternative*. Hanser: Munich, 1994.
- (3) Brown, R. A.; Budd, P. M.; Price, C.; Satgurunathan, R. *European Polymer Journal* **1993**, 29 (2-3), 337-342.
- (4) Ryan, N. M.; McNally, G. M.; Welsh, J. *Developments in Chemical Engineering and Mineral Processing* **2004**, 12 (1-2), 141-148.
- (5) Paul, D. R.; Robeson, L. M. *Polymer* **2008**, 49 (15), 3187-3204.
- (6) Bharadwaj, R. K. *Macromolecules* **2001**, 34 (26), 9189-9192.
- (7) Picard, E.; Vermogen, A.; Gerard, J. F.; Espuche, E. *Journal of Membrane Science* **2007**, 292 (1-2), 133-144.

Chapter 6: Water barrier properties of polymer/graphite nanocomposites

- (8) Delassus, P. Barrier Polymers. In *The Wiley Encyclopedia of Packaging Technology*, 2nd edition; Brody, A.; Marsh, K., Eds.; John Wiley & Sons, Inc.: New York, 1997; pp 71-77.
- (9) Comyn, J., *Polymer Permeability*. Elsevier Applied Science Publishers: New York, 1986.
- (10) Crank, J., *Diffusion in Polymers*. Academic Press: London and New York, 1968.
- (11) Nielsen, L. E. *Journal of Macromolecular Science: Part A - Chemistry* **1967**, 1 (5), 929-942.
- (12) Bunch, J. S.; Verbridge, S. S.; Alden, J. S.; van der Zande, A. M.; Parpia, J. M.; Craighead, H. G.; McEuen, P. L. *Nano Letters* **2008**, 8 (8), 2458-2462.
- (13) Kim, H.; Macosko, C. W. *Macromolecules* **2008**, 41 (9), 3317-3327.
- (14) Kim, H.; Macosko, C. W. *Polymer* **2009**, 50 (15), 3797-3809.
- (15) Kim, H.; Miura, Y.; Macosko, C. W. *Chemistry of Materials* **2010**, 22 (11), 3441-3450.
- (16) Prud'homme, R. K.; Ozbas, B.; Aksay, I. A.; Register, R. A.; Adamson, D. H. W. O. Patent 2008045778 A1. 2008.
- (17) Kim, H.; Abdala, A. A.; Macosko, C. W. *Macromolecules* **2010**, 43 (16), 6515-6530.
- (18) Kalaitzidou, K.; Fukushima, H.; Drzal, L. T. *Carbon* **2007**, 45 (7), 1446-1452.
- (19) Compton, O. C.; Kim, S.; Pierre, C.; Torkelson, J. M.; Nguyen, S. T. *Advanced Materials* **2010**, 22 (42), 4759-4763.
- (20) Stankovich, S.; Dikin, D. A.; Dommett, G. H. B.; Kohlhaas, K. M.; Zimney, E. J.; Stach, E. A.; Piner, R. D.; Nguyen, S. T.; Ruoff, R. S. *Nature* **2006**, 442 (7100), 282-286.
- (21) Hummers, W. S.; Offeman, R. E. *Journal of the American Chemical Society* **1958**, 80, 1339.
- (22) Stankovich, S.; Piner, R. D.; Chen, X.; Wu, N.; Nguyen, S. T.; Ruoff, R. S. *Journal of Materials Chemistry* **2006**, 16 (2), 155-158.
- (23) Bourlinos, A. B.; Gournis, D.; Petridis, D.; Szabo, T.; Szeri, A.; Dekany, I. *Langmuir* **2003**, 19 (15), 6050-6055.
- (24) Mills, N., *Plastics: Microstructure, Properties and Applications*. Edward Arnold Ltd.: Amsterdam, 1986; pp 225-226.
- (25) Lee, J. M.; Kim, O. H.; Shim, S. E.; Lee, B. H.; Choe, S. *Macromolecular Research* **2005**, 13 (3), 236-242.
- (26) Forch, R.; Schonherr, H.; Jenkins, A. T. A., *Surface design: applications in bioscience and nanotechnology*. 1st edition; Wiley-VCH Verlag GmbH & Co. KGaA, Weinheim: 2009; pp 741.
- (27) Adamson, A., *Physical Chemistry of Surfaces*. 2nd edition; John Wiley & Sons, Inc.: New York, 1982; pp 433-460.
- (28) Titelman, G. I.; Gelman, V.; Bron, S.; Khalfin, R. L.; Cohen, Y.; Bianco-Peled, H. *Carbon* **2005**, 43 (3), 641-649.
- (29) Despond, S.; Espuche, E.; Cartier, N.; Domard, A. *Journal of Applied Polymer Science* **2005**, 98, 704-710.
- (30) Keddie, J. *Materials Science and Engineering* **1997**, 21, 101-170.

Chapter 6: Water barrier properties of polymer/graphite nanocomposites

- (31) Juhue, D.; Lang, J. *Colloids and Surfaces A: Physicochemical and Engineering Aspects* **1994**, 87, 177.
- (32) Tzitzinou, A.; Jenneson, P.; Clough, A.; Keddie, J.; Lu, J.; Zhdan; Treacher, K.; Satguru, R. *Porogress in Organic Coatings* **1999**, 35, 89-99.
- (33) Zhao, C.; Holl, Y.; Pith, T.; Lambla, M. *Colloid & Polymer Science* **1987**, 265, 823-829.
- (34) Aramendia, E.; Barandiaran, M.; Grade, J.; Blease, T.; Asua, J. *Langmuir* **2005**, 21, 1428-1435.

CONCLUSIONS, HIGHLIGHTS AND RECOMMENDATIONS

7.1 Conclusions

The following conclusions are made to the objectives stated in Section 1.4.

Poly (styrene-co-butyl acrylate) (poly(St-co-BA) nanocomposite latices containing the intercalated graphite oxide (GO) nanosheets were successfully synthesized using miniemulsion polymerization. Natural graphite was oxidized by a strong oxidizing agent (KMnO_4) in the presence of a strong mineral acid (H_2SO_4) to obtain GO nanosheets. The GO was mixed with styrene (St) and n-butyl acrylate (BA), and emulsified in the presence of a hydrophobe (HD) and a surfactant (SDBS). The GO was intercalated during the emulsification step followed by miniemulsion polymerization process. The polymerization proceeded to relatively high monomer conversion and produced stable nanocomposite latices. XRD analysis indicated that the nanocomposites exhibited mainly an intercalated morphology, irrespective of the percentage of GO filler loading. Examination of the nanocomposites by TEM proved the formation of intercalated morphology.

2-Acrylamido-2-methyl-1-propanesulfonic acid (AMPS) was successfully used to modify GO nanosheets by mixing the GO with AMPS, to yield AMPS-modified GO. The AMPS-modified GO was used for the miniemulsion polymerization of St and BA. The polymerization resulted in encapsulated GO nanosheets in poly(St-co-BA) particles, and the nanocomposites were exfoliated during polymerization. The modification with AMPS increased the gap between graphene oxide nanosheets in GO, resulting in the synthesis of polymer nanocomposites with exfoliated structure. The exfoliated structure in the nanocomposites was determined by X-ray diffraction (XRD) measurements. Transmission electron microscopy (TEM) confirmed that the graphene nanoplatelets in GO were exfoliated ($\sim 2\text{--}5$ layers thick) in the nanocomposites. The nanocomposites had structures ranging from intercalated to largely exfoliated, and the degree of graphene exfoliation was enhanced as the AMPS-modified GO loading increased. The nanocomposites prepared here had better thermal and mechanical properties than the neat copolymer. Furthermore, the nanocomposites that were made with AMPS-modified GO had better thermal and mechanical properties compared to those made with unmodified GO (i.e., as-prepared).

Dodecyl isobutyric acid trithiocarbonate (DIBTC) RAFT agent was successfully anchored onto GO nanosheets to yield RAFT-immobilized GO. Polystyrene (PS) nanocomposites were subsequently synthesized using the RAFT-immobilized GO by RAFT-mediated miniemulsion polymerization. This study effectively combined the RAFT technology and graphite nanotechnology for the synthesis of polymer nanocomposites in a controlled manner (i.e., low dispersity (\bar{D})). RAFT-mediated polymerization was used to control the morphology and properties of PS nanocomposites. The molar mass and \bar{D} of PS in the nanocomposites decreased markedly as the RAFT-functionalized GO concentration increased, as expected for a typical RAFT-mediated polymerization. The obtained PS-GO nanocomposites had exfoliated morphology, as determined by XRD and TEM analysis. The PS-GO nanocomposites also had improved thermal and mechanical properties relative to neat PS.

The barrier properties of the resulting films obtained from the synthesized poly(St-co-BA) latices to water and water vapor molecules were determined. Functional groups on GO were reduced by using a strong reducing agent, hydrazine hydrate, in order to increase the hydrophobicity of the GO nanosheets. The obtained poly(St-co-BA) films containing the reduced-GO (RGO) were tested for their hydrophobicity and barrier properties, and compared to the films made with unreduced GO (i.e., as-prepared GO). It was determined that the water affinity and barrier properties of the final films were greatly affected by the type of GO used in the miniemulsion formulation. The use of RGO led to a significant increase in the barrier properties and hydrophobicity of the final films. This was mainly due to the hydrophobic nature of graphene nanoplatelets in RGO.

7.2 Highlights

This study describes the synthesis and characterization of polymer nanocomposites by miniemulsion polymerization using graphite oxide (GO) nanosheets. The study confirmed that miniemulsion was a successful method for the preparation of polymer nanocomposites containing intercalated and exfoliated GO nanosheets. The use of miniemulsion polymerization allows the formation of polymer latices, containing the GO nanosheets, which can be exfoliated during the miniemulsion process. This presents a new approach for the preparation of polymer nanocomposites based on GO nanosheets.

The first example of GO modification with a surfmer is described in this study. The modification of GO could significantly change the intercalation behavior of its graphene

oxide nanoplatelets, allowing for the complete exfoliation of graphite into individual graphene nanoplatelets. The obtained modified GO will have a broad gap between its graphene layers, which facilitates the intercalation of monomers into the GO nanogalleries. This provides the needed exfoliation driving force for the formation of polymer nanocomposites with exfoliated structures. The use of miniemulsion as the polymerization method also promotes the intercalation of monomers into the modified graphite nanosheets.

To date, most researchers in the field of nanotechnology have focused mainly on the synthesis and characterization of polymer/graphite nanocomposites (PGNs) using conventional free radical polymerization. Only a few articles on the use of CLRP, such as the RAFT method, focus on the use of clay and carbon nanotubes. In this study, the use of graphite-anchored RAFT agent in miniemulsion polymerization has been reported for the first time. The study showed that a RAFT agent was successfully attached to the surface of GO sheets via an esterification reaction. The use of an anchored RAFT agent results in controlled living radical polymer growth from the graphite surface. The use of a combination of RAFT technology and graphite nanosheets for the synthesis of PGNs by RAFT-mediated polymerization allows for the preparation of tailor-made polymer composites with enhanced properties. This opens the possibility for the synthesis of a wide range of polymer functional GO nanosheets due to the versatility of the RAFT polymerization process.

Results of this study also showed that the use of graphite (i.e., RGO) in polymer nanocomposites will lead to the formation of polymer films with good water resistance properties. The nanolayered structure of graphene leads to low water diffusion through the polymer film by providing a tortuous path across the polymer matrix. The synthesis of polymer/graphite lattices by miniemulsion polymerization could provide new industrial applications for emulsion coatings. The obtained emulsions, for instance, can be easily applied on permeable surfaces such as paper, which is widely used in food packaging applications.

7.3 Recommendations

Recently, there has been growing interest in Pickering emulsions^{1,2} because they open new avenues of particle stabilization and have numerous practical applications. These include commercial applications such as in cosmetics, petrochemicals and oil refining. In Pickering emulsions, solid particles of intermediate wettability in the size range from several

nanometres to several micrometers attach to the liquid-liquid interface and provide particle stability. Different solid particles, such as silica³ and clay,^{4,5} have been previously used for the synthesis of these surfactant-free Pickering emulsions. However, the use of graphite nanosheets in such emulsions has not yet been investigated.

Further work should investigate the use of graphite (such as GO and modified GO) nanoparticles for the synthesis of solid-stabilized (i.e., surfactant-free) polymer latices. Miniemulsion polymerizations using graphite nanosheets as stabilizer, of which the surface of the particles is covered and stabilized with graphene nanoplatelets, could be investigated. The resulting polymer latices are expected to exhibit good colloidal stabilities. Subsequently, coatings prepared from these waterborne polymer/graphite latices should be devoid of the common adverse effects provoked by the presence of conventional surfactants.

Therefore, the following areas could be studied:

- Modification of graphite nanoparticles to produce modified graphene platelets of intermediate wettability.
- Preparation of surfactant-free polymer emulsions and miniemulsions using the modified graphene nanosheets as stabilizers.
- Possibility of using the obtained surfactant-free latices for film formation (coatings), and investigation of their barrier properties (i.e., to water, oxygen and nitrogen).

7.4 References

- (1) Pickering, S. U. *Journal of the Chemical Society, Transactions* **1907**, 91, 2001-2021.
- (2) Ramsden, W. *Proceedings of the Royal Society of London* **1903**, 72 (477-486), 156-164.
- (3) Ma, H.; Luo, M.; Sanyal, S.; Rege, K.; Dai, L. *Materials* **2010**, 3 (2), 1186-1202.
- (4) Bon, S. A. F.; Colver, P. J. *Langmuir* **2007**, 23 (16), 8316-8322.
- (5) Zhang, J.; Chen, K.; Zhao, H. *Journal of Polymer Science Part A: Polymer Chemistry* **2008**, 46 (8), 2632-2639.

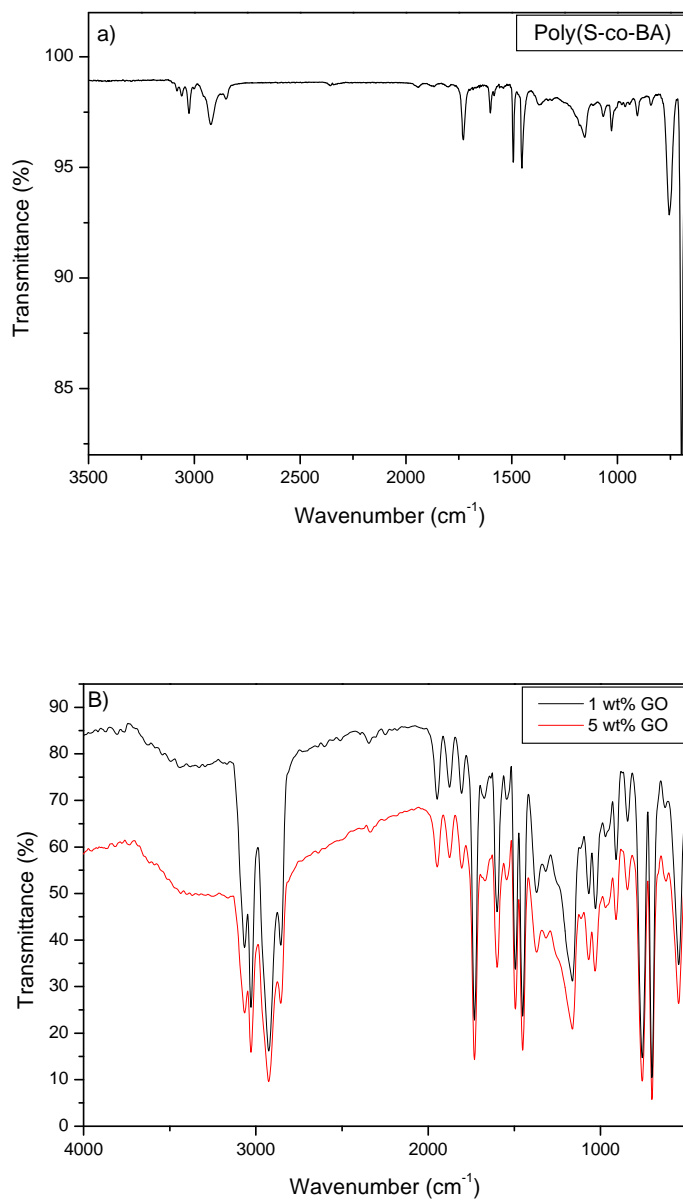
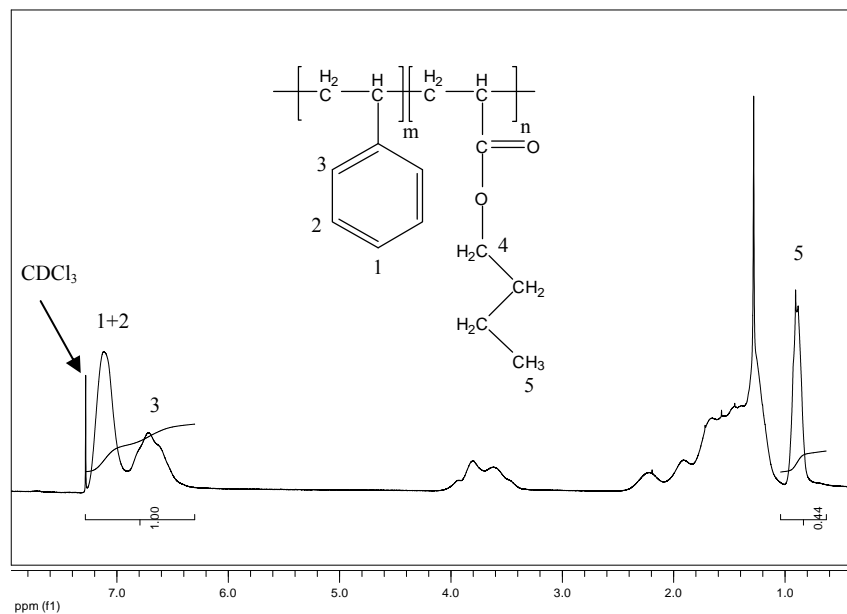
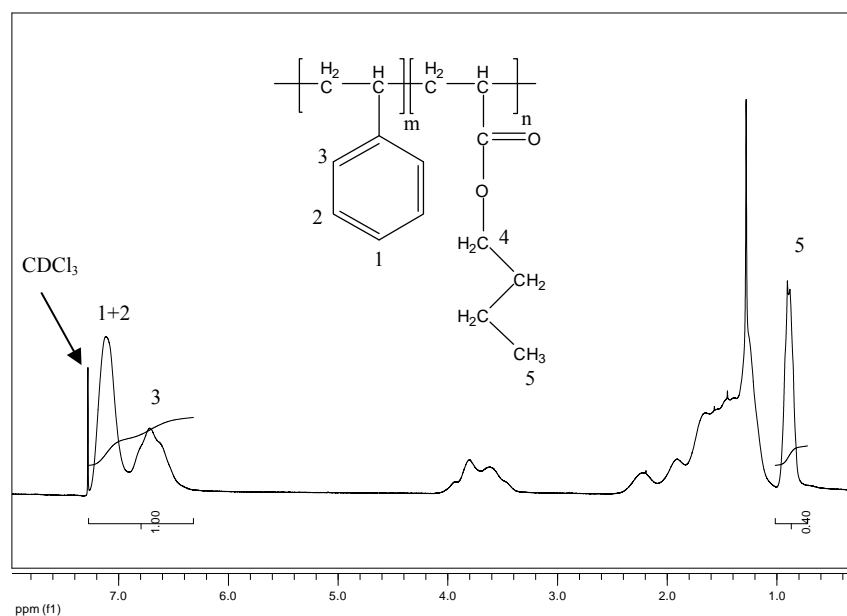
Appendix A: FT-IR spectra for pure poly(St-co-BA) and poly(St-co-BA)/GO nanocomposites

Figure A.1: FT-IR spectrum of (a) pure poly(St-co-BA) and (b) poly(St-co-BA)/GO nanocomposite containing 1 and 5 wt% of GO.

Appendices

Appendix B: NMR data for pure poly(St-co-BA) and poly(St-co-BA) in the nanocomposites.**Figure B.1: ¹H-NMR spectrum (CDCl₃) of pure poly(St-co-BA).****Figure B.2: ¹H-NMR spectrum (CDCl₃) of poly(St-co-BA)/GO nanocomposite at 1 wt% GO loading.**

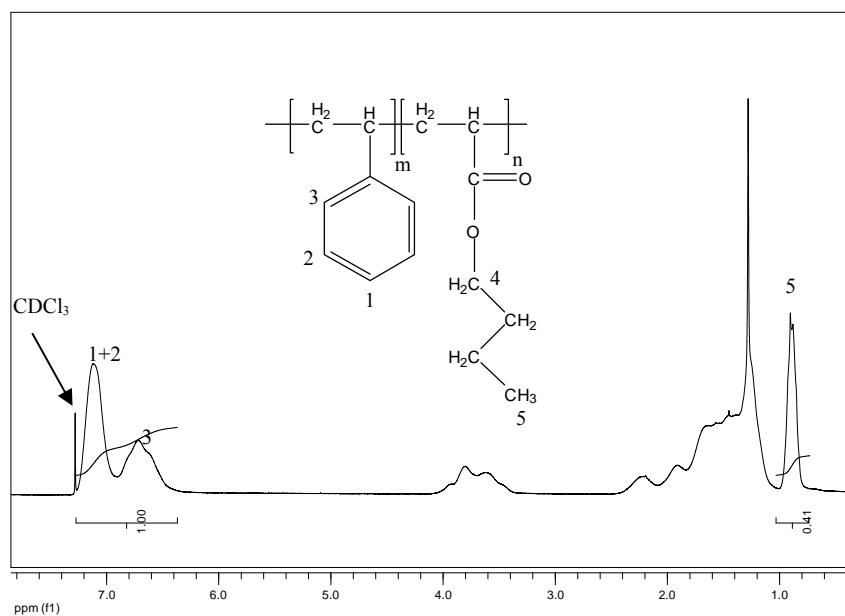


Figure B.3: ¹H-NMR spectrum (CDCl₃) of poly(St-co-BA)/GO nanocomposite at 3 wt% GO loading.

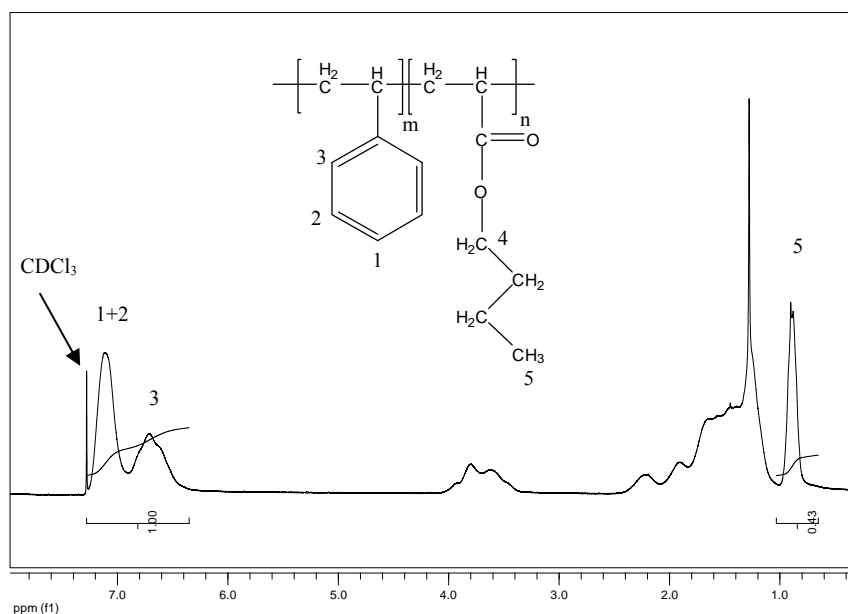
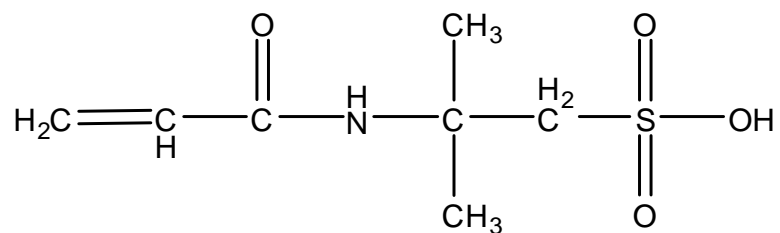


Figure B.4: ¹H-NMR spectrum (CDCl₃) of poly(St-co-BA)/GO nanocomposite at 5 wt% GO loading.

Appendix C: Chemical structure of the surfmer that was used to modify GO**Figure C.1: 2-Acrylamido-2-methyl-1-propane sulfonic acid (AMPS).**

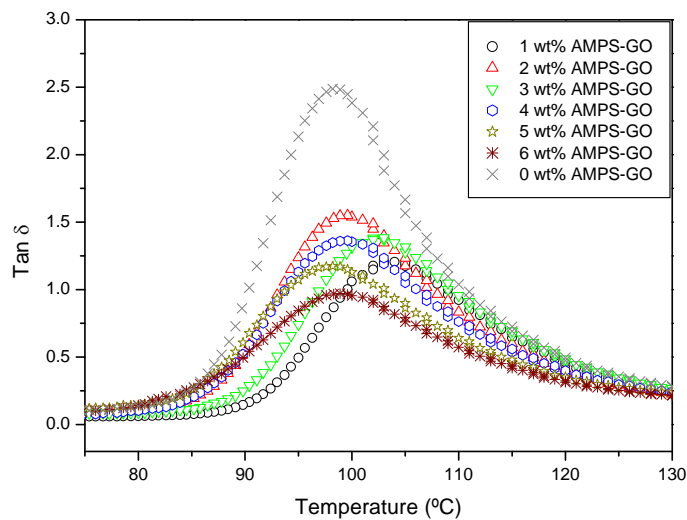
Appendix D: Tan δ curves of poly(St-co-BA)/GO nanocomposites

Figure D.1: Tan δ as function of temperature of poly(St-co-BA)/GO nanocomposites, at graphite loadings of 0–6 wt%.

Appendix E: NMR data for DIBTC RAFT agent

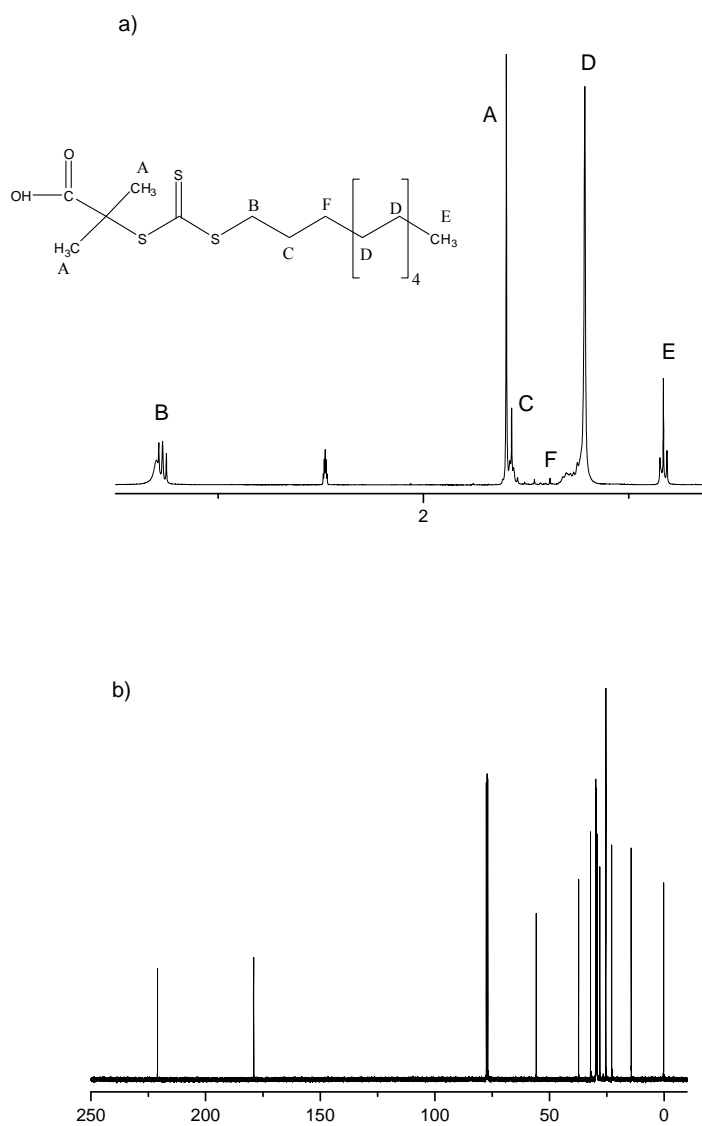


Figure E.1: NMR data for DIBTC RAFT agent: a) ^1H -NMR spectrum ($\text{DMSO-}d_6$) and b) ^{13}C -NMR spectrum (CDCl_3).